TESIS DOCTORAL

Estudio de las interacciones microbianas de comunidades planctónicas en gradientes ambientales

Study of the microbial interactions of the planktonic communities in environmental gradients

Sara Soria Píriz

Universidad de Cádiz

Facultad de Ciencias del Mar y Ambientales

Departamento de Biología-Área de Ecología

Cádiz, Febrero - 2020

Estudio de las interacciones microbianas de comunidades planctónicas en gradientes ambientales

Memoria presentada por Sara Soria Píriz para optar al Grado de Doctor en Ciencias y Tecnologías Marinas por la Universidad de Cádiz

Fdo. **Sara Soria Píriz**

_____

Los directores: **Dr. D. Alfonso Corzo Rodríguez**, Catedrático del Área de Ecología de la Universidad de Cádiz y **Dr. D. Sokratis Papaspyrou**, Profesor Titular del Área de Ecología de la Universidad de Cádiz.

CERTIFICAN:

Que la presente memoria titulada, "**Estudio de las interacciones microbianas de comunidades planctónicas en gradientes ambientales**", presentada por Sara Soria Píriz, ha sido realizada bajo su dirección y autorizan su presentación y defensa, para optar al Grado de Doctor por la Universidad de Cádiz

Y para que así conste y surta los efectos oportunos, firman la presente memoria de tesis doctoral en Puerto Real (Cádiz), a 28 de noviembre de dos mil diecinueve.

Dr. D. Alfonso Corzo Rodríguez **Dr. D. Sokratis Papaspyrou**

_____ _____

Para la realización de esta Tesis doctoral, Sara Soria Píriz, ha disfrutado de dos contratos anuales asociados al proyecto "*Interacción de los procesos microbianos y geoquímicos en la atenuación natural de la contaminación por drenaje acido de minas en embalses y estuarios*" (P11-RNM-7199, Proyecto Excelencia Junta de Andalucía) y "Producción primaria y metabolismo neto en gradientes ecológicos. Estuarios y lagos ácidos" (20.DG.UE.II.05, Plan Propio Universidad de Cádiz). La realización de la Tesis también ha sido financiada por los proyectos: 1) "*Desarrollo y Consolidación de la investigación en ecología microbiana y biogeoquímica marina en costa rica* (A1/037457/11 y D/031020/10), financiados por la Agencia Española de cooperación internacional para el desarrollo (AECID). 2) "*Interacción de los procesos microbianos y geoquímicos en la atenuación natural de la contaminación por drenaje acido de minas en embalses y estuarios*" (P11-RNM-7199), Proyecto de Excelencia Junta de Andalucía. 3) "*Producción primaria y metabolismo neto en gradientes ecológicos. Estuarios y lagos ácidos*" (20.DG.UE.II.05), Plan Propio Universidad de Cádiz). 4) *"Ecología microbiana y biogeoquímica de los sedimentos intermareales: Efectos del forzamiento físico de las mareas, el fotoperiodo y los eventos climáticos extremos"* (CTM2017-82274-R), Plan Nacional de I+D+i, Ministerio de Economía y Competitividad.

Esta tesis doctoral se ha realizado en el Laboratorio de Ecología Microbiana y Biogeoquímica (http://www2.uca.es/grup-invest/microbentos/), dentro del grupo de investigación Estructura y Dinámica de Ecosistemas Acuáticos (EDEA, RNM-214) del Departamento de Biología de la Universidad de Cádiz.

Parte de los resultados presentados en esta memoria de Tesis Doctoral han sido publicados en revistas internacionales indexadas (Capítulo II y IV en *Limnology and Oceanography*), presentados en diversos congresos nacionales e internacionales o bien se encuentran en preparación para su publicación

GRACIAS!

Bueno, bueno…no puedo creer estar escribiendo esta parte!! Después de tanto tiempo, cuesta creerlo…:-D

Pues empezaré dando las gracias a Alfonso y Sokratis, Gracias por permitirme hacer la tesis en el MEBlab. Sobre todo a Alfonso, por seguir aceptándome a pesar de renunciar a una tesis doctoral con otra temática y dejarme ser la oveja "pelágica" del lab. Aunque no ha sido un camino fácil, pero si una se empeña, las cosas salen, tarde o temprano. Siempre serás mi padre en la ciencia ☺. Y a Sokratis, gracias por sacar siempre 10 minutos para resolver las dudas que tuviera, sobre todo del mundo complejo de la estadística.

A Emilio, porque todo esto empezó por tu idea en una inocente entrevista para la campaña de Costa Rica. Nombraste la parte da la campaña relacionada con la columna de agua y yo decir… Me encargo! Una cosa llevó a la otra, y hasta ahora. Gracias por instruirme en mis inicios en el mundo de la investigación!

A mis coleguis del lab! Han sido muchos los que han pasado por allí, pero sobre todo a Julio, Juanlu, y Eddy. Por la de horas que hemos trabajo juntos, sobre todo en los muestreos, ya sean los de Costa Rica o los del El Sancho! Siempre quedarán en el recuerdo anécdotas divertidas, que al final es con lo que te quedas!

A Sara, Maca y Juan! Qué de ratitos güenos que hemos echado al lado del mar, con nuestras conversaciones profundas de la vida. Extrañaré los momentos en los que uno decía por lo bajini en el lab…, mm una cerveza rápida? Y al final siempre nos animábamos a por unas cuentas más! Y a Yoni! por echarnos unas risas cada vez que venías y por ser el soporte informático cuando lo he necesitado.

A Miguel. Como ya te dije, el secreto de acabar bien un trabajo es la buena comunicación que hemos tenido y la predisposición por escuchar. Para mí, es el secreto para sacar adelante las cosas. Además, nos hemos animado el uno al otro en los momentos más desesperantes y eso ayuda mucho!

A Vicky, por tu paciencia desde el otro lado del charco en resolverme dudas sobre el citómetro. Facilitaste mucho mi aprendizaje y si algún día volvemos a encontrarnos por este tema, que sean análisis en un citómetro con autosampling!….La de tiempo que hubiéramos ahorrado! Bueno, mejor ni pensarlo ☺

Al equipo de Costa Rica-UCA. Esas campañas fueron algo especial para mí. No solo porque fue mi primera experiencia en cruzar el charco y ver el Océano Pacífico, pero sobre todo al equipo humano y al buen ambiente que hubo siempre. A pesar de dormir 3 horas diarias, siempre hubo una sonrisa en cada uno de vosotros. Pura vida!

Al equipo de Aquatic Bio Technology, en especial a Sergio, nuestro MacGyver de los muestreos en el Sancho. Gracias por tu buen carácter y tu manera elegante de trabajar, siempre intentado solucionar cualquier cosa que surgiera. Y a Asier y a Enaitz, porque de algún modo, fuisteis mis primeros "jefes oficiales", jeje.

Cómo no mencionar a Juan, el guarda de El Sancho. He de reconocer que la primera vez que te vi, me asusté de ver aquel hombre tan desaliñado al que costaba entender lo que decía (sin ánimo de ofender, jeje)…Pero cuando te conocimos, pudimos ver a una persona entrañable al que se le coge mucho cariño. Además, con tu buen humor, pusiste la guinda dulce a los "ácidos" muestreos en El Sancho.

A Iria y a Eli! Por ese trio consejero (aunque una servidora nunca apareció, :-P). Por los ratitos de risas que hemos echado en la cafetería y esos ánimos sobre todo en la última etapa! También recordaré aquel

turno de madrugada en la campaña MEGAN, que aunque estuviéramos agotadas, siempre hubo tiempo para reír ☺

A Ángel, Pablo y Alberto, los camareros de la cafetería del CASEM. Gracias por recibirme siempre con una sonrisa por las mañanas temprano y prepararme un desayuno de "café explosivo", si me veían muy cansada, con "happy cream" (paté ibérico) acompañando a la tostada y empezar el día con energía. Cómo dice Ángel, todo es posible en el CASEM!

A Lara y a Edurne, mis compis de sufrimiento desde la distancia. Siempre habéis estado ahí con vuestro apoyo...Espero que nos volvamos a encontrar en algún lugar, a ser posible de fiesta, para celebrar que hemos superado esta fase ☺. Y a Dan! Por esos consejos y ánimos como post-doc a una doctoranda.

A Meu, Edurne, Fini, Laura, Marta, Maca, Sol, y Tom. Gracias por confiar en mis ilustraciones en un momento crítico de la tesis. Con vuestros encargos, contribuisteis a que volviera a sentir la energía y motivación que hace falta para seguir luchando por lo que quieres.

A Laura. Mi amiga más longeva de tierras gaditanas. Qué decir de ti Laurilla? Que me acogiste cuando no tenía casa en mis comienzos, y siempre has estado ahí. Gracias por tu generosidad y tu nobleza.

A mis compis isleños. Gracias por acogerme en vuestro grupo de cervezas de "el viernes a las 11 en la escalerilla", jaja. La verdad que hemos echado buenos momentos por la Isla, aunque a veces se hablara demasiado de trabajo, :-P. Y aunque ya pocos quedamos por aquí, pero siempre recordaré las fiestas que nos echábamos, sobre todo con vosotros, Fran, Juanlu y Eddy. A Sole, Nono, Sara, Ricardo y Carmen, Rosa, que aunque vosotros estuvierais en mi misma situación (o peor), nunca faltaron vuestros ánimos. Las conversaciones con Sol sobre la vida, acompañadas de un cafelito/cerveza en cualquier momento para desconectar un ratito. Y a Isa, que aunque te conocí por poquito tiempo, pero supe que nuestra amistad iría para largo.

A mis "queridas titis" como no, que a pesar de que os veo una vez o dos al año, siempre estáis ahí, como si nos hubiéramos visto ayer, y eso no es fácil de conservar! Espero que a partir de ahora, podamos vernos más a menudo, o por lo menos, venir a visitarme esté donde esté!…que allí por Olivenza, hay poco donde trabajar sobre comunidades planctónicas microbianas :-D

A Luisa, Pepe y Alicia. Por vuestra constante ayuda durante este periodo. Sin vuestro apoyo, económico y sobre todo emocional, no hubiera podido acabar la tesis. Gracias por ser la familia que sois ☺.

Y a Ale. Aunque nos haya tocado vivir una relación a distancia la mayor parte del tiempo, siempre has estado ahí. Esto nos ha curtido para cualquier cosa que se nos presente de aquí en adelante. Y también por tu santa paciencia, de tener una novia monotemática, sobretodo esta última temporada. Espero que a partir de ahora tengamos más tiempo para compartir y disfrutar más aventuras juntos!!

A tod@s vosotr@s, GRACIAS!

Sara

x_____

ABSTRACT

Microbial communities play a primordial role in the biogeochemical cycles in nature. Phytoplankton and bacterioplankton are at the base of the microbial food web in aquatic systems, being the main producer and decomposer of organic carbon, respectively. In aquatic systems, these communities are controlled by the characteristic dynamism and heterogeneity of the environmental variables in pelagic ecosystems. One of the best ways to understand how communities are affected by environmental variables is by studying ecological gradients, which are progressive spatiotemporal changes of biotic and/or abiotic characteristics within an ecosystem.

Many ecosystems present remarkable environmental gradients in which the interactions between the microbial communities and the effect these strong abiotic gradients have on them are poorly known. Without this information it is difficult to predict how the structure of microbial community, its functionality and in a greater extent the ecosystem itself, might respond to future environmental changes. Here we show how the microbial communities and their interactions in the environmental gradients studied here, a longitudinal transect in a tropical estuary and a vertical gradient in an acid reservoir, are strongly affected by the changes in the environmental conditions in space and time. In the tropical estuary, a marked zonation in terms of productivity was observed from the head to the mouth of the estuary, being daily net production only positive in the middle of the estuarine gradient. The strong dissolved organic carbon inflows to the tropical estuary during the rainy season could potentially change the ecosystem to a system driven in a higher degree by allochthonous carbon leading to a higher importance of bacterioplankton activity. In contrast, during the dry season, remarkable direct (by dissolved organic carbon) coupling between phyto- and bacterioplankton groups were revealed from the similarity of the patterns. In the acid reservoir, during stratification, a strong coupling between the phytoplankton that forms a deep chlorophyll maximum in the metalimnion and the bacterial carbon dioxide production in the hypolimnion was demonstrated by a 1-D reactive transport model, indicating that inorganic carbon can be the limiting nutrient for phytoplankton community in acid lakes. The phylogenetic composition and cell traits of bacterioplankton changed in parallel between stratification and mixing seasons suggesting that both structural levels of this community are linked each other and are affected by the environmental variables. Overall, our results demonstrate how the environmental gradients affect the microbial communities at different levels, including single cell characteristics, physiology, phylogenetic structure, spatiotemporal distributions of different populations and ecosystem level properties like net ecosystem production and metabolism. This multilevel approach is essential to understand the ecological function of the microbial community in complex ecosystems and predict future changes in response to climate and anthropogenic forcing.

RESUMEN

Las comunidades microbianas juegan un papel crucial en los ciclos biogeoquímicos en la naturaleza. El fitoplancton y el bacterioplancton están en la base de la red alimentaria microbiana en los sistemas acuáticos, siendo el principal productor y descomponedor de carbono orgánico, respectivamente. En los sistemas acuáticos, estas comunidades están controladas por el dinamismo característico y la heterogeneidad de las variables ambientales en los ecosistemas pelágicos. Una de las mejores maneras de entender cómo las comunidades se ven afectadas por las variables ambientales es estudiando los gradientes ecológicos, que son cambios espaciotemporales progresivos de características bióticas y / o abióticas dentro de un ecosistema.

Muchos ecosistemas presentan notables gradientes ambientales, en los que las interacciones entre las comunidades microbianas y el efecto que estos fuertes gradientes abióticos tienen sobre ellos, son poco conocidos. Sin esta información, es difícil predecir cómo la estructura de la comunidad microbiana, su funcionalidad y, en mayor medida, el ecosistema mismo, podrían responder a los cambios ambientales futuros. Aquí mostramos cómo las comunidades microbianas y sus interacciones en los gradientes ambientales estudiados aquí, un transecto longitudinal en un estuario tropical y un gradiente vertical en un embalse ácido, se ven fuertemente afectados por cambios en las condiciones ambientales en el espacio y el tiempo. En el estuario tropical, se observó una marcada zonación en términos de productividad desde la cabeza hasta la boca del estuario, siendo la producción neta diaria positiva sólo en el medio del gradiente del estuario. Las fuertes entradas de carbono orgánico disuelto al estuario tropical durante la temporada de lluvias podrían potencialmente cambiar el ecosistema a un sistema impulsado en mayor grado por el carbono alóctono, lo que lleva a una mayor importancia de la actividad del bacterioplancton. En contraste, durante la estación seca, los patrones de similaridad revelaron un notable acoplamiento directo (por carbono orgánico disuelto) entre grupos de fitoplancton y bacterioplancton. En el embalse ácido, durante la estratificación, se demostró un fuerte acoplamiento entre el fitoplancton que forma un máximo profundo de clorofila en el metalimnion y la producción de dióxido de carbono por parte del bacterioplancton en el hipolimnion, mediante un modelo de transporte reactivo 1-D, lo que indica que el carbono inorgánico puede ser el nutriente limitante de la comunidad de fitoplancton en lagos ácidos. La composición filogenética y los rasgos celulares del bacterioplancton cambiaron en paralelo entre las fases de estratificación y de mezcla, lo que sugiere que ambos niveles estructurales de esta comunidad están vinculados entre sí y se ven afectados por las variables ambientales. En general, nuestros resultados demuestran cómo los gradientes ambientales afectan a las comunidades microbianas a diferentes niveles, incluidas las características celulares, fisiología, estructura filogenética, distribuciones espacio-temporales de diferentes poblaciones y propiedades a nivel del ecosistema, como la producción neta del ecosistema y el metabolismo. Este enfoque de múltiples niveles es esencial para comprender la función ecológica de la comunidad microbiana en ecosistemas complejos y predecir cambios futuros en respuesta al forzamiento climático y antropogénico.

CONTENTS

"Unless we appreciate the importance of microbial processes, we fundamentally limit our understanding of Earth's biosphere and response to climate change and thus jeopardize efforts to create an environmentally sustainable future"

(United Nations, 2018)

CHAPTER I

General Introduction and Objectives

1. GENERAL INTRODUCTION

1.1. Research motivation: the role of microbial communities in pelagic systems

Understanding the role of microorganisms in maintaining ecosystem health is a central goal in ecology (Prosser et al. 2007; Fuhrman 2009). Microorganisms constitute the life support system of the biosphere having an enormous impact on all biogeochemical cycles. Despite their small size, aquatic microorganisms are the dominant organisms in the plankton ($>10^{30}$ cells) providing, from an anthropocentric point of view, many ecosystem services, such as clean drinking water, fisheries sustainability, bioenergy, or simply, being largely responsible for the O_2 that we breathe (Thingstad et al. 2005; Reynolds 2006), and controlling to a great extent, through metabolic pathways, the pelagic energy flow of carbon and the nutrient cycles (Cole and Cole 1982; Whitman et al. 1998).

Phytoplankton, the photoautotrophic component of the plankton community, and *bacterioplankton*, the prokaryotic community mainly responsible of the decomposition of pelagic detritic matter, form the basis of the microbial food web in aquatic systems. Phytoplankton assimilates CO_2 and greatly influences the energy and resource fluxes through the entire biosphere, accounting for ~45% of the global carbon fixation (Field et al. 1998; Reynolds 2006; Litchman and Klausmeier 2008). Bacterioplankton plays a key role in the transfer of C and other essential nutrients (i.e. N and P) between the dissolved and the particulate fractions, consuming DOC released by phytoplankton and releasing dissolved compounds from particulate detritic matter (Azam et al. 1983; Ducklow 1983; Fuhrman 1992). Therefore, bacterioplankton plays an essential role in the biochemical transformation of particulate and dissolved detrital organic matter, nutrient recycling, and energy fluxes within aquatic ecosystems (Sherr and Sherr 1988; del Giorgio and Cole 1998). These microbial communities exhibit a number of emergent properties such as stability, productivity or resiliency, based on their metabolic and taxonomic diversity, which convert them to main players in biogeochemical cycles and ecological processes (Konopka 2009). Hence, the study of the interactions between the different components of the community (phytoplankton and bacterioplankton), at different levels, taxonomic, physiological and functional, provides essential information about and insight into ecological processes (Fig. 1) (Azam and Worden 2004).

The ecological n-dimensional space in which a species can survive and reproduce, maintaining viable populations, defines its *ecological niche* (Hutchinson 1957, Ter Braak and Prentice 1988, Ackerly 2003). This concept is fundamental in the analysis of biodiversity, species distribution, and other aspects related to the composition and dynamics of communities including ecosystem stability (Lewis 2009). In the pelagic environment, the spatiotemporal distribution of these ecological niches are controlled by the adaptations of microorganisms to the characteristic heterogeneity and dynamism of the environmental variables (Fig. 2, 3) (Margalef 1978; Green and Bohannan 2006; Mitchell et al. 2008). Margalef stated that “the knowledge of the relations among elements is more important to the understanding of a system than knowledge of the precise nature of its constituents” (Margalef, 1992). Therefore, improving our understanding on the diversity of potential microbial niches, the microorganisms related to them, and how the changes in these ecological niches, and their associated microbial communities occur in space and time will benefit our predictive models on the role of microorganisms can play in the response of the ecosystems to climate change (Fuhrman 2009; Tylianakis and Morris 2017; Cavicchioli et al. 2019). Moreover, human-induced global change will

likely alter the microbial community structure in a short time span, making its understanding even more pressing for the future of our planet (Litchman and Klausmeier 2008, Cavicchioli et al. 2019).

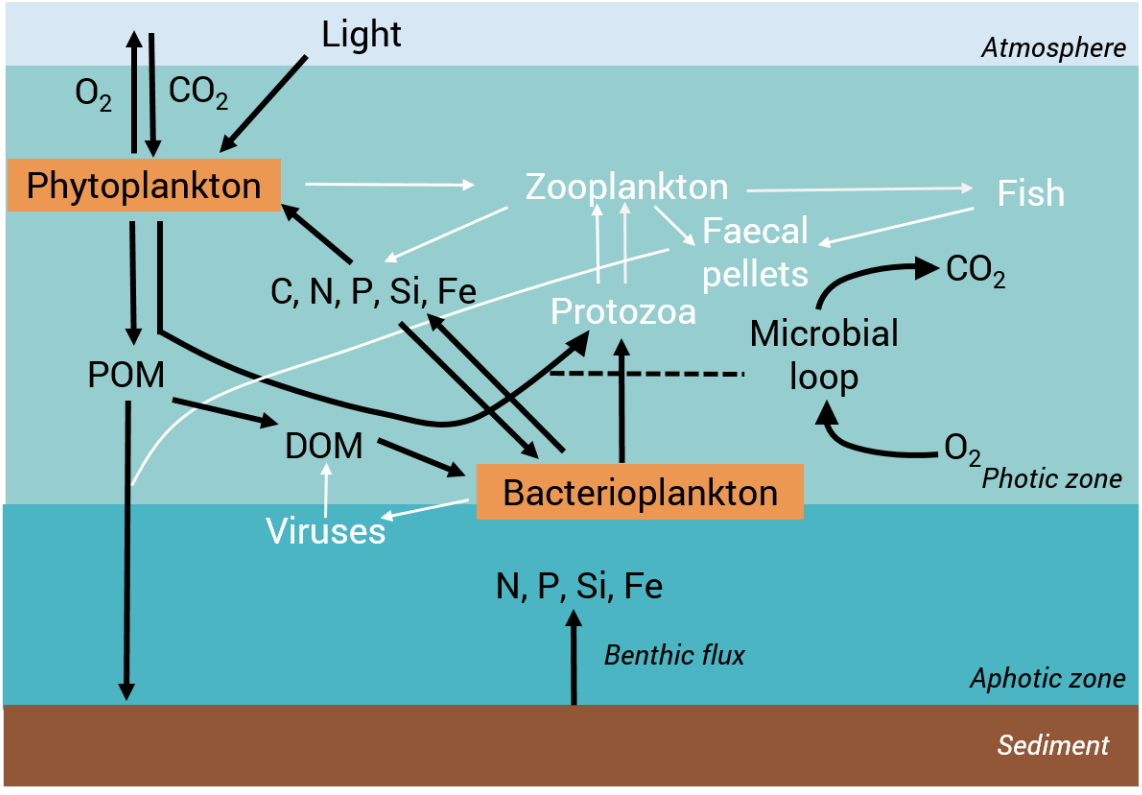

Fig.1: Idealized *microbial food web***.** Most of the organic matter synthesized by primary producers (phytoplankton) becomes dissolved organic matter (DOM) and is taken up almost exclusively by bacterioplankton. This DOM is respired to carbon dioxide (CO_2), being anew available by phytoplankton (Microbial loop, Azam et al. 1983). Another fraction is assimilated and re-introduced into the classical food chain (phytoplankton to zooplankton to fish, white arrows). Phytoplankton and bacterioplankton form the basis of pelagic trophic web, being grazed by heterotrophic or mixotrophic protozoa or by viruses (white arrows). Modified from Azam and Malfatti (2007).

1.2. The e*nvironmental gradient* concept in aquatic ecosystems

In nature, temporal and spatial variability are omnipresent as already expressed by Herakleitos as *panta rhei* (everything flows) (Diels 1895, Schweiger et al. 2016). The essential mission of ecology is to find general rules which explain how, when, and why environmental factors influence the distribution of organisms and ecological processes within the variability and heterogeneity of nature, and reciprocally, how the changes in the distributions of the organisms influence ecological patterns (Unban et al 1987; Turner 1989; Cushman et al. 2010). Understanding how communities are affected by the environment is most easily achieved by investigating their variations along gradients of different factors (Mcgill et al. 2006). The term *ecological gradient* refers to gradual changes or transitions, both

in space and in time, of biotic or abiotic variables within an ecosystem (Gosz 1992). Spatial gradients can range from small-scale variation in different ecological factors across several types of interfaces, i.e. the sediment-water interface, the thermocline, land-water zonation in the shoreline of aquatic environments etc., to large-scale geographical and climatic variability gradients (e.g. latitudinal and altitudinal) (Gaston 2000). Temporal gradients refer to changes in time of the ecological factors, which can include short (e.g. seasonal) or long-term changes (e.g. associated to changing climatic conditions) (Serreze et al 2000). The study of ecological gradients have enhanced our understanding of the structure and function of ecosystems allowing us to assess the dynamics, structure, and function of communities in a multidimensional way, and in turn, predict how, when and why the communities can change in response to these ecological gradients (Gosz 1992).

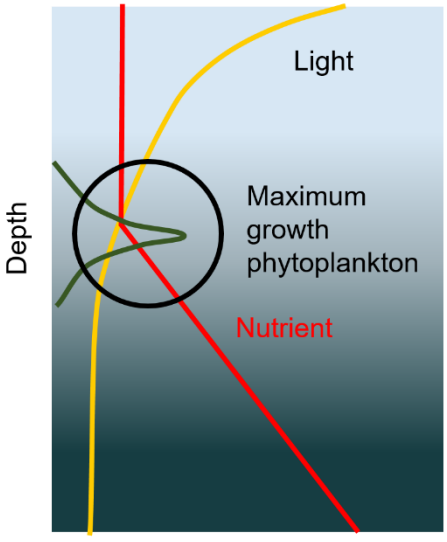

Fig.2: Example of an *ecological niche* of a phytoplankton species which depends on the opposite gradients of the main resources for phytoplankton growth (light and nutrients) along the water column. Modified from Litchman (2007).

Although research on gradients has generally focused on vegetation ecology, in terms of species' abundances and diversity (Whittaker 1967; Austin 1985; Peterson et al. 1997; Mcgill et al. 2006, among others), the study of microorganisms along gradients, especially in phytoplankton ecology, is not novel. In 1978, Margalef defined his classical *mandala* concept on how phytoplankton composition varies depending on the nutrient-turbulence space gradients (Fig. 3). Studies on microbial community structure along environmental gradients in aquatic systems has increased in the last decades (Bouvier and del Giorgio 2002; Cotner and Biddanda 2002; del Giorgio and Bouvier 2002; Delong et al. 2007). However, there are still many ecosystems, with marked environmental gradients, in which the interactions between different components of microbial communities are still unknown.

Two different environmental gradients were selected in this PhD thesis. The first one was a horizontal gradient in an estuarine system, and the second one a vertical gradient in an acid freshwater reservoir. In the estuary, the mixing of riverine fresh water with seawater along the estuarine

longitudinal axis, from head to mouth, creates steep changes in many environmental variables between the two dominant end-members (the river and the ocean), which in addition change seasonally in parallel to the river flow (Figs. 4, 5). In the reservoir, the water column is fully mixed during the winter and strongly stratified into several layers during summer (Fig. 6), leading to a complex ecosystem structure with marked vertical environmental gradients (Fig. 7). Therefore, both ecosystems are ideal candidates to study microbial interactions and biogeochemical processes giving insights into ecosystem functioning in gradient systems.

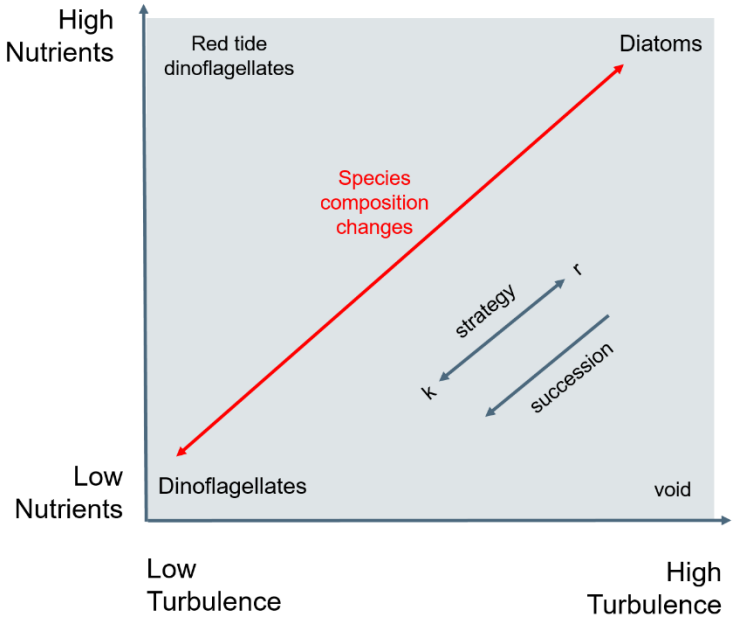

Fig.3: The *mandala* of Margalef shows how different environmental conditions in the pelagic environment determine different suitable niches for different phytoplanktonic assemblages. Modified from Margalef (1978, Fig. 2).

1.2.1. Longitudinal gradient in estuarine systems

Estuaries, as transitional systems, are ideal natural laboratories for studying microbial interactions and biogeochemical processes because of the sharp natural gradients in light, nutrient, salinity, and temperature that typically exist associated with the freshwater river plumes (O'Donohue and Dennison 1997; Bouvier and del Giorgio 2002; Li et al. 2017; Xenopoulos et al. 2017). Mixing of the fresh water riverine inputs with saline water is the dominant feature of these systems (Mclusky 1993; Bouvier and del Giorgio 2002). Due to the strong salinity gradient, estuaries can be considered a separate class of ecosystem having complex and diverse spatial patterns, with unique species assemblage and transport processes (Attrill and Rundle 2002; Quinlan and Phlips 2007; Muylaert et al. 2009).

Estuaries are systems of special relevance for human societies since they provide important ecosystem services, being included among the most biologically valuable areas of the world (Costanza et al. 1998; Barbier et al. 2011). Indeed, even though they only represent about 1-2% of the surface of the ocean, their primary production accounts for 20% of the its global production (Smith 1981; Charpy-Roubaud and Sournia 1990; Cloern et al. 2014). Anthropogenic activities affect ecological and biogeochemical processes in estuaries, modifying the structure of their food web, from microbial communities to macroorganisms, including species of economic interest (Burford et al. 2008; Blaber 2013; Cloern et al. 2016). Of all the estuaries, tropical ones are being particularly affected as they are often located in developing or recently industrialized countries, usually characterized by high population growth rates (Alongi 2002; Barbier et al. 2011).

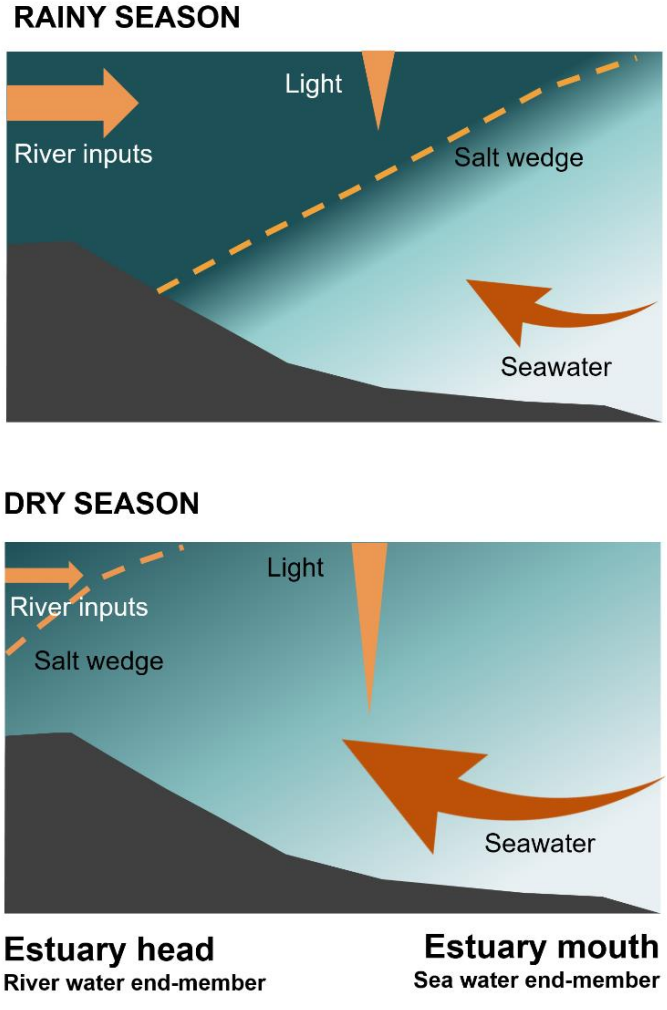

Fig. 4: Idealized *longitudinal cross section views* along an estuary during the typical rainy and dry seasons in tropical areas. During the rainy season, discharges from the river are higher than during the dry season resulting in a more pronounced salt wedge and a higher turbidity in the water column.

Although tropical estuaries share a number of features with temperate ones, such as salinity gradients, tidal variations, and terrestrial inputs (Eyre and Balls 1999), they also have singular characteristics, i.e. larger variations in river runoff and higher and more constant levels of irradiance and temperature year round (Nittrouer et al. 1995; Cloern et al. 2014). Changes in the riverine flow regime are much higher in the tropical estuaries whose regimes are determined by the rainy (wet) and dry seasons. In fact, discharge differences between dry and rainy seasons are generally two orders of magnitude higher than those observed in temperate estuaries over the course of a year (Eyre and Balls 1999). Increased riverine discharge plays an important role, increasing nutrient concentrations, turbidity and sediment loads to the estuary, promoting changes in water residence time, decreasing the salinity and causing variations in plume characteristics (Eyre and Balls 1999; Eyre 2000; Burford et al. 2012). All these changes, ultimately, affect the biota and the ecology of estuarine ecosystems (Xenopoulos et al. 2017).

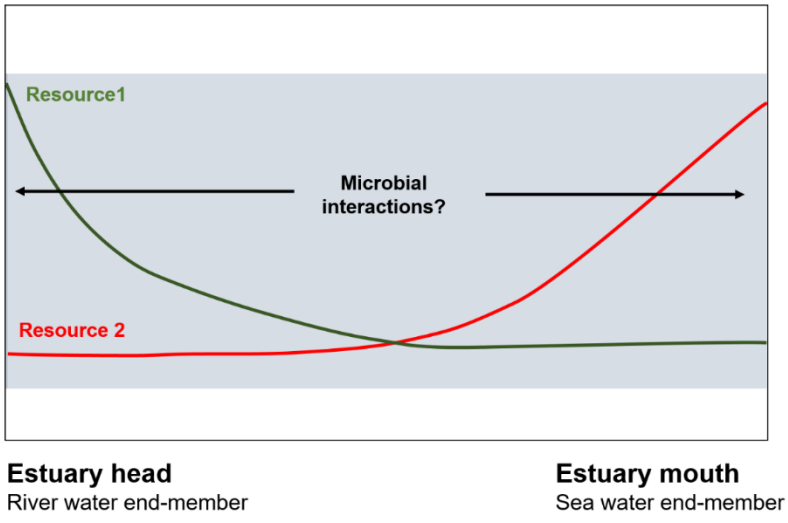

Fig.5: Idealized *longitudinal-section view* along a typical estuary showing opposing gradients of resources such as higher concentrations of nutrients in the head of the estuary due to the river discharges and increased light penetration at the estuary mouth. The shaded area represents the unknown longitudinal zonation of the possible microbial communities and their interactions.

1.2.2. Vertical gradient in freshwater systems

Freshwater systems represent only 0.009% of the total water on Earth (Wetzel 2001). They are the most extensively and rapidly altered ecosystems, enduring changes in physical structure, chemical processes and biotic characteristics (Carpenter et al. 2011). The most severe impact is the strong degradation of freshwater quality caused by pollutants (Wetzel 1992), reducing severely the water supply available for different purposes to both wildlife and humans (Wetzel 2001).

Many lakes exhibit thermal stratification for a substantial portion of the year, developing marked vertical gradients in physical and chemical properties (Boehrer and Schultze 2008). These

gradients influence biogeochemical processes such as the cycling of organic and inorganic matter (Coloso et al. 2008; Van de Bogert et al. 2012) and alter the patterns of metabolism and energy flow through the food web (Wilkinson et al. 2015). Fluxes between layers are limited, but can be facilitated by episodic deepening of the mixed layer (Imberger 1985), penetrative convection (Jonas et al. 2003) and upwelling or internal wave breaking (Wüest et al. 1996, Boegman et al. 2005, Staehr et al. 2012). In contrast, during winter, mixing of the water column prevails, with nutrients and other dissolved compounds being transported from the deeper to the upper layers and vice versa, resulting in the homogeneous distribution of substances and organisms through the water column and the fueling important biogeochemical reactions (Lawson and Anderson 2007; Deemer et al. 2015)

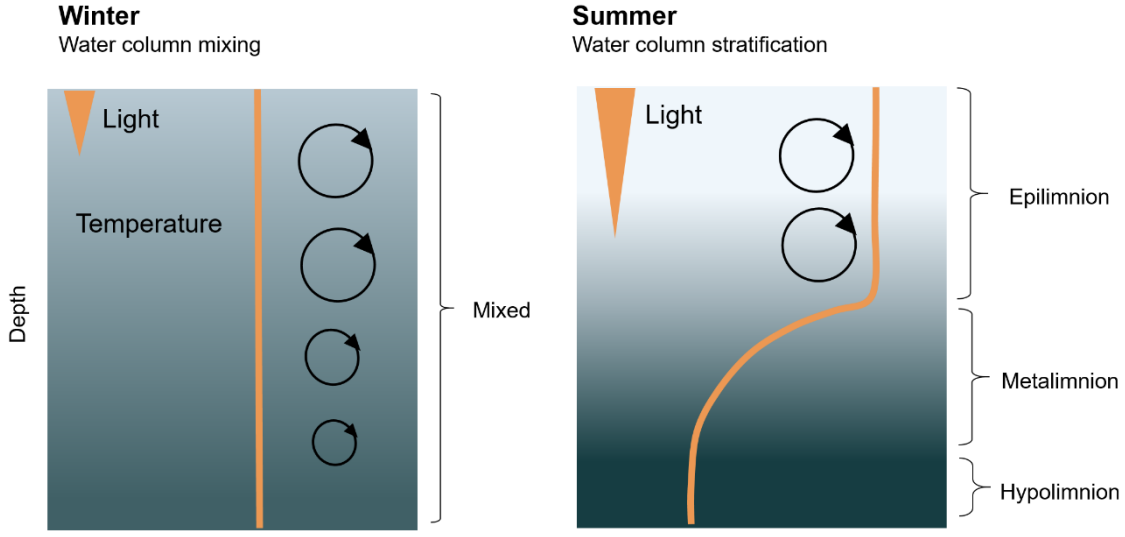

Fig.6: Idealized *cross section view* through the water column of a temperate lake or reservoir during the winter and summer seasons. During the winter season, the homogeneous vertical profile of temperature favours mixing, whereas during the summer, the water column is well stratified in different layers due to the higher difference in temperatures and therefore density.

In general, thermally driven changes and nutrient fluxes through the water column are well understood in freshwater systems. However, little is known about how thermal changes in the water column affect microbial interactions and biogeochemistry in lakes with a complex chemistry, such as those affected by acid mine drainage (AMD). AMD represents one of the main environmental problems associated with the exploitation of sulfide minerals, and can pose serious ecological and public health problems since it can affect aquatic systems in numerous ways (Azapagic 2004). In these systems, biological niches are shaped by certain environmental conditions, such as concentrations of dissolved metals and other solutes, being low pH the most important (Méndez-García et al. 2015).

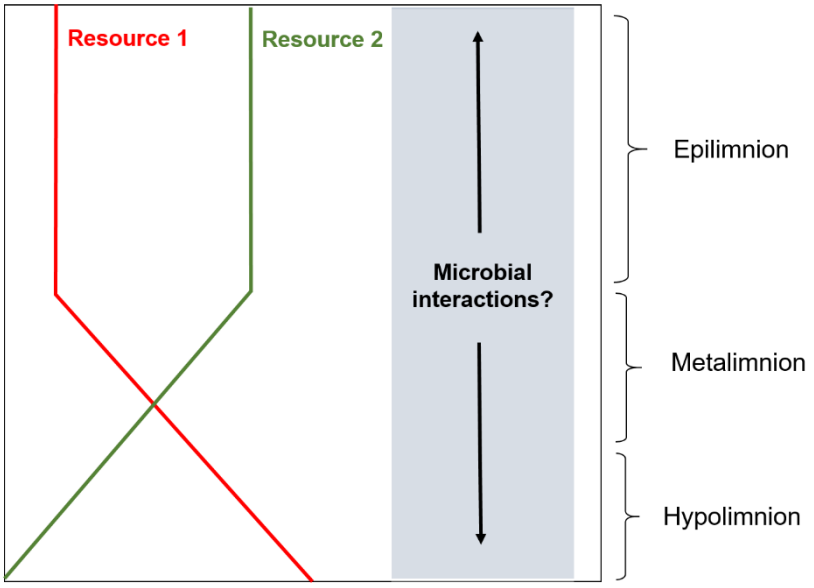

Fig.7: Idealized *cross-section of a lake* or reservoir showing the strong vertical gradients of the environmental variables during stratification. The shaded area represents the unknown vertical zonation of the possible microbial communities and their interactions.

The effects of AMD on the community structure at an ecological level are related to the reduction of biodiversity and the simplification of the food chain, thus significantly reducing the stability and resilience of these aquatic ecosystems (Gray 1997; Levings et al. 2004). The seasonal changes of the acidophilic community in AMD polluted environments and their ecological drivers are poorly understood (Edwards et al., 1999, Tan et al., 2009; Volant et al., 2012). Spatiotemporal studies combining a detailed description of the community at several levels, the relationship between the different functional components of the community and the biogeochemical environment are essential, since they provide a comprehensive insights into the ability and dynamics of acidophilic microorganisms to thrive in extreme acidic environments.

2. References

Ackerly, D.D. 2003. Community assembly, niche conservatism, and adaptive evolution in changing environments. Int. J. Plant. Sci. **164**: S165–S184

Alongi, D. M. 2002. Present State and Future of the World ' s Mangrove Forests Present state and future of the world ' s mangrove forests.doi:10.1017/S0376892902000231

Attrill, M. J., and S. D. Rundle. 2002. Ecotone or Ecocline : Ecological Boundaries in Estuaries. 929–936. doi:10.1006/ecss.2002.1036

Austin, M. P. 1985. Continuum concept, Ordination Methods, and Niche Theory. Ann. Rev. Ecol. Syst. **16**: 39–61.

Azam, F., T. Fenchel, J. G. Field, J. S. Gray, L. A. Meyer-Reil, and F. Thingstad. 1983. The Ecological Role of Water-Column Microbes in the Sea *. **10**: 257–263.

Azam, F., and J. S. Graf. 1983. The Ecological Role of Water-Column Microbes in the Sea *. **10**: 257–263.

Azam, F., and F. Malfatti. 2007. Microbial structuring of marine ecosystems. Nat Rev Micro **5**: 782-791. Nat. Rev. Microbiol. **5**: 782–791. doi:10.1038/nrmicro1747

Azam, F., and A. Z. Worden. 2004. Microbes, molecules, and marine ecosystems. Science (80-.). **303**: 1622–1624.

Azapagic, A. 2004. Developing a framework for sustainable development indicators for the mining and minerals industry. J. Clean. Prod. **12**: 639–662. doi:10.1016/S0959-6526(03)00075-1

Barbier, E. B., S. D. Hacker, C. Kennedy, E. W. Koch, C. Stier, and B. R. Silliman. 2011. The value of estuarine and coastal ecosystem services. **81**: 169–193.

Blaber, S. J. M. 2013. Fishes and fisheries in tropical estuaries: The last 10 years. Estuar. Coast. Shelf Sci. **135**: 57–65. doi:10.1016/j.ecss.2012.11.002

Boehrer, B., and M. Schultze. 2008. Stratification of lakes. Rev. Geophys. **46**: 1–27. doi:10.1029/2006RG000210

Van de Bogert, M. C., D. L. Bade, S. R. Carpenter, J. J. Cole, M. L. Pace, P. C. Hanson, and O. C. Langman. 2012. Spatial heterogeneity strongly affects estimates of ecosystem metabolism in two north temperate lakes. Limnol. Oceanogr. **57**: 1689–1700. doi:10.4319/lo.2012.57.6.1689

Bouvier, T. C., and P. A. del Giorgio. 2002. Compositional changes in free-living bacterial communities along a salinity gradient in two temperate estuaries. **47**: 453–470.

Ter Braak, C. J., and I. C. Prentice. 1988. A Theory of Gradient Analysis, p. 271–317. *In* Advances in Ecological Research.

Burford, M. A., D. M. Alongi, A. D. McKinnon, and L. A. Trott. 2008. Primary production and nutrients in a tropical macrotidal estuary, Darwin Harbour, Australia. Estuar. Coast. Shelf Sci. **79**: 440–448. doi:10.1016/j.ecss.2008.04.018

Burford, M. A., I. T. Webster, A. T. Revill, R. A. Kenyon, M. Whittle, and G. Curwen. 2012. Estuarine , Coastal and Shelf Science Controls on phytoplankton productivity in a wet e dry tropical estuary. Estuar. Coast. Shelf Sci. **113**: 141–151. doi:10.1016/j.ecss.2012.07.017

Boegman, L., G. N. Ivey, and J. Imberger. 2005. The energetics of large-scale internal wave degeneration in lakes. J. Fluid Mech. **531**: 159–180, doi:10.1017/S0022112005003915

Carpenter, S. R., E. H. Stanley, and M. J. Vander Zanden. 2011. State of the World's Freshwater Ecosystems: Physical, Chemical, and Biological Changes. Ssrn. doi:10.1146/annurev-environ-021810-094524

Cavicchioli, R., L. R. Bakken, M. Baylis, and others. 2019. Scientists's warning to humanity: microoganims and climate change. Nat. Rev. Microbiol. **17**. doi:10.1038/s41579-019-0222-5

Charpy-Roubaud, C., and A. Sournia. 1990. The comparative estimation of phytoplanktonic and microphytobenthic production in the oceans. Mar. Microb. Food Webs **4**: 31–57.

Cloern, J. E., P. C. Abreu, J. Carstensen, and others. 2016. Human activities and climate variability drive fast-paced change across the world's estuarine-coastal ecosystems. Glob. Chang. Biol. **22**: 513–529. doi:10.1111/gcb.13059

Cloern, J. E., S. Q. Foster, and A. E. Kleckner. 2014. Phytoplankton primary production in the world ' s estuarine-coastal ecosystems. 2477–2501. doi:10.5194/bg-11-2477-2014

Cole, J. J., and J. J. Cole. 1982. Interactions between bacteria and algae in aquatic ecosystems. Ann. Rev. Ecol. Syst. **13**: 291–314.

Coloso, J. J., J. J. Cole, P. C. Hanson, and M. L. Pace. 2008. Depth-integrated, continuous estimates of metabolism in a clear-water lake. Can. J. Fish. Aquat. Sci. **65**: 712–722. doi:10.1139/F08-006

Costanza, R., R. D'Arge, R. de Groot, and others. 1998. The value of the world's ecosystem services and natural capital. Nature **387**: 253–260. doi:10.1038/387253a0

Cotner, J. B., and B. A. Biddanda. 2002. Small Players , Large Role : Microbial Influence on Biogeochemical Processes in Pelagic Aquatic Ecosystems. Ecosystems **5**: 105–121. doi:10.1007/s10021-001-0059-3

Cushman, S. A., K. Gutzweiler, J. S. Evans, and K. Mcgarigal. 2010. The Gradient Paradigm : A Conceptual and Analytical Framework for Landscape Ecology. 83–108. doi:10.1007/978-4-431-87771-4

Deemer, B. R., S. M. Henderson, and J. A. Harrison. 2015. Chemical mixing in the bottom boundary layer of a eutrophic reservoir: The effects of internal seiching on nitrogen dynamics. Limnol. Oceanogr. **60**: 1642–1655. doi:10.1002/lno.10125

Delong, E. F., E. F. Delong, C. M. Preston, and others. 2007. No Title. **496**. doi:10.1126/science.1120250

Ducklow, H. W. 1983. Production and Fate of Bacteria in the Oceans. Bioscience **33**: 494–501. doi:10.2307/1309138

Edwards,K.J., P.L., Bond, T.M. Gihring, and J.F Banfield. 2000. An archaeal iron-oxidizing extremeacidophile important in acid mine drainage. Science **287**:1796–1799.doi:10.1126/science.287.5459.1796

Eyre, B. 2000. Regional evaluation of nutrient transformation and phytoplankton growth in nine river-dominated sub-tropical east Australian estuaries. Mar. Ecol. Prog. Ser. **205**: 61–83.

Eyre, B., and P. Balls. 1999. A Comparative Study of Nutrient Behavior along the Salinity Gradient of Tropical A Comparative Study of Nutrient Behavior along the Salinity Gradient of Tropical and Temperate Estuaries. Estuaries 313–326. doi:10.2307/1352987

Field, C. B., M. J. Behrenfeld, J. T. Randerson, and P. Falkowski. 1998. Primary Production of the Biosphere: Integrating Terrestrial and Oceanic Components. Science. **281**: 237–240. doi:10.1126/science.281.5374.237

Fuhrman, J. A. 1992. Bacterioplankton roles in cycling of organic matter: The microbial food web, *In* Primary productivity and Biogeochemical Cycles in the Sea.

Fuhrman, J. A. 2009. Microbial community structure and its functional implications. Nature **459**: 193–199. doi:10.1038/nature08058

Gaston, K. J. 2000. Global patterns in biodiversity. Nature **405**. doi:10.1038/35012228

del Giorgio, P. A., and T. C. Bouvier. 2002. Linking the physiologic and phylogenetic successions in free-living bacterial communities along an estuarine salinity gradient. Limnol. Oceanogr. **47**: 471–486. doi:10.4319/lo.2002.47.2.0471

del Giorgio, P. A., and J. J. Cole. 1998. Bacterial growth efficiency in Natural Aquatic systems. Annu. Rev. Ecol. Syst. **29**: 503–541.

Gosz, J. R. 1992. Gradient Analysis of Ecological Change in Time and Space : Implications for Forest Management. Ecol. Appl. **2**: 248–261.

Gray, N. 1997. Environmental impact and remediation of acid mine drainage: A management problem. Environ. Geol. **30**: 62–71.

Green, J., and B. J. M. Bohannan. 2006. Spatial scaling of microbial biodiversity. Trends Ecol. Evol. **21**: 501–507. doi:10.1016/j.tree.2006.06.012

Hutchinson, G. E. 1957. Concluding remarks. In: Cold Spring Harbour Symposium on Quantitative Biology, 22:415-427

Imberger, J. 1985. The diurnal mixed layer. Limnol. Oceanogr. **30**: 737–770. doi:10.4319/lo.1985.30.4.0737

Jonas, T., A. W.E., Stips, and A.Wüest. 2003. Observations of a quasi shear-free lacustrine convective boundary layer: Stratification and its implications on turbulence. J. Geophys. Res. Oceans 108: 33128, doi:10.1029/2002JC001440

Konopka, A. 2009. What is microbial community ecology ? 1223–1230. doi:10.1038/ismej.2009.88

Lawson, R., and M. A. Anderson. 2007. Stratification and mixing in Lake Elsinore, California: An assessment of axial flow pumps for improving water quality in a shallow eutrophic lake. Water Res. **41**: 4457–4467. doi:10.1016/j.watres.2007.06.004

Levings, C. D., K. L. Barry, J. A. Grout, G. E. Piercey, A. D. Marsden, A. P. Coombs, and B. Mossop. 2004. Effects of acid mine drainage on the estuarine food web, Britannia Beach, Howe Sound, British Columbia, Canada. Hydrobiologia **525**: 185–202. doi:10.1023/B:HYDR.0000038866.20304.3d

Lewis, W. M. 2009. The Ecological Niche in Aquatic Ecosystems.

Li, J., X. Jiang, Z. Jing, and others. 2017. Spatial and seasonal distributions of bacterioplankton in the Pearl River Estuary: The combined effects of riverine inputs, temperature, and phytoplankton. Mar. Pollut. Bull. **125**: 199–207. doi:10.1016/j.marpolbul.2017.08.026

Litchman, E.2007. Resource competition and the ecological success ofphytoplankton, inEvolution of Primary Producers in the Sea,editedby P. G. Falkowski and A. H. Knoll, pp. 351–375, Elsevier, Amsterdam,doi:10.1016/B978-012370518-1/50017-5

Litchman, E., and C. A. Klausmeier. 2008. Trait-Based Community Ecology of Phytoplankton. 615–639. doi:10.1146/annurev.ecolsys.39.110707.173549

Litchman, E., C. A. Klausmeier, J. R. Miller, O. M. Schofield, and P. G. Falkowski. 2006. Multi-nutrient, multi-group model of present and future oceanic phytoplankton communities. Biogeosciences **3**: 585–606. doi:10.5194/bg-3-585-2006

Margalef, R. 1978. Life-forms of phytoplankton as survival alternatives in an unstable environment.

Margalef, R. 1992. Selforganization and response to disturbance, a key time/space patterns in ecosystems. Proceed. 1st Intern. Symp. on Conceptual tools for understanding

Nature: 91-99.

Mcgill, B. J., B. J. Enquist, E. Weiher, and M. Westoby. 2006. Rebuilding community ecology from functional traits. **21**. doi:10.1016/j.tree.2006.02.002

Mclusky, D. S. 1993. Marine and estuarine gradietns - An Overview. Netherlands J. Aquat. Ecol. **27**: 489–493.

Méndez-García, C., A. I. Peláez, V. Mesa, J. Sánchez, O. V. Golyshina, and M. Ferrer. 2015. Microbial diversity and metabolic networks in acid mine drainage habitats. Front. Microbiol. **6**: 1–17. doi:10.3389/fmicb.2015.00475

Mitchell, J. G., H. Yamazaki, L. Seuront, F. Wolk, and H. Li. 2008. Phytoplankton patch patterns : Seascape anatomy in a turbulent ocean. J. Mar. Syst. **69**: 247–253. doi:10.1016/j.jmarsys.2006.01.019

Muylaert, K., K. Sabbe, and W. Vyverman. 2009. Changes in phytoplankton diversity and community composition along the salinity gradient of the Schelde estuary (Belgium/The Netherlands). Estuar. Coast. Shelf Sci. **82**: 335–340. doi:https://doi.org/10.1016/j.ecss.2009.01.024

Nittrouer, C. A., G. J. Brunskill, and A. G. Figueiredo. 1995. Importance of tropical coastal environments. Geo-Marine Lett. **15**: 121–126. doi:10.1007/BF01204452

O'Donohue, M. J. H., and W. C. Dennison. 1997. Phytoplankton Productivity Response to Nutrient Concentrations, Light Availability and Temperature Along an Australian Estuarine Gradient. **20**: 521–533.

Peterson, D. L., E. G. Schreiner, and N. M. Buckingham. 1997. Gradients, vegetation and climate: Spatial and temporal dynamics in the Olympic Mountains, U.S.A. Glob. Ecol. Biogeogr. Lett. **6**: 7–17. doi:10.2307/2997523

Prosser, J. I., B. J. M. Bohannan, T. P. Curtis, and others. 2007. The role of ecological theory in microbial ecology. **5**: 384–392.

Le Quere, C., S. P. Harrison, I. Colin Prentice, and others. 2005. Ecosystem dynamics based on plankton functional types for global ocean biogeochemistry models\rdoi:10.1111/j.1365-2486.2005.1004.x. Glob. Chang. Biol. **11**: 2016–2040. doi:10.1111/j.1365-2486.2005.01004.x

Quinlan, E. L., and E. J. Phlips. 2007. Phytoplankton assemblages across the marine to low-salinity transition zone in a blackwater dominated estuary. J. Plankton Res. **29**: 401–416. doi:10.1093/plankt/fbm024

Reynolds, C. S. 2006. The ecology of phytoplankton, Cambridge University Press.

Schweiger, A. H., S. D. H. Irl, M. J. Steinbauer, and C. Beierkuhnlein. 2016. Optimizing sampling approaches along ecological gradients. 463–471. doi:10.1111/2041-210X.12495

Serreze, M.C., J.E.Walsh, F.S. Chapin III,T. Osterkamp, M. Dyurgerov, V. Romanovsky,W.C. Oechel, J. Morison,T. Zhang and R.G. Barry, 2000. Observational evidence of recent change in the northern high latitude environment. Climatic Change, 46:159–207

Sherr, E. B., and B. F. Sherr. 1988. Role of Microbes in Pelagic Food Webs: A Cevised Concept. Limnol. Oceanogr. **33**: 1225–1227.

Smith, S. V. 1981. Macrophytes as a Global Carbon Sink. Science (80-.). **211**: 838–840.

Staehr, P. A., J. P. A. Christensen, R. D. Batt, and J. S. Read. 2012. Ecosystem metabolism in a stratified lake. Limnol. Oceanogr. **57**: 1317–1330. doi:10.4319/lo.2012.57.5.1317

Tan,G.L., W.S. Shu, W.H. Zhou, X.L. Li, C.Y. Lan, and L.N. Huang. 2009. Seasonal and spatial variations in microbial community structure and diversity in the acid stream draining across an ongoing surface mining site. FEMS Microbiol.Ecol. **70**:121–129.doi:10.1111/j.1574-6941.2009.00744.x

Thingstad, T. F., R. G. J. Bellerby, G. Bratbak, K. Y. Børsheim, J. K. Egge, M. Heldal, A. Larsen, and C. Neill. 2008. Counterintuitive carbon-to-nutrient coupling in an Arctic pelagic ecosystem. **455**. doi:10.1038/nature07235

Thingstad, T. F., L. Øvreås, J. K. Egge, T. Løvdal, and M. Heldal. 2005. Use of non-limiting substrates to increase size; a generic strategy to simultaneously optimize uptake and minimize predation in pelagic osmotrophs? Ecol. Lett. **8**: 675–682. doi:10.1111/j.1461-0248.2005.00768.x

Turner, M. G. 1989. Landscape Ecology: The Effect of Pattern on Process. Annu. Rev. Ecol. Syst. **20**: 171–197. doi:10.1146/annurev.es.20.110189.001131

Tylianakis, J. M., and R. J. Morris. 2017. Ecological Networks Across Environmental Gradients.

Urban, D.L., R.V. O'Neill, and H.H. Shugart Jr. 1987. Landscape Ecology. A Hierarquical Perspective Can Help Scientists Understand Spatial Patterns. Bioscience, 37, 119-127.doi.org/10.2307/1310366

Volant, A., A. Desoeuvre ,C. Casiot, B. Lauga, S. Delpoux, G. Morin. and others. 2012. Archaeal diversity:temporal variation in the arsenic-rich creek sediments of Carnoules Mine,France. Extremophiles **16**:645–657.doi:10.1007/s00792-012-0466-8

Wetzel, R. G. 1992. Clean water: a fading resource. Hydrobiologia **243**–**244**: 21–30. doi:10.1007/BF00007017

Wetzel, R. G. 2001. Limnology: Lake and River Ecosystems, Elsevier Science.

Whitman, W. B., D. C. Coleman, and W. J. Wiebe. 1998. Perspective Prokaryotes : The unseen majority. **95**: 6578–6583.

Whittaker, R. H. 1967. Gradient Analysis of Vegetation. Biol. Rev. **42**: 207–264.

Wilkinson, G. M., J. J. Cole, M. L. Pace, R. A. Johnson, and M. J. Kleinhans. 2015. Physical and biological contributions to metalimnetic oxygen maxima in lakes. Limnol. Oceanogr. **60**: 242–251. doi:10.1002/lno.10022

Wüest A, D.C. Van Senden, J. Imberger, G. Piepke, and M. Gloor. 1996. Comparison of diapycnal diffusivity measured by tracer and microstructure techniques. Dyn. Atmos. Oceans **24**:27–39

Xenopoulos, M. A., J. A. Downing, S. Menden-deuer, M. Voss, and M. D. Kumar. 2017. Headwaters to oceans : Ecological and biogeochemical contrasts across the aquatic continuum. Limnol. Oceanogr. **62**: S3-S14. doi:10.1002/lno.10721

3. OBJECTIVES

The main objective of the present PhD thesis is to evaluate the microbial interactions in the pelagic system along two distinct environmental gradients; an intense estuarine horizontal gradient and a vertical gradient in a stratified acid reservoir. Major emphasis was put in describing the ecological characteristics of autotrophic and heterotrophic microbial communities, and quantifying the phytoplankton primary production and net metabolism of the plankton community. This main objective can be divided into 5 specific objectives:

1. Quantify the primary production, total net metabolism and the relative contribution to net metabolism of the different sized fractions of the plankton, i.e. pico-, nano- and microplankton in the water column along the inner part of the Gulf of Nicoya (Costa Rica) and determine biogeochemical factors and processes which control the phytoplankton size distribution and primary production. (Chapter II).

2. Characterize the microbial groups (phytoplankton and bacterioplankton) in terms of the abundance and single cells-traits and determine the possible spatiotemporal interactions among them along inner part of the Gulf of Nicoya (Costa Rica) (Chapter III).

3. Quantify the phytoplanktonic primary production and the net metabolism of the plankton community in the water column of El Sancho reservoir (Huelva, Spain), paying special attention to the deep chlorophyll maximum (DCM), which develops during the stratification in response to the contrasting gradients of irradiance and nutrients (nitrogen and inorganic carbon) (Chapter IV).

4. Determine through a 1D biogeochemical model whether the inorganic carbon production in the hypolimnion by bacterial respiration can support the carbon photosynthetic demand at the DCM and therefore its formation (Chapter IV).

5. Characterize the bacterioplankton community in terms of abundances, single-cell traits and taxonomic composition in the water column in El Sancho reservoir (Huelva, Spain) during stratification and mixing, determine how these different aspects of the bacterioplankton community covariates and if they are affected by the same environmental changes (Chapter V).

CHAPTER II

Size fractionated phytoplankton biomass and net metabolism along a tropical estuarine gradient

Size fractionated phytoplankton biomass and net metabolism along a tropical estuarine gradient

Sara Soria-Píriz [1*], Emilio García-Robledo[1,a], Sokratis Papaspyrou [1,b], Virginia Aguilar [1], Isabel Seguro[1,c], Jenaro Acuña, [2,4], Álvaro Morales [2,3], Alfonso Corzo[1]

[1]Departamento de Biología, Universidad de Cádiz, Polígono Rio San Pedro s/n, 11510 Puerto Real, Spain
[2]Centro de Investigación en Ciencias del Mar y Limnología (CIMAR), P.O. Box 2060 San Pedro de Montes de Oca, Costa Rica.
[3]Escuela de Biología, Universidad de Costa Rica. P.O. Box 2060 San Pedro de Montes de Oca, Costa Rica
[4]Escuela de Química, Universidad de Costa Rica. P.O. Box 2060 San Pedro de Montes de Oca, Costa Rica

Present address:
[a]Microbiology Section, Department of Biosciences. Aarhus University. Ny Munkegade 116, DK-8000, Aarhus, Denmark
[b]Laboratorio de Microbiología y Genética, Departamento de Biomedicina, Biotecnología y Salud Pública, Facultad de Ciencias, Universidad de Cádiz,11510 Puerto Real, Spain.
[c]Centre for Ocean and Atmospheric Sciences, School of Environmental Sciences, University of East Anglia, Norwich, NR4 7TJ, United Kingdom

ABSTRACT: Size structure of phytoplankton determines to a large degree the trophic interactions in oceanic and coastal waters and eventually the destiny of its biomass. Although, tropical estuarine systems are some of the most productive systems worldwide compared to temperate systems, little is known about phytoplankton biomass size fractions, their contribution to net metabolism, or the ecological factors driving phytoplankton size distribution in tropical estuaries. Hence, we measured the size-fractionated biomass and net metabolism of the plankton community along a salinity and nutrient gradient in the Gulf of Nicoya estuary (Costa Rica), during the dry season. Respiration (23.6 mmol O_2 m^{-3} h^{-1}) was highest at the estuary head, whereas maximum net primary production (23.1 mmol O_2 m^{-3} h^{-1}) was observed in the middle of the estuary, coinciding with the chlorophyll a maximum (15.9 mg m^{-3}). Thus, only the middle section of the estuary was net autotrophic (2.9 g C m^{-2} d^{-1}), with the rest of the estuary being net heterotrophic. Regression analysis identified light availability, and not nutrients, as the principal factor limiting primary production in the estuary due to increased turbidity. The changes in net metabolism along the estuary were also reflected in the phytoplankton's size structure. Although micro- and picophytoplankton were the most productive fractions overall, in the middle section of the estuary nanophytoplankton dominated primary production, chlorophyll, and autotrophic biomass.

KEYWORDS: primary production, tropical estuary, phytoplankton community, size fractionation, estuarine gradient

Published in *Limnology and Oceanography* (2017) doi: 10.1002/lno.10562

1. Introduction

Estuaries are transitional systems providing important ecosystem services such as fisheries maintenance, nutrient cycling, water supply and purification, and recreation (Costanza et al. 1997; Barbier et al. 2011). However, estuaries are under serious threat worldwide due to anthropogenic activities, such as pollution, deforestation, and urbanization. These activities affect ecological and biogeochemical processes in estuaries, altering the structure of the estuarine food webs from phytoplanktonic primary producers to macroorganisms, including shellfish and fish species of economic interest (Bianchi 2007; Burford et al. 2008; Blaber 2013). Tropical estuaries are being particularly affected as they are often located in developing or recently industrialized countries, with usually high population growth rates (Alongi 2002; Barbier et al. 2011).

Approximately 50 % of total production in estuaries is due to pelagic primary producers (Meyercordt et al. 1999; Underwood and Kromkamp 1999) which span a wide range of size classes across several taxonomic groups i.e. cyanobacteria, diatoms, dinoflagellates, and chlorophytes (Devassy and Goes 1988; Sin et al. 2000; Huang et al. 2004). The abundance and relative contribution of each size class and taxonomic group, and consequently their contribution to planktonic primary production, are affected by changes in the abiotic and biotic environmental factors (e.g. light limitation, mixing, shelf water intrusions) (Lancelot and Muylaert 2011). In addition, the relative contribution of the different phytoplankton size classes to total planktonic community influence the functioning of the ecosystem due to the effects of cell size on growth rates, trophic interactions, and sinking and resuspension rates (Malone 1980; Goldman 1988; De Madariaga et al. 1989; Cermeño et al. 2006).

Primary production rates in tropical estuaries are typically much higher than in temperate ones (Nittrouer et al. 1995; Cloern et al. 2014). These high production rates are due to a comparatively higher nutrient availability, irradiance, and temperature year-round (Nittrouer et al. 1995). Nonetheless, increased turbidity due to high inputs of suspended solids from rivers and sediment resuspension has been shown to limit primary production in many tropical estuaries (Cloern 1987; Fichez et al. 1992; Nittrouer et al. 1995; Burford et al. 2008). Despite the high phytoplankton productivity in tropical estuaries, many important aspects of phytoplankton ecology have been poorly studied compared with temperate ones (Bianchi 2007; Burford et al. 2008; Rochelle-Newall et al. 2011; Cloern et al. 2014). Only in a few cases is there information available on phytoplankton biomass size classes in tropical or subtropical estuaries (Sin et al. 2000; Li et al. 2013; Zhang et al. 2013). As far as we know, no information exists on the contribution of these size classes to primary production and net metabolism. This lack of information might limit our ability to 1) understand and model the trophic interactions and C and N biogeochemical cycling in these highly productive and valuable ecosystems, thus impacting negatively their scientific-based management, and 2) to evaluate quantitatively the contribution of subtropical and tropical estuaries to global biogeochemical cycles (Cloern et al. 2014).

The Gulf of Nicoya is one of the most productive estuaries in the world (Gocke et al. 1990; Córdoba-Muñoz 1998; Gocke et al. 2001a and 2001b; Cloern et al. 2014) and represents a model system for the estuaries of Central America. This gulf is a tropical estuary of about 80 km length from the Tempisque River down to the Pacific Ocean, clearly divided into an inner and outer basin with strong differences in bathymetry and hydrographic conditions (Peterson 1958; Voorhis et al. 1983). Tempisque River freshwater discharges to the inner basin are high and with a clear seasonality. Nine-year period averages show discharges up to 390 $m^3 s^{-1}$ during the rainy (May – November) and 162 $m^3 s^{-1}$ during the dry seasons (December – April) (Kress et al. 2002). The seasonal changes in river discharges largely

control hydrodynamic characteristics of the inner basin of the Gulf of Nicoya, resulting in the estuary being partially stratified during the rainy season and fully mixed during the dry season (Kress et al. 2002; Palter et al. 2007; Seguro et al. 2015).

The few existing studies on phytoplankton in the Gulf of Nicoya, dealing mainly with large nanophytoplankton and microphytoplankton, showed a dominance of diatoms and dinoflagellates in these size classes, and the existence of clear changes in the abundance of microphytoplankton along the riverine-marine gradient in the estuary (Hargraves and Víquez, 1985; Brugnoli-Olivera and Morales-Ramírez 2001 and 2008; Seguro et al. 2015). The importance of the different size fractions, pico-, nano-, and microphytoplankton for the standing stocks of phytoplankton and their relative contribution to total primary production and net metabolism in the water column were investigated along the riverine-marine gradient in the estuary of the Gulf of Nicoya. In addition, the environmental factors which are likely controlling primary production and phytoplankton size distribution in the inner part of the Gulf of Nicoya were measured in order to explain the changes in total and size fractionated community net metabolism and autotrophic biomass along the gradient in the environmental conditions along this tropical estuary.

2. Materials and Methods

2.1. Study site and sampling

The inner part of the Gulf of Nicoya extends from the Tempisque River mouth down to near the Puntarenas channel (Fig. 1). It is a shallow area (< 20 m) with extensive tidal flats surrounded mainly by mangroves. Tides are semidiurnal with mean amplitude of 2.5 m (MIO-CIMAR 2012).

Five stations, one station per day, were sampled along the inner Gulf of Nicoya during the dry-season in 2012 (14th - 18th April). The innermost station was located near the Amistad Bridge, close to the Tempisque River mouth (Station, St., 1) and the most marine station (Station 5) close to the Caballo Island (Fig.1). Water column temperature (ºC) and salinity profiles (psu) were measured using a multiparameter probe (YSI 6600). Photosynthetically active irradiance profiles (PAR) were measured using a radiometer (LiCor 250A with a spherical sensor). Based on the registered light profiles and depending on the station's maximum water depth, 3 to 4 depths were selected within the 1 to 100 % range of incident irradiance plus an additional depth, 1 m from the bottom. Water from each depth was collected using a 10 L Niskin bottle and was used for the determination of chlorophyll *a* concentration (Chl *a*), total suspended material (TSS), particulate organic carbon content (POC), inorganic nutrients and for in situ incubations to measure net production and respiration rates of the whole community. While onboard, all samples were stored on ice and darkness until further analysis in the laboratory. In addition, 30 L of surface water were carried each day to the laboratory in Estación Nacional de Ciencias Marino-Costeras (ECMAR, Universidad Nacional de Costa Rica) for fractionation trough successive filtration and incubations as described below.

2.2. Chlorophyll, total suspended material, and organic matter

Five water samples (110 – 550 mL) (which $n = 3$ per Chl *a*, $n = 2$ per TSS and $n = 1$ per POC) from each depth and station were filtered through pre-combusted Whatman GF/F glass fiber (0.7 μm nominal pore size) filters. For the determination of Chl *a*, filters were placed in individual tubes with 4

mL of methanol at 4 °C for 12 hours. Tubes were then centrifuged (3000 rpm, 5 min) and the absorbance of the extract were measured on a UNICAM UV/Vis spectrometer. Chl *a* concentration was calculated according to Ritchie (2008). Filters for TSS determination were dried at 60 °C for 24 h and weighed. POC content was determined as the difference between total particulate carbon measured in non-combustioned filters and particulate inorganic carbon measured on a second replicate filter after combustion at 450 ºC. Both filters were analysed on an elemental analyzer (LECO CHNS 932).

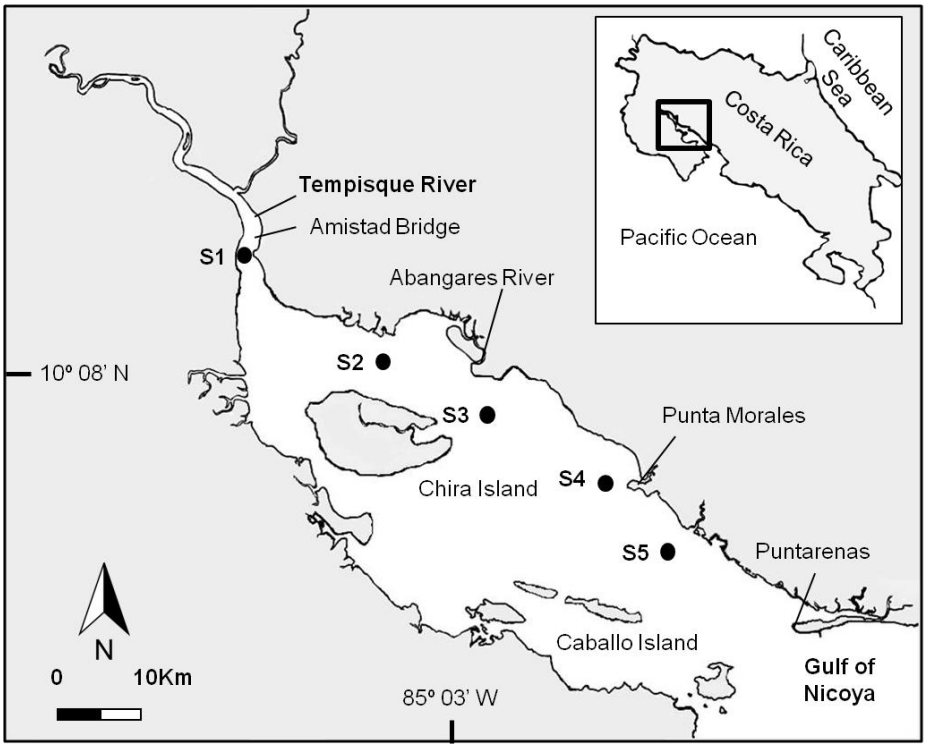

Fig.1: The inner basin of the Gulf of Nicoya. Map of the study area and the sampling stations.

2.3. Inorganic nutrients

Samples for inorganic nutrients (n = 3 per depth) were filtered through a glass fiber 0.7 μm filter (Fisherbrand®) in polyethylene vials and stored in darkness at -20º C until analysed manually. Ammonium (NH_4^+) was determined according to Bower and Holm-Hansen (1980), phosphate (PO_4^{3-}) and silicate (SiO_4^{4-}) according to Grasshoff et al. (1999) and nitrate (NO_3^-) and nitrite (NO_2^-) according to García-Robledo et al. (2014). Spectrophotometric measurements were done using an UV 1700 Pharmaspec Shimadzu spectrophotometer.

Salinity has been used as a conservative tracer, i.e. a tracer no affected by biological activity, to calculate the theoretical spatial distribution of a given nutrient along the estuary (Boyle et al. 1974; Fisher et al. 1988). This approach assumes that mixing of freshwater and marine water in different proportions along the estuarine gradient is the only cause of change in the concentration of nutrients, same as it occurs for salinity. When the spatial distribution of a given nutrient along the estuary is equal to that expected from simple mixing, the nutrient behaves conservatively like salinity, and therefore

there is not apparent consumption or production of this nutrient along the estuary. Correspondingly, the non-conservative distribution of a given nutrient is interpreted as evidence of biological consumption when measured concentrations are lower than those expected from conservative mixing. In contrast, when the measured concentrations are higher than the ones expected by mixing, either the nutrient is net produced within the estuary or an additional nutrient source exists. Nutrient concentrations for each end member, riverine fresh water and marine water, were calculated from the regression lines between nutrients and salinity (Table 1). This information was used to calculate the theoretical concentration of every nutrient, assuming a conservative behavior identical to salinity, as a result of the mixing of both end members for a given salinity according to following equations:

$$S_i = V_i^R S^R + V_i^M S^M \quad (1)$$
$$V_i^R + V_i^M = 1 \quad (2)$$
$$V_i^M = (Si - (V_i^R S^R))/S^M \quad (3)$$
$$V_i^R = 1 - V_i^M \quad (4)$$
$$C_i = V_i^R C^R + V_i^M C^M \quad (5)$$

Where, S_i was the salinity at a given *i* position in the estuary, $V^R{}_i$ and $V^M{}_i$ are the volume fractions of the river and marine end members respectively in a liter of water of a given salinity S_i. C_i is the concentration of any given compound at the *i* position resulting from mixing alone, which can be calculated from the concentration in the river and marine end members, C^R and C^M respectively, and the corresponding volume fractions assuming conservative behavior (Yin et al. 1995).

2.4. In situ measurements of planktonic net production and respiration

Water from the selected depths was used to fill three transparent and three dark Winkler bottles and were closed and incubated in situ at the corresponding depth for 1.5 - 3 hours. Short incubation times were chosen to avoid any bottle effect given 1) the high productivity in the gulf (Córdoba-Muñoz 1998; Gocke 2001a and b) and 2) our preliminary tests before the sampling cruises where we obtained a significant change (consumption or production) in the oxygen (O_2) concentration in incubation bottles with water samples from the gulf measured continuously with O_2 microsensors. Samples for the measurement of initial (n = 3 per depth) and final (n = 2 per Winkler bottle) O_2 concentrations were taken in 12 mL Exetainer tubes (Labco, UK) and fixed with the Winkler reagents on board. O_2 samples were analyzed according to Labasque et al. (2004) on a SHIMADZU PharmaSpec/UV-1700/UV-VISIBLE spectrophotometer. The volumetric dark respiration rate (R) was measured as the O_2 consumption in the dark bottles and the volumetric net primary production rate (Pn) from the O_2 changes (positive or negative) in the transparent bottles (Gaarder and Gran 1927). Daily depth integrated of net plankton community production (P_n^d), gross production (P_g^d) and respiration (R^d) rates for the photic layer were calculated from the integrated volumetric rates according to the following equations:

$$P_g^d = P_n^d + R^d \quad (6)$$
$$P_n^d = (\alpha Pn) - (\beta R) \quad (7)$$
$$R^d = (\alpha + \beta)R = 24R \quad (8)$$

The terms α and β represent the local daily light and dark periods in hours at the sampling dates (12.35 and 11.65 h, respectively).

2.5. Size fractionated metabolism, chlorophyll, and organic matter

Size fractionation was carried out by two consecutive filtrations through 20 and 2 μm nylon filters (47 mm diameter, Millipore®) using only surface water (0.5 m depth) from every sampling station. P_n and R were measured for each of the following fractions in triplicate: 1) 300 mL of an unfiltered water subsample, 2) 300 mL of a water subsample filtered by 20 μm nylon filter and 3) 300 mL of water subsample filtered by 2 μm nylon filter. All fractions were incubated in light at 530 μmol photons m^{-2} s^{-1} and in darkness to measure P_n and R rates respectively. Incubations were performed in 300 mL Winkler bottles with a magnetic stirrer to ensure internal turbulence and mixing. Bottles were sealed with rubber stoppers holding a 50 μm tip O_2 microsensor (UNISENSE®, Denmark), allowing the continuous measurement of O_2 with time. P_n and R rates were calculated as the time evolution (30 minutes per incubation) of the O_2 concentration. O_2 microsensors have been used in previous studies to measure continuously planktonic respiration (Briand et al. 2004; García-Martín et al. 2011). Microplankton P_n and R were calculated from the differences between the rates measured for the whole community minus the rates measured for the < 20 μm fraction ($\boldsymbol{P_{n\ micro}} = P_{n\ whole} - P_{n\ <20\mu m}$, $\boldsymbol{R_{micro}} = R_{whole} - R_{<20\mu m}$). Nanoplankton contribution was calculated as the rates measured in the < 20μm fraction minus those in < 2 μm fraction ($\boldsymbol{P_{n\ nano}} = P_{n\ <20\mu m} - P_{n\ <2\mu m}$, $\boldsymbol{R_{nano}} = R_{<20\mu m} - R_{<2\mu m}$). Picoplankton rates were directly measured in the < 2μm fraction ($\boldsymbol{P_{n\ pico}} = P_{n\ <2\mu m}$, $\boldsymbol{R_{pico}} = R_{<2\mu m}$).

Table 1. End members for Tempisque River fresh water, with Salinity (S) = 0 and marine water, with Salinity (S) = 35, mixing in the inner part of the Gulf of Nicoya in the dry season. Marine water here corresponds to the so-called intermediate water which is the surface water of the lower Gulf of Nicoya. Values were either calculated from regression lines of nutrients (μM) against salinity (psu) in this study or obtained from published previous studies when calculation from regression lines produced negatives estimates. * From Table 1 in Kress et al 2002, ** estimates from regression lines produced negatives value for the river end member and nitrite was below detection limit in directed measurement in surface water of more marine Sts 4 and 5 in this study. Regression equations, determination coefficient and number of data for the river end and the marine end are presented in the table in brackets (regression equation; R^2; n).

	End member River water (S = 0)		End member Marine water (S = 35)	
NO_3^-	35.6	(NO_3^- = -0.81**S** + 35.62; 0.86;7)	1.4*	-
NO_2^-	0**	-	0**	-
NH_4^+	2.3	(NH_4^+ = -0.05**S** + 2.3; 0.40;7)	0.4	(NH_4^+ = -0.05**S** + 2.27; 0.28;19)
PO_4^{3-}	8.7	(PO_4^{3-} = -0.14**S** + 8.72; 0.98;7)	0.2*	-
SiO_4^{4-}	1200.9	(SiO_4^{4-} = -32.11**S** + 1200.9; 0.99;7)	27.3	(SiO_4^{4-} = -34.30**S** + 1227.63; 0.99;19)

Once the incubation finished, two water samples from each Winkler bottle (three replicates), one for Chl *a* and one for POC, were filtered through pre-combusted glass fiber filters (0.7 μm nominal pore size, 47 mm diameter, Whatman GF/F) and were analysed using the methods previously described.

The same calculation procedure described above for P_n and R was used to determine Chl *a* and POC in the micro-, nano- and picoplankton size fractions.

2.6. Phytoplankton abundance, biovolume and biomass

Unfiltered samples (n = 2) of in situ surface water (20 cm depth) were taken for the measurements of prokaryotic and eukaryotic pico- (0.2 – 2 μm) and nanophytoplankton (2 – 20 μm) abundance. Samples were fixed using glutaraldehyde (1% final concentration) and stored at - 80 ºC until analyzed by flow cytometry in the laboratory. Microphytoplankton was concentrated by filtering 4-8 L of surface water through a 10 μm mesh. The samples were preserved with formaldehyde (4 % final concentration) and stored in dark bottles for later analysis by optical microscopy. A certain overlap might exist between the abundances of nanoplankton determined by flow cytometry and microplankton determined by microscopy.

Analyses of pico- and nanophytoplankton abundances were carried out on a Dako CyAnTM ADP (Beckman Coulter™) flow cytometer using fluorescent microspheres (1.1 μm, Ex/Em: 430/465 nm, FluoSpheres® Molecular Probes Inc.™) as standard. Side Scattered Light (SSC), red fluorescence from Chl *a*, and orange fluorescence from phycobiliproteins were used to characterize each population (Corzo et al. 1999; Gasol and del Giorgio 2000; Marie et al. 2005). The relationship between cell size and SSC was calibrated using reference microspheres of known sizes ranging from 0.49 to 9.9 µm (FluoSpheres® Molecular Probes Inc.™). Thereby, biovolumes (μm^3/cell) were calculated assuming cells as spheres. The abundance (cell mL^{-1}) of microphytoplankton was determined by the inverted microscopy technique on a Nikon Eclipse Ti-U microscope (Seguro et al. 2015). Biovolume (μm^3/cell) was calculated considering the cell shape of each species according to different geometric forms following Hillebrand et al. (1999).

Based on the calculated biovolume, the carbon biomass was then determined for the picophytoplankton (*Prochlorococcus*, *Synechococcus* and picoeukaryotes), nanophytoplankton (nanoeukaryotes) (V. Aguilar, unpubl.) and the most abundant microphytoplankton species (representing more than 75 % of the total at each station): *Actinoptychus undulatus, Cerataulina dentata, Chaetoceros curvisetus, Chaetoceros subtilis var. abnormis, Cylindrotheca closterium, Cyclotella* spp.*, Guinardia striata, Paralia sulcata, Prorocentrum minimum, Protoperidinium pallidum, Scenedesmus opoliensis, Strobilidium* spp.*, Thalassionema nitzschioides and Thalassiosira* spp.) (Seguro et al. 2015).

There is significant uncertainty over carbon conversion factors for prokaryotic picophytoplankton derived from uncertainties in both, size and carbon density estimates (DuRand et al. 2001; Shalapyonok et al. 2001). In this study, a conversion factor of 0.235 pg C μm^{-3} was used for prokaryotic phytoplankton, which is an average of CHN (Carbon: Hydrogen: Nitrogen: ratio) measurements for the cyanobacteria of interest: *Synechococcus sp*. and *Prochlorococcus sp*.as determined by other studies (Shalapyonok et al. 2001; Worden et al. 2004).

The biomass (μg C L^{-1}) of the prokaryotic phytoplankton (*Synechococcus* and *Prochlorococcus*), picoeukaryotes, nanoeukaryotes and microphytoplankton community was calculated using the equations 9 and 10 according to Strickland (1970).

$$Log\ C_{\left(\frac{pg}{cell}\right)} = 0.76 LogV_{(\mu m^3)} - 0.29^{(*)} \quad (9)$$

$$LogC_{\left(\frac{pg}{cell}\right)} = 0.94 LogV_{(\mu m^3)} - 0.60^{(**)} \quad (10)$$

(*) for diatoms
(**) for all other cells

2.7. Statistical methods

Simple and multiple linear correlation and regression analyses were used to test statistical significance of covariation between different variables and to estimate river and marine end-member nutrient concentrations. The relationship between P_n and the product between the concentration of Chl *a* and the ratio between incident irradiance and the extinction coefficient was tested using linear regression (Cole and Cloern 1984, 1987). In an attempt to increase the explained variability of net production we progressively included the concentration of different inorganic nutrients (NO_3^-, PO_4^3, SiO_4^{4-}) and temperature in a statistical model of stepwise multiple regression (PRIMER). Linear correlation between fractionated Chl *a* and total Chl *a* concentrations were tested for surface water samples (n = 15). Since the relationships between any given nutrient and salinity were not linear at the estuary scale, two separate linear regressions were used to estimate the river and marine end member nutrient concentrations more accurately, one for the river end (Sts 1 and 2, n = 7) and another for the marine end (Sts 3 to 5, n =19).

3. Results

3.1. Hydrographic conditions and inorganic nutrients

Physicochemical variables were strongly influenced by the Tempisque River water discharge, showing in general a gradient along the estuary (Fig. 2). Salinity increased progressively from the river to the more marine stations, whereas temperature presented a maximum centered in surface waters at St. 3 (Fig. 2a, b). The vertical profiles of temperature and salinity indicated complete vertical mixing closer to the river (St. 1 and 2) and a certain degree of stratification with minimal gradients for temperature in the more marine stations (Fig. 2b). NO_3^-, NO_2^-, PO_4^{3-} and SiO_4^{4-} concentrations were generally highest at the innermost stations (St. 1 and 2), decreasing progressively towards the marine end. NO_2^- showed a clear maximum in St. 2, whereas no clear patterns were observed for NH_4^+, which was the least abundant of all inorganic nutrients measured.

Comparison of the observed nutrient concentration with the theoretical one derived from the mixing model (Fig. 3) indicates: 1) that most of the decrease in NO_3^-, PO_4^{3-} and SiO_4^{4-} along the estuary is due to dilution, 2) an additional source of NO_3^- and PO_4^{3-} seems to exist between Sts 1 and 2 and 3) the large deviation of bottom concentrations from the theoretical ones suggests that the sediment is an additional source of nutrients.

Total suspended material increased from the river towards St. 2 and 3, where the maximum was found and decreased thereafter towards the sea. Photic layer was < 1m at St. 1, increasing progressively with increasing distance from the river down to 10 m depth at St. 5 (Fig. 4a).

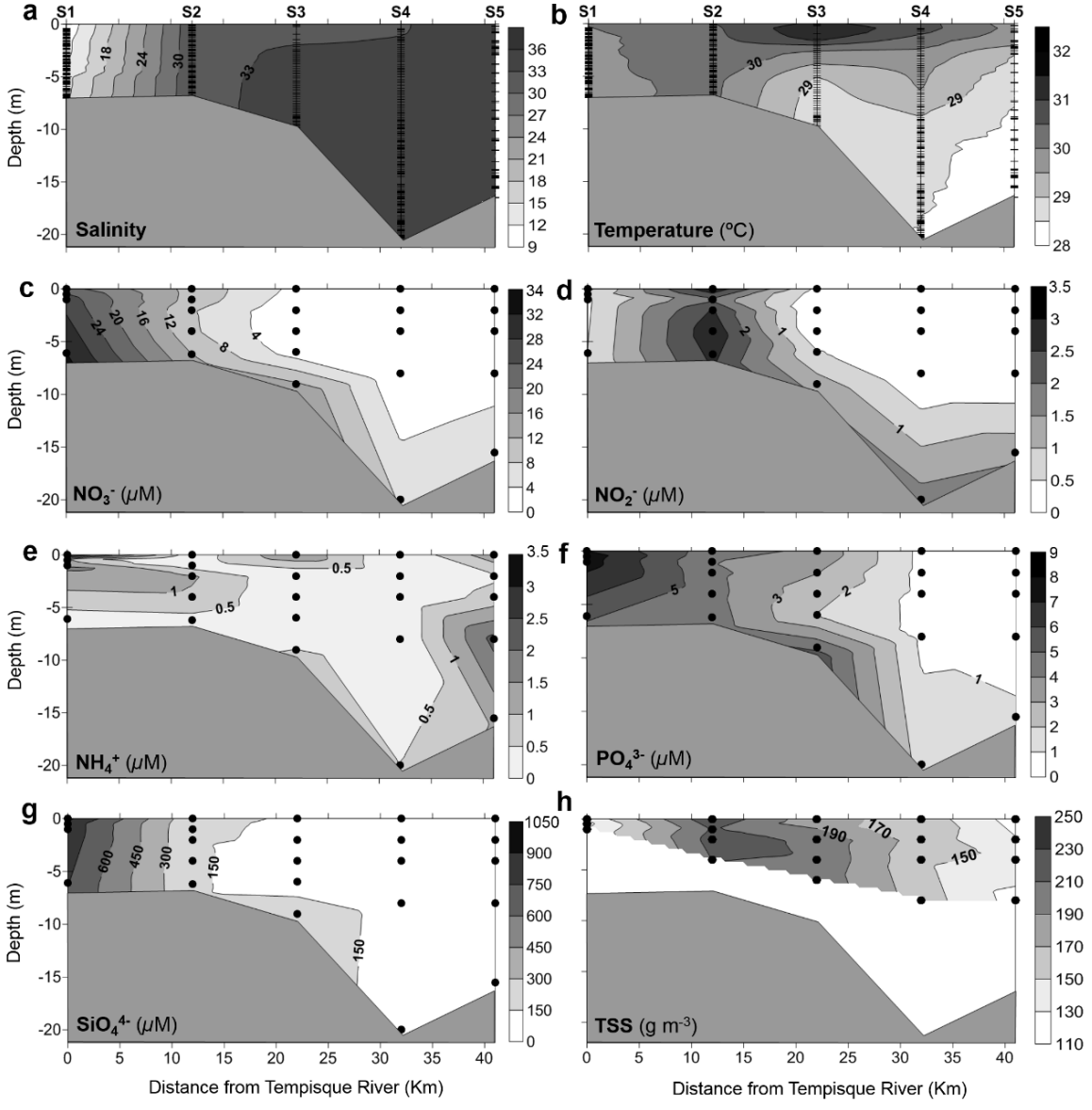

Fig.2: *Vertical distributions* of (**a**) salinity, (**b**) temperature (ºC); (**c**) nitrate (NO_3^-), (**d**) nitrite (NO_2^-), (**e**) ammonium (NH_4^+), (**f**) phosphate (PO_4^{3-}) and (**g**) silicate (SiO_4^{4-}) concentrations (μmol L^{-1}), and (**h**) total Suspended material (TSS) (g m^{-3}) along the sampled area. Data are n = 1 for temperature and salinity, means of *n* = 3 for inorganic nutrients and means of *n* = 2 for TSS.

3.2. Chlorophyll, organic carbon and phytoplankton biomass

Total Chl *a* concentration showed the highest value in the middle of the estuary at 2 m depth (St. 3) and the lowest in the surface water of St. 5 (Fig. 4b). Fractionated chlorophyll, measured only in surface water samples, showed that nanoplankton (2 – 20 μm) was the dominant fraction of Chl *a* throughout the estuary representing 51 - 78 % of total Chl *a* (Fig. 5b). Picoplankton (< 2 μm) and microplankton (> 20 μm) chlorophyll fractions represented up to a maximum of 31% (St. 2) and 37% (St. 4), respectively. Microplankton was more abundant in the more marine areas of the estuary, while picoplankton did not show any clear pattern along the estuary (Fig. 5b).

Particulate organic carbon concentration had very similar pattern to total Chl *a*, both along the estuary and with depth with high values at the intermediate St. 3 (Fig. 4b). However, the highest POC concentration was measured at St. 1, near the river mouth (Fig. 4b). POC size fractionation of surface samples showed that pico-particles (< 2 μm) represented the main fraction of the total POC, accounting for 45 to 81 % of the total (Fig. 5b). Nano-particles (2 – 20 μm) accounted for almost 50 % of the total POC at St. 1, but did not exceed 30 % at the remaining Stations (Fig. 5b). Micro-particles (> 20 μm) represented less than 15 % of the total POC. The relative contribution of nano- and micro-particles to the total Chl *a* was comparatively larger than to the total POC, however the pico-particles fraction was considerably depleted in Chl *a* with respect to POC (Fig. 6b).

Estimated phytoplankton biomass ranged between 600 and 1600 μg C L^{-1} and showed a spatial distribution along the estuary similar to Chl *a*; a maximum at St. 3 and a minimum at St. 2 (Fig. 5c). Direct counts of phytoplankton confirmed the considerable contribution of nanophytoplankton (always > 92%) to the total autotrophic biomass compared to microplankton (1.3 – 6.8 %) and picoplankton (0.2 - 1.1%) (Fig. 5c). The contribution of pico- and microplankton to the total autotrophic biomass was similar to the one for total Chl *a*. However nanoplankton had a higher contribution to total biomass than Chl *a* (Fig. 6a).

3.3. Total and size-fractionated net production and respiration rates

Total P_n rates, determined by in situ incubations, presented a maximum in the middle of the estuary, being the highest total P_n rates (23.1 mmol O_2 m^{-3} h^{-1}) measured at 2 m depth in St. 3 (Fig. a). In contrast, the entire water column had negative P_n rates at St. 1. Compensation depth ($P_n = 0$) increased from St. 1 to St. 3, and decreased again at St. 4 (Fig. 7a). *R* rates were highest (23.6 mmol O_2 m^{-3} h^{-1}) in the surface at St. 1, decreasing with the distance from the river and with the depth in each station (Fig. 7b). O_2 in the water column was subsaturated in the riverine station and in the bottom layer along the estuary and oversaturated in the surface water from St. 2 seawards (Fig. 7c).

Net production in estuaries has been previously related to a composite parameter calculated as the product between the Chl *a* concentration and the ratio between the incident irradiance (I_o) and the extinction coefficient (k) (Cole and Cloern 1984, 1987). The application of this empirical model to our data produced a significant linear correlation ($P_n = 0.0016[\text{Chl } a\ [I_o/k]] - 9.1623$, $r = 0.540$, $p = 0.021$, $n = 18$), with P_n expressed in mmol O_2 m^{-3} h^{-1}, Chl *a* in mg m^{-3}, I_o in μmol m^{-2} s^{-1} and k in m^{-1}. However, this composite parameter that accounts for the Chl *a* concentration and the light availability only explains about half of the variability of P_n along the estuary. Attempts to increase the explained P_n variation by including the concentration of different inorganic nutrients (NO_3^-, PO_4^{-3}, SiO_4^{4-}) and

temperature in a statistical model of stepwise multiple regression did not increase the percentage of P_n explained variation (results not shown).

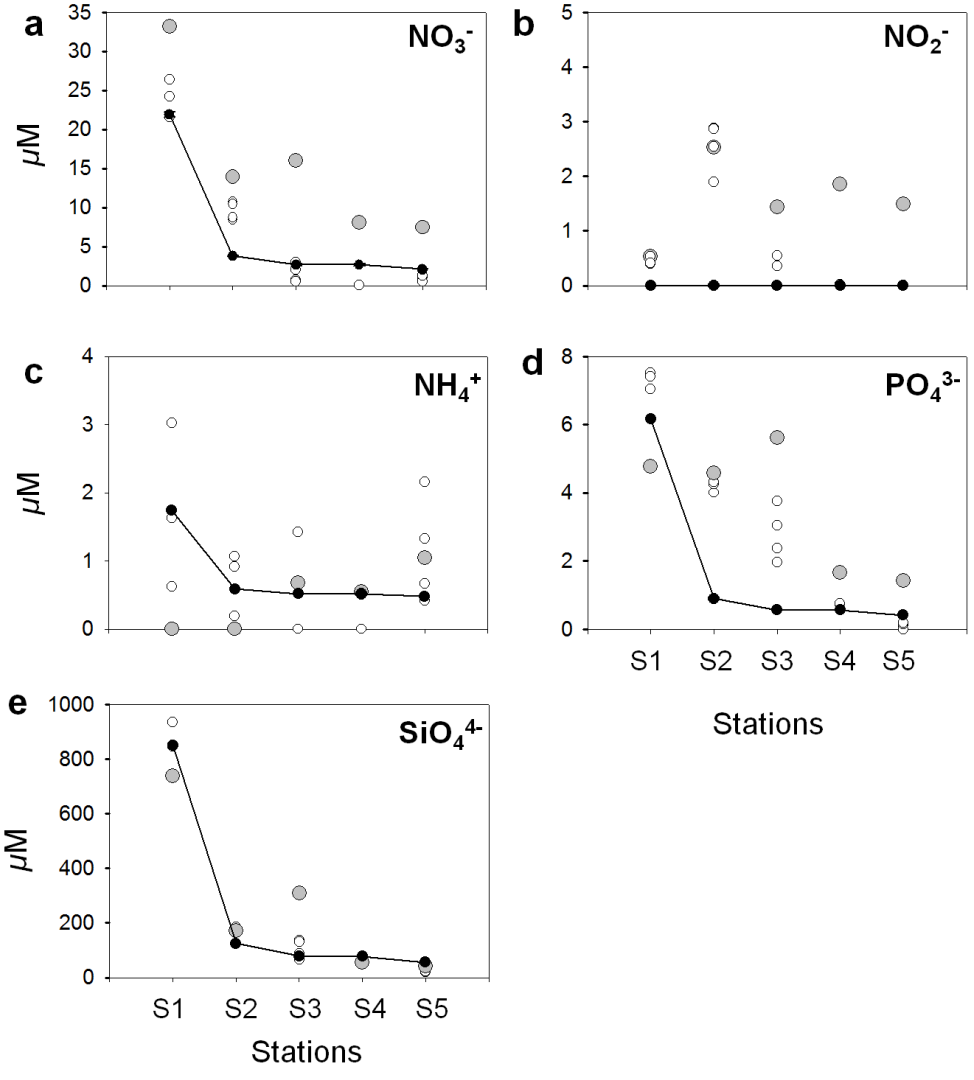

Fig.3: Observed (○ and ●) and calculated (⟶) nutrient concentrations from a mixing model using salinity as a conservative property along the study are. The concentrations of nutrients were measured at different depth in the water column, the bottom water samples have been marked with a different symbol (large grey circle). The calculated nutrient concentrations are presented as the water column mean ± standard error for simplicity. (**a**) nitrate (NO_3^-), (**b**) nitrite (NO_2^-), (**c**) ammonium (NH_4^+), (**d**) phosphate (PO_4^{3-}) and (**e**) silicate (SiO_4^{4-}) concentrations (μM).

The relative contribution of different planktonic size classes to pelagic primary production and respiration in the inner part of the gulf changed along the estuary (Fig. 8). The picoplankton fraction accounted from 40 to 60 % of the net community production in the inner basin except at St. 3, where

its contribution was lower, i.e. 35 %. The contribution of picoplankton to net metabolism of the pelagic community was comparatively higher than its contribution in terms of Chl *a* (Fig. 8c). In general, the picoplankton fraction showed the highest *R* rates and accounted for almost 54 ± 4 % of the total respiration at all stations (Fig. 8b). The importance of picoplankton contribution to total *R* agrees well with the importance of this size class in terms of POC (Figs. 5b, 8d). Nanoplankton had a high contribution to the total P_n at Sts. 3 and 4, being up to 55 % of the P_n at St. 3. However, surprisingly nano-phytoplankton contributed very little to the total P_n in surface samples in the rest of the stations (Fig. 8a).

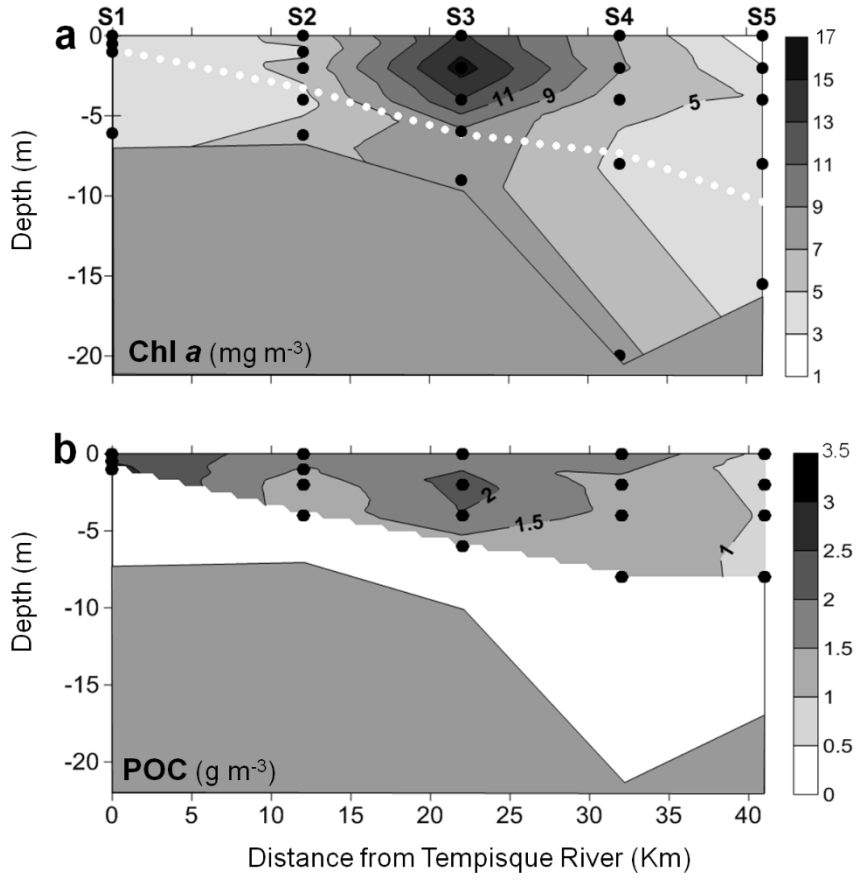

Fig.4: *Vertical distribution* of (**a**) chlorophyll *a* (Chl *a)* (mg m^{-3}), and (**b**) particulate organic carbon (POC) (g m^{-3}) along the study area. White circles line represent photic layer depth (m). Data are means of *n* = 3 for Chl *a*, and *n* = 1 for POC.

The contribution of nanoplankton to the total Chl *a*, was comparatively higher than to P_n along the estuary (Fig. 8c). The contribution of microplankton to the total community net production was maximum at St. 2 and at the most marine station (about 50 %) and in general represented a higher contribution to P_n than to Chl *a* along the estuary (Fig. 8c). Microplankton respiration was the second most important contributor to total community respiration, accounting for up to 43.3 ± 5.8 % (Fig. 8b) and its contribution to total *R* was comparatively higher than to POC (Fig. 8d).

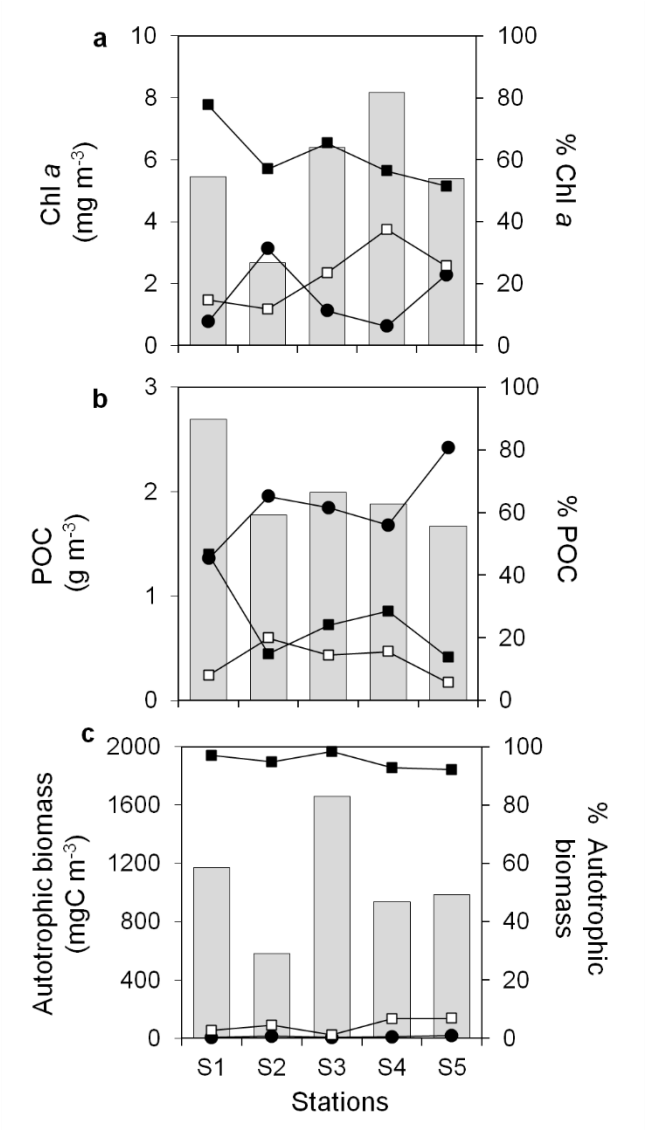

Fig.5: Total concentration ( ) of (**a**) chlorophyll a (Chl *a*) (mg m^{-3}) (n = 3), (**b**) particulate organic carbon (POC) (g m^{-3}) (*n* = 3), and (**c**) biomass of phytoplankton (mg C m^{-3}) (*n* = 2), and their relative contribution (%) of pico- (< 2 μm,), nano- (2 - 20 μm,), and microplankton (> 20 μm,) along the sampling stations.

3.5. Photic layer net ecosystem production

Daily depth integrated net metabolism for the photic layer along the estuarine gradient was calculated from volumetric rates, the duration of local day and night periods and assuming a photosynthesis quotient (PQ) of 1.2 and a respiration quotient (RQ) of 0.8 (Ryther 1956) (Fig. 9). P_g^d (1.5 – 7.2 g C m^{-2} d^{-1}) and R^d rates (4.3 – 8.9 g C $m^{-2}d^{-1}$) changed along the estuary, both showing maximum values at St. 3, where the maxima in Chl *a* and P_n were measured as well (Figs. 4a, 7a). P_n^d was only positive in this sampling station along the estuary (2.9 g C m^{-2} d^{-1}) being the photic layer in the rest of the estuary net heterotrophic (Fig. 9).

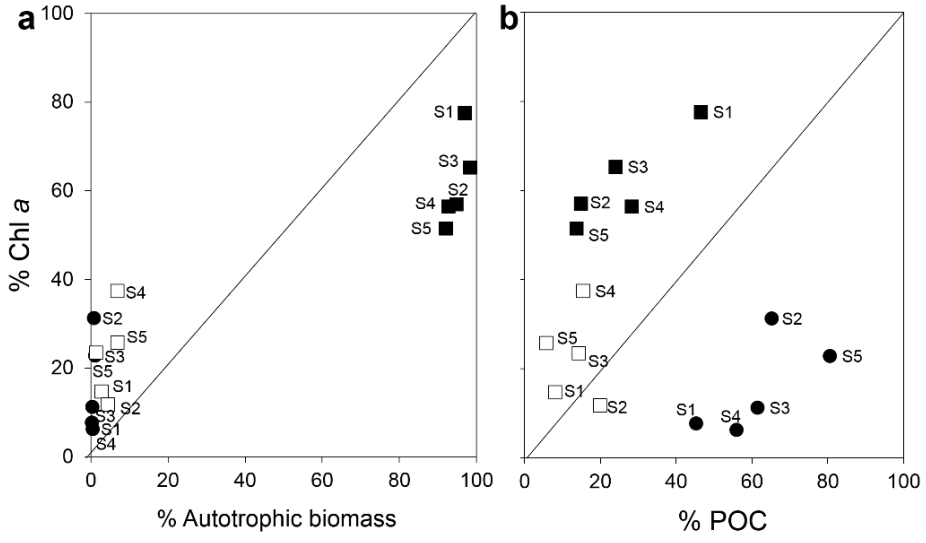

Fig.6: *Relative contribution* (%) of pico- (< 2 μm, ●), nano- (2 - 20 μm, ■), and microplankton (> 20 μm, □) in terms of (**a**) chlorophyll a (Chl *a*) versus autotrophic biomass in carbon (C) units, and (**b**) Chl *a* versus particulate organic carbon (POC) along the estuarine gradient. Diagonal lines represent identical contribution to both variables. S1 to S5 represent the sampling stations.

4. Discussion

4.1. The influence of Tempisque River on phytoplankton

The flow of the Tempisque River affects phytoplankton abundance, community structure and primary production in the inner basin of the Gulf of Nicoya due to its effects on water column stability, nutrient concentration, and light availability. Fresh water flow changes seasonally and controls the stability of the water column (Voorhis et al. 1983, Seguro et al. 2015). During the dry season, tidal and residual currents mix the water column between St. 1 and 2, where the steepest salinity gradient was observed (Fig. 2). Nonetheless, a certain degree of stratification was also observed at St. 3 due to the presence of a warm water mass (Fig. 2b), probably due to warmer water discharge from the Abangares River (Lizano and Vargas 1993).

The Tempisque River represents a considerable source of nutrients for the estuarine phytoplankton community during the rainy and dry seasons (Palter et al. 2007, Seguro et al. 2015). NO_3^-, PO_4^{3-}, and SiO_4^{4-} concentrations at the more riverine stations were higher than those reported previously for the Gulf of Nicoya (Palter et al. 2007) and other tropical estuaries (Rochelle-Newall et al. 2011; Burford et al. 2012; Pamplona et al. 2013). Mixing calculations using salinity as a conservative property clearly show that the general decrease of inorganic nutrients along the estuary was mainly due to dilution by mixing with seawater of lower nutrient concentrations (Fig. 3, Table 1). This was particularly clear for SiO_4^{4-} due its high discharge into the estuary, being always in stoichiometric excess with respect to total inorganic N and P. The general decrease of NO_3^-, and PO_4^{3-} concentrations along the estuary was due to dilution by mixing as well.

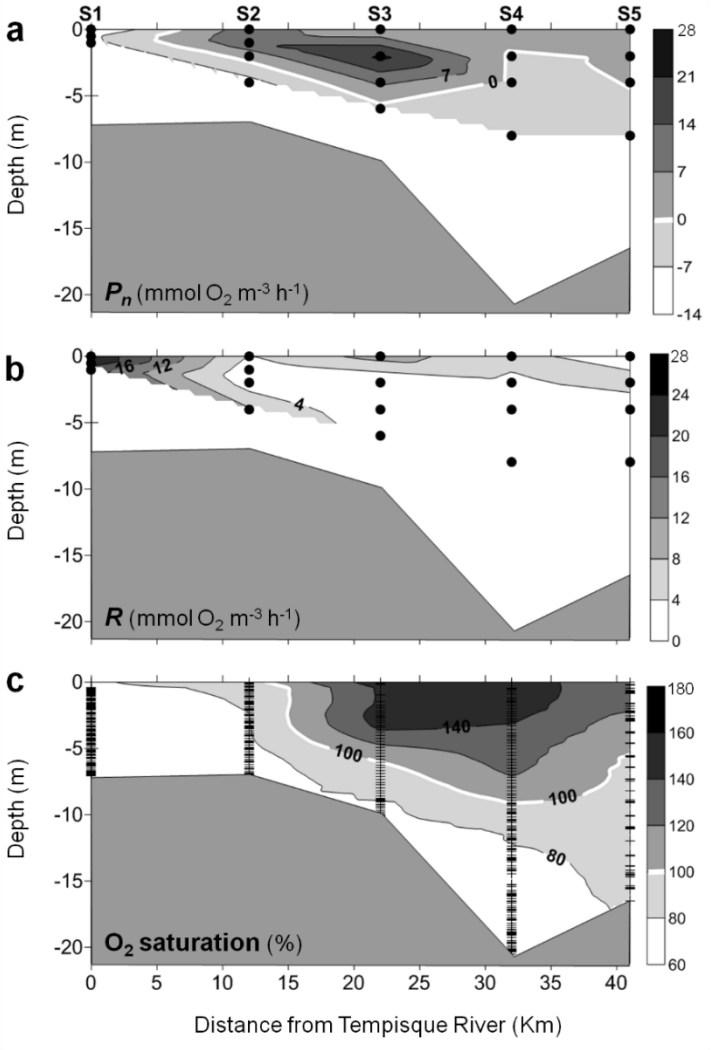

Fig.7: *Vertical distribution* of (**a**) volumetric net primary production rates (P_n), (**b**) volumetric dark respiration rates (R) (mmol O_2 m^{-3} h^{-1}) and (**c**) % of oxygen (O_2) saturation along the studied transect.

However, additional sources of these nutrients existed in St. 2 and 3, as their concentrations were higher than those predicted by dilution. Intense remineralization in the sediment is the most likely source, since NO_3^-, NO_2^-, and PO_4^{3-} concentrations close to the sediment were generally higher than those at the water surface (Fig. 2c, d, f) and showed a wider deviation from theoretical values, assuming conservative mixing (Fig. 3). This is expected as estuarine sediments are an important source of regenerated nutrients for the water column (Fisher et al. 1982; Cowan and Boynton 1996; Corbett 2010).

In addition to inorganic nutrients, fresh water discharge from the Tempisque River supplies high levels of allochthonous dissolved and particulate matter, which increases turbidity in the inner gulf (Gocke et al. 2001; Kress et al. 2002; Palter et al. 2007; Seguro et al. 2015). TSS presented highest values at St. 2, likely due to flocculation of dissolved organic matter favored by the freshwater and marine water mixing (Bell et al. 2000; Thill et al. 2001; Verney et al. 2009). Therefore, the relatively high concentrations of nutrients and the very shallow photic layer suggest that primary production in

the inner basin of the Gulf of Nicoya is likely more limited by light availability rather than by inorganic nutrients as shown in other estuaries (Cloern 1987; Fichez et al. 1992; Nittrouer et al. 1995; Burford et al. 2008).

4.2. Phytoplankton spatial distribution and size structure

The maximum of total Chl *a* recorded in the middle of the inner gulf in the dry season (Fig. 4a) was also observed during the rainy season (Seguro et al. 2015), being located, similarly to other estuaries, after the maximum salinity gradient (Cloern 1987; Humborg et al. 1997). The Chl *a* concentration range was similar to that found previously in the Gulf of Nicoya (Kress et al. 2002; Palter et al. 2007, Seguro et al. 2015) and in other tropical and subtropical estuaries (Burford et al. 2012; Rochelle-Newall et al. 2011; Li et al. 2013). The maximum in phytoplankton biomass in St. 3 likely explains the maximum observed in POC as well, whereas in the most riverine station, a large fraction of the high POC concentration was of detrital origin since the input of total Chl *a* concentration with the riverine water was proportionally lower (Fig. 4).

The relative importance of the different size classes in terms of Chl *a*, POC and autotrophic biomass (C units) was not fully coincident (Fig. 5, Table 2). Nonetheless, the dominance of nanoplanktonic fraction was confirmed in terms of Chl *a* and of autotrophic C units; nanoplankton contributed more than 61 and 95 %, respectively. The higher relative importance of nanoplankton with respect to micro- and picoplankton has been reported for temperate estuaries (Iriarte and Purdie 1994; Sin et al. 2000). Surprisingly, nanoplanktonic POC was only about 25.5 % of total POC, being POC largely abundant in the picoplankton size fraction (61.7 ± 5.8 %), which likely suggest a higher relative contribution of either detritus or heterotrophs to the pico-particle size class. The cell carbon content of bacterioplankton ($3 \times 10^5 – 2 \times 10^6$ cell mL^{-1}, V. Aguilar, unpubl. data) might explain the important contribution of picoplankton size fraction to total POC but not to total Chl *a* and total autotrophic C. Moreover, Chl *a* content in the picoplankton fraction might have been underestimated in our study since the complete extraction of Chl *a* from picocyanobacteria is usually difficult, typically requiring mechanical disruption of cells (Stauffer et al. 1979, Howard and Joint 1989). Based on the picoplankton abundance measured by flow cytometry during the same cruise (V. Aguilar, unpubl. data) and a cell content of 1.9×10^{-11} mg Chl *a* $cell^{-1}$ for picoplankton (Collier et al. 1994), Chl *a* concentration in the picoplankton fraction would be between 2.5 and 4.4 times higher than that obtained from our extractions here.

The concentration of Chl *a* in larger size fractions in marine and freshwater systems has been shown to be related to the trophic state of the system, increasing as total Chl *a* increases both in space and seasonally (Chisholm 1992; Iriarte and Purdie 1994; Bell and Kalff 2001). In the Gulf of Nicoya, microplankton Chl *a* increased as the total Chl *a* increased ($r = 0.463$, $p = 0.0263$, $n = 15$) extending the pattern frequently observed in temperate estuaries to tropical estuaries. The contribution of nanoplankton to phytoplankton biomass decreased along the estuarine gradient as observed in other estuaries (Sin et al. 2000), while the contribution of microplankton tended to increase seawards (Fig. 5). The observed changes in the size structure of phytoplankton community along the estuarine gradient likely have strong functional implications. Generally, large-size phytoplankton transfers organic matter to higher trophic levels through short, herbivore-based food chains, whereas communities dominated by small-sized phytoplankton are characterized by complex microbial food webs that favor the recycling of organic matter within the system (Cushing 1989, Reynolds 2006).

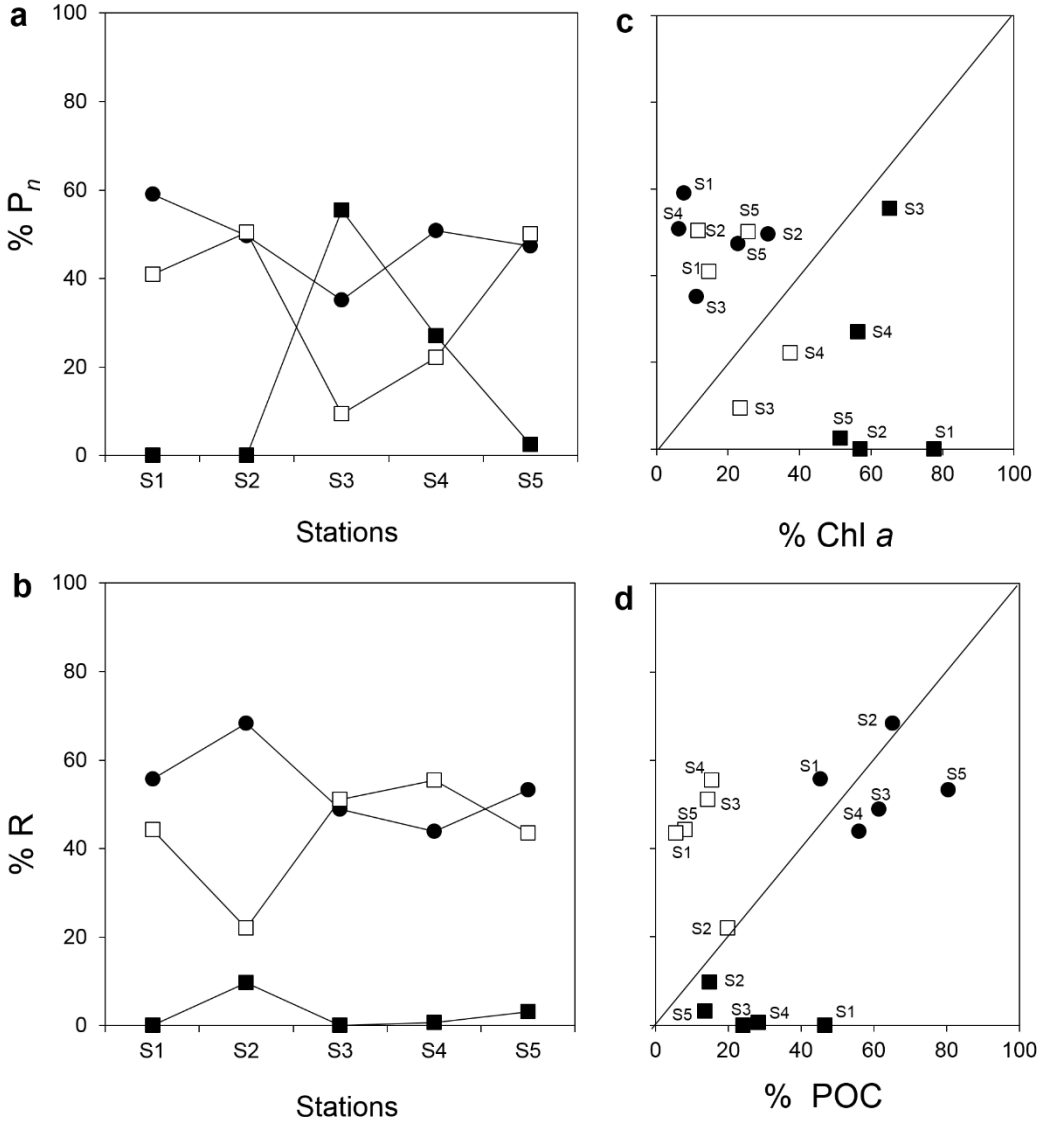

Fig.8: *Relative contribution* (%) of pico- (< 2 μm, ●), nano- (2 - 20 μm, ■), and microplankton (> 20 μm, □) in terms of (**a**) volumetric net primary production rates *(P_n)* and (**b**) volumetric dark respiration rates *(R)*. Data are means of n = 3. Relative contribution (%) of pico- (< 2 μm, ●), nano- (2 - 20 μm, ■), and microplankton (> 20 μm, □) of (**c**) P_n versus Chlorophyll a (Chl *a)*, and (**d**) *R* versus particulate organic carbon (POC). Diagonal lines represent identical contribution to both variables. S1 to S5 represent the sampling stations.

4.3. Zonation of net metabolism along the estuary

Seasonal changes in the water column stability due to differences in river flow are a common feature of many tropical estuaries and are known to affect phytoplankton abundance and primary

production (Ram et al. 2003; Costa et al. 2009; Burford et al. 2012). The spatial distribution of P_n matches well the observed pattern in phytoplankton abundance in the inner basin of the Gulf of Nicoya (Figs. 4a, 7a). P_g^d along the inner gulf ranged from 120 to 580 mg C m^{-2} h^{-1}, being in general higher than those measured in previous studies (Gocke et al. 1990; Córdoba-Muñoz 1998; Gocke et al. 2001a, b). Our results confirm that the inner Gulf of Nicoya is one of the most productive estuaries worldwide (Cloern et al. 2014). Primary production in this estuarine gradient seems to be limited by light availability due to high turbidity as suggested by the relation between P_n and I_o/k (Cole and Cloern 1984, 1987) and the existence of a mixed layer deeper than the photic layer (Figs. 2a, 4a). However, light availability explained less than half of the variation in P_n in the inner gulf. When nutrients were added to light as independent variables in a stepwise multiple regression analysis, the % of variance explained did not increase. This result confirms that variability of primary production along the inner Gulf of Nicoya is not dependent on nutrient availability. Other ecological drivers, together with light availability and water column stability, might explain the observed spatial pattern of net primary production. Top-down control of phytoplankton biomass and primary production is likely an obvious candidate and it has been observed in other estuaries, but no such information exists for the Gulf of Nicoya (Tackx et al. 2003; Lancelot et al. 2011).

Table 2. Relative contribution (%) of pico-, nano- and microplankton size fractions to total chlorophyll *a* (Chl *a*), particulate organic carbon (POC) and biomass abundance (expressed in C units using suitable conversion factors, see M&M section) along the inner section of the Gulf of Nicoya. Data are expressed as mean percentage ± standard deviation for the 5 sampling stations.

	Picoplankton	Nanoplankton	Microplankton
Chl *a*	15.9 ± 10.8	61.6 ± 10.3	22.6 ± 10.1
POC	61.7 ± 13.0	25.5 ± 13.3	12.7 ± 5.8
Autotrophic biomass (C units)	0.6 ± 0.3	95.1 ± 2.7	4.4 ± 2.5

The inner basin of the Gulf of Nicoya can be divided into three different zones (*Zone 1*, *Zone 2* and *Zone 3*) based on daily integrated rates of organic carbon production and consumption (Fig. 9). In *Zone 1* (St. 1 and 2), net microbial plankton community production was negative, resulting in a daily net heterotrophic metabolism (P: R < 1) for the photic layer (Fig. 9). This was probably due to the combination of two factors: 1) the low primary production rates in this zone due to the light-limitation, since mixing depth exceeded the euphotic depth (Grobbelaar 1985; Domingues et al. 2011), and 2) the high planktonic microbial respiration due to the input of allochthonous organic matter (Figs. 4b,7b,c).

Zone 2 was located in the middle of the estuarine gradient (St. 3), where maximum values of primary production, Chl *a*, and POC were registered (Figs. 4, 7). Despite the high daily respiration rates, daily integrated net community production was positive, indicating the existence of a net autotrophic microbial community (P: R > 1) in the photic layer (Fig. 9), which led to a strong O_2 oversaturation during the day (Fig. 7c). This high net primary production is due to a combination of several factors. The photic layer was deeper than the mixing layer due to a decrease in turbidity (Seguro et al. 2015) and to an increase in thermohaline stratification (Fig. 2B), which resulted in higher residence time for phytoplankton in the photic layer under conditions of high nutrient availability (Cole and Cloern 1984, 1987; Cloern 1987, Lancelot and Muylaert 2011).

Finally, in *Zone 3* (St. 4 and 5), net daily integrated primary production showed negative values with the microbial pelagic community being net heterotrophic (P:R ratio <1) as *Zone 1*(Fig. 9). The mixing layer was again deeper than the photic layer once the thermohaline stratification of St. 3 disappeared (Fig. 2a). In addition, nutrient limitation in *Zone 3* might also contribute to the decrease in primary production since NO_3^-, PO_4^{3-}, and SiO_4^{4-} concentrations were the lowest along the estuarine gradient and below the theoretical values calculated from the conservative mixing model (Fig. 3).

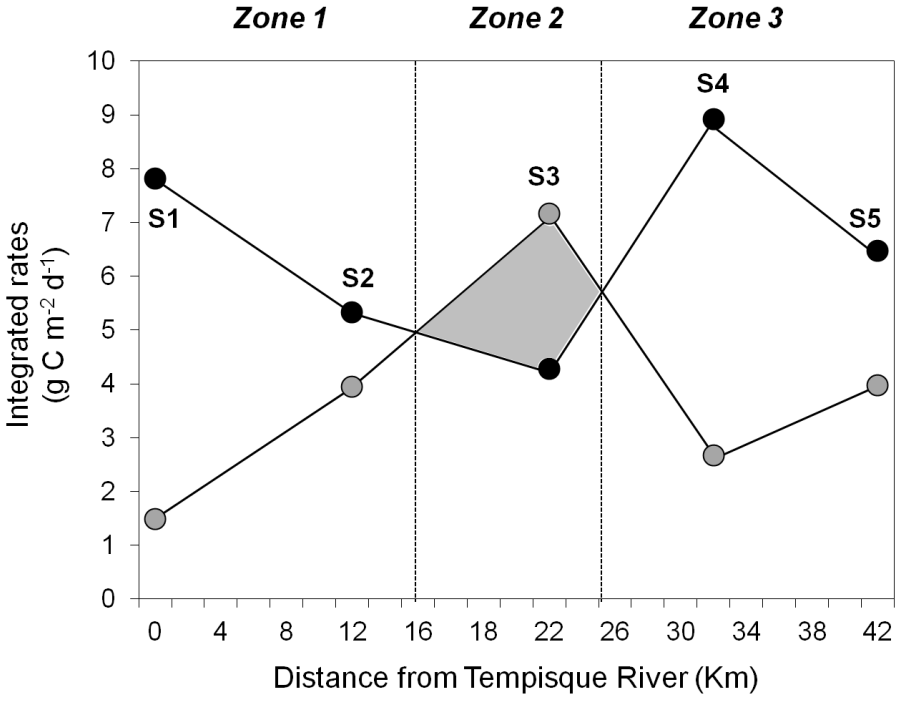

Fig. 9: Daily depth integrated of gross production rates (P_g^d, —●—) and daily depth integrated respiration rates (R^d, —●—) (g C m^{-2} d^{-1}) in the photic layer along the estuarine gradient. Grey area represents the region where the microbial community production in the photic layer was positive.

The relative contribution of the different size classes to net primary production and respiration did not match their relative contribution to biomass. An uncoupling between the relative contribution of different size classes to total phytoplankton biomass and primary production has been reported in oceanic waters as well (Malone et al. 1993; Marañón et al. 2003). This observation has been typically explained either as a consequence of a top-down control of the phytoplankton community by grazers (Banse 1995) or by physiological changes that affect the photosynthetic efficiency of phytoplankton (Chisholm 1992; Geider et al. 1997; Cermeño et al. 2006). The contribution of picoplankton in terms of net primary production, Chl *a*, and biomass was the lowest in Zone 2; in combination with the increase in the contribution of nanoplankton to primary production, these data indicate a shift in the size structure of primary production towards higher cell sizes. Seawards, the contribution of nanoplankton to net community production decreased, but the contribution of microplankton increased, further

shifting the size structure of phytoplankton biomass and production towards higher size classes (Figs. 5, 8a). This shift would likely increase further the direct transfer of primary production from microphytoplankton to large herbivorous grazers (Thingstad and Rassoulzadegan 1999), such as copepods which are actually the dominant group of phytoplankton metazoan grazers in the Gulf of Nicoya (Brugnoli-Olivera and Morales-Ramírez 2008).

In this contribution we have shown that the size structure of the phytoplankton community changed considerably along the estuarine gradient in the Gulf of Nicoya, both in terms of standing stock (biomass) and net metabolism (primary production and respiration). In addition, phytoplankton biomass and net metabolism size distributions were partially uncoupled along the estuarine gradient. However, information on what environmental factors, including bottom-up and top-down drivers, explain the observed patterns in phytoplankton size structure in the inner part of the Gulf of Nicoya and others tropical estuaries is still lacking. Bridging this gap of knowledge is critical because such shifts in size distribution of primary production and phytoplankton biomass along an estuarine gradient are likely to have major implications for the entire trophic network and biogeochemical cycling in these highly productive systems.

5. Acknowledgments

This study was funded by projects C/023621/09, D/031020/10, and A1/037457/11 from Spanish Agency for International Development and Cooperation (AECID), the projects CTM2013-43857-R and P11-RNM-7199 from the Spanish Ministry of Economy and Competitiveness and Andalusian Regional Government and supported by the project 808-B3-127 at the University of Costa Rica (UCR). We thank all colleagues and the staff from UCA and CIMAR-UCR that contributed to the realization of this study for their personal and logistic support.

6. References

Alongi, D.M. 2002. Present state and future of the world's mangrove forests. Environ. Conserv. 29: 331–349. doi:10.1017/S0376892902000231

Banse, K. 1995. Community response to IRONEX. Nature 375: 112. doi:10.1038/375112a0

Barbier, E.B., S.D. Hacker, C. Kennedy, E.W. Koch, A.C. Stier, and B.R. Silliman. 2011. The value of estuarine and coastal ecosystem services. Ecol. Monogr. 81: 169–193. doi: 10.1890/10-1510.1

Bell, R., M. Green, T. Hume, and R. Gorman. 2000. What Regulates Sedimentation in Estuaries? Water Atmos. 8:13–16.

Bell, T., and L. Kalff. 2001. The contribution of picophytoplankton in marine and freshwater systems of different trophic status and depth. Limnol. Oceanogr. 46: 1243–1248. doi: 10.4319/lo.2001.46.5.1243

Bianchi, T., 2007. Biogeochemistry of Estuaries. Oxford University Press, New York.

Blaber, S.J.M. 2013. Fishes and fisheries in tropical estuaries, the last 10 years. Estuar., Coast. Shelf Sci. 135: 57–65. doi:10.1016/j.ecss.2012.11.002

Bower, C.E., and T. Holm-Hansen. 1980. A salicylate-hypochlorite method for determining ammonia in seawater. Can. J. Fish. Aquat. Sci. 37: 794–798.

Boyle, E., R. Collier, A.T. Dengler, J.M. Edmond, A.C. Ng, and R.F. Stallard. 1974. On the chemical mass-balance in estuaries. Geochim. Cosmochim. Acta 38: 1719–1728. doi:10.1016/0016-7037(74)90188-4

Briand, E., O. Pringault, S. Jacquet, and J.P Torréton. 2004. The use of oxygen microprobes to measure bacterial respiration for determining bacterioplankton growth efficiency. Limnol. Oceanogr. Methods 2: 406–416.

Brugnoli-Olivera, E., and A. Morales-Ramírez. 2001. La comunidad fitoplanctónica de Punta Morales, Golfo de Nicoya, Costa Rica. Rev. Biol. Trop. 49: 11–17.

Brugnoli-Olivera, E., and A. Morales-Ramírez. 2008. Trophic planktonic dynamics in a tropical estuary, Gulf of Nicoya, Pacific coast of Costa Rica during El Niño 1997 event. Rev. Biol. Mar. Oceanogr. 43: 75–89.

Burford, M.A., D.M. Alongi, A.D. McKinnon, and L.J. Trott. 2008. Primary production and nutrients in a tropical macrotidal estuary, Darwin Harbour, Australia. Estuar. Coast. Shelf Sci. 79: 440–448. doi:10.1016/j.ecss.2008.04.018

Burford, M.A., I.T. Webster, A.T Revill, R. Kenyon, AM. Whittle, and G. Curwen. 2012. Controls on phytoplankton productivity in a wet-dry tropical estuary. Estuar. Coast. Shelf Sci. 113: 141–151. doi:10.1016/j.ecss.2012.07.017

Cermeño, P., E. Marañón, V. Pérez, P. Serret, E. Fernández, and C.G. Castro. 2006. Phytoplankton size structure and primary production in a highly dynamic coastal ecosystem Ría de Vigo, NW-Spain, Seasonal and short-time scale variability. Estuar. Coast. Shelf Sci. 671: 251–266. doi:10.1016/j.ecss.2005.11.027

Chisholm, S.W. 1992. Phytoplankton size. In Falkowski, P.G.,and Woodhead, A.D., ed. Primary Productivity and Biogeochemical Cycles in the Sea. Plenum press, New York.

Cloern, J.E. 1987. Turbidity as a control on phytoplankton biomass and productivity in estuaries. Cont. Shelf Res. 7: 1367–1381. doi:10.1016/0278-4343(87)90042-2

Cloern, J.E., S.Q. Foster, and A.E. Kleckner. 2014. Review: phytoplankton primary production in the world's estuarine-coastal ecosystems. Biogeosciences 11: 2477–2501. doi:10.5194/bg-11-2477-2014

Cole, B.E. and J.E. Cloern. 1984. Significance of biomass and light availability to phytoplankton productivity in San Francisco Bay. Mar. Ecol. Prog. Ser. 17: 15–24. doi: 10.3354/meps017015

Cole, B.E. and J.E. Cloern. 1987. An empirical model for estimating phytoplankton productivity in estuaries. Mar. Ecol. Prog. Ser. 36: 299–305. doi: 10.3354/meps036299

Collier J.L., S.K. Herbert, D. C. Fork, and A. R. Grossman 1994. Changes in the cyanobacterial photosynthetic apparatus during acclimation to macronutrient deprivation. Photosynth Res. 42: 173-183. doi: 10.1007/BF00018260

Corbett, D.R. 2010. Resuspension and estuarine nutrient cycling: insights from the Neuse River Estuary. Biogeosciences 7: 3289 – 3300. doi:10.5194/bg-7-3289-2010

Córdoba-Muñoz, R. 1998. Primary productivity in the water column of Estero de Morales, a mangrove system in the Gulf of Nicoya, Costa Rica. Rev. Biol. Trop. 46: 257–262.

Corzo, A., F. Jiménez-Gómez, F.J.L. Gordillo, R. García-Ruíz, and F.X. Niell. 1999. Synechococcus and Prochlorocccus-like populations detected by flow cytometry in a eutrophic reservoir in summer. J. Plankton Res. 21: 1575–1581. doi: 10.1093/plankt/21.8.1575

Costa, L.S., V.L.M. Huszar, and A.R. Ovalle. 2009. Phytoplankton functional groups in a tropical estuary: hydrological control and nutrient limitation. Estuaries Coasts 32: 508–521. doi: 10.1007/s12237-009-9142-3

Costanza, R., R. d'Arge, R. de Groot and others. 1997. The value of the world's ecosystem services and natural capital. Nature 387: 253–260. doi:10.1038/387253a0

Cowan, J.L.W., and W.R. Boynton. 1996. Sediment-water oxygen and nutrient exchanges along the longitudinal axis of Chesapeake Bay: seasonal patterns, controlling factors and ecological significance. Estuaries Coasts 19: 562–58. doi: 10.2307/1352518

Cushing, D.H. 1989. A difference in structure between ecosystems in strongly stratified waters and in those that are only weakly stratified. J. Plankton Res. 11: 1-13. doi: 10.1093/plankt/11.1.1

de Madariaga, I., and E. Orive. 1989. Spatio-temporal variations of size-fractionated primary production in the Gernika estuary. J. Exp. Mar. Biol. Ecol. 127: 273–288. doi: 10.1016/0022-0981(89)90079-8

Devassy, V.I., and J.I. Goes. 1988. Phytoplankton Community Structure and Succession in a Tropical Estuarine Complex (Central West Coast of India). Estuar. Coast. Shelf Sci. 27: 671–685. doi: 10.1016/0272-7714(88)90074-1

Domingues, R.B., T.P. Anselmo, A.B. Barbosa, U. Sommer, and H.M. Galvão. 2011. Light as a driver of phytoplankton growth and production in the freshwater tidal zone of a turbid estuary. Estuar. Coast. Shelf Sci. 91: 526–535. doi: 10.1016/j.ecss.2010.12.008

DuRand, M.D., R.J. Olson, and S.W. Chisholm. 2001. Phytoplankton population dynamics at the Bermuda Atlantic Time-series station in the Sargasso Sea. Deep Sea Res. Part II: Top. Stud. Oceanogr. 48: 1983–2003. doi:10.1016/S0967-0645(00)00166-1

Fichez, R., T.D. Jickells, and H.M. Edmunds. 1992. Algal blooms in the high turbidity, a result of the conflicting consequences of turbulence on nutrient cycling in a shallow water estuary. Estuar. Coast. Shelf Sci .35: 577–592. doi:10.1016/S0272-7714(05)80040-X

Fisher, T.R., P.R. Carlson, and R.T. Barber. 1982. Sediment nutrient regeneration in three North Carolina estuaries. Estuar. Coast. Shelf Sci. 14: 101–116. doi: 10.1016/S0302-3524(82)80069-8

Fisher, T.R., L.W. Harding, and L.G. Ward. 1988. Phytoplankton, nutrients and turbidity in the Chesapeake, Delaware and Hudson estuaries. Estuar. Coast. Shelf Sci. 27: 61–93. doi: 10.1016/0272-7714(88)90032-7

Gaarder, T., and H.H. Gran. 1927. Investigation on the production of plankton in the Oslo-Fjord. Rapp. P.-v. Réun. Cons. Int. Explor. Mer 42:1–48.

García-Martín, E.E., P. Serret, and M. Pérez-Lorenzo. 2011. Testing potential bias in marine plankton respiration rates by dark bottle incubations in the NW Iberian shelf: incubation time and bottle volume. Cont. Shelf Res. 31: 496–506. doi:10.1016/j.csr.2010.07.006

García-Robledo, E., A. Corzo, and S. Papaspyrou. 2014. A fast and direct spectrophotometric method for the sequential determination of nitrate and nitrite at low concentrations in small volumes. Mar. Chem. 162: 30–36. doi:10.1016/j.marchem.2014.03.002

Gasol, J.M., and P. del Giorgio. 2000. Using flow cytometry for counting natural planktonic bacteria and understanding the structure of planktonic bacterial communities. Sci. Mar. 64: 197–224.

Geider, R.J., H.L. MacIntyre, and T.M. Kana. 1997. Dynamic model of phytoplankton growth and acclimation: responses of the balanced growth rate and the chlorophyll a: carbon ratio to light, nutrient-limitation and temperature. Mar. Ecol. Prog. Ser. 148:187–200. doi: 10.3354/meps148187

Gocke, K., J. Cortés, and C. Villalobos. 1990. Effects of red tides on oxygen concentration and distribution in the Golfo de Nicoya, Costa Rica. Rev. Biol. Trop. 38: 401–407.

Gocke, K., J. Cortés, and M.M. Murillo. 2001a. The annual cycle of primary productivity in a tropical estuary, the inner regions of the Golfo de Nicoya, Costa Rica. Rev. Biol. Trop. 49: 289–306.

Gocke, K., J. Cortés, and M.M. Murillo. 2001b. Planktonic primary production in a tidally influenced mangrove forest on the Pacific coast of Costa Rica. Rev. Biol. Trop. 49: 279–288.

Goldman, C.R., 1988. Primary productivity, nutrients, and transparency during the early onset of eutrophication in ultra-oligotrophic Lake Tahoe, California-Nevada. Limnol. Oceanogr. 33: 1321–1333. doi: 10.4319/lo.1988.33.6.1321.

Grasshoff K., K. KremLing, and M. Ehrhardt. 1999. Frontmatter, in Methods of Seawater Analysis, 3rd ed. Wiley-VCH Verlag GmbH, Weinheim, Germany.

Grobbelaar, J.U. 1985. Phytoplankton productivity in turbid waters. J. Plankton Res. 7: 653–663. doi: 10.1093/plankt/7.5.653

Hargraves, P.E., and R. Víquez. 1985. Spatial and temporal distribution of phytoplankton in the Gulf of Nicoya, Costa Rica. Bull. Mar. Sci. 37: 557–585.

Hillebrand, H., C.D. Dürselen, D. Kirschtel, T. Zohary, and U. Pollingher. 1999. Biovolume calculation for pelagic and benthic microalgae. J. Phycol. 35: 403–424. doi: 10.1046/j.1529-8817.1999.3520403.x

Howard, K. M., and L. R. Joint. 1989. Physiological ecology of picoplankton in the North Sea. Mar. Biol. 102: 275-281. doi: 10.1007/BF00428289

Huang, L., W. Jian, X. Song, X. Huang, S. Liu, P. Qian, K. Yin, and M. Wu. 2004. Species diversity and distribution for phytoplankton of the Pearl River Estuary during rainy and dry seasons. Mar. Pollut. Bull. 49: 588–596. doi:10.1016/j.marpolbul.2004.03.015

Humborg, C., V. Ittekkot, A. Cociasu, and B.V. Bodungen. 1997. Effect of Danube River dam on Black Sea biogeochemistry and ecosystem structure. Nature. 386: 385–8. doi:10.1038/386385a0

Iriarte, A., and D. A. Purdie. 1994. Size distribution of chlorophyll a biomass and primary production in a temperate estuary (Southampton Water): the contribution of photosynthetic picoplankton. Mar. Ecol. Prog. Ser. 115: 283–297. doi: 10.3354/meps115283

Kress, N., S. Brenner, S. León Coto, C.L. Brenes, and C. Arroyo. 2002. Horizontal transport and seasonal distribution of nutrients, dissolved oxygen and chlorophyll-a in the Gulf of Nicoya, Costa Rica: a tropical estuary. Cont. Shelf Res. 22: 51– 66. doi: 10.1016/S0278-4343(01)00064-4

Labasque, T., C. Chaumery, A. Aminot, and G. Kergoat. 2004. Spectrophotometric Winkler determination of dissolved oxygen: re-examination of critical factors and reliability. Mar. Chem. 88: 53 – 60. doi: 10.1016/S0304-4203(04)00058-1.

Lancelot, C., and K. Muylaert. 2011. Trends in Estuarine Phytoplankton Ecology. Treatise on Estuarine and Coastal Science 7: 5–16. doi:10.1016/B978-0-12-374711-2.00703-8

Li, L., L. SongHui, J. Tao, and L. Xia. 2013. Seasonal variation of size-fractionated phytoplankton in the Pearl River Estuary. Chinese Sci. Bull. 58: 2303–2314. doi: 10.1007/s11434-013-5823-1

Lizano, O.G., and J.A. Vargas. 1993. Distribución espacio-temporal de temperatura y salinidad en la parte interna del Golfo de Nicoya. Tecnol. Marcha. 12: 3–16.

Malone, T.C., 1980. Algal size. In I. Morris, ed. The physiological ecology of phytoplankton. University of California Press, Berkeley.

Malone, T.C., S.E. Pike, and D.J. Conle. 1993. Transient variations in phytoplankton productivity at the JGOFS Bermuda time series station. Deep Sea Res. Part I: Oceanogr. Res. Pap. 40: 903–924. doi:10.1016/0967-0637(93)90080-M

Marañón, E., M.J. Behrenfield, N. González, B. Mourino, and M. Zubvok. 2003. High variability of primary production in oligotrophic waters of the Atlantic Ocean: Uncoupling from phytoplankton biomass and size structure. Mar. Ecol. Prog .Ser. 257: 1–11. doi:10.3354/meps257001

Marie, D., Simon N., and Vaulot D. 2005. Phytoplankton cell counting by flow cytometry. In Andersen R.A., ed. Algal Culturing Techniques. Academic Press, London.

Meyercordt, J., S. Gerbersdorf, and L.A. Meyer-Reil. 1999. Significance of pelagic and benthic primary production in two shallow coastal lagoons of different degrees of eutrophication in the southern Baltic Sea. Aquat. Microb. Ecol. 20: 273–284. doi: 10.3354/ame020273

Nittrouer, C., G.J. Brunskill, and A.G. Figueiredo. 1995. Importance of tropical coastal environments. Geo-Mar. Lett. 15: 121–126.

Palter, J., S. León Coto, and D. Ballestero. 2007. The distribution of nutrients, dissolved oxygen and chlorophyll a in the upper Gulf of Nicoya. Costa Rica, a tropical estuary. Rev. Biol. Trop. 55: 427–436.

Pamplona, F.C, E.T. Paes, and A. Nepomuceno. 2013. Nutrients fluctuations in the Quatipuru River: A macrotidal estuarine mangrove system in the Brazilian Amazonian basin. Estuar. Coast. Shelf Sci. 133: 273–284. doi: 10.1016/j.ecss.2013.09.010

Peterson, C.L. 1958. The physical oceanography of the Gulf of Nicoya, Costa Rica, a tropical estuary. Bull. Inter. Am. Trop. Tuna Comm 4: 137–216.

Ram, A.S.P., S. Nair, and D. Chandramohan. 2003. Bacterial growth efficiency in the tropical estuarine and coastal waters of Goa, southwest coast of India. Microb. Ecol. 45: 88–96.

Reynolds, C. S. 2006. Ecology of phytoplankton. Cambridge University Press. 551 p. doi: 10.1017/CBO9780511542145

Ritchie, R.J. 2008. Universal chlorophyll equations for estimating chlorophylls a, b, c, and d and total chlorophylls in natural assemblages of photosynthetic organisms using acetone, methanol, or ethanol solvents. Photosynthetica 46: 115–126. doi: 10.1007/s11099-008-0019-7

Rochelle-Newall, E.J., V.T. Chu, O. Pringault, D. Amouroux, R. Arfi, Y. Bettarel, and J. P. Torréton. 2011. Phytoplankton distribution and productivity in a highly turbid, tropical coastal system (Bach Dang Estuary, Vietnam). Mar. Pollut. Bull. 62: 2317–2329. doi:10.1016/j.marpolbul.2011.08.044

Ryther, J. H. 1956. The measurement of primary production. Limnol. Oceanogr. 1: 72–84. doi: 10.4319/lo.1956.1.2.0072

Seguro, I., C.M. García, S. Papaspyrou, and others. 2015. Seasonal changes of the microplankton community along a tropical estuary. Reg. Stud. Mar. Sci. 2: 189-202. doi:10.1016/j.rsma.2015.10.006

Shalapyonok, A., R.J. Olson, and L.S. Shalapyonok. 2001. Arabian Sea phytoplankton during southwest and northeast monsoons 1995: composition, size structure and biomass from individual cell properties measured by flow cytometry. Deep Sea Res. Part II: Top. Stud. Oceanogr. 48: 1231–1261. doi: 10.1016/S0967-0645(00)00137-5

Sin, Y., R.L. Wetzel, and I.C. Anderson. 2000. Seasonal variations of size-fractionated phytoplankton along the salinity gradient in the York River estuary, Virginia (USA). J. Plankton Res. 22: 1945–1960. doi: 10.1093/plankt/22.10.1945

Stauffer, R. E., G. F. Lee, and D. E. Armstrong. 1979. Estimating chlorophyll extraction biases. J. Fish. Res. Bd Can. 36:152-157. doi: 10.1139/f79-024

Strickland, J.D.H. 1970. The Ecology of the Plankton Off La Jolla, California, in the Period April Through September, 1967. Bull. Scripps Inst. Oceanogr.

Tackx, M.L.M. , P.J.M. Herman, S. Gasparini, X. Irigoien, R. Billiones, M.H. Daro. 2003. Selective feeding of *Eurytemora affinis* (Copepoda, Calanoida) in temperate estuaries: model and field observations. Estuar. Coast. Shelf Sci. 56: 305–311. doi: 10.1016/S0272-7714(02)00182-8.

Thill, A., S. Moustier, J.M. Garnier, C. Estournel, J.J. Naudin, and J.Y. Bottero. 2001. Evolution of particle size and concentration in the Rhone river mixing zone: influence of salt flocculation. Cont. Shelf Res. 21: 2127–2140. doi: 10.1016/S0278-4343(01)00047-4

Thingstad, T.F., and F. Rassoulzadegan. 1999. Conceptual models for the biogeochemical role of the photic zone microbial food web, with particular reference to the Mediterranean Sea. Prog. Oceanogr. 44: 271–286. doi:10.1016/S0079-6611(99)00029-4

Underwood, G.J.C., and J. Kromkamp. 1999. Primary Production by Phytoplankton and Microphytobenthos in Estuaries. Adv. Ecol. Res. 29: 93–153. doi: 10.1016/S0065-2504(08)60192-0

Verney, R., R. Lafite, and J.C. Brun-Cottan. 2009. Flocculation Potential of Estuarine Particles: The Importance of Environmental Factors and of the Spatial and Seasonal Variability of Suspended Particulate Matter. Estuaries Coasts 324: 678–693. doi: 10.1007/s12237-009-9160-1

Voorhis, A., C.E. Epifanio, D. Maurer, A.I. Dittel, and J.A. Vargas. 1983. The estuarine character of the Gulf of Nicoya and embayment on the Pacific coast of Central America. Hydrobiologia 99: 225–237. doi: 10.1007/BF00008774

Worden, A.Z., J.K. Nolan, and B. Palenik. 2004. Assessing the dynamics and ecology of marine picophytoplankton, the importance of the eukaryotic component. Limnol. Oceanogr. 49: 168–179.

Yin, K., P.J. Harrison, S. Pond, and R.J. Beamish. 1995. Entrainment of nitrate in the Fraser River Estuary and its biological implications. Estuar. Coast. Shelf Sci. 40: 505–528. doi:10.1006/ecss.1995.0036

Zhang, X., Z. Shi, X. Huang, F. Ye, and Q. Liu. 2013. Phytoplankton abundance and size-fractionated structure in three contrasting periods in the Pear River Estuary. J. Mar. Res. 71: 187–210. doi: 10.1357/002224013807719464

CHAPTER III

Spatiotemporal changes in microbial patterns based on abundances and single-cell traits along a tropical estuarine gradient

Spatiotemporal changes in microbial patterns based on abundances and single-cell traits along a tropical estuarine gradient

Sara Soria-Píriz[1*], Virginia Aguilar[1], Sokratis Papaspyrou[1], Emilio García-Robledo[1], Isabel Seguro[1+], Álvaro Morales Ramírez[2] and Alfonso Corzo[1]

[1]Department of Biology, Faculty of Marine and Environmental Sciences, University of Cádiz, Campus of International Excellence (CEIMAR), Polígono Rio San Pedro s/n 11510 Puerto Real, (Cádiz) Spain.

[2]Centro de Investigación en Ciencias del Mar y Limnología (CIMAR), P.O. Box 2060 San Pedro de Montes de Oca, Costa Rica.

* corresponding author: Department of Biology, Faculty of Marine and Environmental Sciences, University of Cádiz, Polígono Río San Pedro s/n 11510 Puerto Real (Cádiz), Spain Tel. 34-956-016774

Present address

+ Centre for Ocean and Atmospheric Sciences, School of Environmental Sciences, University of East Anglia, Norwich, NR4 7TJ, United Kingdom.

ABSTRACT: The interactions between the different components of the microbial food web are still poorly studied in tropical estuaries. The Gulf of Nicoya (northwest Pacific coast of Costa Rica) is considered one of the most productive estuaries in the world and represents a model system for the estuaries of Central America. We examined the spatiotemporal changes in the environmental gradient along the estuary and the interactions among the main components of the microbial community i.e., photosynthetic picocyanobacteria, pico- and nanoeukaryotes and heterotrophic bacteria based on their abundance and single-cell properties during the rainy and the dry seasons along the riverine-marine gradient. Multivariate ordination of the microbial assemblages revealed different ecological relationships among the phyto- and bacterioplankton assemblages between seasons (rainy and dry). Our results clearly show that the patterns among the microbial assemblages were more similar during the dry season. This suggests that seasonal changes in allochthonous organic carbon inputs, inorganic nutrients and solar radiation could be the major driver of the degree of coupling between the phyto- and bacterioplankton assemblages along this tropical estuarine gradient.

KEYWORDS: phytoplankton, bacterioplankton, niche ordination, tropical estuary, seasonal, single-cell traits

1. Introduction

The aquatic microbial food web, which comprises of prokaryotic and eukaryotic organisms, plays an essential role in the recycling of nutrients and organic matter (OM) and the regulation of energy transfer to higher trophic levels (Pomeroy 1974; Azam et al. 1983; Fenchel and Finlay 2008). Nowadays, it is assumed that these interactions and carbon flow patterns are being altered by global warming (von Scheibner et al. 2014). Interactions between phytoplankton and bacterioplankton communities in terms of production rates, biomass or diversity have been demonstrated in freshwater and marine systems (Bird and Kalff 1984; Weisse et al. 1990; Gasol and Duarte 2000; Paver et al. 2013). However, the information on spatiotemporal distribution and interactions among different components of microbial communities on changing environmental conditions are still limited.

Flow cytometry (FCM) techniques allow to describe simultaneously the relative abundance of various components of the microbial community and their cell-specific properties, like intensity of fluorescence in different spectral windows, related to pigment or nucleic acid content, and light scatter, related to cell size and cell granularity. This information allows to investigate spatiotemporal changes in the structure of the microbial assemblage (Rodríguez 1994; Dubelaar and Jonker 2000; Gasol and Del Giorgio 2000; Bouvier et al. 2007) and can provide insight into the processes or environmental factors driving microbial community structure and functions (Horner-Devine et al. 2007; Borcard 2012).

Estuaries are among the most productive systems worldwide and are under increasing human pressure. Estuaries represent natural laboratories to investigate microbial interactions since they exhibit strong spatiotemporal gradients of salinity, turbidity and resources availability. Consequently, microbial communities show highly variable characteristics across these conditions, affecting the fate of organic carbon (Bouvier and del Giorgio 2002; Crump et al. 2007; Li et al. 2017; Xenopoulos et al. 2017). Within the estuaries, tropical ones have some singular additional characteristics: they are exposed to high constant irradiance and temperature year round and large variations in river runoff during the two contrasting seasons, the rainy (wet) and dry seasons. In addition, in tropical estuaries many important aspects regarding the functioning of the pelagic microbial web and the interactions between the different components of the microbial community are still poorly studied (Nittrouer et al. 1995; Roland et al. 2010, Cloern et al. 2014).

The present article describes, for the first time, the structure and dynamics of the pelagic microbial community of the inner part of the Gulf of Nicoya (northwest Pacific coast of Costa Rica) along the riverine-marine gradient, based on their abundance and single-cell properties during the rainy and the dry seasons. This estuary is considered one of the most productive estuaries in the world and represents a model system for the estuaries of Central America (Gocke et al. 1990, 2001a; b; Córdoba-Muñoz 1998; Cloern et al. 2014; Soria-Píriz et al. 2017). Thus, our aims were to (1) analyze the spatiotemporal changes in the structure of the microbial community in terms of the abundance and single-cells characteristics of its major components (photosynthetic picocyanobacteria, pico- and nanoeukaryotes and heterotrophic bacteria); (2) link the spatiotemporal changes in the microbial community to changes in relevant environmental properties along the estuarine gradient; and (3) investigate the possible similarity among the spatiotemporal distributions of the different microbial assemblages to examine the degree of coupling between them. The results show differences in the response of the different microbial assemblages to the spatiotemporal changes along the estuarine gradient and a higher degree of coupling among the phototrophic and heterotrophic components of the pelagic microbial community during the dry season.

2. Materials and Methods

2.1. Study site and sampling

The inner basin of the Gulf of Nicoya (northwest Pacific coast of Costa Rica) extends from the Tempisque River mouth down to near the Puntarenas channel (Fig. 1). This section is strongly influenced by seasonal changes in the Tempisque River freshwater discharges, being the estuary partially stratified during the rainy season and fully mixed during the dry season (Kress et al. 2002; Seguro et al. 2015; Soria-Píriz et al. 2017). It is a shallow area (< 20 m) with extensive tidal flats surrounded mainly by mangroves. Tides are semidiurnal with mean amplitude of 2.5 m (MIO-CIMAR 2012).

Samplings were carried out along the transect spanning the salinity gradient divided in five stations, one station per day, during both rainy (31th July - 5th August 2011) and dry seasons (14th - 18th April 2012) in flood tide conditions. The innermost station (St. 1) was located close to the Tempisque River mouth and the most marine station (St. 5) close to the Caballo Island (Fig.1). Water column salinity, temperature (T, ºC), and fluorescence (r.u) were measured in situ using a multiparameter probe (YSI 6600). Water samples were collected with a 10 L Niskin bottle from the surface layer (0.5 m depth) and one meter under the halocline during the rainy season or one meter above the bottom during the dry season.

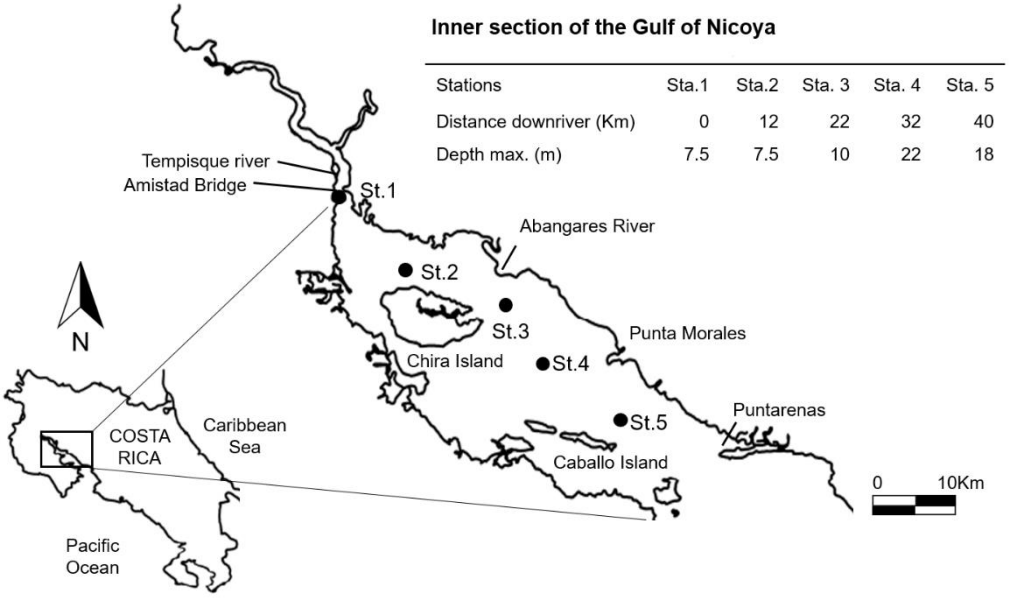

Fig. 1. Map of the Gulf of Nicoya (Costa Rica). The longitudinal transect spanned the entire length of the inner part of the Gulf of Nicoya from the riverine station (St.1) to the more marine station (St.5).

2.2. Inorganic nutrients, chromophoric dissolved organic matter and dissolved organic carbon

Inorganic nutrients were analyzed in filtered water samples (MF 300, 0.7 µm, 47 mm, Fisherbrand™), stored on ice and frozen at -20 ºC upon return to the laboratory. Ammonium (Bower

and Holm-Hansen 1980), nitrate and nitrite (García-Robledo et al. 2014), and phosphate (PO_4^{3-}) (Grasshoff et al. 1999) were measured with detection limits ranging between 0.2 and 0.8 µmol L^{-1}.

For determination of chromophoric dissolved organic matter (CDOM), samples were filtered in situ through double filters (GF/F glass fiber filters, 0.7 µm, 47 mm, Whatman® and a cellulose acetate filter, 0.2 µm, 47 mm, Fisher Scientific™) in combusted glass vials, stored at 4 °C and analysed the following day on a Shimadzu UV-1700 spectrophotometer on 10 cm quartz cells. Light absorption (m^{-1}) at 440 nm was used as a proxy of CDOM concentration. The spectral region between 400 to 440 nm was used to determine the slope of the CDOM light absorption spectrum (Stedmon et al. 2000; Seguro et al. 2015).

Dissolved organic carbon (DOC) was measured in water samples (approximately 20 mL) during the dry season, filtered through nylon filters (Nylon Syringe filters, 0.2 µm, 30 mm, Thermo Scientific™) in acid washed glass vials (n = 1) and stored at 4ºC. DOC contents were determined on a Shimadzu TOC-5050 analyzer on acidified samples (1 mL of phosphoric acid 1:3) (ICMAN-CSIC external services).

2.3. Chlorophyll concentrations and depth integrated net community production

Chlorophyll concentration was estimated from the fluorescence signal of the YSI 6600 multiparameter probe. Photosynthetically active irradiance profiles (PAR, µmol photons m^{-2} s^{-1}) were determined by a LiCor (Li-250A) radiometer. Profiles were used to measure I_o and calculate k as the slope of decreasing exponential function of PAR irradiance with depth (Kirk 1994), during the dry and the rainy seasons (Table S1).

During the dry season, volumetric rates of net community planktonic production ($Pn_)$ were determined *in situ* for selected depths using the light and dark bottle incubation technique. Rates were transformed to daily rates and integrated for the photic layer to calculate the net daily depth-integrated plankton community production (NCP) as described in Soria-Píriz et al (2017). Unfortunately, during the rainy season, *in situ* measurements of Pn failed. In this case, P*n* (mmol O_2 m^{-3} h^{-1}) for the rainy season was estimated using the experimental linear correlation obtained for the dry season data (Pn = 0.0016 [Chl *a* [Io/k]] – 9.1623, r = 0.54, p = 0.021, Soria-Píriz et al 2017) between Pn and the product of chlorophyll a concentration (Chl *a*, mg m^{-3}) by the ratio between incident irradiance at the surface (I_o, µmol photons m^{-2} s^{-1}) and the extinction coefficient (k, m^{-1}) according to the empirical model of Cole and Cloern (1984, 1987) (Table 1).

2.4. Flow cytometry analyses

Water samples (n = 2) were fixed in cryotubes (4.5 mL) using glutaraldehyde (1% final concentration) (Vaulot et al. 1989) and frozen at – 80 ºC until analysis. Samples were left to thaw at room temperature. Phytoplankton groups were identified based on their autofluorescence, while for bacterioplankton groups, 10 µL of SYBR® Green-I (Molecular Probes #S7563) were added to 1 mL water sample (2.5 µM final concentration) and incubated for 10 min at room temperature in darkness before analysis (Lebaron et al. 2001; Corzo et al. 2005). A known amount of autofluorescent beads (1.1 µm diameter, Ex/Em: 430/465 nm, FluoSpheres® Molecular Probes Inc.™) were added to each sample as an internal standard. Samples were analyzed by the same researcher on a Dako CyAnTM ADP (Beckman Coulter™) flow cytometer at low flow rate, and were run until at least 30000 counts were recorded.

Cells were excited at 488 and 635 nm and the different populations were distinguished according to their 90° light scatter (SSC) and several fluorescence bands (red and orange fluorescences for the phytoplankton cells and green fluorescence for the stained bacterial cells). The average

fluorescence and SSC values of phyto- and bacterioplankton subgroups were standardized to those of the reference beads to account for potential differences in measurement conditions. Phytoplankton cells were classified in four assemblages based on their orange (phycoerythrin) or red (chlorophyll) fluorescence signals when excited by 488 nm laser, the red florescence signal (phycocyanin) when excited by the 635 nm laser and SSC signals (Marie et al. 2005; Calvo-Díaz and Morán 2006; Liu et al. 2014). Two populations of *Synechococcus*, one containing only phycocyanin (Syn-PC) and another one with both phycocyanin and phycoerythrin (Syn-PE) were distinguished according to their differences in the phycocianin fluorescence signal (Rajaneesh and Mitbavkar 2013; Liu et al. 2014). Picoeukaryotes (PEuk) and nanoeukaryotes (NEuk) were quantified as well (Fig. S1a-c). SSC signal was used as a proxy of cell size and the fluorescence-to-SSC ratio by cell (FL/SSC) was used here as a proxy for cellular pigment content to cell size ratio. Two populations of non-photosynthetic prokaryotes (bacteria in a general sense) were classified and quantified by their green fluorescence and SSC signals as high nucleic acid content (HNA) and low nucleic acid content bacteria (LNA) (Lebaron et al. 1998; Corzo et al. 1999; Gasol and del Giorgio 2000) SSC signal was used as a proxy of bacterial cell size and the green fluorescence-to-SSC ratio by cell (FL/SSC) as a proxy of cellular nucleic acid content to cell size ratio. We were able to distinguish photosynthetic picoplankton (picocyanobacteria) from non-photosynthetic picoplankton (heterotrophic bacteria) by inspecting the green fluorescence versus orange or red fluorescence cytograms. Events corresponding to picocyanobacteria were removed to avoid overlapping with heterotrophic bacteria. The sample at Sta. 5 from the bottom layer during the rainy season was not available.

Statistical analyses

Simple linear correlation analyses (Spearman) were used to test statistical significance of covariation between the environmental variables and the salinity gradients in both seasons and layers. Environmental and cytometric variables were normalized (0 to 1) to remove differences in scales prior to multivariate statistical analyses. Non-metric multidimensional scaling (nMDS) ordination analysis of Euclidean distances of environmental gradients and of every microbial subgroup in each season (rainy and dry) was performed using the metaMDS() function (R package vegan version 2.5-4) (Oksanen et al. 2019). Spearman correlations were determined to assess relationships between the environmental variables and the axes of every microbial community subgroup ordination plot. The envfit() function was used for fitting environmental variables, where the length of the arrow is proportional to the correlation between ordination and environmental variable. The number of permutations in the envfit() function was set at 9999. Relate resemblance matrices of every microbial subgroup based on their abundance and single-cells traits in each season were calculated based on ρ (Spearman rank correlation) values of all pairwise comparisons between those matrices using the metaMDS() function (R package vegan version 2.5-4) (Oksanen et al. 2019). These data were represented on a second-stage nMDS plot (Clarke et al. 2006).

3. Results

3.1 Environmental gradient along the estuary

In the inner part of the Gulf of Nicoya, similar salinity trends were observed in both seasons, with salinity increasing progressively from the river seaward (Fig 2). However, during the rainy period, due to the higher discharges from the Tempisque River, the increase was more gradual than during the dry season (Fig. 2a). Temperature values were around 26 – 31 ºC, with the highest values being observed

at the surface of St. 2 during the rainy season and from the middle of the estuary seaward during the dry season; the lowest values were registered in the bottom layer (Fig. 2b). Dissolved inorganic nitrogen (DIN=NH_4^++NO_3^-+NO_2^-) concentrations were always higher at the estuary head, slightly more in the bottom layer, and decreased seawards (Fig. 2c). PO_4^{3-} concentrations also decreased seaward, but showed higher values during the dry season (Fig. 2d). PO_4^{3-} concentrations showed high and negative correlations with salinity during the rainy season in both layers ($r = -0.99$, $p < 10^{-5}$, $n = 5$). CDOM presented its highest values during the rainy season at the head of the estuary, especially in the surface layer, with values decreasing seawards in both seasons. During the dry season, CDOM values in both layers were one order of magnitude lower compared to the rainy season. CDOM showed negative correlations with salinity in both layers ($r = -0.99$, $p < 10^{-5}$, $n = 5$) (Fig. 2e). The slope of the CDOM absorbance spectra, considered a proxy of the degree of OM lability, increased seaward in both seasons (Fig. S1a). DOC, measured only in the dry season, correlated linearly with CDOM ($r^2 = 0.89$, $p = 0.0006$, $n = 10$, Fig. S1b). The integrated net plankton community production (NCP) showed a similar pattern in both seasons with positive values only in the middle of the estuary (Sta. 3), with values being higher during the dry season than during the rainy season (Fig. 2f).

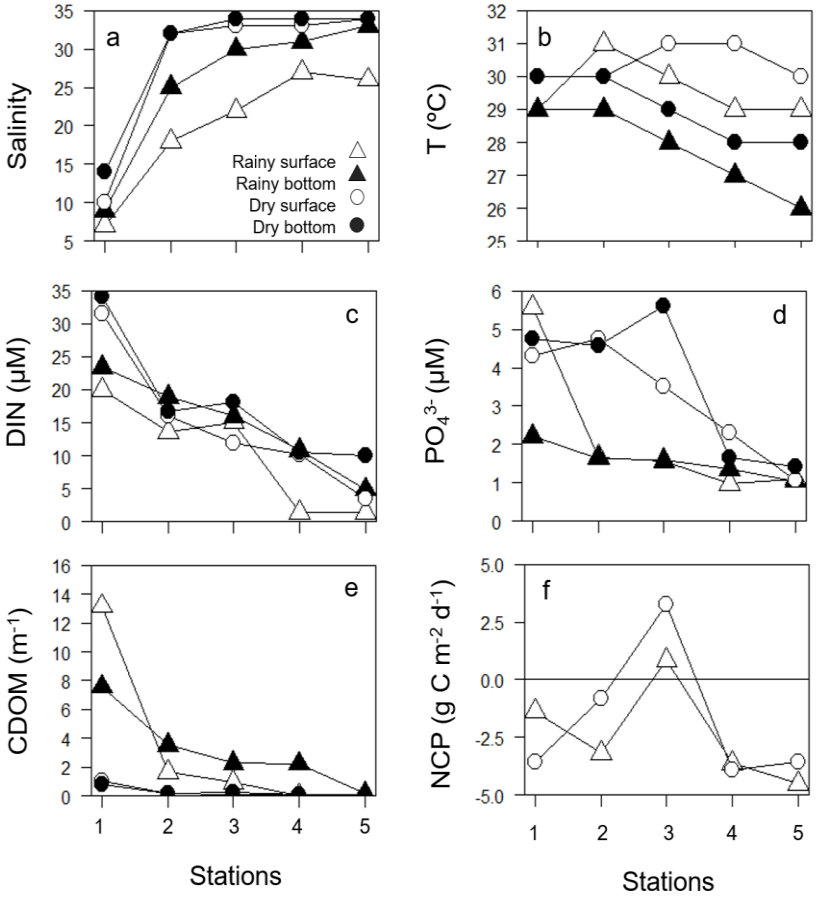

Fig. 2: *Longitudinal distribution* of (a) Salinity, (b) Temperature (T), (c) dissolved inorganic nitrogen (DIN), (d) phosphate (PO_4^{3-}), (e) chromophoric dissolved organic matter (CDOM) and (f) daily net depth-integrated planktonic community production (NCP) at the surface and bottom layers of the five stations sampled along the inner part of the Gulf of Nicoya during July 2011 (rainy) and April 2012 (dry).

Multivariate analysis of the environmental variables using nMDS confirmed the existence of strong gradients (salinity, CDOM, PO_4^{3-}) and the separation between the riverine (St. 1) and the more marine stations (St. 4 and 5) during the rainy season on the horizontal axis, especially in the surface layer (Fig. 3a). In the bottom layer, variability was less compared to the surface layer. On the vertical axis, differences were minor and correlated with temperature and NCP. During the dry season, a separation along the horizontal axis was observed as well, between the riverine (St. 1) and marine stations (St. 4 and 5), although less pronounced. In contrast, on the vertical axis, differences were higher than the rainy season correlating with the NCP (Fig. 3b).

3.2. Abundance and cell traits of phytoplankton assemblages

The four phytoplankton assemblages distinguished in the Gulf of Nicoya by FCM showed contrasting spatiotemporal distributions along the estuarine gradient. The Syn-PE was the most abundant photoautotrophic assemblage in the inner part of the Nicoya Gulf and increased seaward reaching very high values during the rainy season in the more marine sampling stations (Fig. 4d). The single cell traits measured in the study, SSC and FL/SSC, changed clearly along the estuary as well. Syn-PE SSC decreased along the estuary showing an inverse relation with abundance ($r = -0.99$, $p < 10^{-5}$, $n = 5$) (Fig. 4e). In contrast, Syn-PE FL/SSC did not correlate with Syn-PE abundance; values increased from the river to the middle of the estuary (Fig. 4f), being more variable further along.

The spatial distribution of Syn-PC abundance contrasted dramatically with that of Syn-PE abundance and was higher at the estuary head, especially in the bottom layer of both seasons (Fig. 4a). Abundance decreased seawards, except in the surface layer of the more marine stations during the rainy season, where its abundance increased considerably. Syn-PC SSC changed remarkably between seasons, depths and to a lesser degree along the estuary. Despite this high variability, as in the case of Syn-PE, the mean Syn-PC SSC showed a general trend to decrease seaward (Fig. 4b). Syn-PC FL/SSC ratio was higher in the middle of the estuary, except in the surface layer during the dry season that it varied more (Fig. 4c).

PEuk abundance did not show a clear seasonal pattern; low values were observed in the riverine station (St. 1), with maximum abundances in the middle of the inner gulf (Fig. 4g). Contrary to Syn-PE and Syn-PC, SSC of PEuk cells tended to increase seaward (Fig. 4h), suggesting a general increase in cell size. PEuk FL/SSC showed a very clear seasonality in the surface layer, increasing considerably seaward in the rainy season (Fig. 4i).

NEuk showed a general trend to decrease seaward in both seasons (Fig. 4j), while their SSC tended to reach a plateau in the middle of the estuary, except for the high value observed in the bottom water layer of St. 5 during the dry season (Fig. 4k). As with PEuk, NEuk FL/SSC was highest during the rainy season in the surface water layer, showing the same increasing trend seaward (Fig. 4l).

3.3. Abundance and cell traits of bacterioplankton assemblages

Two cytometric bacterial subpopulations or assemblages (HNA and LNA cells) were observed in all samples (Fig. S1d). Both HNA and LNA bacterial groups showed a general trend to increase toward the more marine stations except for HNA in the bottom water layer during the rainy season (Fig. 5a). HNA bacteria in the surface layer reached maximum abundances in the middle of the estuary (St. 3) during the rainy season and in the more marine stations during the dry season (Fig. 5a). LNA abundance showed a clear seasonality, being considerably higher during the dry season (Fig. 5d). In general, in each sample, LNA bacteria were slightly more abundant that the HNA, except for the bottom layer in St.1 and the surface layer in St. 3 during the rainy season, as indicated by the HNA/LNA ratio

ratio (Fig. 5g). This ratio showed a rather consistent pattern to decrease along the estuary, except for the high value observed in surface at Sta. 3 during the rainy season. HNA/LNA values along the estuary were generally higher during the rainy season.

SSC was generally higher in HNA than LNA bacteria, reaching maximum values at the surface layer of Sta. 3 during the rainy season (Fig. 5b). HNA SSC showed a larger variability, whereas LNA SSC was stable along the estuary. Minimum values of LNA SSC were observed in the surface layer along the estuary during the dry season (Fig. 5e). FL/SSC increased along the estuary for both HNA and LNA bacteria, suggesting a higher relative content of nucleic acid per cell seawards (Fig. 5c, f). LNA abundance was positively correlated to its respective FL/SSC signal in the surface water layer of the rainy season ($r = 0.9$, $p = 0.04$, $n = 5$) and in the bottom layer of the dry season ($r = 0.9$, $p = 0.04$, $n = 5$).

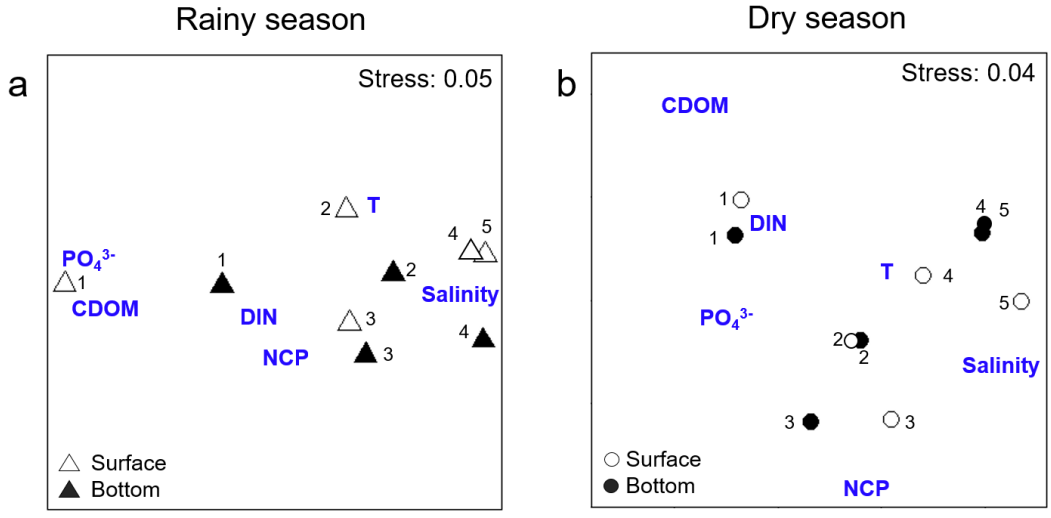

Fig. 3: *Two-dimensional nMDS ordination* of dissimilarity matrix (Euclidean distances) based on the normalized environmental variables (0 to 1) at the surface and bottom layers of the five stations sampled along the inner part of the Gulf of Nicoya during July 2011 (rainy) and April 2012 (dry). Variables in blue indicate the environmental factors i.e. Salinity, Temperature (T), dissolved inorganic nitrogen (DIN), phosphate (PO_4^{3-}), chromophoric dissolved organic matter (CDOM) and daily net depth-integrated planktonic community production (NCP).

3.4. Multivariate ordination of photoautotrophic community

The nMDS ordination of the sampling stations along the estuarine gradient, based on the abundance, SSC, and FL/SSC, of the various photoautotrophic assemblages, produced different results depending on the assemblage and season considered (Fig. 6).

The ordination of samples based on Syn-PE abundance and single-cell traits revealed a clear separation between the most riverine (St. 1) from the more marine stations (St. 4 and 5) in the surface and bottom water layers during both rainy and dry seasons. However, during the rainy season a smoother change was observed along the horizontal axis, whereas during the dry season, St. 1 was clearly separated from the rest of the stations that were grouped closely together (Fig. 6b). Among the

environmental variables, DIN showed a high correlation with the ordination plot during the rainy (r = 0.79, p = 0.009) and dry seasons (r = 0.71, p = 0.011). Salinity also significantly correlated with the ordination plot during the dry season (r = 0.59, p = 0.041) (Fig. 6b).

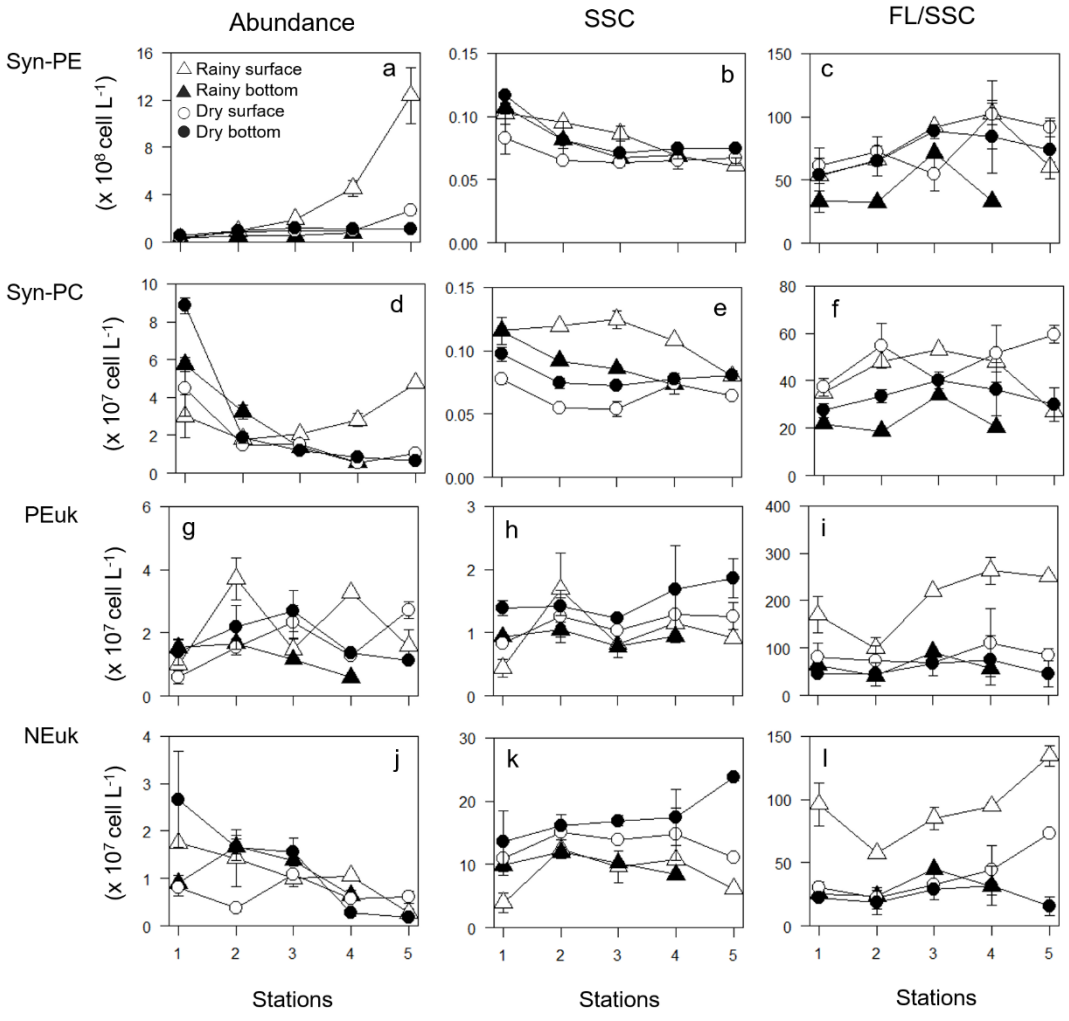

Fig. 4: *Longitudinal distribution* of the abundance and the single-cell characteristics i.e. Side scatter (SSC) and the Fluorescence-to-Side Scatter ratio (FL/SSC) of the photoautotrophic groups: (a-c) *Synechococcus* phycoerythrin-rich cells (Syn-PE), (d-f) *Synechococcus*- phycocyanin-rich cells (Syn-PC), (g-i) PicoEukaryotes (PEuk) and (j-l) NanoEukaryotes (NEuk) at the surface and bottom layers of the five stations sampled along the inner part of the Gulf of Nicoya during July 2011 (rainy) and April 2012 (dry).

Samples ordination based on Syn-PC abundance and single-cell traits showed that during the rainy season samples were quite dissimilar with more differences observed between bottom layer samples. In contrast, during the dry season, with the exception of St.1, samples were grouped close together (Fig. 6c, d). In the rainy season, temperature and salinity correlated marginally with the

ordination plot ($r = 0.65$, $p = 0.048$ and $r = 0.66$, $p = 0.041$ respectively) (Fig. 6c). In the dry season, DIN ($r = 0.82$, $p = 0.002$), salinity ($r = 0.76$, $p = 0.015$) and CDOM ($r = 0.69$, $p = 0.016$) showed high correlations with the ordination plot (Fig. 6d).

The nMDS ordination obtained from PEuk showed a clear separation between surface and bottom layers in both seasons but it did not present any clear pattern along the estuarine gradient (Fig. 6e, f). No environmental variable correlated significantly with the axes of PEuk-based ordination during either the rainy or the dry seasons.

The ordination based on NEuk during the rainy season presented a separation between the surface and bottom samples along the horizontal axis and between the riverine and the more marine stations in the surface layer associated to the vertical axis, while samples in the bottom layer were not clearly separated (Fig. 6g). During the dry season, a separation between surface and bottom layers samples was observed but only the bottom layer showed a clear distribution of samples along the estuary. Like previously observed for PEuk-based nMDS, no significant correlations between the NEuk-based habitats ordination and environmental variables were found during either of the seasons (Fig. 6h).

3.5. Multivariate ordination of bacterial assemblages

The nMDS of HNA abundance and single-cell traits showed considerable scattering suggesting large variations of this group during the rainy season, particularly for the surface samples. Only DIN showed a high correlation with the ordination plot ($r = 0.64$, $p = 0.046$) (Fig. 7a). During the dry season, the horizontal axis showed a clear separation between layers. DIN showed the highest correlation ($r = 0.84$, $p = 0.002$), followed by CDOM ($r = 0.67$, $p = 0.014$) and in a lesser extent salinity ($r = 0.59$, $p = 0.038$). In the bottom water layer, St. 4 and 5 were grouped closely together suggesting that HNA assemblage showed similar characteristics (Fig. 7b).

The LNA trait-based ordination in the rainy season showed a clear separation of the surface layer at St.1 and St. 5 with the rest of the samples which were grouped closely together. PO_4^{3-} ($r = 0.97$, $p = 0.024$), CDOM ($r = 0.84$, $p = 0.013$), and salinity ($r = 0.58$, $p = 0.047$) showed significant correlations with the ordination plot (Fig. 7c). In contrast, during the dry season, the samples along the estuary were distributed along the horizontal axis, whereas samples from the surface and bottom layers were separated along the vertical axis. In the bottom layer, St. 4 and St. 5 were very close, suggesting that LNA bacterial assemblage showed similar characteristics as observed previously for HNA bacteria. The horizontal axis of the nMDS plot correlated with DIN ($r = 0.94$, $p = 0.001$), salinity ($r = 0.69$, $p = 0.007$), CDOM ($r = 0.74$, $p = 0.002$) and PO_4^{3-} ($r = 0.56$, $p = 0.046$) (Fig. 7d).

3.6. Similarities in the ordination patterns of environmental variables and microbial assemblages

Second stage nMDS based on the individual ordinations of the environmental variables and the distinct microbial assemblages, including both primary producers and bacteria, revealed differences between the rainy and the dry season (Fig. 8, Table S2). During the rainy season, ordination patterns based on the abundance and single-cell traits of the different microbial groups and environmental variables were quite dissimilar, showing weaker relationships. Syn-PE showed a high correlation with Syn-PC, NEuk and HNA assemblages and LNA with the environmental ordination and NEuk assemblage (Fig. 8a, Table S2).

Interestingly, during the dry season, ordination patterns among the microbial assemblages were more similar, with microbial groups clustering closer together. The only exception was PEuk which only correlated with the environmental ordination. Syn-PE showed a high correlation with Syn-PC,

HNA and LNA. Syn-PC also showed a strong resemblance pattern with NEuk, HNA and LNA. NEuk with both HNA and LNA fractions. LNA sample ordinations were closely correlated to HNA and with environmental ordination (Fig. 8b, Table S2).

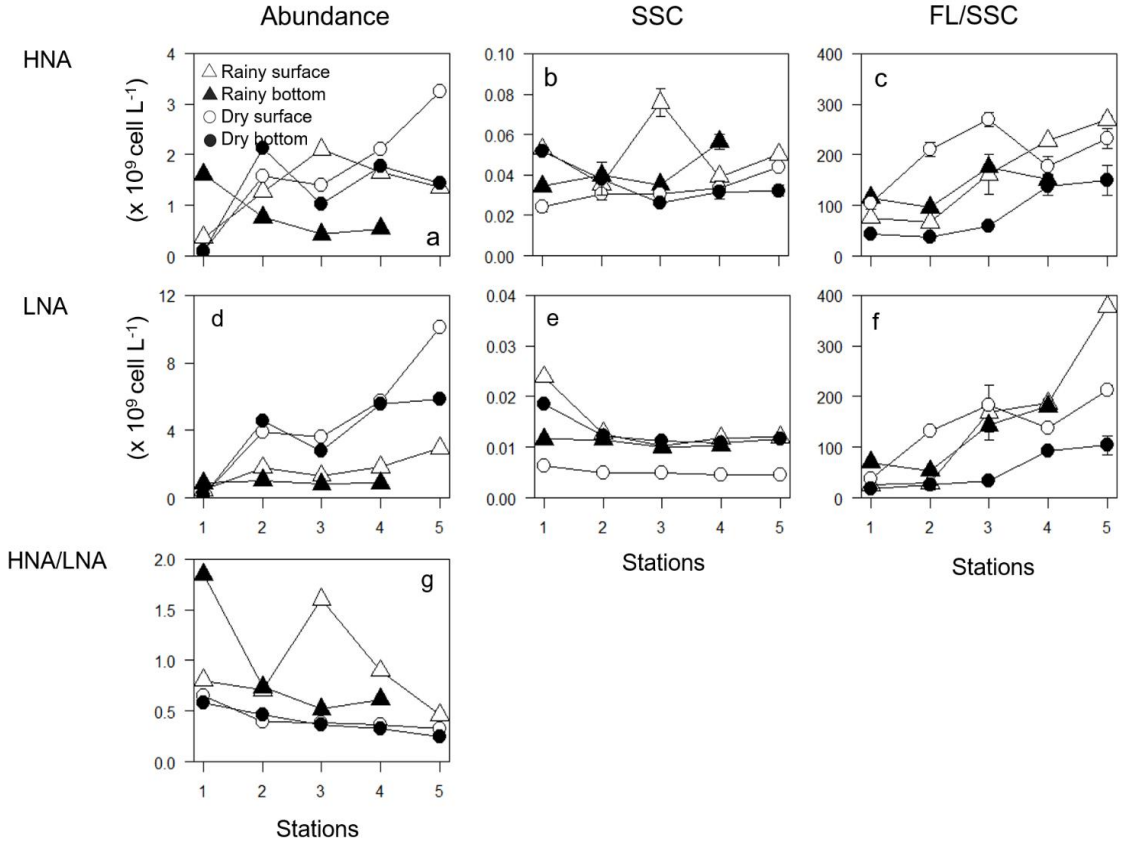

Fig. 5: *Longitudinal distribution* of the abundance and the single-cell characteristics i.e. Side scatter (SSC) and the Fluorescence-to-Side Scatter ratio (FL/SSC) of the of the bacterial groups: (a-c) high nucleic acid bacterial (HNA), (d-f) low nucleic acid bacterial (LNA) and (g) HNA-to-LNA ratio (HNA/LNA) at the surface and bottom layers of the five stations sampled along the inner part of the Gulf of Nicoya during July 2011 (rainy) and April 2012 (dry).

4. Discussion

4.1. Spatiotemporal changes in the environmental gradient along the estuary

Different estuarine zones were clearly distinguished based on the strong physicochemical gradients in both seasons (Fig. 2 and 3). The opposing gradients of decreasing nutrients (DIN and PO_4^{3-}) and CDOM and increasing salinity along the estuary and the clear separation between Sta. 1 and the rest of the stations in the ordination (Fig. 3), certainly indicate that the Tempisque River is the main contributor of allochthonous nutrients, and organic matter, for the microbial community in the inner part of the Gulf of Nicoya (Palter et al. 2007; Seguro et al. 2015; Soria-Píriz et al. 2017). The variations in the Tempisque freshwater discharge with season affect the hydrological circulation, water column

stability, residence time, turbidity, and resources availability. All the above, can result in the development of different microbial assemblages along the estuarine gradient (del Giorgio and Bouvier 2002; Crump et al. 2004; Lancelot and Muylaert 2011; Seguro et al. 2015).

Inorganic nutrients, CDOM and DOC concentrations decreased along the estuary in both seasons (Seguro et al. 2015, Soria-Píriz et al 2017). Interestingly, the concentration of inorganic nutrients (DIN and PO_4^{3-}) was similar in both seasons except for the high concentration of PO_4^{3-} found in Sta. 2 and 3, which could be associated with discharges of anthropogenic origin from the Abangares River (Soria-Píriz et al 2017). In contrast, the concentration of CDOM was considerably higher during the rainy season (Fig. 2e), suggesting a strong contribution of allochthonous OM from the watershed soils. Since the river flow doubles during the rainy season (Kress et al. 2002), the load of both inorganic nutrients and CDOM to the estuary is considerably higher during that season. Large inputs of allochthonous DOM, associated to higher river flow into the estuaries, are known to promote bacterial production, allowing the decoupling from autochthonous primary production (Figueroa et al. 2016; Andersson et al. 2018). The dramatic increase of CDOM during the rainy season went in parallel to a higher contribution of refractory organic compounds, characteristic of terrestrial soils (Bianchi et al. 1997; Abril et al. 2002) as suggested by the lower slope of CDOM absorption spectrum during this season. The relevance of the refractory material decreased seawards as the CDOM spectral slope increased (Fig. S1a). In contrast, the CDOM spectral slope indicated a higher lability of CDOM during the dry season with respect to the rainy season, particularly near the estuary head. This higher lability of CDOM during the dry season could be due to a higher proportion of *in situ* produced OM by phytoplankton (autochthonous origin). Net community production was indeed higher during the dry season despite the similar DIN and PO_4^{3-} concentrations in both seasons (Fig. 2f). During the dry season, incident irradiance was higher (Table 1), likely due to lower cloud cover in this season, favoring higher primary production rates (Cloern 1999). In addition, NCP showed a marked zonation with positive values only in the middle of the estuary in both seasons, as observed in other similar systems (Cloern 1987; Xiuren et al. 1988; Barrera-Alba et al. 2008). The positive NCP at this zone is a compromise between different cross-gradients along the estuary, i.e. nutrient and light availability, water column stability, and residence time (Cole and Cloern 1984, 1987; Cloern 1987; Lancelot and Muylaert 2011; Soria-Píriz et al. 2017). Overall, seasonal changes in terrestrial organic carbon inputs, inorganic nutrients and solar radiation could be the major drivers of the coupling between the phyto- and bacterioplankton assemblages along this tropical estuarine gradient as it has been suggested in other aquatic systems (Hitchcock and Mitrovic 2015; Figueroa et al. 2016; Andersson et al. 2018).

4.2. Changes in the phytoplankton assemblages along the estuarine gradient

The abundances of the photoautotrophic assemblages observed in the Gulf of Nicoya were similar to those reported in other tropical and subtropical estuaries (Li and Li 2012; Mitbavkar et al. 2012; Liu et al. 2014; Rajaneesh et al. 2018). The four assemblages showed very distinct spatiotemporal distributions in terms of both abundances and single cell traits along the estuary, which indicates their different niche preferences in response to the prevailing environmental gradients. In general, Syn-PC and NEuk decreased seaward, whereas the opposite was true for Syn-PE, particularly in the surface layer during the rainy season. In contrast, PEuk abundances were higher in the middle of the estuary, where maxima of NCP were observed in both dry and rainy seasons (Fig. 2, Soria-Píriz et al 2017).

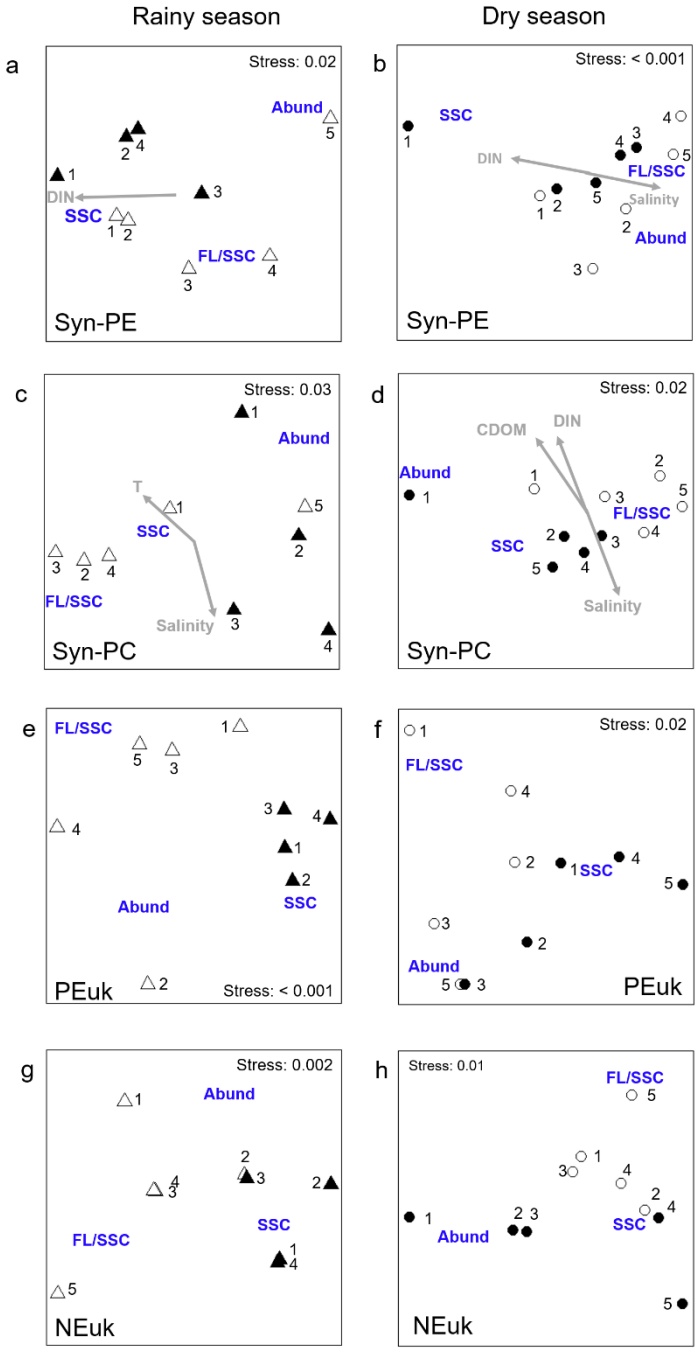

Fig. 6: *nMDS ordination* of the dissimilarity matrix (Euclidean distances) of the photoautotrophic groups: (a-b) *Synechococcus* phycoerythrin-rich cells (Syn-PE), (c-d) *Synechococcus*- phycocyanin-rich cells (Syn-PC), (e - f) picoeukaryotes (PEuk) and (g – h) nanoeukaryotes (NEuk) at the surface and bottom layers of the five stations sampled along the inner part of the Gulf of Nicoya during July 2011 (rainy) and April 2012 (dry). Variables in blue indicate the abundance (Abund) and the single cell traits i.e. side scatter (SSC) and fluorescence-to-side scatter ratio (FL/SSC). Arrows indicate significant Spearman correlations of environmental variables with the ordination axes ($p < 0.05$).

Syn-PC cells have a flow cytometry signature similar to that of *Prochlorococcus* sp. when they are analysed only with a single laser (488 nm) FCM and in the past they may have been misidentified by a freshwater or brackish water *Prochlorococcus*-like population (Vaulot et al. 1990; Corzo et al. 1999; Shang et al. 2007). However, these populations can be distinguished by using two lasers (488 and 635 nm) FCM (Murrell and Lores 2004; Rajaneesh and Mitbavkar 2013; Liu et al. 2014).

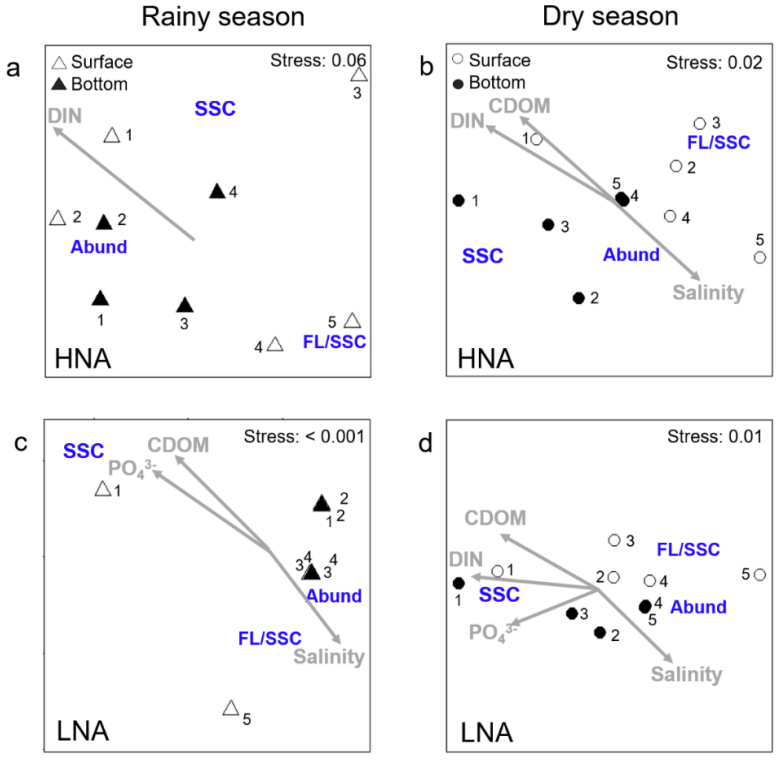

Fig.7: *nMDS ordination* of the dissimilarity matrix (Euclidean distances) of the bacterial groups: (a – b) high nucleic acid bacterial cells (HNA) and (c- d) low nucleic acid bacterial cells (LNA) at the surface and bottom layers of the five stations sampled along the inner part of the Gulf of Nicoya during July 2011 (rainy) and April 2012 (dry). Variables in blue indicate the abundance (Abund) and the single cell traits i.e. side scatter (SSC) and fluorescence-to-side scatter ratio (FL/SSC). Arrows indicate significant Spearman correlations of environmental variables with the ordination axes ($p < 0.05$).

A *Prochlorococcus*–like population, in addition to one of Syn-PC, has been recently reported in the Zuari estuary using two lasers FCM (Rajaneesh et al. 2018). However, in our samples from the Tempisque River estuary, no *Prochlorococcus* DNA was detected (Joe Taylor, unpublished data). Therefore, we think that in the inner part of the Nicoya Gulf the picocyanobacterial community is dominated by at least two different lineages of *Synechococcus*; Syn-PC is more abundant at lower salinities and Syn-PE more abundant at higher salinities seaward (Fig. 4), as has been observed in other estuaries and bays (Wang et al. 2011; Xia et al. 2015, 2017). In the inner Gulf of Nicoya, salinity, DIN and CDOM were the environmental factors significantly related with the spatiotemporal distribution of Syn-PC and Syn-PE (Fig. 6a-d). Our result are coincident with other studies where the abundance and diversity of the Synechococcus assemblage has been shown to be affected by nutrient availability (nitrate and phosphate) and salinity (Rajaneesh and Mitbavkar 2013; Xia et al. 2015, 2017; Sohm et al. 2016). Preferences of Syn-PC for rich-nutrients and high turbid waters and Syn-PE for oligotrophic and transparent waters have been seen in other aquatic systems (Pick 1991; Vörös et al. 1998; Camacho et al. 2003; Stomp et al. 2007). This may explain the inverse spatial pattern of *Synechococcus* assemblages observed in the Gulf of Nicoya.

PEuk and NEuk assemblages are characterised by a high functional and phylogenetic diversity (Worden and Not 2008; Hug et al. 2016), higher than that of *Synechococcus*, which likely involves differences in niche preference, including light and nutrient availability preferences. This was reflected in the higher dispersion in their nMDS ordination and the lack of significant correlations with environmental variables (Fig. 6 e-h). Regardless, PEuk and NEuk showed clearly different distributions along the estuarine gradient (Fig. 4). The highest abundance of PEuk were measured at or after the salt wedge during the rainy and dry seasons, where turbidity decreases considerably and NCP begins to shift to positive values (Fig 2). These changes were associated to an increase in terms of total Chl *a* and primary production (Seguro et al 2015, Soria et al 2017). This is consistent with the increase of relative and absolute importance of PEuk with increasing total Chl *a* in nutrient-rich ecosystems due to their higher growth rates than picocyanobacteria (Raven 1986, Weisse 1993, Bec et al 2005). NEuk, on the other hand, showed a general trend to decrease towards the sea (Fig. 4j). NEuk was the dominant biomass fraction in the Gulf of Nicoya, contributing 83 and 90 % of the total phytoplankton biomass during the dry and rainy seasons, respectively, and substantial fractions of the chlorophyll concentrations and net primary production rates at sampling St. 3 and 4 (Soria-Píriz et al. 2017). A similar quantitative importance of NEuk has been found in other coastal systems, including tropical estuaries (Ansotegui et al. 2003; Piwosz et al. 2015; Madhu et al. 2017).

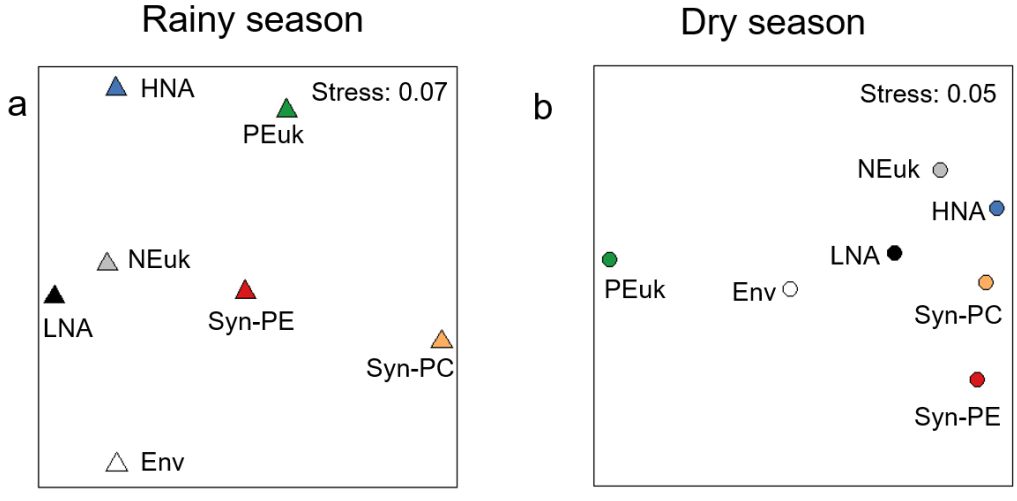

Fig. 8: *Two-dimensional second-stage nMDS* based on pairwise rank comparisons (Spearman correlation) between individual nMDS plots of environmental and microbial assemblages along the inner part of the Gulf of Nicoya during July 2011 (rainy) and April 2012 (dry). The closer two symbols are located to each other, the more their observed multivariate patterns are related to each other. Env, environmental variables; Syn-PE, *Synechococcus* phycoerythrin-rich cells; Syn-PC, *Synechococcus* phycocyanin-rich cells; PEuk, picoeukaryotes; NEuk , nanoeukaryotes; HNA, high nucleic acid bacterial cells; LNA, low nucleic acid bacterial cells.

In addition to the changes in abundance, changes in single-cell traits were also evident along the estuarine gradient for the four phytoplankton assemblages (Fig. 4). In general, SSC patterns along the estuary differed between the prokaryotic and eukaryotic phytoplanktonic assemblages. SSC can be used as a proxy of cell size (Echevarria et al. 2009), although internal and cell surface characteristics affect it as well (Gasol and del Giorgio 2000; Lebaron et al. 2002; Morán et al. 2007). SSC of Syn-PC and Syn-PE decreased seaward, while SSC of PEuk and NEuk tended to increase along the estuarine

gradient. The different response in cell size along the estuary between phytoplankton prokaryotes and eukaryotes could be due to bottom-up and top-down processes (Raven 1998; Ward et al. 2012; Marañón 2015), including constraints that cell organization and mean cell size impose on metabolism and growth in response to nutrient and light availability (DeLong et al. 2010; Marañón 2015). In contrast to SSC, FL/SSC of phytoplankton, which represents an estimate of Chl *a* normalized to cell size, tended to increase seaward in all assemblages, although differences were observed with season. FL/SSC of PEuk and NEuk in the surface water layer was considerably higher during the rainy season with respect to the dry one, an observation we cannot explain for now. The changes in FL/SSC toward the sea could be due to both changes in phylogenetic composition and physiology, permitting to increase the assemblage's fitness to the changing conditions along the estuarine gradient (Demers et al. 1989; Olson et al. 1990). In that direction, changes in fluorescence in phytoplankton have been related to photoacclimation due to changes in light conditions, cellular division, changes in quantum yield and shifts in species composition (Olson et al. 1990; Vaulot et al. 1990; Campbell and Vaulot 1993).

nMDS ordination analysis based on abundance and single cell traits of the different phytoplanktonic assemblages showed strong changes in the spatial patterns along the estuarine gradient and between seasons (Fig. 6). The clear separation of St. 1, especially in the dry season, from the rest of the sampling stations suggests the potential presence of an ecotone (Attrill and Rundle 2002; Muylaert et al. 2009) for the estuarine microbial community between St.1 and St.2, which is where the steepest salinity gradient occurred (Fig. 2, 3). This ecotone was observed for the microphytoplankton community in the Gulf of Nicoya, whereas in the rest of the estuary, changes in the community phylogenetic structure follow better an ecocline model (Seguro et al 2015). However, the smaller phytoplanktonic size classes investigated here behaved in a more complex and contradicting way. On the one hand, the nMDS ordination seems to suggest the existence of an ecotone at the maximum salinity gradient for Syn-PC and Syn-PE, with salinity, DIN, CDOM and temperature best correlating with the changes of both assemblages along the estuary (Fig. 6). On the other hand, a separation of St.1 was less clear for PEuk and NEuk; in addition, no environmental variable correlated significantly with their ordination along the estuary

4.3. Changes in the bacterial assemblages along the estuarine gradient

The range of abundances of the free-living bacterioplankton assemblages observed in the inner part of the Gulf of Nicoya ($1 – 12 \times 10^9$ cell L^{-1}) were similar to those of other tropical areas (Pradeep Ram et al. 2003; Barrera-Alba et al. 2008; Li et al. 2017). Bacteria attached to particles were not measured in this study, however, the higher turbidity, particulate organic C and total respiration rate measured at St. 1 in the Gulf of Nicoya (Soria-Píriz et al 2017) suggests a higher importance of the attached bacterial community in the estuary head and a decrease seawards as observed elsewhere (Griffith et al. 1994; Crump et al. 1998; Barrera-Alba et al. 2008).

Although the relative contribution of HNA has been considered as an index of bacterial activity and as a tracker of the system's productivity, being highly correlated to chlorophyll stocks (Corzo et al. 2005; Morán et al. 2007) other studies consider that LNA bacteria are metabolically active as well, with specific growth rates even higher than HNA cells, and play an essential role in the microbial food web (Zubkov et al. 2001; Jochem et al. 2004; Longnecker et al. 2005; Bouvier et al. 2007). The % HNA (20 – 64 %) was always lower than the % LNA (36 – 80 %) in all stations, layers and seasons except during the rainy season at St. 1 (bottom layer) and St. 3 (surface layer). The % HNA was within the range reported by other estuarine systems (del Giorgio and Bouvier 2002; Bouvier et al. 2007; Liu et al. 2016).

The abundance of HNA and LNA bacterial assemblages presented evident spatiotemporal changes along the estuary, increasing clearly seaward, except HNA in the bottom layer during the rainy

season (Fig. 5). This trend of increasing bacterial abundances along the estuarine gradient has been observed in some temperate estuaries in the transition zone where fresh and marine water mix (del Giorgio and Bouvier 2002; Cottrell and David 2003). In contrast, an inverse trend or no trend at all has been found in other systems (Urakawa et al. 2013; Li et al. 2017). Frequently, bacterioplankton abundance and diversity show a negative correlation with salinity (Painchaud et al. 1996; Troussellier et al. 2002; Campbell and Kirchman 2012), although the response of bacteria to salinity has been shown to be taxon dependent in estuaries, with some taxa increasing seaward, like *α-Proteobacteria*, including the SAR11 clade, and other decreasing, like β-Proteobacteria and Actinobacteria (Kirchman et al. 2005; Campbell and Kirchman 2012). In other systems, differences in water residence time have been suggested to affect the abundance and structure of the bacterial community (Crump et al. 2004). Likely, the environmental drivers behind these differences depend on the system studied. In terms of their relative abundance, the general decrease of HNA vs LNA (HNA/LNA ratio) (Fig 2, Fig S1b) suggests a limitation of the more "active" and larger HNA bacteria which could be due to the reduced availability of organic substrates seaward (CDOM and DOC) (Fig S1b). However, this interpretation contradicts the observed absolute increase in HNA and LNA abundances and the increased FL/SSC for both assemblages along the estuary.

FL/SSC in heterotrophic bacteria is an estimator of the size-specific content of nucleic acid per bacterial cell and therefore its values can change in response to differences in metabolic activity and growth rate, but also to phylogenetic differences in nucleic acid content (Gasol et al. 1995; Lebaron et al. 2002; Vadia et al. 2017). In the Gulf of Nicoya, the seaward increase of FL/SSC of HNA and LNA assemblages coincided with an increase in the slope of the CDOM spectra along the estuary in both seasons (Fig. S1a). A greater slope in CDOM spectra indicates a relative increase of more labile DOM, likely from autochthonous primary production, and a dilution of the more refractory allochthonous component of terrestrial and mangrove origin. This increase in the pool of labile carbon substrates could stimulate bacterial production and growth increasing the FL/SSC ratio (Bertilsson and Tranvik 1998; Stedmon and Markager 2003; Bertilsson et al. 2005; Galgani et al. 2011). In addition, the differences in availability of specific organic substrates can also affect the phylogenetic composition of the bacterial community along the estuarine gradient and the FL/SSC ratio (Campbell and Kirchman 2012; Urakawa et al. 2013; Jeffries et al. 2016). Lastly, differences in grazing and viral lysis rates upon HNA and LNA assemblages along the estuary, although not available for the Gulf of Nicoya, can also significantly affect HNA/LNA ratios (Gonzalez et al. 1990; Bouvier and del Giorgio 2002; Crump et al. 2004; Campbell and Kirchman 2012).

In contrast with the clear trend of FL/SSC, SSC changed little along the estuary, contrary to what it was reported for the temperate Haihe River estuary (China), where SSC varied more than FL suggesting that both cellular properties could be related to different factors (Liu et al 2016). The highest values of SSC occurred in the rainy season, at St. 1 for LNA, where the inputs of allochthonous material from the river was higher (Seguro et al 2015, Soria-Píriz et al 2017), and at St. 3 for HNA, where the maxima in NCP was located (Fig. 2). This suggest that HNA and LNA fractions comprise of different compositions and/or the cells size of both LNA and HNA fractions along the estuarine gradient could differed in their response to increasing levels of nutrients and Chl *a* (Corzo et al. 2005, Liu et al 2017).

The nMDS analysis based on abundance and single cell traits of HNA and LNA assemblages showed important differences between the two (Fig. 7). Ordination of the stations based on the HNA assemblage presented a larger dispersion than that based on LNA bacteria, particularly during the rainy season. This suggests that the HNA assemblage could be more sensitive to the spatial variability of abiotic and or biotic factors along the estuary (Liu et al. 2016). Another important difference was the dissimilarity of St. 1 compared to the rest of the stations, particularly for the LNA assemblage during the dry season. The riverine bacterial assemblage was clearly different in terms of abundances and

single cell traits from the rest of the estuarine community, similarly to what we observed for prokaryotic phytoplankton assemblages, Syn-PE and Syn-PC, and microphytoplankton (Seguro et al 2015), but not the case for PEuk and NEuk (Fig. 6). The environmental variables that best correlated with the ordination based on single cell HNA and LNA traits, were rather similar in both seasons. Salinity, CDOM, and DIN correlated with the ordination of both bacterial assemblages, while PO_4^{3-} correlated specifically with LNA (Fig. 7). These variables, not always in the same order or with the same importance, have been shown to have a role in the spatiotemporal distribution of the abundance and phylogenetic structure of the bacterial community in different estuaries (Crump et al. 2004; Hitchcock and Mitrovic 2010; Liu et al. 2016). These differences between systems suggest the weight of the different abiotic and biotic factors in shaping the dynamics of microbial communities are system specific.

4.4. Seasonal differences in the similarity between environmental and microbial assemblages ordinations

Our results clearly show that multivariate ordinations based on abiotic factors and the microbial assemblages traits were more concordant during the dry season (Fig. 8, Table S2). The weak similarities in the ordination patterns within each functional group, i.e. phytoplankton (Syn-PE, Syn PC, PEuk and NEuk) and bacterioplankton assemblages (HNA, LNA), during the rainy season, suggests that their dynamics are more uncoupled responding in distinct ways to the prevailing environmental conditions or that to different abiotic and biotic drivers during this period of the year (Huete-Stauffer and Morán 2012; Liu et al. 2016). The higher allochthonous organic carbon discharges from the Tempisque River and the lower autochthonous NCP in rainy season due to the higher turbidity and reduced light availability, likely led to a higher uncoupling of bacterial assemblages from phytoplankton, as observed elsewhere (Barrera-Alba et al 2008, Figueroa et al 2016, Andersson et al 2018). Under non-limiting DOC conditions, bacterioplankton outcompetes phytoplankton for N and P, taking advantage of their low surface/volume ratio (Le et al. 1994; Findlay 2003; Hitchcock and Mitrovic 2010). Therefore, during the rainy season, the high DOC inflow to the Gulf of Nicoya could potentially change the system to an allochthonous C dominated system, with enhanced importance of bacterioplankton in the transfer of carbon to higher trophic levels, via the detrital food chain (Jassby et al. 1993; Sherr and Sherr 2000; Barrera-Alba et al. 2009). By contrast, the greater similarity in the ordination of phyto- and bacterial assemblages during the dry season was likely the consequence of a higher coupling between these two functional components of the pelagic trophic web due to a higher autochthonous primary production and the lower DOC inflows from the river discharges. Therefore, the spatiotemporal changes in the relative contribution of allochthonous and autochthonous C along the estuarine gradient is a strong determinant for the degree of coupling between phytoplankton and bacterioplankton, driving changes in the transfer of energy and mass of the pelagic microbial food web and the functioning of the ecosystem in its entirety.

5. Acknowledgement

This study was funded by projects C/023621/09, D/031020/10, and A1/037457/11 from Spanish Agency for International Development and Cooperation (AECID), the projects CTM2013-43857-R and P11-RNM-7199 from the Spanish Ministry of Economy and Competitiveness and Andalusian Regional Government and supported by the project 808-B3-127 at the University of Costa Rica (UCR). We thank all colleagues and the staff from UCA and CIMAR-UCR that contributed to the realization of this study for their personal and logistic support.

6. References

Abril, G., M. Nogueira, H. Etcheber, G. Cabec, and E. Lemaire. 2002. Behaviour of Organic Carbon in Nine Contrasting European Estuaries. 241–262. doi:10.1006/ecss.2001.0844

Andersson, A., S. Brugel, J. Paczkowska, O. F. Rowe, and D. Figueroa. 2018. Estuarine , Coastal and Shelf Science In fl uence of allochthonous dissolved organic matter on pelagic basal production in a northerly estuary. **204**: 225–235. doi:10.1016/j.ecss.2018.02.032

Ansotegui, A., A. Sarobe, J. María Trigueros, I. Urrutxurtu, and E. Orive. 2003. Size distribution of algal pigments and phytoplankton assemblages in a coastal-estuarine environment: Contribution of small eukaryotic algae. J. Plankton Res. **25**: 341–355. doi:10.1093/plankt/25.4.341

Attrill, M. J., and S. D. Rundle. 2002. Ecotone or Ecocline : Ecological Boundaries in Estuaries. 929–936. doi:10.1006/ecss.2002.1036

Azam, F., T. Fenchel, J. G. Field, J. S. Gray, L. A. Meyer-Reil, and F. Thingstad. 1983. The Ecological Role of Water-Column Microbes in the Sea *. **10**: 257–263.

Barrera-Alba, J., M. Flores, G. Aparecida, O. Moser, and M. P. Saldanha-corre. 2009. Estuarine , Coastal and Shelf Science Influence of allochthonous organic matter on bacterioplankton biomass and activity in a eutrophic , sub-tropical estuary. **82**: 84–94. doi:10.1016/j.ecss.2008.12.020

Barrera-Alba, J. J., S. M. Gianesella, G. A. Oliveira Moser, and F. M. Prado Saldanha-COrrea. 2008. Bacterial and phytoplankton dynamics in a sub-tropical estuary. Hydrobiologia 229–246. doi:10.1007/s10750-007-9156-4

Bec, B., J. Husseini-ratrema, Y. Collos, and P. Souchu. 2005. Phytoplankton seasonal dynamics in a Mediterranean coastal lagoon : emphasis on the picoeukaryote community. J. Plankton Res. **27**: 881–894. doi:10.1093/plankt/fbi061

Bertilsson, S., O. Berglund, M. J. Pullin, and S. W. Chisholm. 2005. Release of dissolved organic matter by Prochlorococcus. Vie Milieu **55**: 225–231.

Bertilsson, S., and L. J. Tranvik. 1998. Photochemically produced carboxylic acids as substrates for freshwater bacterioplankton. **43**: 885–895.

Bianchi, T. S., M. Baskaran, J. Delord, and M. Ravichandran. 1997. Carbon cycling in a shallow turbid estuary of Southeast Texas: The use of plant pigment biomarkers and water quality parameters. Estuaries **20**: 404–415. doi:10.2307/1352353

Bird, D. F., and J. Kalff. 1984. Empirical Relationships between Bacterial Abundance and Chlorophyll Concentration in Fresh and Marine Waters. Can. J. Fish. Aquat. Sci. **41**: 1015–1023. doi:10.1139/f84-118

Borcard, D. 2012. Partialling out the Spatial Component of Ecological Variation Author (s): Daniel Borcard , Pierre Legendre and Pierre Drapeau Reviewed work (s): Published by : Ecological Society of America Stable URL : http://www.jstor.org/stable/1940179 . PARTIALLIN. **73**: 1045–1055.

Bouvier, T. C., and P. A. del Giorgio. 2002. Compositional changes in free-living bacterial communities along a salinity gradient in two temperate estuaries. **47**: 453–470.

Bouvier, T., P. A. del Giorgio, and J. M. Gasol. 2007. A comparative study of the cytometric characteristics of High and Low nucleic-acid bacterioplankton cells from different aquatic ecosystems. Environ. Microbiol. **9**: 2050–2066. doi:10.1111/j.1462-2920.2007.01321.x

Bower and Holm-Hansen. 1980. A salicylate-Hypochlorite method for determining amonia in seawater. Can. J. Fish. Aquat. Sci. **37**: 794–798. doi:10.1139/f80-106

Calvo-Díaz, A., and X. A. G. Morán. 2006. Seasonal dynamics of picoplankton in shelf waters of the southern Bay of Biscay. Aquat. Microb. Ecol. **42**: 159–174. doi:10.3354/ame042159

Camacho, A., M. R. Miracle, and E. Vicente. 2003. Which factors determine the abundance and distribution of picocyanobacteria in inland waters? A comparison among different types of lakes and ponds. Arch. für Hydrobiol. **157**: 321–338. doi:10.1127/0003-9136/2003/0157-0321

Campbell, B. J., and D. L. Kirchman. 2012. Bacterial diversity , community structure and potential growth rates along an estuarine salinity gradient. **7**: 210–220. doi:10.1038/ismej.2012.93

Campbell, L., and D. Vaulot. 1993. Photosynthetic picoplankton community structure in the subtropical North Pacific Ocean near Hawaii (station ALOHA). Deep. Res. I **40**: 2043–2060.

Clarke, K., P. Somerfield, L. Airoldi, and R. Warwick. 2006. Exploring interactions by second-stage analysis. J. Exp. Mar. Bio. Ecol. **338**: 179–192. doi:10.1016/j.jembe.2006.06.019

Cloern, J. 1987. Turbidity as a control on phytoplankton biomass and productivity in estuaries. Cont. Shelf Res.

7: 1367–1381. doi:https://doi.org/10.1016/0278-4343(87)90042-2

Cloern, J. 1999. The relative importance of light and nutrient limitation of phytoplankton growth: A simple index of coastal ecosystem sensitivity to nutrient enrichment. Aquat. Ecol. **33**: 3–15. doi:10.1023/A:1009952125558

Cloern, J. E., S. Q. Foster, and A. E. Kleckner. 2014. Phytoplankton primary production in the world ' s estuarine-coastal ecosystems. 2477–2501. doi:10.5194/bg-11-2477-2014

Cole, B. E., and J. E. Cloern. 1984. Significance of biomass and light availability to phytoplankton productivity in San Francisco Bay. **17**: 15–24.

Cole, B. E., and J. E. Cloern. 1987. An empirical model for estimating phytoplankton productivity in estuaries. Mar. Ecol. Prog. Ser. **36**.

Córdoba-Muñoz, R. 1998. Primary productivity in the water column of Estero Morales, a mangrove system in the Gulf of Nicoya, Costa Rica. Rev. Biol. Trop. **46**: 257–262.

Corzo, A., F. Jiménez-Gómez, F. J. L. Gordillo, R. García-Ruíz, and F. X. Niell. 1999. Short communication. Synechococcus and Prochlorococcus-like populations detected by flow cytometry in a eutrophic reservoir in summer. J. Plankton Res. **21**: 1575–1581. doi:10.1093/plankt/21.8.1575

Corzo, A., S. Rodríguez-Gálvez, L. Lubian, C. Sobrino, P. Sangrá, and A. Martínez. 2005. Antarctic marine bacterioplankton subpopulations discriminated by their apparent content of nucleic acids differ in their response to ecological factors. Polar Biol. **29**: 27–39. doi:10.1007/s00300-005-0032-2

Cottrell, M. T., and K. L. David. 2003. Contribution of major bacterial groups to bacterial biomass production (thymidine and leucine incorporation) in the Delaware estuary. Limnol. Oceanogr. **48**: 168–178.

Crump, B. C., J. A. Baross, and C. A. Simenstad. 1998. Dominance of particle-attached bacteria in the Columbia River estuary, USA. Aquat. Microb. Ecol. **14**: 7–18.

Crump, B. C., C. S. Hopkinson, M. L. Sogin, and J. E. Hobbie. 2004. Microbial Biogeography along an Estuarine Salinity Gradient : Combined Influences of Bacterial Growth and Residence Time. **70**: 1494–1505. doi:10.1128/AEM.70.3.1494

Crump, B. C., C. Peranteau, B. Beckingham, and J. C. Cornwell. 2007. Respiratory succession and community succession of bacterioplankton in seasonally anoxic estuarine waters. Appl. Environ. Microbiol. **73**: 6802–6810. doi:10.1128/AEM.00648-07

DeLong, J. P., J. G. Okie, M. E. Moses, R. M. Sibly, and J. H. Brown. 2010. Shifts in metabolic scaling, production, and efficiency across major evolutionary transitions of life. Proc. Natl. Acad. Sci. **107**: 12941 LP-12945. doi:10.1073/pnas.1007783107

Demers, S., K. Davis, T. L. Cucci, I. Maurice-lamontagne, P. Oceans, G. H. C. S. D, and O. Dominion. 1989. A Flow Cytometric Approach to Assessing the Environmental and Physiological Status of Phytoplankton '. **652**: 644–652.

Dubelaar, G. B. J., and R. R. Jonker. 2000. Flow cytometry as a tool for the study of phytoplankton. Sci. Mar. **64**: 135–156. doi:10.3989/scimar.2000.64n2135

Echevarria, F., L. Zabala, A. Corzo, G. Navarro, L. Prieto, and D. Macías. 2009. Spatial distribution of autotrophic picoplankton in relation to physical ´ diz , Strait of forcings : the Gulf of Ca ´ n Sea case study Gibraltar and Albora. J. Plankton Res. **31**. doi:10.1093/plankt/fbp070

Fenchel, T., and B. Finlay. 2008. Oxygen and the spatial structure of microbial communities. Biol. Rev. **83**: 553–569. doi:10.1111/j.1469-185X.2008.00054.x

Figueroa, D., O. F. Rowe, J. Paczkowska, C. Legrand, and A. Andersson. 2016. Allochthonous Carbon — a Major Driver of Bacterioplankton Production in the Subarctic Northern Baltic Sea. 789–801. doi:10.1007/s00248-015-0714-4

Findlay, S. 2003. 15 - Bacterial Response to Variation in Dissolved Organic Matter, p. 363–379. *In* S.E.G. Findlay and R.L.B.T.-A.E. Sinsabaugh [eds.], Aquatic Ecology. Academic Press.

Galgani, L., A. Tognazzi, C. Rossi, and others. 2011. Journal of Photochemistry and Photobiology B : Biology Assessing the optical changes in dissolved organic matter in humic lakes by spectral slope distributions. J. Photochem. Photobiol. B Biol. **102**: 132–139. doi:10.1016/j.jphotobiol.2010.10.001

García-Robledo, E., A. Corzo, and S. Papaspyrou. 2014. A fast and direct spectrophotometric method for the sequential determination of nitrate and nitrite at low concentrations in small volumes. Mar. Chem. **162**: 30–36. doi:10.1016/j.marchem.2014.03.002

Gasol, J. M., and C. M. Duarte. 2000. Comparative analyses in aquatic microbial ecology : how far do they go ? **31**: 99–106.

Gasol, J. M., and P. A. del Giorgio. 2000. Using flow cytometry for counting natural planktonic bacteria and

understanding the structure of planktonic bacterial communities. Sci. Mar. **64**: 197–224. doi:10.3989/scimar.2000.64n2197

Gasol, J. M., P. A. Del Giorgio, R. Massana, and C. M. Duarte. 1995. Active versus inactive bacteria: size-dependence in a coastal marine plankton community. Mar. Ecol. Prog. Ser. **128**: 91–97. doi:10.3354/meps128091

del Giorgio, P. A., and T. C. Bouvier. 2002. Linking the physiologic and phylogenetic successions in free-living bacterial communities along an estuarine salinity gradient. Limnol. Oceanogr. **47**: 471–486. doi:10.4319/lo.2002.47.2.0471

Gocke, K., J. Cortés, and M. M. Murillo. 2001a. Planktonic primary production in a tidally influenced mangrove forest on the Pacific coast of Costa Rica. **1**: 279–288.

Gocke, K., J. Cortés, M. M. Murillo, and others. 2001b. The annual cycle of primary productivity in a tropical estuary : The inner regions of the Golfo de Nicoya , Costa Rica Study area : The Golfo de Nicoya is a tropical estuary situated on the Pacific coast of Costa. 289–306.

Gocke, K., J. Cortés, C. Villalobos, C. De Investigación, and U. D. C. Rica. 1990. Effects of red tides on oxygen concentration and distribution in the Golfo de Nicoya , Costa Rica. **38**: 401–407.

Gonzalez, J. M., E. B. Sherr, and B. F. Sherr. 1990. Size-selective grazing on bacteria by natural assemblages of estuarine flagellates and ciliates. Appl. Environ. Microbiol. **56**: 583–589.

Grasshoff, K., K. Kremling, and M. Ehrhardt. 1999. Methods of Seawater analysis, Wiley Online Library.

Griffith, P., F.-K. Shiah, K. Gloersen, H. W. Ducklow, and M. Fletcher. 1994. Activity and distribution of attached bacteria in Chesapeake Bay *. Mar. Ecol. Prog. Ser. **108**: 1–10.

Hitchcock, J. N., and S. M. Mitrovic. 2010. Responses of Estuarine Bacterioplankton , Phytoplankton and Zooplankton to Responses of Estuarine Bacterioplankton , Phytoplankton and Zooplankton to Dissolved Organic Carbon (DOC) and Inorganic Nutrient Additions.doi:10.1007/s12237-009-9229-x

Hitchcock, J. N., and S. M. Mitrovic. 2015. Estuarine , Coastal and Shelf Science Highs and lows : The effect of differently sized freshwater in fl ows on estuarine carbon , nitrogen , phosphorus , bacteria and chlorophyll a dynamics. Estuar. Coast. Shelf Sci. **156**: 71–82. doi:10.1016/j.ecss.2014.12.002

Horner-Devine, M. C., J. M. Silver, M. A. Leibold, and others. 2007. A comparison of taxon co-occurrence patterns for macro- and microorganisms. Ecology **88**: 1345–1353. doi:10.1890/06-0286

Huete-Stauffer, T. M., and X. A. G. Morán. 2012. Dynamics of heterotrophic bacteria in temperate coastal waters: Similar net growth but different controls in low and high nucleic acid cells. Aquat. Microb. Ecol. **67**: 211–223. doi:10.3354/ame01590

Hug, L. A., B. J. Baker, K. Anantharaman, and others. 2016. A new view of the tree of life. Nat. Microbiol. **1**: 16048. doi:10.1038/nmicrobiol.2016.48

Jassby, A. D., J. E. Cloern, and T. M. Powell. 1993. Organic carbon sources and sinks in San Francisco Bay: variability induced by river flow. Mar. Ecol. Prog. Ser. **95**: 39–54.

Jeffries, T. C., M. L. Schmitz Fontes, D. P. Harrison, V. Van-Dongen-Vogels, B. D. Eyre, P. J. Ralph, and J. R. Seymour. 2016. Bacterioplankton Dynamics within a Large Anthropogenically Impacted Urban Estuary. Front. Microbiol. **6**: 1438. doi:10.3389/fmicb.2015.01438

Jochem, F., A. Biofuels, and P. Lavrentyev. 2004. Growth and grazing rates of bacteria groups with different apparent DNA content in the Gulf of Mexico.doi:10.1007/s00227-004-1406-7

Kirchman, D. L., A. I. Dittel, R. R. Malmstrom, and M. T. Cottrell. 2005. Biogeography of major bacterial groups in the Delaware Estuary. Limnol. Oceanogr. **50**: 1697–1706. doi:10.4319/lo.2005.50.5.1697

Kirk, J. T. O. 1994. Light and photosynthesis in aquatic ecosystems, Cambridge university press.

Kress, N., S. Leon, C. L. Brenes, and S. Brenner. 2002. Horizontal transport and seasonal distribution of nutrients , dissolved oxygen and chlorophyll -a in the Gulf of Nicoya , Costa Rica : a tropical estuary. **22**: 51–66.

Lancelot, C., and K. Muylaert. 2011. Trends in Estuarine Phytoplankton Ecology, Elsevier Inc.

Le, J., J. D. Wehr, and L. Campbell. 1994. Uncoupling of bacterioplankton and phytoplankton production in fresh waters is affected by inorganic nutrient limitation. Appl. Environ. Microbiol. **60**: 2086–2093.

Lebaron, P., N. Parthuisot, P. Catala, and O. Oce. 1998. Comparison of Blue Nucleic Acid Dyes for Flow Cytometric Enumeration of Bacteria in Aquatic Systems. Appl. Environ. Microbiol. **64**: 1725.

Lebaron, P., P. Servais, H. Agogué, C. Courties, and F. Joux. 2001. Does the High Nucleic Acid Content of Individual Bacterial Cells Allow Us to Discriminate between Active Cells and Inactive Cells in Aquatic Systems? Appl. Environ. Microbiol. **67**: 1775–1782. doi:10.1128/AEM.67.4.1775-1782.2001

Lebaron, P., P. Servais, A. Baudoux, M. Bourrain, C. Courties, and N. Parthuisot. 2002. Variations of bacterial-specific activity with cell size and nucleic acid content assessed by flow cytometry.doi:10.3354/ame028131

Li, J., X. Jiang, Z. Jing, G. Li, Z. Chen, L. Zhou, and C. Zhao. 2017. Spatial and seasonal distributions of bacterioplankton in the Pearl River Estuary : The combined e ff ects of riverine inputs , temperature , and phytoplankton. **125**: 199–207. doi:10.1016/j.marpolbul.2017.08.026

Li, Y., and D. Li. 2012. Spatial Distributions of Picoplankton and Viruses in the Changjiang Estuary and Its Adjacent Sea Area during Summer. **2012**. doi:10.1155/2012/465168

Liu, H., H. Jing, T. H. C. Wong, and B. Chen. 2014. Co-occurrence of phycocyanin- and phycoerythrin-rich Synechococcus in subtropical estuarine and coastal waters of Hong Kong. Environ. Microbiol. Rep. **6**: 90–99. doi:10.1111/1758-2229.12111

Liu, J., Z. Hao, L. Ma, Y. Ji, M. Bartlam, and Y. Wang. 2016. Spatio-temporal variations of high and low nucleic acid content bacteria in an exorheic river. PLoS One **11**. doi:10.1371/journal.pone.0153678

Liu, J., D. Ma, L. Ma, Y. Song, G. Gao, and Y. Wang. 2017. Geographic distribution pattern of low and high nucleic acid content bacteria on a river-catchment scale. Mar. Freshw. Res. **68**: 1618–1625. doi:10.1071/MF16068

Longnecker, K., B. F. Sherr, and E. B. Sherr. 2005. Activity and phylogenetic diversity of bacterial cells with high and low nucleic acid content and electron transport system activity in an upwelling ecosystem. Appl. Environ. Microbiol. **71**: 7737–7749. doi:10.1128/AEM.71.12.7737-7749.2005

Madhu, N. V., G. D. Martin, C. K. Haridevi, M. Nair, K. K. Balachandran, and N. Ullas. 2017. Differential environmental responses of tropical phytoplankton community in the southwest coast of India. Reg. Stud. Mar. Sci. **16**: 21–35. doi:10.1016/j.rsma.2017.07.004

Marañón, E. 2015. Cell Size as a Key Determinant of Phytoplankton Metabolism and Community Structure. Ann. Rev. Mar. Sci. **7**: 241–264. doi:10.1146/annurev-marine-010814-015955

Marie, D., N. Simon, and D. Vaulot. 2005. Phytoplankton cell counting by flow cytometry. Algal Cult. Tech. **1**: 253–267.

Mitbavkar, S., K. M. Rajaneesh, A. C. Anil, and D. Sundar. 2012. Estuarine , Coastal and Shelf Science Picophytoplankton community in a tropical estuary : Detection of Prochlorococcus -like populations. Estuar. Coast. Shelf Sci. **107**: 159–164. doi:10.1016/j.ecss.2012.05.002

Morán, X. A. G., A. Bode, L. Á. Suárez, and E. Nogueira. 2007. Assessing the relevance of nucleic acid content as an indicator of marine bacterial activity. Aquat. Microb. Ecol. **46**: 141–152. doi:10.3354/ame046141

Murrell, M. C., and E. M. Lores. 2004. Phytoplankton and zooplankton seasonal dynamics in a subtropical estuary: importance of cyanobacteria. J. Plankton Res. **26**: 371–382. doi:10.1093/plankt/fbh038

Muylaert, K., K. Sabbe, and W. Vyverman. 2009. Estuarine , Coastal and Shelf Science Changes in phytoplankton diversity and community composition along the salinity gradient of the Schelde estuary (Belgium / The Netherlands). Estuar. Coast. Shelf Sci. **82**: 335–340. doi:10.1016/j.ecss.2009.01.024

Nittrouer, C. A., G. J. Brunskill, and A. G. Figueiredo. 1995. Importance of tropical coastal environments. Geo-Marine Lett. **15**: 121–126. doi:10.1007/BF01204452

Oksanen, J. , F. Guillaume Blanchet, Michael Friendly, Roeland Kindt, Pierre Legendre, Dan McGlinn, Peter R. Minchin, R. B. O'Hara, Gavin L. Simpson, Peter Solymos, M. Henry H. Stevens, Eduard Szoecs and Hele ne Wagner 2019. vegan: Community Ecology Package. R package version 2.5-6.

Olson, R. J., S. W. Chisholm, E. R. Zettler, and E. V. Armbrust. 1990. Pigments, size, and distributions of Synechococcus in the North Atlantic and Pacific Oceans. Limnol. Oceanogr. **35**: 45–58. doi:10.4319/lo.1990.35.1.0045

Painchaud, J., D. Lefaivre, J. C. Therriault, and L. Legendre. 1996. Bacterial dynamics in the upper St. Lawrence estuary. Limnol. Oceanogr. **41**: 1610–1618. doi:10.4319/lo.1996.41.8.1610

Palter, J., S. L. Coto, and D. Ballestero. 2007. The distribution of nutrients , dissolved oxygen and chlorophyll a in the upper Gulf of Nicoya , Costa Rica , a tropical estuary. **55**: 427–436.

Paver, S. F., K. R. Hayek, K. A. Gano, and others. 2013. Interactions between specific phytoplankton and bacteria affect lake bacterial community succession. **15**: 2489–2504. doi:10.1111/1462-2920.12131

Pick, F. 1991. The abundance and composition of freshwater picocyanobacteria in relation to light penetration. Limnol. Oceanogr. **36**: 1457–1462. doi:10.4319/lo.1991.36.7.1457

Piwosz, K., K. Spich, J. Całkiewicz, A. Weydmann, A. M. Kubiszyn, and J. M. Wiktor. 2015. Distribution of small phytoflagellates along an Arctic fjord transect. Environ. Microbiol. **17**: 2393–2406. doi:10.1111/1462-2920.12705

Pomeroy, L. R. 1974. The Ocean's Food Web, A Changing Paradigm. Bioscience **24**: 499–504.

Pradeep Ram, A. S., S. Nair, and D. Chandramohan. 2003. Bacterial growth efficiency in the tropical estuarine

and coastal waters of Goa, southwest coast of India. Microb. Ecol. **45**: 88–96. doi:10.1007/s00248-002-3005-9

Rajaneesh, K. M., and S. Mitbavkar. 2013. Factors controlling the temporal and spatial variations in Synechococcus abundance in a monsoonal estuary. Mar. Environ. Res. **92**: 133–143. doi:https://doi.org/10.1016/j.marenvres.2013.09.010

Rajaneesh, K. M., S. Mitbavkar, and A. C. Anil. 2018. Dynamics of size-fractionated phytoplankton biomass in a monsoonal estuary: Patterns and drivers for seasonal and spatial variability. Estuar. Coast. Shelf Sci. doi:10.1016/j.ecss.2018.04.026

Raven, J. A. 1986. Physiological consequences of extremely small size for autotrophic organisms in the sea. Can. J. Fish. Aquat. Sci. **214**: 1–70.

Raven, J. A. 1998. The twelfth Tansley Lecture . Small is beautiful : the picophytoplankton. 503–513.

Rodríguez, J. 1994. Some comments on the size-based structural analysis of the pelagic ecosystem. Sci. Mar. **58**: 1–10.

Roland, F., L. M. Lobão, L. O. Vidal, E. Jeppesen, R. Paranhos, and V. L. M. Huszar. 2010. Relationships between pelagic bacteria and phytoplankton abundances in contrasting tropical freshwaters. **60**: 261–272. doi:10.3354/ame01429

von Scheibner, M., P. Dorge, A. Biermann, U. Sommer, H.-G. Hoppe, and K. Jurgens. 2014. Impact of warming on phyto-bacterioplankton coupling and bacterial community composition in experimental mesocosms. Environ. Microbiol. **16**. doi:10.1111/1462-2920.12195

Seguro, I., C. M. García, S. Papaspyrou, J. A. Gálvez, and E. García-robledo. 2015. Seasonal changes of the microplankton community along a tropical estuary. Reg. Stud. Mar. Sci. **2**: 189–202. doi:10.1016/j.rsma.2015.10.006

Shang, X. P., L. H. Zhang, and J. O. Zhang. 2007. Prochlorococcus -like populations detected by £ ow cytometry in the fresh and brackish waters of the Changjiang Estuary.doi:10.1017/S0025315407055191

Sherr, E. B., and B. F. Sherr. 2000. Microbial Ecology of the Oceans ed DL Kirchman.

Sohm, J. A., N. A. Ahlgren, Z. J. Thomson, C. Williams, J. W. Moffett, M. A. Saito, E. A. Webb, and G. Rocap. 2016. Co-occurring Synechococcus ecotypes occupy four major oceanic regimes defined by temperature, macronutrients and iron. ISME J. **10**: 333–345. doi:10.1038/ismej.2015.115

Soria-Píriz, S., E. Garc, S. Papaspyrou, V. Aguilar, I. Seguro, J. Acu, A. Morales, and A. Corzo. 2017. Size fractionated phytoplankton biomass and net metabolism along a tropical estuarine gradient. Limnol. Oceanogr. **62**: 309–326. doi:10.1002/lno.10562

Stedmon, C. A., and S. Markager. 2003. Behaviour of the optical properties of coloured dissolved organic matter under conservative mixing. **57**: 973–979. doi:10.1016/S0272-7714(03)00003-9

Stedmon, C. A., S. Markager, and H. Kaas. 2000. Optical Properties and Signatures of Chromophoric Dissolved Organic Matter (CDOM) in Danish Coastal. 267–278. doi:10.1006/ecss.2000.0645

Stomp, M., J. Huisman, L. Vörös, F. R. Pick, M. Laamanen, T. Haverkamp, and L. J. Stal. 2007. Colourful coexistence of red and green picocyanobacteria in lakes and seas. Ecol. Lett. **10**: 290–298. doi:10.1111/j.1461-0248.2007.01026.x

Troussellier, M., H. SchÃƒ Â¤fer, N. Batailler, L. Bernard, C. Courties, P. Lebaron, G. Muyzer, and P. Servais. 2002. Bacterial activity and genetic richness along an estuarine gradient (Rhone River plume, France) . Aquat. Microb. Ecol. **28**: 13–24.

Urakawa, H., J. Ali, R. D. J. Ketover, S. D. Talmage, J. C. Garcia, I. S. Campbell, A. N. Loh, and M. L. Parsons. 2013. Shifts of Bacterioplankton Metabolic Profiles along the Salinity Gradient in a Subtropical Estuary L.B. Cahoon, J.L. Zhou, D. Alongi, M. Lipinski, and S. Ishman [eds.]. ISRN Oceanogr. **2013**: 410814. doi:10.5402/2013/410814

Vadia, S., J. L. Tse, R. Lucena, Z. Yang, D. R. Kellogg, J. D. Wang, and P. A. Levin. 2017. Fatty Acid Availability Sets Cell Envelope Capacity and Dictates Microbial Cell Size. Curr. Biol. **27**: 1757–1767.e5. doi:10.1016/j.cub.2017.05.076

Vaulot, D., C. Courties, and F. Partensky. 1989. A simple method to preserve oceanic phytoplankton for flow cytometric analyses. Cytom. Part A **10**: 629–635.

Vaulot, D., F. Partensky, N. Jacques, R. Mantoura, and C. Llewellyn. 1990. Wintertime presence of Prochlorophytes in surface waters of the North-Western Mediterranean Sea. Limnol. Oceanogr. **35**: 1156–1164. doi:10.4319/lo.1990.35.5.1156

Vörös, L., C. Callieri, K. V Balogh, and R. Bertoni. 1998. Freshwater picocyanobacteria along a trophic gradient and light quality range. Hydrobiologia **369**: 117–125. doi:10.1023/A:1017026700003

Wang, K., K. E. Wommack, F. Chen, W. E. T. Al, and A. P. P. L. E. N. M. Icrobiol. 2011. Abundance and Distribution of Synechococcus spp . and Cyanophages in the Chesapeake Bay □ †. **77**: 7459–7468. doi:10.1128/AEM.00267-11

Ward, B. A., S. Dutkiewicz, O. Jahn, and M. J. Follows. 2012. A size-structured food-web model for the global ocean. Limnol. Oceanogr. **57**: 1877–1891. doi:10.4319/lo.2012.57.6.1877

Weisse, T. 1993. Dynamics of Autotrophic Picoplankton in Marine and Freshwater Ecosystems, *In* J. Gwynfryn [ed.], Advances in Microbial Ecology. Plenum Press, New York.

Weisse, T., H. Miiller, R. A. L. Pinto-coelho, A. Schweizer, D. Springmann, and G. Baldringer. 1990. Response of the microbial loop to the phytoplankton spring bloom in a large prealpine lake. **35**: 781–794.

Worden, A. Z., and F. Not. 2008. Ecology and Diversity of Picoeukaryotes. Microb. Ecol. Ocean. Second Ed. 159–205. doi:10.1002/9780470281840.ch6

Xenopoulos, M. A., J. A. Downing, S. Menden-deuer, M. Voss, and M. D. Kumar. 2017. Headwaters to oceans : Ecological and biogeochemical contrasts across the aquatic continuum.doi:10.1002/lno.10721

Xia, X., W. Guo, S. Tan, and H. Liu. 2017. Synechococcus Assemblages across the Salinity Gradient in a Salt Wedge Estuary. **8**: 1–12. doi:10.3389/fmicb.2017.01254

Xia, X., N. K. Vidyarathna, B. Palenik, P. Lee, and H. Liu. 2015. Comparison of the seasonal variation of Synechococcus assemblage structure in estuarine waters and coastal waters of Hong Kong.doi:10.1128/AEM.01895-15

Xiuren, N., D. Vaulot, L. Zhensheng, and L. Zilin. 1988. Standing stock and production of phytoplankton in the estuary of the Changjiang (Yangtse River) and the adjacent East China Sea *. Mar. Ecol. Prog. Ser. **49**: 141–150.

Zubkov, M. V., B. M. Fuchs, P. H. Burkill, and R. Amann. 2001. Comparison of Cellular and Biomass Specific Activities of Dominant Bacterioplankton Groups in Stratified Waters of the Celtic Sea. Appl. Environ. Microbiol. **67**: 5210–5218. doi:10.1128/AEM.67.11.5210

7. Supplementary Material

7.1.Tables

Table S1: Spearman rank correlations between individual nMDS plots of environmental and microbial assemblages along the inner part of the Gulf of Nicoya during July 2011 (rainy) and April 2012 (dry). *Synechococcus* phycoerythrin-rich cells (Syn-PE), *Synechococcus*- phycocyanin-rich cells (Syn-PC), PicoEukaryotes (PEuk), NanoEukaryotes (NEuk), high acid nucleic bacterial cells (HNA) and low acid nucleic bacterial cells (LNA) were correlated separately for the rainy and dry seasons. Numbers in bold are significant correlations at ** $p < 0.001$, *$p < 0.05$.

		Env	Syn-PE	Syn-PC	PEuk	NEuk	HNA
Rainy season	Env						
	Syn-PE	0.18					
	Syn-PC	0.04	**0.36***				
	PEuk	-0.02	0.13	0.06			
	NEuk	0.25	**0.49***	0.04	0.27		
	HNA	0.02	**0.38***	0.03	0.19	0.19	
	LNA	**0.54***	0.31	-0.20	0.11	**0.69****	0.23
Dry season	Env						
	Syn-PE	0.26					
	Syn-PC	0.29	**0.66****				
	PEuk	**0.35***	-0.16	-0.06			
	NEuk	0.23	0.25	**0.47***	0.02		
	HNA	0.30	**0.35***	**0.56****	-0.12	**0.43***	
	LNA	**0.61****	**0.42***	**0.61****	0.04	**0.53****	**0.76****

7.2. Figures

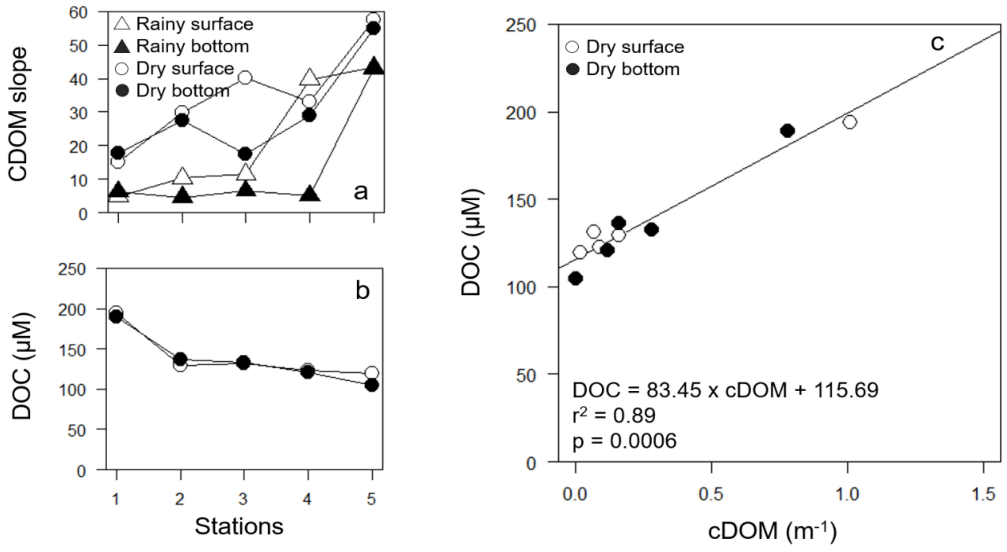

Fig. S1 (a) *Longitudinal distribution* of the slope of CDOM along the five stations in the inner part of the Gulf of Nicoya during both seasons (rainy and dry) in both layers (surface and bottom). **(**b) Relationship between dissolved organic carbon (DOC) and colorimetric dissolved organic matter (CDOM) data during dry season in both layers (surface and bottom). Data from both layers fit significantly.

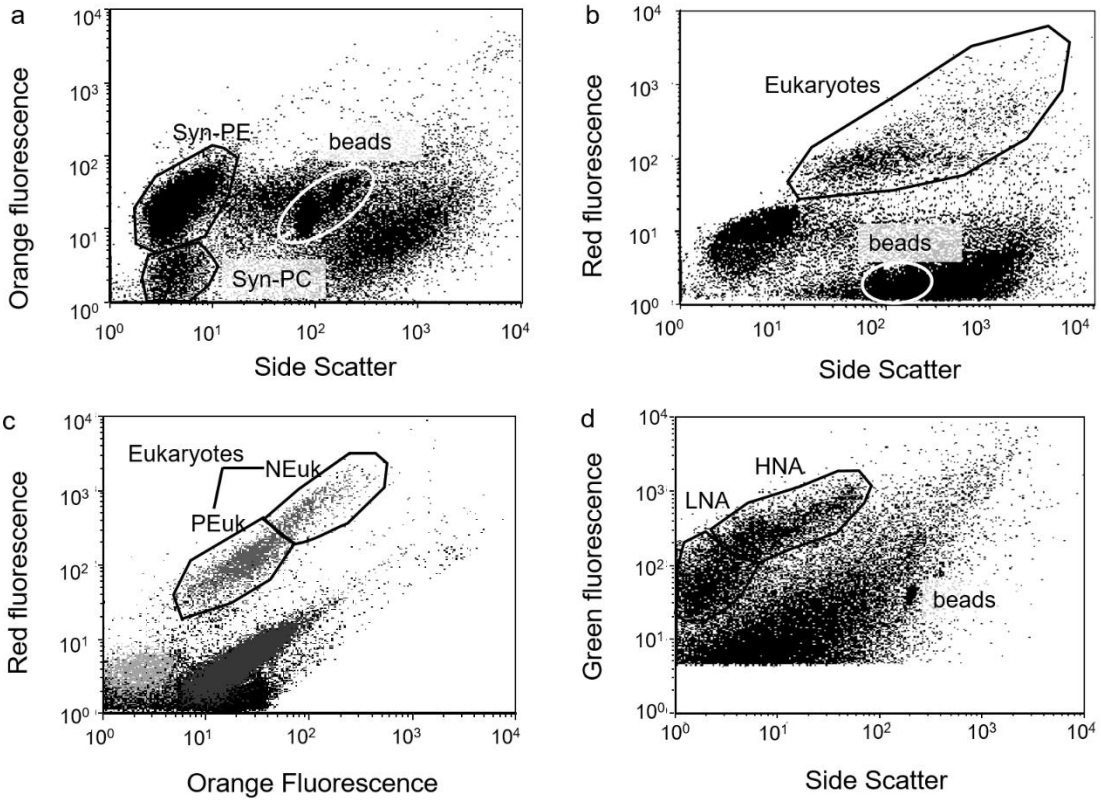

Fig. S2: Examples of cytograms of the four assemblages: *Synechococcus* phycoerythrin-rich cells (Syn-PE), *Synechococcus*- phycocyanin-rich cells (Syn-PC), PicoEukaryotes (PEuk), NanoEukaryotes (NEuk), high acid nucleic bacterial cells (HNA) and low acid nucleic bacterial cells (LNA) identified in the inner part of the Gulf of Nicoya. (a) Windows for photosynthetic picocyanobacteria groups, i.e. *S* Syn-PE and Syn-PC, (b-c) Windows for PEuk and NEuk, and (d) Windows for bacterial groups i.e. high nucleic acid cells (HNA) and low nucleic acid cells (LNA) (red region) after SyBR green I staining. Beads are the internal standard on every sample (1.1 µm).

CHAPTER IV

What supports the deep chlorophyll maximum in acidic lakes? The role of the bacterial CO_2 production in the hypolimnion

What supports the deep chlorophyll maximum in acidic lakes? The role of the bacterial CO_2 production in the hypolimnion

Sara Soria-Píriz [1*], Miguel Lara[1], Juan Luis Jiménez-Arias[1], Sokratis Papaspyrou[1], Bárbara Úbeda[2], Emilio García-Robledo[1, 3], Julio Bohórquez[1], José Ángel Gálvez[1], Niels Peter Revsbech[3], Alfonso Corzo[1]

[1]Department of Biology, Faculty of Marine and Environmental Sciences, University of Cádiz, Campus of International Excellence of the Sea (CEIMAR), Polígono Rio San Pedro s/n 11510 Puerto Real, (Cádiz) Spain.
[2]Instituto Universitario de Investigación Marina (INMAR), University of Cádiz, Campus of International Excellence of the Sea (CEIMAR), Polígono Rio San Pedro s/n 11510 Puerto Real, (Cádiz) Spain.
[3]WATEC, Microbiology Section, Department of Bioscience. Aarhus University. Ny Munkegade 116, DK-8000, Aarhus, Denmark

ABSTRACT: The interactions between phytoplankton, bacteria and resources, irradiance and nutrients, leading to the formation of deep chlorophyll maxima (DCMs), are little understood in acid lakes. In "El Sancho" reservoir (Iberian Pyritic belt, Huelva, Spain), an acid mine drainage impacted water body (pH 3.5 - 4.0), a strong DCM forms in the metalimnion during the stratification period. The DCM was located always below the 1% irradiance level, where the decreasing irradiance profile overlapped with a dissolved inorganic carbon concentration (CO_2) gradient decreasing upward from the hypolimnion. The DCM was dominated by the chlorophyte *Carteria* sp. and showed the highest volumetric photosynthetic and dark respiration rates. The DCM, however, only contributed around 20 % of water column integrated gross primary production, while it accounted for 54 - 66 % of water column chlorophyll. The total bacterial abundance correlated significantly with the CO_2 concentration ($r = 0.74$). To test the hypothesis of a possible dependence of the formation of the DCM in acid lakes on the production of CO_2 by heterotrophic bacteria, a 1-D reactive transport model (DCM-CO_2) was developed and tested. The DCM-CO_2 model simulated the vertical distribution of chlorophyll ($R^2 > 0.63$) and the vertical profile of CO_2 rather accurately ($R^2 > 0.79$), the position of DCM depending on both light penetration and an upward flux of CO_2 produced by hypolimnetic heterotrophic bacteria. Overall, the results support the hypothesis of microbial degradation of organic matter being a source of CO_2 for acid lake primary producers at the DCM.

KEYWORDS: net metabolism, acid lake, microbial community, modelling, fluxes, dissolved inorganic carbon, light, deep chlorophyll maximum

Published in *Limnology and Oceanography* (2019) doi: 10.1002/lno.11391

1. Introduction

Deep chlorophyll maxima (DCMs) are subsurface water layers enriched in chlorophyll commonly found in relatively nutrient-poor stratified open ocean waters (Cullen 1982; Huisman et al. 2006; Martin et al. 2010; Latasa et al. 2017) and lakes (Abbott et al. 1984; Barbiero and Tuchman 2004; Clegg et al. 2012). Generally most DCMs result both from a certain increase in chlorophyll per cell (Latasa et al. 2017) and from the accumulation of phytoplankton cells, forming deep biomass maxima (DBMs) as well. Coinciding DCMs and DBMs can be found at the intersection of two opposite resource gradients, light from the surface and nutrients from the bottom (Abbott et al. 1984; Durham and Stocker 2012).

Acid lakes (Nixdorf et al. 1998; Tittel et al. 2003), due to the high concentration of dissolved metals and low pH in the water column, are extreme environments with specific biogeochemical characteristics and microbiotas (Nixdorf et al. 1998; Torres et al. 2014; Corzo et al. 2018). Thus, while in typical aquatic ecosystems nitrogen and phosphorous are often considered as the primary limiting nutrients, in acid lakes, carbon and phosphorous have been suggested as the main nutrients limiting phytoplankton primary production (Nixdorf et al. 1998). In the epilimnion of these environments, dissolved inorganic carbon (DIC) is available primarily as carbon dioxide (CO_2), at concentrations near the equilibrium with air as determined by Henry´s law (Nixdorf et al. 1998; Tittel et al. 2005). However, although phosphates are highly soluble at low pH, the high concentrations of metals in acid lakes promote their co-precipitation with Fe(III) oxyhydroxides under aerobic conditions, reducing their bioavailability for the photosynthetic organisms in the water column (Nixdorf et al. 2001). Despite these limitations under extreme conditions, DCMs have been reported in acid lakes, where chlorophyll a (Chl *a*) concentrations may reach about 30 µg L^{-1} similar to the values found in eutrophic lakes (Nixdorf et al. 1998). Therefore, DCMs can contribute significantly to the water column-integrated primary production in acid environments. However, the physicochemical and biological processes that determine and favor the development of DCM and whether this coincides with a DBM in different aquatic environments and especially in acid lake settings are still under debate (Fennel and Boss 2003; Cullen 2015).

El Sancho reservoir (SW Spain), located in Iberian Pyritic Belt, is a warm monomictic freshwater reservoir, that has undergone an acidification process over the years (pH 3.5 - 4.5) due to ongoing pollution by acid mine drainage (AMD) (Torres et al. 2013, 2014). In summer, during the stratification season, a sharp DCM appears at the bottom of the photic layer; however, its ecological characteristics, including the vertical distribution of phyto- and bacterioplankton are unknown (Torres et al. 2016). Previously, the microbial community and the limnological characteristics have been studied in small pit acidic lakes in the Iberian Pyritic Belt; however, these systems are not comparable to El Sancho reservoir due to their different origin, small dimensions and more extreme conditions (pH < 3) (Sánchez-España et al. 2012; Santofimia et al. 2013).

Here, we present a detailed description of the conditions under which the seasonal DCM develops in El Sancho, focusing on the net metabolism of the plankton community and on the interactions between the main pelagic microbial communities: phyto- and bacterioplankton. We provide field experimental evidence supporting the hypothesis that bacterial CO_2 production in the hypolimnion is an important source of inorganic carbon contributing to the formation of the DCM. This hypothesis was tested by a 1-D reactive transport model, which predicted the phototrophic biomass and CO_2 vertical distribution as a function of irradiance and the abundance of heterotrophic bacteria.

2. Materials and methods

2.1 Study site and sampling collection

El Sancho Reservoir (4.27 km^2, 58 hm^3) was built in 1962. Its main tributary, the River Meca (pH 2.6) is heavily contaminated by AMD with high concentrations of trace metals, iron and sulfate and is responsible for its acidification (Torres et al. 2013).

Samplings were carried out at one station (37°27'49''N, 6°59'3''W) located at the deepest part of the El Sancho reservoir (34.5 m average depth) four times during the stratification period in 2013 (12th, 18th and 25th September and 8th October 2013) (Fig. S1). Vertical temperature (T, ºC), pH, and fluorescence (relative units, r.u.) profiles were obtained using a multiparameter probe (Hydrolab MS5). Photosynthetically active irradiance profiles (PAR) (µmol photons m^{-2} s^{-1}) were obtained using a LiCor (Li-1400) radiometer equipped with a planar probe; the light extinction coefficient (k) was then calculated (Kirk 1994). Based on the fluorescence profile, water samples were collected using a 10 L Van Dorn bottle (7-17 depths).

Sediment cores (n = 8) (Plexiglas tubes, i.d. 5.8 cm, length 60 cm) were collected using a Kajak corer (KC Denmark A/S), stored on ice (4ºC) in the dark, and kept under water at 13ºC overnight once in the laboratory after 4 - 5 h.

Two independent sets of sediment traps were deployed on 12th September. In each set, four traps (Plexiglas tubes, i.d. 7 cm, length 50 cm) were installed between 23 and 25 m and another four between 31 and 34 m. Traps were left in situ for 28 days.

2.3 Water column and sediment analyses

Samples for dissolved oxygen (O_2) determination (n = 2 per depth) were collected and fixed in 12 mL Exetainer tubes (Labco Ltd, UK) following Labasque et al. (2004), stored in darkness at 4 °C, and analyzed within 24 hours (Limit of detection, LOD: 3.8 µmol L^{-1}). O_2 saturation was determined as a function of the water column temperature according to García and Gordon (1992). High-resolution O_2 profiles were determined on the 2th and 8th October with a modified MP4 Miniprofiler (UNISENSE, Fig. S2). CO_2 samples (n = 1 per depth) were collected in 5 mL Exetainer tubes, fixed with 100 µL saturated $HgCl_2$ and stored in darkness at 4 °C until analysis. CO_2 was measured following the setup of Hall and Aller 1992 on an InfraRed Gas Analyzer (Qubit systems, S151 CO2 analyzer) (LOD: 6.8 µmol L^{-1}).

Inorganic nutrients were analyzed in filtered water samples (MF 300, 0.7 µm, 47 mm, Fisherbrand™), stored on ice and frozen at -20ºC upon return to the laboratory. Ammonium (NH_4^+) (Bower and Holm-Hansen 1980), phosphate (PO_4^{3-}) (Grasshoff et al. 1999) and nitrate (NO_3^-) and nitrite (NO_2^-) (García-Robledo et al. 2014) were measured with LOD between 0.1 and 0.5 µmol L^{-1}.

For determination of Chl *a*, water samples (1 L) were filtered *in situ* through pre-combusted filters (GF/F glass fiber filters, 0.7 µm, 47 mm, Whatman®), stored on ice in darkness, and frozen at -20 °C upon return to the laboratory. Chlorophyll *a* was extracted at 4 °C for 12 hours with 4 mL of acetone 90%, tubes centrifuged (2200 x g, 5 min) and the absorbance of the extracts measured on a UV 1700 Pharmaspec Shimadzu spectrophotometer. Chl *a* concentration was calculated according to Ritchie (2008).

Dissolved organic carbon (DOC) was measured in water samples (approximately 20 mL), filtered through nylon filters (Nylon Syringe filters,0.2 µm, 25 mm, Fisher Scientific™) in acid washed

glass vials (n = 1) and stored at 4ºC. DOC contents were determined on a Shimadzu TOC-5050 analyzer on acidified samples (1 mL of phosphoric acid 1: 3) (ICMAN-CSIC external services). Particulate organic carbon (POC) and total nitrogen (PTN) samples were collected similarly to chlorophyll on preweighed filters and determined on a FlashEA1112 (ThermoFinnigan) elemental analyzer (University of A Coruña external services).

Sediment cores (2 replicates per sampling) were sliced at a 1-cm interval for the first 6 cm and 2-cm intervals down to 18 cm depth within 24 hours of collection under a flow of N_2, and slices from the same depth pooled. Pore water was extracted by centrifugation from each layer, filtered through nylon filters (Nylon Syringe filters,0.2 μm, 25 mm, Fisher Scientific™) and stored at -20ºC until analysis of NH_4^+ and NO_3^- as described previously. Total organic carbon (C_{org}) and total nitrogen contents (N_T) were analysed on a FlashEA1112 (ThermoFinnigan) elemental analyzer using standard protocols (University of A Coruña external services) on sediment samples dried at 60ºC for 24 hours (expressed as g [g dry sediment]$^{-1}$ × 100).

For porewater CO_2 determination, sediment cores (3 replicates) were sliced every 2 cm for the first 6 cm and every 4 cm down to 18 cm depth within 24 hours. Extracted pore water was fixed with 100 μL saturated $HgCl_2$ and stored in darkness at 4 °C until analysis as described previously.

Collected sediment traps, once in the lab, were left undisturbed at 4 ºC to allow the particles to settle, supernatant removed and particulate material dried at 60 °C and analysed for C_{org} and N_T as described previously.

2.4 Fluxes calculation through water column and sediment

Assuming steady state conditions, the net rates of O_2, CO_2, NH_4^+ and NO_3^-production and consumption were calculated for the epilimnion, metalimnion and hypolimnion layers according to Fick´s first law applied to turbulent diffusion (Okubo and Levin 2001).

$$J_C = -K_d \frac{dC}{dz} \qquad (1)$$

where J_c is the net flux of substance C, K_d is the vertical turbulent diffusion coefficient, and dC/dz is the concentration gradient. Here, dC/dz was calculated for each layer from the measured concentration profiles and K_d (m^2 s^{-1}) was calculated by equation 2 (Osborn 1980):

$$K_d = \frac{\gamma \varepsilon}{N^2} \qquad (2)$$

where γ is the mixing coefficient and ε is the dissipation rate of turbulent kinetic energy. Values of 0.15 for γ and 9 x 10^{-9} W kg^{-1} for ε were used (Wuest et al. 2000). The frequency of Brunt-Väisälä (N, s^{-1}), which measures the stability of the water column, was calculated according to equation 3 from the density gradient in depth (dρ/dz) in each layer (Gargett 1984):

$$N^2 = \frac{g}{\rho} \frac{d\rho}{dz} \qquad (3)$$

where g is the gravitational acceleration and ρ is the mean water density for each layer.

CO_2 and NH_4^+ fluxes at the sediment-water interface were calculated using Fick´s law applied to molecular diffusion and the concentration gradient with depth from 2 cm above the sediment surface to 5.5 cm below the sediment surface (maximum linearity). The apparent molecular diffusion coefficient (Ds, $m^2\ d^{-1}$) for each substance was calculated with Marelac R package (version 2.1.9) (Soetaert et al. 2010) the specific *in situ* T and pressure, and taking into account the average porosity (0.88) of the sediment (0 – 5.5 cm) (Torres et al. 2014).

2.5 Microbial community analyses

Water samples were fixed in cryotubes (4.5 mL) using glutaraldehyde (1% final concentration) and frozen at –80 ºC until analysis by flow cytometry. Prior to the analyses, autofluorescent beads (1.1 µm diameter, Ex/Em: 430/465 nm, FluoSpheres® Molecular Probes Inc.™) were added to each sample (1 mL) as an internal standard. Phytoplankton was identified based on autofluorescence. For bacterioplankton, 10 µL of SYBR® Green-I (Molecular Probes #S7563) (2.5 µM final concentration) was added to each sample and incubated for 10 min at room temperature in darkness before analysis. Samples were analyzed on a Dako CyAnTM ADP (Beckman Coulter™) flow cytometer. Further methodological details can be found in Corzo et al. (1999), Gasol and del Giorgio (2000) and Corzo et al. (2005). Biomass of each group (in µg C L^{-1}) was estimated from cell diameter and cell abundance using published empirical equations (Suppl. Material).

Taxonomic identification of phytoplankton was carried on an inverted light microscope (Nikon Eclipse Ti-U) in water samples collected in polyethylene bottles (100 mL), stored *in vivo* at 4 °C in dark and analysed within 24 hours after collection.

2.6 Photosynthesis-Irradiance curves

Water samples from specific depths (0, 5, 16, 22.5 and 30 m depth) were collected using a 10 L Van Dorn bottle (September 25th) and transported to the laboratory. Incubations were performed in special bottles under continuous stirring at 17 ºC under increasing irradiances (0, 50, 100, 200, 400 and 600 µmol photons $m^{-2}\ s^{-1}$). Changes in O_2 concentration to determine net primary production (Pn) and dark respiration (Rd) rates were measured with STOX sensors (Revsbech et al. 2011), with a resolution lower than 2 nmol $O_2\ L^{-1}\ h^{-1}$ (Tiano et al. 2014). Photosynthesis-irradiance ($P - E$) curves for each water depth and the corresponding photosynthetic parameters were obtained after fitting the experimental data to the Jassby and Platt (1976) model (Suppl. Material).

2.7 Numerical modelling of the Chl *a* and CO_2 vertical distributions

A 1-D reactive transport model was developed to predict the spatial distribution of the phototrophic biomass (Chl *a*, mg m^{-3}) for the four sampling dates. The basic equations of this model were based on pre-existing literature about DCM (Fennel and Boss 2003; Huisman et al. 2006; Gong et al. 2015) and coupled the light and inorganic carbon dependency of growth with both turbulent diffusion (mixing) and a sinking term along the vertical axis, according to equation 4:

$$\frac{\partial B}{\partial t} = (\mu - l) * B + K_d\left(\frac{\partial^2 B}{\partial z^2}\right) - W_s\left(\frac{\partial B}{\partial z}\right) \qquad (4)$$

where z is depth (m, in positive values), B is the Chl *a* concentration (mg m^{-3}), μ is the specific growth rate (d^{-1}), l is the natural mortality (d^{-1}), K_d is the turbulent diffusion coefficient (m^2 d^{-1}) and W_s is the bulk sinking velocity of phytoplankton (m d^{-1}). Biomass production was set by the variable μ, which depended on the maximum growth rate μ_{max} and a minimum law (Liebig's law) applied to the two limiting factors, light and inorganic carbon by two respective dependent functions (i.e. f(E) and $f(CO_2)$), according to equation 5:

$$\mu\big(E(z), CO_2(z)\big) = \mu_{max} \min(f\big(E(z)\big), f\big(CO_2(z)\big)) \qquad (5)$$

The f(E(z)) was modelled as an hyperbolic light-production curve (Jassby and Platt 1976), according to the equation 6:

$$f\big(E(z)\big) = tanh\left(\frac{E(z)}{E_k(z)}\right) \qquad (6)$$

where E(z) is the light irradiance at depth z (which obeys to an exponential attenuation) and E_k is the light-saturation of photosynthesis (μmol photons m^{-2} s^{-1}). To account for the photoacclimation of cells, a critical process in oligotrophic lakes (Fennel and Boss 2003; Leach et al. 2018), the E_k parameters which were obtained with the five experimental *P-E* curves (i.e. at 0, 5, 16, 22.5 and 30 m depth, see *Photosynthesis-Irradiance curves* section) were linearly interpolated along profiles. Due to the acidic conditions of the water column in our system, HCO_3^- is < 0.1 % of total dissolved inorganic carbon, therefore CO_2 was the only inorganic carbon specie considered in the model. The $f(CO_2)$ was set to a Monod type response according to the equation 7:

$$f\big(CO_2(z)\big) = \frac{CO_2(z)}{CO_{2\,half} + CO_2(z)} \qquad (7)$$

where CO_2 (z) is the inorganic carbon concentration at depth z (μM) and $CO_{2\,half}$ is the half-saturation constant (μM, Reynolds and Irish 1997). The observed values of CO_2 concentrations at the epilimnion layer were assumed to be close to 0 μM since concentrations were below the detection limit (i.e. < 6.85 μM).

In addition to modelling the DCM, the profiles of CO_2 were modelled as a function of two reaction terms (i.e. CO_2 production by heterotrophic bacteria – CO_2 consumption by primary producers), according to equation 8:

$$\frac{\partial CO2}{\partial t} = K_d\left(\frac{\partial^2 CO2}{\partial z^2}\right) + (R - P) \qquad (8)$$

where *R* is the CO_2 production due to the mineralization of organic matter (OM) (mmol C m^{-3} d^{-1}) and *P* is the CO_2 consumption rate due to the net photosynthesis of phytoplankton (mmol C m^{-3} d^{-1}).

The term *P* was estimated as a function of growth rate, biomass abundance and the carbon-to-chlorophyll a ratio (C:Chl *a*) and represent the CO_2 demand at a given depth (equation 9, Cloern et al. 1995)

$$P(z) = \mu(z) * B(z) * (C{:}Chl\ a) * \left(\frac{1}{12}\right) \qquad (9)$$

where μ was calculated from equation 8 and C:Chl *a* is the mg C: mg Chl *a* ratio. Two different values of the C:Chl *a* were used by the epi- and metalimnion layers since experimental POC:Chl *a* showed a wide range throughout the corresponding depths.

Rates of *Pg* were also extracted from the model, in order to compare with the experimental values calculated from the *P-E* curves. The conversion of P values to *Pg* rates was addressed by considering two respiratory terms, i.e. a basal respiration of phytoplankton (R_{min}) which is independent on the photosynthetic gross production rate, and a second respiration term which increase linearly with photosynthesis (R_{phot}, Eq. 10). These parameters were initially obtained from the universal relationship between growth rate and respiration reported by Cloern et al. (1995), but recalibrated to better fit with our P*g* and Chl *a* data.

$$Pg(z) = \frac{1}{(1-R_{phot})} * (\mu(z) + R_{min}) * B(z) * (C{:}\,Chl\ a) * (\frac{1}{12}) \qquad (10)$$

where R_{min} is the minimum respiration rate (≈ 0.015 d^{-1}) and R_{phot} is the fraction of *Pg* respired (≈ 0.15, Cloern et al. 1995).

Bacterial respiration was considered to be the result of both aerobic and anaerobic respiration since O_2 levels decreases from 400 µM to nearly 0 µM through the water column depth. Therefore, *R* was a function of T, bacterial abundance and O_2 availability (equation 11, Grégoire et al. 2008)

$$R(z) = \left(Bact\ (z) * \left(R_A * \left(\frac{O_2(z)}{O_2(z)+K_S} \right) + R_{An} * \left(1 - \frac{O_2(z)}{O_2(z)+K_I} \right) \right) * f(T) \right) \qquad (11)$$

where Bact (z) is the measured bacterial abundance (cell m^{-3}), R_A is the maximal specific rate of aerobic respiration (mmol C $cell^{-1}$ d^{-1}), R_{An} is the maximal anaerobic respiration (Soetaert et al. 1996), O_2 (z) is oxygen concentration at depth z (µM), K_S is the half-saturation constant for aerobic respiration (µM), K_I is the half-inhibitory constant for anaerobic respiration (µM), and f(T) is a correction factor of *R* as a function of T (equation 12)

$$f(T) = Q_{10}^{\left(\frac{(T(z)-T_{ref})}{10} \right)} \qquad (12)$$

where Q_{10} is the metabolic enhancement factor, $T(z)$ is T at depth z (ºC), and T_{ref} is the superficial temperature for each sampling period (ºC). Note that equation 11 allows a clear vertical structure of metabolisms for extremely high or extremely low values of O_2, but also a coexistence of both anaerobic and aerobic activities for depths with low O_2 concentrations, as other authors confirmed in marine ecosystems (Grégoire et al. 2008; García-Robledo et al. 2017).

Numerical simulations of Chl *a* and CO_2 profiles were carried out by solving the steady state of both Equations 4 and 8 across a 10^{-2} m resolution grid, i.e. with a linear system of 2 x 3300 equations for a maximal depth of ≈ 33 m. Spatial discretization was performed with a second-order approximation of derivatives, but a purely upwind scheme for the sinking term to avoid numerical instabilities (Soetaert and Herman 2009). Boundary conditions for Chl *a* were set as zero-flux at z = 0 (Huisman et al. 2006) and as known Chl *a* values (measured in every sampling date) at the maximum depth, i.e. biomass export toward the sediment was allowed (Torres et al. 2013). Boundary conditions for CO_2 at the water-atmosphere interface followed a piston-based flux according to equation 13 (Schindler 1975; Cole and Caraco 1998; Cole et al. 2002):

$$F_{CO2}^{atm}\ (z = 0) = K_{piston} * \left(C_{eq} - CO_2(z = 0)\right) \quad (13)$$

where F_{CO2}^{atm} (z = 0) (mmol C m^{-2} d^{-1}) and CO_2 (z = 0) (µM) are respectively the imposed flux and concentration at the upper boundary of the profile, K_{piston}=10^{-5} m s^{-1} is the piston velocity of CO_2 with no wind and with no chemical enhancement (Jørgensen 1979a; Jørgensen 1979b) and C_{eq} is the equilibrium concentration according to Henry's law (µM, Soetaert et al. 2010). At the bottom boundary, sediment was a net source of CO_2 due to mineralization of OM. Values of this flux were estimated by inverse modelling considering a range between the zero-flux of CO_2 from the sediment as the "minimum flux" and the flux of CO_2 in the hypolimnion as the "maximum flux", which was determined for each sampling. Sediment CO_2 fluxes were similar to the experimentally determined CO_2 efflux obtained on the 25th September and to previous studies (Torres et al. 2014; Corzo et al. 2018).

The coupled DCM-CO_2 model included a total of 14 parameters that were calibrated simultaneously to fit the experimental information on each sampling date. The minimum and maximum limits for calibrated parameters were taken from the literature (see *References* from Table 3). In addition, W_s was determined from the dominant (in biomass) phytoplankton at the DCM, *Carteria* sp. (ca. 1.9*10^{-5} m s^{-1}, calculated by Stoke's law). Since the error threshold for growth rates according to Cloern et al. (1995) were up to 35%, a reasonable uncertainty in the respiration of phytoplankton was considered accordingly, and the upper and lower limits for R_{min} and R_{phot} were set as ± 20% of the original parameters calculated by these authors. Calibrations were made with ReacTran R package (version 1.4.3.1) by adequately arranging model parameters to the spatial grid (Soetaert and Meysman 2012). Whereas K_d and E_k were measured, the remaining parameters were calibrated by the pseudo-random algorithm of Price until the predicted Chl *a* and the CO_2 profiles fitted with the field observations (EcolMod R package version 1.2.6, Soetaert and Herman 2009). Further details of the model, as well as a description of the R code, are included within Suppl. material.

2.8 Statistical analyses

Simple linear correlation (Spearman correlation) and regression analyses were used to test statistical significance of variation between different variables through both spatial and temporal scales. A correlation of observed versus predicted values was used to check the goodness of fit of the model outputs. Percentage of variation explained by the ecological model was calculated by the R^2 coefficients, testing firstly that the intercept and the slope were not statistically different from zero and from 1 (t-test), respectively. All analyses were made with Stats R package (version 3.5.2) (R Core Team 2014).

3. Results

3.1 Water column structure

The photic layer extended down to 18 – 22 m depth (1% of surface irradiance) depending on sampling date (Fig.1a). The k value for light attenuation increased considerably at 18 - 19 m, from 0.12 - 0.18 m^{-1} in the epilimnion to very high values at the bottom of the thermocline (0.71 - 0.97 m^{-1}). Fluorescence and Chl *a* showed a similar vertical distribution (r = 0.65, p < 0.001, n = 45), showing a pronounced deep chlorophyll maximum (DCM) at the bottom of the photic layer at irradiances between

1.3 – 11.1 µmol photons m^{-2} s^{-1}. Chl *a* concentration was 1 to 2 orders of magnitude higher at the DCM peak compared to surface waters.

POC showed a vertical distribution similar to Chl *a* (r = 0.94, p < 0.001, n = 45), including a peak in POC at the same depth as Chl *a*. POC:Chl *a* ratio (mg C mg $Chla^{-1}$) at the epilimnion changed considerably between samplings but decreased with depth showing a minimum (72.4 ± 4.4) at the DCM. From the DCM toward the bottom, POC:Chl *a* increased due to a relative decrease in Chl *a* (Fig. 2). The POC:PTN ratio decreased from the DCM depth toward the bottom due to the relatively higher decrease of POC with respect to PTN. (Fig. 2).

The water column was stratified showing a marked thermocline between 15 and 24 m depth (Fig.1b). Temperature decreased from 25.5 ºC on average in the epilimnion to less than 13.5 ºC in the hypolimnion. pH was rather constant in the epilimnion and metalimnion (around 3.5), increasing linearly with depth in the hypolimnion up to 4.5 (Fig.1b)

Oxygen concentration was constant in the epilimnion (270 ± 5 µM), increasing sharply right below the beginning of the thermocline where it ranged from 362 to 439 µM (Fig.1c) (129 - 158% saturation) (Fig.1c). From this peak, O_2 decreased down to 20 to 25 m depth to concentrations below 10 µM (often below the LOD) until the bottom (Fig.1c). CO_2 concentrations were below the LOD in the epilimnion and in the upper part of the thermocline, but increased linearly with the depth up to 670 µM near the bottom (r = 0.94, p < 0.001, n = 43) (Fig.1c). CO_2 and O_2 concentrations showed a strong inverse correlation in the hypolimnion (r = -0.97, < 0.001, n = 15).

NH_4^+ concentrations were constant in the epilimnion and increased linearly from the thermocline downwards, reaching concentrations >100 µM close to the sediment surface (Fig.1d). In the hypolimnion, NH_4^+ tended to increase slightly during successive samplings and showed a high positive correlation with CO_2 (r = 0.93, p < 0.001, n = 43). NO_3^- concentrations were much lower (< 3 µM) and showed an inversed vertical distribution to those of NH_4^+ (Fig.1d). PO_4^{3-} and NO_2^- were always below the LOD. DOC concentration did not show any consistent vertical pattern (Fig.1d). DOC:POC in the epilimnion decreased towards the DCM layer and remained constant with depth in the hypolimnion (Fig. 2).

3.2 Water column net fluxes

The shape of the vertical profiles of O_2, CO_2, NH_4^+ and NO_3^- indicated the existence of strong gradients associated with the presence of the DCM (Fig. 1c-d). K_d values were higher and more variable between samplings in the epilimnion, particularly due to a very high value on September 25th, while the values at the hypolimnion and metalimnion were one order and three orders of magnitude lower, respectively, and more constant (Table 1).

Despite the relatively high homogeneity of O_2 concentration in the epilimnion, we calculated a relatively high O_2 production rate and net flux toward the atmosphere due to the high K_d estimated for the epilimnion (Table 1). The O_2 concentration peak in the metalimnion was associated with high O_2 production rates (6.2 ± 0. 4 mmol O_2 m^{-2} d^{-1}) in this layer (15 – 24 m). O_2 net consumption rate in the hypolimnion was very low, mainly due to the very low O_2 available in this lake compartment (Fig. 1, Table 1).

Vertical profiles of CO_2 clearly indicated a strong gradient from the bottom of the reservoir to the metalimnion where it was consumed. While in the hypolimnion's CO_2 presented an upward flux ranging from 19.8 to 46.7 mmol CO_2 m^{-2} d^{-1}, the net flux in the metalimnion was considerably lower

due to both a decrease in the concentration gradient and a much lower K_d than in the hypolimnion (Table 1).

Ammonium net fluxes at the epilimnion were very variable due to the variability of concentrations and the value of K_d across samplings (Table 1). In contrast, NH_4^+ was always consumed in the metalimnion, whereas a high net upward flux in the hypolimnion toward the DCM was detected in all samplings (4 ± 0.3 mmol m^{-2} d^{-1}). CO_2:NH_4^+ upward flux stoichiometry was about 8.5 ± 0.9. Nitrate net fluxes were always one to several orders of magnitude lower than those calculated for NH_4^+ (Table 1). In the epilimnion, NO_3^- was generally produced, while it was consumed in the meta- and hypolimnion.

Sedimentation rate of OM from the DCM, measured with sediment traps, was 19.9 ± 3.2 mmol C_{org} m^{-2} d^{-1} with a C:N stoichiometry of 9.6 ± 0.3, similar to the CO_2:NH_4^+ upward flux stoichiometry. An estimate for the average sedimentation velocity (v) of POC, calculated from POC sedimentation rates (traps) and POC concentration at the DCM peak (v = POC downward flux / POC concentration at DCM), gives values between 0.15 and 0.23 m d^{-1}. These values are much lower than those calculated using the cell size of the main contributor to the phytoplanktonic biomass (*Carteria* sp., see below) using the Stokes equation (0.78 – 1.68 m d^{-1}).

3.3 Sediment concentrations and net fluxes to the water column

C_{org} and N_T decreased considerably from ~ 12 to 3 % and from ~ 1.4 to 0.3 %, respectively, in upper 7.5 cm sediment layer, remaining constant with depth below (Fig. 3a). C_{org}:N_T was 10.1 ± 0.1 at the sediment surface and changed very little with depth (Fig. 3a). The CO_2 profile indicated net production in the uppermost sediment layers increasing from 640 µM in the bottom water to about 2500 µM at 5 cm depth within the sediment, remaining constant or even decreasing slightly at higher depths (Fig. 3b). CO_2 production rate and subsequent efflux to the water column was 2.6 mmol CO_2 m^{-2} d^{-1} (Table 1). Porewater NH_4^+ profiles indicated a net production of NH_4^+ within the sediment (Fig. 3b) and a net efflux of NH_4^+ to the water column of 1.19 ± 0.3 mmol NH_4^+ m^{-2} d^{-1} (Table 1). Interestingly, CO_2:NH_4^+ stoichiometric efflux from the sediment was about ~ 2, much lower than the stoichiometry of the upward flux in the hypolimnion and the downward flux of OM.

3.4 Microbial community structure

Three main phytoplankton populations were discriminated in El Sancho by their flow cytometry signatures (result not shown). Two of them were in the pico- size fraction, identified as PicoEukaryotes (PEuk) and *Synechococcus–like* cells (Synech), while the other one was in the nano- size fraction. These cells were identified by optical microscopy as the Chlorophyte *Carteria* sp.

Phytoplanktonic groups presented a clear niche separation. PEuk (1.4×10^6 - 1.5×10^7 cells L^{-1}) was the only fraction observed in the epilimnion, whereas the DCM was formed by the accumulation of Synech (3.3×10^6 - 7.2×10^7 cells L^{-1}) and *Carteria* sp. (1.7×10^5 - 3.2×10^6 cells L^{-1}). Despite being less abundant, *Carteria* represented most of the phytoplankton biomass (> 99 %) at the DCM and in the hypolimnion due to their much higher cell size (Table 2). In addition, of the three phytoplanktonic groups, *Carteria* abundance showed the highest correlation with Chl *a* (r = 0.79, < 0.001, n = 43). The coincidence of vertical distributions of total phytoplankton biomass, Chl *a* concentration and fluorescence clearly confirmed that the DCM was a biomass maximum as well (Fig. 4).

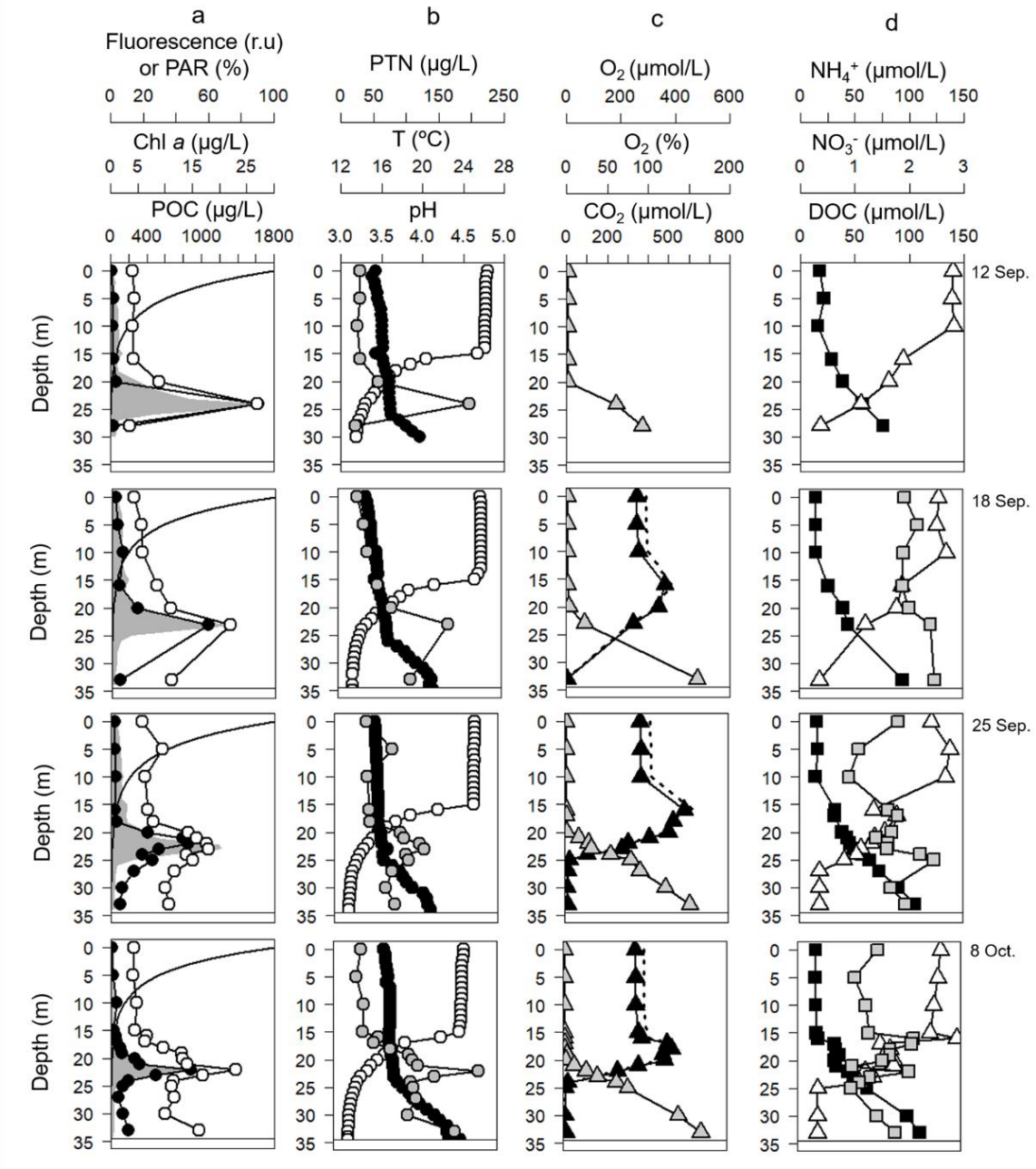

Fig.1. Depth profiles of *water column* variables during the sampling period in El Sancho reservoir. (a) chlorophyll *a* (Chl *a*,), particulate organic carbon (POC,), fluorescence ( ), and irradiance expressed as percent of photosynthetically active radiation at the surface (PAR,); (b) particulate total nitrogen (PTN,), temperature (T,) and pH ( );(c) dissolved oxygen (O_2,), percent saturation of dissolved oxygen (O_2,), and carbon dioxide (CO_2,); (d) ammonium (NH_4^+,), nitrate (NO_3^-,) and dissolved organic carbon (DOC,). The bottom of reservoir is shown with a horizontal black line.

Bacterioplankton abundance ranged between 4×10^7 and 5.2×10^8 cells L^{-1} depending on sampling date and depth. Bacterial biomass was low and rather constant in the epilimnion as observed previously for the phytoplanktonic biomass. It increased with depth from the thermocline to the hypolimnion, especially in the last sampling (Fig. 4) and was clearly associated with the DCM's position. From the thermocline down to the bottom of the hypolimnion, total bacterial biomass was highly correlated with CO_2 concentration ($r = 0.68$, $p < 0.001$, $n = 31$).

Table 1. Mean turbulent diffusion coefficient (K_d, $m^2\ s^{-1}$) and mean net fluxes of O_2, CO_2, NH_4^+ and NO_3^- (mmol $m^{-2}\ d^{-1}$) within every layer i.e. epilimnion, metalimnion, hypolimnion and sediment and their thickness (m for water column layers and cm for sediment layer) calculated from the corresponding observed vertical profiles. Fluxes within the sediment were calculated using different apparent molecular diffusion coefficients (Ds, $m^2\ d^{-1}$) for every substance and taking into account the sediment porosity. Mean molecular diffusion coefficients: CO_2: 1.17×10^{-4}, NH_4^+: 1.31×10^{-4}. Positive and negative signs are net production and net consumption rates respectively within the corresponding layer. Data are $n = 4 \pm$ se (standard error).

Layer	Thickness	K_d	O_2	CO_2	NH_4^+	NO_3^-
Epilimnion	0 - 15	$7.3 \times 10^{-5} \pm 4 \times 10^{-5}$	+ 2.7 ± 1	-	- 0.5 ± 0.4	+ 0.12 ± 0.11
Metalimnion	15 - 24	$5.2 \times 10^{-7} \pm 1.4 \times 10^{-8}$	+ 6.2 ± 0.4	+ 0.8 ± 0.2	+ 0.1 ± 0.02	- 0.004 ± 0.001
Hypolimnion	24 - 33	$8.6 \times 10^{-6} \pm 5.4 \times 10^{-7}$	- 7.3 ± 0.5	+ 34 ± 5.6	+ 4 ± 0.3	- 0.08 ± 0.01
Sediment	-2 – 5.5	-	~ 0	+ 2.62	+ 1.2 ± 0.3	-

3.5 *P-E* curves

P - E curves showed marked difference in the photosynthetic characteristics of the phytoplankton communities at the DCM and other depths (Fig. 5). Surprisingly, there was no evidence of photoinhibition (up to 600 µmol photons $m^{-2}\ s^{-1}$ tested) at any depth, despite the much lower *in situ* irradiance observed at increasing depths (Fig. 1a). Highest values of Pg^{max} and α were observed at the DCM (22.5 m depth), being much lower in the rest of the water column (Fig. 6a). The lowest *Ec* was determined for the DCM (19 ± 3 µmol photons $m^{-2}\ s^{-1}$), while the lowest *Ek* was at 16 m depth (Fig. 6a). *Rd* rates were less variable along the water column, showing a minimum at 30 m depth (Fig. 6a). Rates normalized to Chl *a* showed a different pattern. Maxima of $Pg^{\text{max Chla}}$ and Rd^{Chla} were at the surface and the highest α^{Chla} was determined at 16 m depth (Fig 6b). Ec^{Chla} and Ek^{Chla} had similar values and vertical pattern to those obtained when *Pg* was expressed by volume (Fig. 6b).

3.6 Numerical simulation of the coupled Chl *a* and CO_2 profiles

We tested through the DCM-CO_2 model whether the CO_2 produced from the mineralization of the OM in the hypolimnion and in the sediments can be the main source for photosynthetic carbon fixation at the DCM. The values obtained for the calibrated parameters were consistent with values reported in the literature (Table 3).

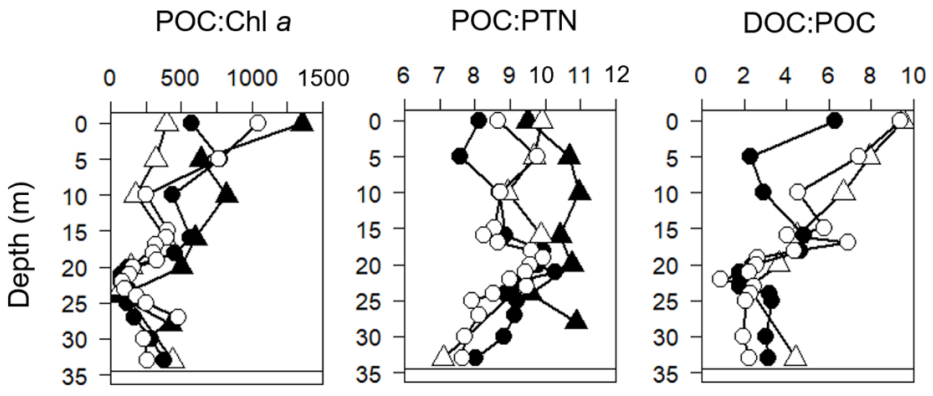

Fig. 2. *Water column* depth profiles of the particulate organic carbon to chlorophyll *a* ratio (POC: Chl *a*), particulate organic carbon to particulate total nitrogen ratio (POC: PTN) and dissolved organic carbon to particulate organic carbon ratio (DOC: POC) during the sampling period in El Sancho reservoir: 12th (—▲—), 18th (—△—), and 25th September (—●—) and 8th October (—○—) of 2013. The bottom of reservoir is shown with a horizontal black line.

The modelled Chl *a*, CO_2 and P*g* values agreed well with the experimental data (Fig. 7 and 8a). Correlation between modelled and observed data yielded values of R^2 between 0.63 - 0.77 for Chl *a* ($p < 0.001$), between 0.79 - 0.91 for CO_2 ($p < 0.001$) and 0.65 for P*g* ($p = 0.1$). The model reproduced rather accurately the DCM in the last two samplings in which the spatial resolution of the experimental data was higher. In addition, the model also reproduced well the temporal evolution of the DCM towards shallower peaks along the studied period (Fig. 7). However, the model estimates of Chl *a* at the DCM were always lower than the observed values. When the contribution of the sediment mineralization to the DCM was analyzed by running the model assuming zero CO_2 release from the sediment, we observed a general but very variable decrease of the DCM peak. The model reproduced well the changes in the observed CO_2 vertical profiles, except in the abrupt change of slope in the metalimnion–hypolimnion transition, likely due to the imposed abrupt changes in K_d, that likely did not exist *in situ* (Table 1, Fig. 7). Despite an evident resemblance, the correlation between modelled and experimentally determined vertical changes in P*g* rates as not statistically significant (only 5 pairs of points were available for the statistical correlation). Nonetheless, the model reproduced well the high rates observed in the upper part of the epilimnion and at the DCM (Fig. 8a) Phytoplankton growth rates extracted from the model (0.1 – 0.3 d^{-1}) showed a maximum at about 20.7 m depth, 2 m shallower than the peak of DCM (Fig. 8b). Phytoplankton growth was generally limited by CO_2 in the epilimnion, while it was light-limited in the meta- and in the hypolimnion.

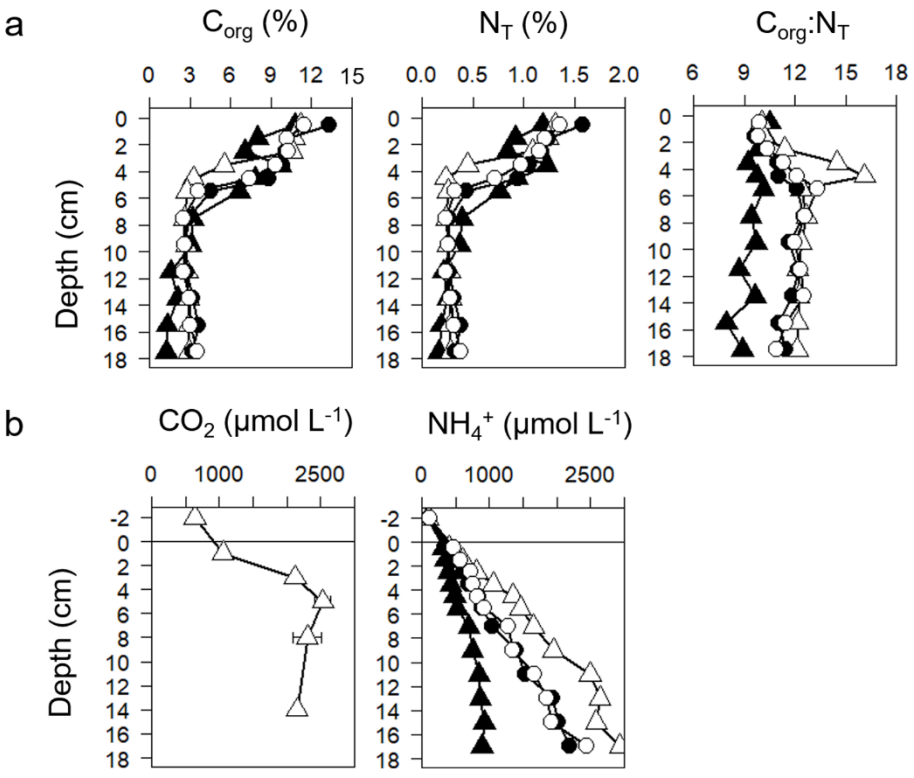

Fig. 3. *Sediment* depth profiles of (a) percent of organic carbon (C_{org}), percent of total nitrogen (N_T), carbon to nitrogen ratio (C_{org}: N_T), (b) carbon dioxide (CO_2) (n = 3) and ammonium (NH_4^+) during the sampling period. : 12th (▲), 18th (△), and 25th September (●) and 8th October (○) of 2013. CO_2 data correspond to a single sampling (16th September, △). The bottom of reservoir is shown with a horizontal black line.

4. Discussion

4.1 The ecological "niche" of the DCM in El Sancho

The DCM in El Sancho represents a DBM as observed in other freshwater (Gálvez et al. 1988, Sterner 2010, Leach et al. 2018) and marine ecosystems (Latasa et al. 2017) (Fig. 1, 4). Chl *a* at the DCM represented 54 - 66 % of the Chl *a* integrated in the entire water column. Nonetheless, the low POC:Chl *a* ratio observed at the DCM suggests the presence of photoacclimation mechanisms (Fennel and Boss 2003; Clegg et al. 2012) and it was in the typical range of actively growing phytoplankton (Cloern et al. 1995; Wang et al. 2009; Yacobi and Zohary 2010). DCM usually develop in a stable water column at the depth where at least two opposed resource gradients, e.g. light and nutrients, interact in the right proportion (Abbott et al. 1984; Camacho 2006; Martin et al. 2010; Durham and Stocker 2012). In El Sancho reservoir, due to a highly transparent epilimnion, the photic layer (Z_{eu}) extended down to 18 - 22 m, well below the bottom of the surface mixing layer (Z_{sml}) found at 15 m (Fig. 1). Therefore,

the formation and the vertical position of the DCM (22.5 m depth) fulfilled the condition of $Z_{eu} > Z_{sml}$ (Hamilton et al. 2010; Brentrup et al. 2016).

Table 2: The relative biomass contribution (%) of the main phytoplankton groups, i.e. *Synechococcus-like* (Synech), PicoEukaryotes (PEuk) and Carteria sp., within the thermal layers of the water column in El Sancho reservoir. Data are $n = 4 \pm$ se (standard error).

Layers	Synech	PEuk	*Carteria* sp.
Epilimnion	0.0	100.0	0.0
Metalimnion	0.1	0.7 ± 0.1	99.2 ± 0.1
Hypolimnion	0.1± 0.1	0.4 ± 0.4	99.4 ± 0.5

In El Sancho, the DCM was located mainly in the metalimnion, where the low K_d reduces the exchange of solutes and particles with the epi- and hypolimnion (Martin et al. 2010). This favours the accumulation of cells and other particles in this layer and reduces the dispersion of phytoplankton by wind-induced turbulence as might occur in the epilimnion (Abbott et al. 1984). Therefore, in addition to the $Z_{eu}>Z_{sml}$ condition, our results suggest that the formation and maintenance of the DCM is facilitated by a layer with reduced K_d , where the phytoplankton growth rate plus the sedimentation from the epilimnion is higher than the losses due to grazing, viral lysis, and sedimentation towards the hypolimnion (Gong et al. 2015; Leach et al. 2018).

In the epilimnion, CO_2 concentration was below our detection limit and below the equilibrium with the atmosphere according to Henry´s law (about 13 µmol L^{-1}) suggesting a net consumption by the planktonic community. This low CO_2 concentration likely limits primary production in the epilimnion of acid lakes and reservoirs (Satake and Saijo 1974; Nixdorf et al. 1998; Tittel et al. 2005). However, in the hypolimnion, the concentration of CO_2 was much higher and increased with depth. This suggests that the source of CO_2 in the hypolimnion can be the mineralization of OM, either in the water column or in the sediment (Satake and Saijo 1974). The observed strong positive correlations of CO_2 with NH_4^+ and the bacterial abundance support the role of microbial degradation as the main source of CO_2 in the hypolimnion. Therefore, the CO_2 produced by OM microbial degradation in the hypolimnion likely fuels the photosynthetic CO_2 fixation at the DCM. Most of the CO_2 consumed at the DCM was provided by the mineralization of OM in the hypolimnion (90 %), whereas the degradation of OM in the sediment contributed marginally (7 %). It is interesting to note that the sediment in El Sancho released less CO_2 than expected according to the stoichiometry of the sedimenting OM, which might indicate the possibility of an important consumption of CO_2 within the sediment by methanogenesis and other chemoautotrophic metabolisms.

In addition to CO_2, phosphorus has been considered a potential limiting nutrient for primary production in acid lakes due to the precipitation of phosphate with Fe (III) oxyhydroxides (Nixdorf et al 1998, Tittel et al., 2005). Since phosphate was below our detection limit in the water column of El Sancho, even in the anoxic hypolimnion, it is a strong candidate to, at least, co-limit primary production in these systems, although phosphate limitation is unlikely to be responsible for the DCM formation.

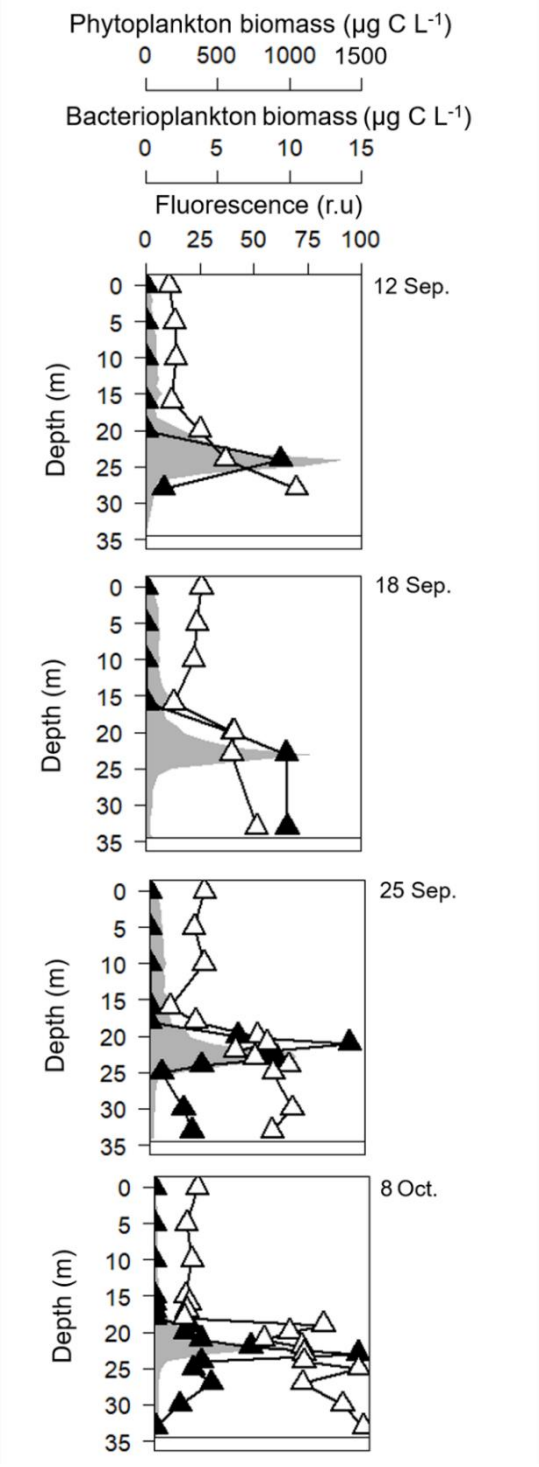

Fig. 4. *Water column* depth profiles of phytoplankton ( ) and bacterioplankton ( ) biomass during the sampling period in El Sancho reservoir. Fluorescence ( ) profiles are also shown for comparison. The bottom of reservoir is shown with a horizontal black line.

Dissolved organic compounds containing phosphorous might be a potential source of this nutrient for phytoplankton in El Sancho reservoir as has been found elsewhere (Boavida and Heath 1986).

Contrary to CO_2 and phosphate, the inorganic nitrogen concentration in El Sancho was high, indicating that primary production in El Sancho was not N-limited. In the epilimnion, NH_4^+ and NO_3^- remained constant with depth but presented inverse trends in the meta- and hypolimnion, NO_3^- presented a typical consumption profile suggesting that it was being used for phytoplankton growth at the DCM and in the oxidation of OM by dissimilatory nitrate reduction in the hypoxic hypolimnion (Tiedje 1988). In contrast, NH_4^+ profiles showed a characteristic increase with depth in the hypolimnion, same as for CO_2, which suggests that it was being produced during the degradation of OM and consumed in the DCM as a N source for phytoplankton growth.

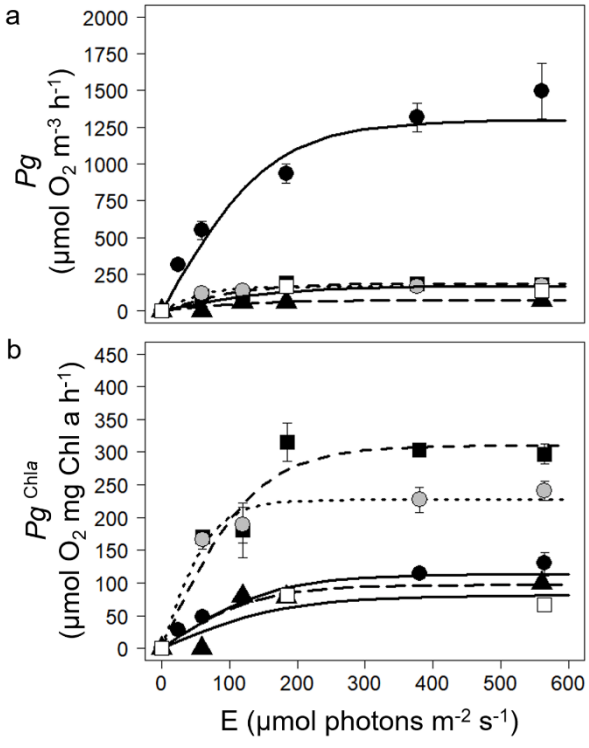

Fig 5. (a) Photosynthesis-irradiance (*P* – *E*) curves (volumetric rates) and (b) *P* – *E* curves normalized to Chl *a* on 25th September of the phytoplankton community at different depths: 0 m (—■- -), 5 m (- -▲- -), 16 m (- -●- -) , 22.5 m (—●—) and 30 m (—□—) depth under increasing irradiance. Data are means ± se (standard error) (*n* = 3 or 5 depending on the depth).

Metalimnetic O_2 maxima are typically associated to DCMs in lakes and the sea (Matthews and Deluna 2008; Wilkinson et al. 2015; Latasa et al. 2017). The cause of the formation and persistence of these O_2 maxima is under debate, with both physical and biological processes being likely involved. The change in O_2 solubility due to thermal difference between the warm epilimnion and the cooler

metalimnion (4 - 5 ºC between the epilimnion and the O_2 maximum in the metalimnion) only represents an increase in O_2 concentration of 26 µmol L^{-1}, whereas the observed differences were between 95 and 159 µmol L^{-1}. Therefore, the O_2 maximum in El Sancho and its position above the DCM peak is mainly the result of a highly positive net photosynthetic O_2 production (Fig. 8b) due to a to a higher light availability at that depth (Clegg et al. 2012; Latasa et al. 2017). Additionally, the low turbulent diffusivity in the metalimnion likely favored the accumulation of photosynthetically produced O_2. Below the metalimnetic peak, O_2 decreased quickly with depth because its consumption, in the aerobic oxidation of OM by heterotrophic bacteria and the oxidation of reduced inorganic compounds formed during the anaerobic mineralization of OM, exceeded its supply from the DCM (Friedrich et al. 2014).

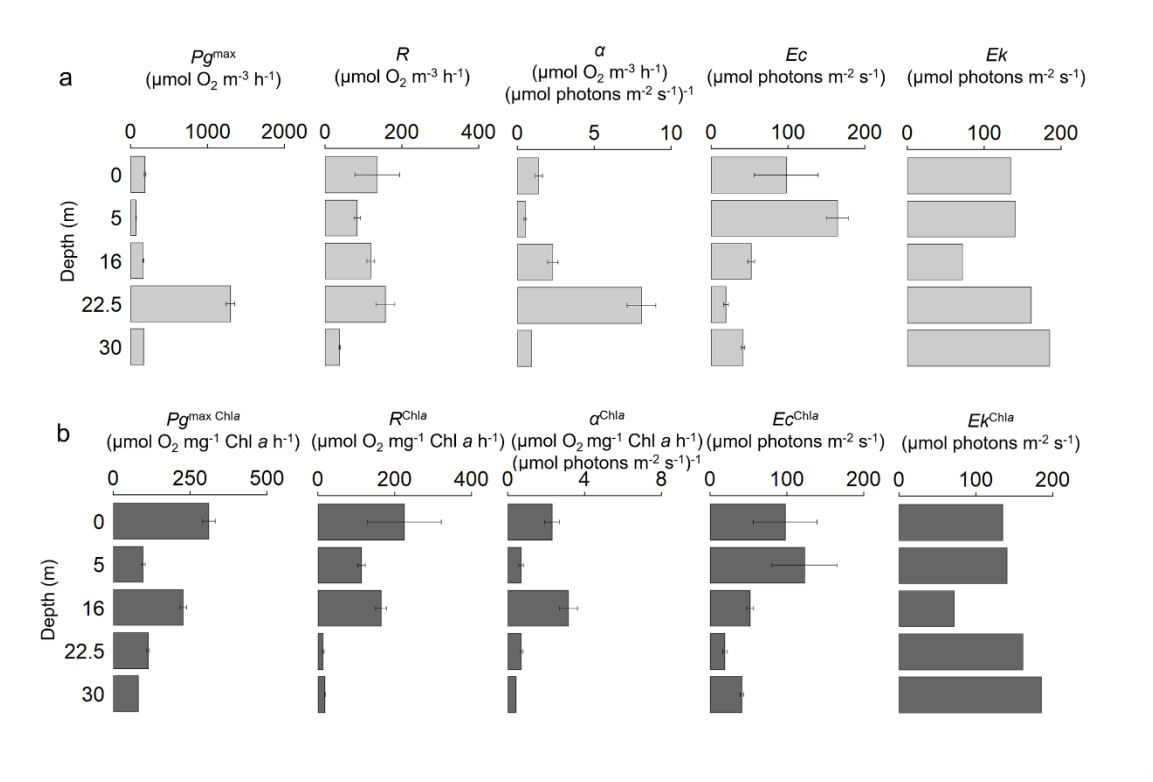

Fig. 6. *Water column* depth profiles of (a) photosynthetic parameters and respiration rate (▭, volume units) and (b) photosynthetic parameters and respiration rate normalized to Chl *a* (▬) on 25th September at 0 m, 5 m, 1 6m, 22.5 m and 30 m depth. P_g^{max} is the maximum gross production, *R* is the respiration rate in the dark, α is the photosynthetic efficiency, *Ec* is the light compensation point and *Ek* is the light saturation point.

4.2 Primary production and net metabolism

Production and net metabolism measurements in acidic lakes are scarce (Nixdorf et al. 2003). The phytoplankton community at the DCM in El Sancho reservoir was highly productive. *Pg* and Pg^{Chla} rates reached values that were 2-30 times higher than those measured in some pit lakes with lower pH (Nixdorf et al. 2003; Gerloff-Elias et al. 2005; Kamjunke et al. 2005), but were far lower than those found in DCM in circumneutral lakes (Sadro et al. 2011; Staehr et al. 2012).

Photoacclimation of the phytoplankton community to the *in situ* light environment in the water column was evident in the *P-E* curves when *Pg* was normalized by Chl *a* (Fig. 5b). Pg^{Chla} was clearly higher at the epilimnion than at the DCM for a given irradiance, suggesting an increase of Chl *a* per cell where irradiance is lower. Photosynthetic parameter $Pg^{max\ Chla}$ and α^{Chla} presented similar patterns with depth showing higher values at the surface and at 16 m depth, just above the DCM (Fig. 6b), as observed in other acidic lakes (see Table 1 in Gerloff-Elias et al. 2005).

The planktonic community inhabiting the DCM (dominated by *Carteria* sp.) presented an *Ec* of 19 ± 3 µmol photons m^{-2} s^{-1}, similar to that of the phylogenetically related *Chlamydomonas acidophila* (Clegg et al. 2012). Since this irradiance was higher than the irradiance measured at the peak of the DCM *in situ* (1.3 – 11.1 µmol photons m^{-2} s^{-1}), net autotrophic growth at the DCM peak was not possible. However, vertical migration and mixotrophic growth have been suggested as fitness traits favoring the survival and growth at the light limiting conditions of DCM (Tittel et al. 2003, 2005; Clegg et al. 2012). Nonetheless, another explanation is possible. The peaks of net primary production and biomass are uncoupled in El Sancho reservoir. The primary production peak occurs 3 - 4 m above the maximum of biomass, where *in situ* irradiance (14 - 39.6 µmol photons) is generally above *Ec*. Therefore, net autotrophic growth is possible at that depth (Fig. 8b). The mismatch between the depth of maximum net growth rate and the DCM has been demonstrated to depend on the sinking rate and the turbulent diffusivity coefficient (Gong et al. 2015). Maximum growth rate is estimated to be found at 19.3 m depth, 3 - 4 m above the mean depth of the DCM in El Sancho according to Eq. 12 from Gong et al. (2015). This estimation is remarkably close to the maximum growth rate depth predicted by our model (20.7 m).

The R^{Chla} were higher than those reported for *in situ* incubations and cultures of *C. acidophila* at different irradiances (Gerloff-Elias et al. 2005; Clegg et al. 2012) but in the low range of those measured in neutral lakes per unit of volume (Pace and Prairie 2005). The high respiration rate in the epilimnion is likely supported by the relatively high concentration of DOC, and the high POC:Chl *a* and DOC:POC ratios observed *in situ* (Fig. 1 and 2), that likely favored an intense heterotrophic bacterial activity. The lowest values of O_2 consumption rate measured at 30 m depth suggest a shift from aerobic to anaerobic pathways of OM oxidation at the bottom part of the hypolimnion and sediment.

4.3 Coupling carbon fixation at the DCM and CO_2 production by heterotrophic respiration: a modelling approach

In the DCM-CO_2 coupled model presented here, the vertical distribution of Chl *a* was modelled as a function of phytoplankton net growth - dependent on the opposite vertical gradients of CO_2 and light -, turbulent mixing processes and sedimentation (Huisman and Sommeijer 2002; Fennel and Boss 2003; Gong et al. 2015). The bulk sinking rates obtained from the model were similar to those measured with the sedimentation traps. However, both were lower than those calculated for passively sinking *Carteria* cells, likely due to their capacity to compensate sinking by vertical migration. In addition, the model takes into account the differences in the phytoplanktonic communities between the epilimnion and the DCM by using two different C:Chl *a* ratios. The calibrated C:Chl *a* ratios produced by the model were very close to those calculated from experimental data according to Geider (1987), 114 and 22.05 mg C mg Chl a^{-1} for the epi- and metalimnion respectively (Fig. S3) and within the range of

published values (Table 3). This distinction improved the simulation of the vertical profile of primary production, specifically the surprisingly high production rates measured in the epilimnion (Fig. 8a). Modelled daily Pg (0.1 – 1.7 mmol C m^{-3} d^{-1}) were similar to the daily Pg at *in situ* irradiances determined from experimental *P-E* curves (0.02 – 1.9 mmol C m^{-3} d^{-1}) (Fig. 8a). The model predicted the high daily Pg observed in the epilimnion and at the DCM, but slightly underestimated daily Pg in the epilimnion and overestimated it at the DCM. The fraction of Pg being consumed by respiration according to the model was about 12 – 16 %, which is consistent with the 12% determined from the *P-E* curves at the DCM depth and the 13 –18% value determined from *C. acidophila* cultures (Clegg et al. 2012). Altogether, the model is able to reproduce noticeably well the Pg and the Chl *a* profiles with a high correlation between experimental data and model estimates (Table 3). This good agreement supports our initial hypothesis, suggesting that the vertical position of the DCM and its existence in El Sancho depends on both the light penetration and the supply of CO_2 from the hypolimnion. The systematic underestimation of the Chl *a* concentration measured at the peak of DCM could be due to the existence of a detrital Chl *a* fraction at the DCM which is not considered in the present model formulation.

The DCM-CO_2 coupled model takes into account three CO_2 inputs to the water column, i.e. from the atmosphere (upper boundary flux), from bacterial respiration in the water column and from the sediment (lower boundary flux). This is a major difference with other models where nutrients are only recycled from the bottom boundary (Huisman and Sommeijer 2002; Fennel and Boss 2003; Gong et al. 2015). Our model suggests that the CO_2 distribution through the water column can be explained basically by the bacterial respiration in the water column. Detrital OM produced in the DCM sunk through the hypolimnion and was degraded by microorganisms releasing CO_2 in the process. This led to an upward net CO_2 flux by turbulent diffusion, which is essential to support the photoautotrophic primary production and growth at the DCM. The model takes into account that the mineralization of OM in the hypolimnion occurs by aerobic and anaerobic processes. The values of the half-saturation constant for aerobic respiration K_S and the half-inhibitory constant for anaerobic respiration K_I and the profiles of the bacterial respiration rates extracted from the model (results not shown) suggest that in the hypoxic conditions prevailing at the bottom of the metalimnion and in the hypolimnion, both aerobic and anaerobic metabolism occur at the same time (Gerritse et al. 1990). Closer to the sediment, the O_2 availability decreases, and a higher fraction of the OM is probably mineralised by anaerobic respiration pathways (Torres et al. 2014; Corzo et al. 2018).

Table 3. Parameter values of the model and their description

Simulations	Parameter	Description	Min	Max	Units	Range values (Reference)
Chl a ($\mu g\ L^{-1}$)	μ_{max}	Maximal specific growth rate of phytoplankton	1.1	3	d^{-1}	0.44 – 3 (Fennel and Boss 2003; Tittel et al. 2005)
	K_{CO2}	Half-saturation constant for CO_2 uptake	16.3	208.6	$\mu mol\ C\ L^{-1}$	0.1 – 200 (Hein 1997; Reynolds and Irish 1997; Monorey 2001)
	l	Natural mortality rate of phytoplankton	0.02	0.1	d^{-1}	0.03 – 0.14 (Soetaert et al. 2001; Huisman et al. 2004; Torres et al. 2016)
	W_s	Bulk sinking velocity of phytoplankton	0.1	0.2	$m\ d^{-1}$	0.1 – 7.7 (Gálvez et al. 1993, Present study, calculated from Stokes equation)
	R^2		0.63	0.77		
	p		1.3×10^{-11}	6.6×10^{-8}		
CO_2 ($\mu mol\ L^{-1}$)	R_A	Maximal specific rate of aerobic respiration	1.3×10^{-12}	3×10^{-12}	mmol C $cell^{-1}$ d^{-}	8.2×10^{-13} – 1.4×10^{-11} (Smith and Prairie 2004)
	K_I	Half-inhibitory constant for anaerobic respiration	1.3	4.7	$\mu mol\ O_2\ L^{-1}$	1 – 30 (Soetaert et al. 1996; Grégoire et al. 2008)
	K_S	Half-saturation constant for aerobic respiration	2.2	5	$\mu mol\ O_2\ L^{-1}$	0.1 – 5 (Grégoire et al. 2008)
	$Flux_{CO2}^{sed}$	Flux of CO_2 from the sediment	2.9	4.2	mmol C m^{-2} d^{-1}	0.02 – 7 (Torres et al. 2015; Corzo et al. 2018)
	$Flux_{CO2}^{atm}$	Flux of CO_2 from the atmosphere	4.3	7.6	mmol C m^{-2} d^{-1}	(-40 – 8) (Emerson and Broecker 1973; Kelly et al. 2001; Morales-Pineda et al. 2016)
	$C:Chl_{epi}$	Particulate organic carbon-to-chlorophyll a in epilimnion	95.6	149.2	mg C mg $Chla^{-1}$	10 – 333 (Falkowski and Kiefer 1985; Geider 1987; Yacobi and Zohary 2010; Clegg et al. 2012)
	$C:Chl_{meta}$	Particulate organic carbon-to-chlorophyll a in metalimnion	15.1	34.4	mg C mg $Chla^{-1}$	10 – 333 (Falkowski and Kiefer 1985; Geider 1987; Yacobi and Zohary 2010; Clegg et al. 2012)
	Q_{10}	Temperature coefficient	1.91	2		1 – 3 (Jørgensen 1979b)
	R_{min}	Minimum basal respiration rate	0.012	0.012	d^{-1}	0.01– 0.2 (Geider and Osborne 1989; Van Den Meersche et al. 2004; Clegg et al. 2012)
	R_{phot}	Part of photosynthesis used for respiration	0.12	0.16		0.1 – 0.25 (Cloern et al. 1995; Van Den Meersche et al. 2004; Gal et al. 2009)
	R^2		0.79	0.91		
	p		2×10^{-6}	7.2×10^{-3}		

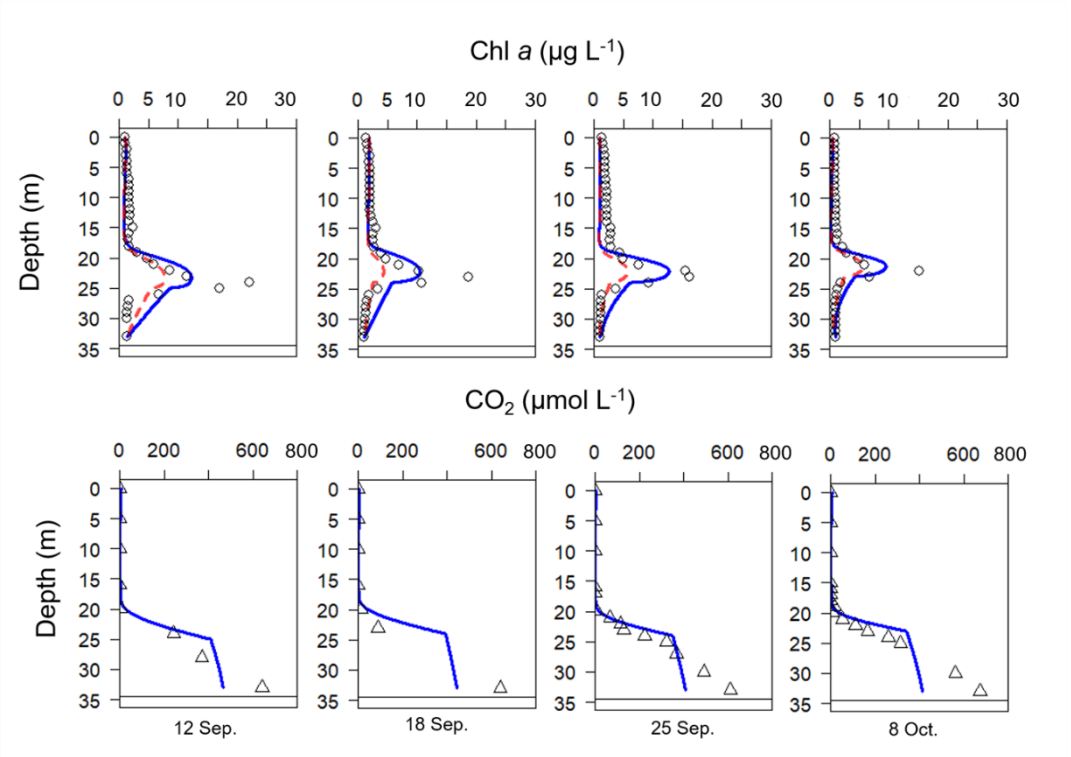

Fig.7. Comparison of Chl *a* (○) and CO_2 (△) depth profiles data against model prediction values with ( ) and without sediment CO_2 fluxes ( ) during the sampling period in El Sancho reservoir. The bottom of reservoir is shown with a horizontal black line.

Experimental evidence and the model simulations suggest that both the input of CO_2 from the atmosphere and the release from the sediment might represent important contributions to the C budget in acid lakes. In the epilimnion, CO_2 was in equilibrium with the atmosphere through a piston flux (Grégoire et al. 2008). Due to the low pH and the efficient consumption of the CO_2 regenerated in the metalimnion by the DCM, the CO_2 demand for the primary production in the epilimnion was supported from the atmosphere (Gross 2000). The areal gross primary production in the epilimnion on September 25th, estimated from the *P-E* curves and *in situ* irradiance and from the DCM-CO_2 model, was similar; 14.9 and 12 mmol CO_2 m^{-2} d^{-1}, respectively. This areal Pg rates represented 69 - 67 % of total water column integrated Pg. Although the fraction of water column integrated Chl *a* was larger in the DCM (56 %) than in the epilimnion (30 %), the contribution of the DCM to the integrated areal Pg was lower; 4.3 and 5.9 mmol CO_2 m^{-2} d^{-1}, 19.8 and 32.5 %, respectively. The epilimnetic CO_2 flux from the atmosphere was completely consumed by primary producers at the epilimnion, i.e. virtually no atmospheric CO_2 reached the DCM layer. Using the DCM-CO_2 coupled model, we could test, for the first time as far as we know, the potential contribution of the CO_2 released from the sediment to support the primary producers' CO_2 demand at the DCM. This contribution ranged between 36 and 58% of the DCM integrated Chl *a* (Fig. 7), bearing in mind that we are using here a 1D model which does not take into account any potential lateral transport within the reservoir. The estimated contribution of the

sediment using the model was higher than that calculated from the observed CO_2 profiles at the hypolimnion and sediment (Table 1), probably because the modelled CO_2 profile in the hypolimnion systematically underestimated the observed profiles. Without the contribution of the CO_2 from the sediment, the intensity of the DCM in El Sancho would be lower.

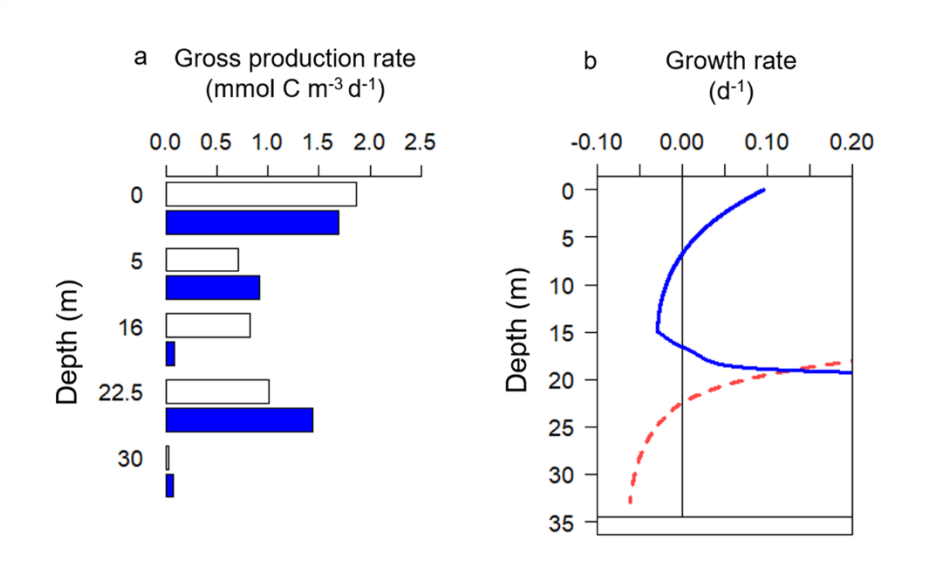

Fig. 8 (a) Comparisons of modelled ( ) and observed ( ) gross production rates (Pg, mmol C m^{-3} d^{-1}) on 25th September. Observed Pg rates were calculated from experimentally determined *P- E* curves at 0 m, 5 m, 16 m, 22.5 m and 30 m depth and the irradiance corresponding to each depth *in situ*. (b) Modeled vertical profiles of phytoplankton net growth rate (d^{-1}) assuming saturating irradiance ( ), therefore microalgae are limited only by CO_2, and limited by light (PAR) at saturating CO_2 concentrations ( ). The bottom of reservoir is shown with a horizontal black line.

In conclusion, the DCM-CO_2 model is able to reproduce noticeably well both the Chl *a* and CO_2 profiles, with a high correlation between experimental and modelled data. This good agreement supports our initial hypothesis that the vertical position of the DCM and its existence in El Sancho depends on both the light penetration and the supply of CO_2, which is regenerated by the hypolimnetic heterotrophic bacteria from the water column and the sediment.

5. Acknowledgement

The research was funded by projects P11-RNM-7199 from the Junta de Andalucía, CTM2017-82274-R from the Spanish I+D+I Program and 20.DG.UE.II.05 from University of Cadiz. Support for the work with microsensors was obtained from the Poul Due Jensen Foundation.

6. References

Abbott, M. R., K. L. Denman, T. M. Powell, P. J. Richerson, R. C. Richards, and C. R. Goldman. 1984. Mixing and the dynamics of the deep chlorophyll maximum in Lake Tahoe. Limnol. Oceanogr. **29**: 862–878. doi:10.4319/lo.1984.29.4.0862

Barbiero, R. P., and M. L. Tuchman. 2004. The Deep Chlorophyll Maximum in Lake Superior. J. Gt. Lakes Res. **30**: 256–268. doi:10.1016/S0380-1330(04)70390-1

Boavida, M. J., and R. T. Heath. 1986. Phosphatase activity of Chlamydomonas acidophila Negoro (Volvocales, Chlorophyceae). Phycologia **25**: 400–404. doi: 10.2216/i0031-8884-25-3-400.1

Bower, C. E., and T. Holm-Hansen. 1980. Salicylate-Hypochlorite Method for Determining Ammonia in Seawater1. Can. J. Fish. Aquat. Sci. **37**: 794–798. doi:10.1139/f80-106

Brentrup, J. A., C. E. Williamson, W. Colom-Montero, and others. 2016. The potential of high-frequency profiling to assess vertical and seasonal patterns of phytoplankton dynamics in lakes: an extension of the Plankton Ecology Group (PEG) model. Inl. Waters **6**: 565–580. doi:10.5268/IW-6.4.890

Camacho, A. 2006. On the occurrence and ecological features of deep chlorophyll maxima (DCM) in Spanish stratified lakes. Limnetica **25**: 453–478. doi: 10.23818/limn.25.32

Clegg, M. R., U. Gaedke, B. Boehrer, and E. Spijkerman. 2012. Complementary ecophysiological strategies combine to facilitate survival in the hostile conditions of a deep chlorophyll maximum. **169**: 609–622. doi:10.1007/s00442-011-2225-4

Cloern, J. E., C. Grenz, and L. Videgar-Lucas. 1995. An empirical model of the phytoplankton chlorophyll: carbon ration-the conversion factor between productivity and growth rate. Limnol. Oceanogr. **40**: 1313–1321. doi: 10.4319/lo.1995.40.7.1313

Cole, J. J., and N. F. Caraco. 1998. Atmospheric exchange of carbon dioxide in a low-wind oligotrophic lake measured by the addition of SF6. Limnol. Oceanogr. **43**: 647–656. doi:10.4319/lo.1998.43.4.0647

Cole, J. J., S. R. Carpenter, J. F. Kitchell, and M. L. Pace. 2002. Pathways of organic carbon utilization in small lakes: Results from a whole-lake ^{13} C addition and coupled model. Limnol. Oceanogr. **47**: 1664–1675. doi:10.4319/lo.2002.47.6.1664

Corzo, A., J. L. Jiménez-Arias, E. Torres, E. García-Robledo, M. Lara, and S. Papaspyrou. 2018. Biogeochemical changes at the sediment–water interface during redox transitions in an acidic reservoir: exchange of protons, acidity and electron donors and acceptors. Biogeochemistry **139**: 241–260. doi:10.1007/s10533-018-0465-7

Corzo, A., F. Jiménez-Gómez, F. J. L. Gordillo, R. García-Ruíz, and F. X. Niell. 1999. Short communication. Synechococcus and Prochlorococcus-like populations detected by flow cytometry in a eutrophic reservoir in summer. J. Plankton Res. **21**: 1575–1581. doi:10.1093/plankt/21.8.1575

Corzo, A., S. Rodríguez-Gálvez, L. Lubian, C. Sobrino, P. Sangrá, and A. Martínez. 2005. Antarctic marine bacterioplankton subpopulations discriminated by their apparent content of nucleic acids differ in their response to ecological factors. Polar Biol. **29**: 27–39. doi:10.1007/s00300-005-0032-2

Cullen, J. J. 1982. The deep chlorophyll maximum: comparing vertical profiles of chlorophyll a. Can. J. Fish. Aquat. Sci. **39**: 791–803. doi: 10.1139/f82-108

Cullen, J. J. 2015. Subsurface Chlorophyll Maximum Layers: Enduring Enigma or Mystery Solved? Ann. Rev. Mar. Sci. **7**: 207–239. doi:10.1146/annurev-marine-010213-135111

Durham, W. M., and R. Stocker. 2012. Thin Phytoplankton Layers: Characteristics, Mechanisms, and Consequences. Ann. Rev. Mar. Sci. **4**: 177–207. doi:10.1146/annurev-marine-120710-100957

Emerson, S., and W. Broecker. 1973. Gas-Exchange Rates in a Small Lake as Determined by the Radon Method. J. Fish. Res. Board Canada **30**: 1475–1484. doi:https://doi.org/10.1139/f73-237

Falkowski, P. G., and D. a Kiefer. 1985. Chlorophyll a fluorescence in phytopankton: relationship to photosynthesis and biomass. J. Plankton Res. **7**: 715–731. doi:10.1093/plankt/7.5.715

Fennel, K., and E. Boss. 2003. Surface maxima of phytoplankton and chlorophyll: Stady-state solutions from a simple model. Limnol. Ocean. **48**: 1521–1534. doi: 10.4319/lo.2003.48.4.1521

Friedrich, J., F. Janssen, D. Aleynik, and others. 2014. Investigating hypoxia in aquatic environments: Diverse approaches to addressing a complex phenomenon. Biogeosciences **11**: 1215–1259. doi:10.5194/bg-11-1215-2014

Gal, G., M. R. Hipsey, A. Parparov, U. Wagner, V. Makler, and T. Zohary. 2009. Implementation of ecological modeling as an effective management and investigation tool : Lake Kinneret as a case study. Ecol. Modell. **220**: 1697–1718. doi:10.1016/j.ecolmodel.2009.04.010

Gálvez, J. A., F. X. Niell, and J. Lucena. 1988. Description and mechanism of formation of a deep chlorophyll maximum due to Ceratium hirundinella (OF Müller) Bergh. Arch. für Hydrobiol. **112**: 143–155.

Gálvez, J. A., F. X. Niell, and J. Lucena. 1993. Sinking velocities of principal phytoplankton species in a stratified reservoir: ecological implications. Int. Vereinigung für Theor. und Angew. Limnol. Verhandlungen **25**: 1228–1231. doi:https://doi.org/10.1080/03680770.1992.11900363

García-Robledo, E., A. Corzo, and S. Papaspyrou. 2014. A fast and direct spectrophotometric method for the sequential determination of nitrate and nitrite at low concentrations in small volumes. Mar. Chem. **162**: 30–36. doi:10.1016/j.marchem.2014.03.002

García-Robledo, E., C. C. Padilla, F. J. Stewart, and O. Ulloa. 2017. Cryptic oxygen cycling in anoxic marine zones. PNAS **114**: 8319–8324. doi:10.1073/pnas.1619844114

García, H. E., and L. I. Gordon. 1992. Oxygen solubility in seawater: Better fitting equations. Limnol. Oceanogr. **37**: 1307–1312. doi:10.4319/lo.1992.37.6.1307

Gargett, A. E. 1984. Vertical eddy diffusivity in the ocean interior. 359–393. doi: 10.1357/002224084788502756

Gasol, J. M., and P. A. del Giorgio. 2000. Using flow cytometry for counting natural planktonic bacteria and understanding the structure of planktonic bacterial communities. Sci. Mar. **64**: 197–224. doi:10.3989/scimar.2000.64n2197

Geider, R. J. 1987. Light and temperature dependence of the carbon to chlorophyll a ratio in microalgae and cyanobacteria: Implications for physiology and growth of phytoplankton. New Phytol. **106**: 1–34. doi:10.1111/j.1469-8137.1987.tb04788.x

Geider, R. J., and B. A. Osborne. 1989. Respiration and microalgal growth : a review of the quantitative relationship between dark respiration and growth. New Phytol. **112**: 327–341. doi:10.1111/j.1469-8137.1989.tb00321.x

Gerloff-Elias, A., E. Spijkerman, and H. Schubert. 2005. Light acclimation of Chlamydomonas acidophila accumulating in the hypolimnion of an acidic lake (pH 2.6). Freshw. Biol. **50**: 1301–1314. doi:10.1111/j.1365-2427.2005.01400.x

Gerritse, J., F. Schut, and J. C. Gottschal. 1990. Mixed chemostat cultures of obligately aerobic and fermentative or methanogenic bacteria grown under oxygen-limiting conditions. FEMS Microbiol. Lett. **66**: 87–93. doi:10.1016/0378-1097(90)90263-P

Gong, X., J. Shi, H. W. Gao, and X. H. Yao. 2015. Steady-state solutions for subsurface chlorophyll maximum in stratified water columns with a bell-shaped vertical profile of chlorophyll. Biogeosciences **12**: 905–919. doi:10.5194/bg-12-905-2015

Grasshoff, K., K. Kremling, and M. Ehrhardt. 1999. Methods of Seawater analysis.Publisher: Wiley

Grégoire, M., C. Raick, and K. Soetaert. 2008. Numerical modeling of the central Black Sea ecosystem functioning during the eutrophication phase. Prog. Oceanogr. **76**: 286–333. doi:10.1016/j.pocean.2008.01.002

Gross, W. 2000. Ecophysiology of algae living in highly acidic environments. Hydrobiologia 433. 31–37. doi: 10.1023/A:1004054317446

Hall, P. O. J., and R. C. Aller. 1992. Rapid, small volume, flow injection analysis for CO_2 and NH_4^+ in marine and freshwaters. Limnol. Ocean. **37**: 1113–1119. doi:http://www.jstor.org/stable/2837857

Hamilton, D. P., K. R. O'Brien, M. A. Burford, J. D. Brookes, and C. G. McBride. 2010. Vertical distributions of in deep, warm monomictic lakes. Aquat. Sci. **72**: 295–307. doi: 10.1007/s00027-010-0131-1

Hein, M. 1997. Inorganic carbon limitation of photosynthesis in lake phytoplankton. Freshw. Biol. **37**: 545–552. doi:10.1046/j.1365-2427.1997.00180.x

Huisman, J., and B. Sommeijer. 2002. Population dynamics of sinking phytoplakton in light-limited environments: simulation techniques and critical parameters. J. Sea Res. **48**: 83–96. doi: 10.1016/S1385-1101(02)00137-5

Huisman, J., J. Sharples, J. M. Stroom, P. M. Visser, W. E. A. Kardinaal, J. M. H. Verspagen, and B. Sommeijer. 2004. Changes in turbulent mixing shift competition for light between phytoplankton species. Ecology **85**: 2960–2970. doi:10.1890/03-0763

Huisman, J., N. N. Pham Thi, D. M. Karl, and B. Sommeijer. 2006. Reduced mixing generates oscillations and chaos in the oceanic deep chlorophyll maximum. Nature **439**: 322–325. doi:10.1038/nature04245

Jassby, A. D., and T. Platt. 1976. Mathematical formulation of the relationship between photosynthesis and light for phytoplankton. Limnol. Oceanogr. **21**: 540–547. doi: 10.4319/lo.1976.21.4.0540

Jørgensen. 1979a. G3 - Diffusion and dispersion, p. 943–988. *In* S.E. JØRGENSEN [ed.], Handbook of Environmental Data and Ecological Parameters. Pergamon.

Jørgensen. 1979b. G5 - Stoichiometric ratio temperature coefficients transfer rates water emissions, p. 1025–1034. *In* S.E. JØRGENSEN [ed.], Handbook of Environmental Data and Ecological Parameters. Pergamon.

Kamjunke, N., J. Tittel, H. Krumbeck, C. Beulker, and J. Poerschmann. 2005. High Heterotrophic Bacterial Production in Acidic , Iron-Rich Mining Lakes. **49**: 425–433. doi:10.1007/s00248-004-0270-9

Kelly, C. A., E. Fee, P. S. Ramlal, J. W. M. Rudd, R. H. Hesslein, C. Anema, and E. U. Schindler. 2001. Natural

variability of carbon dioxide and net epilimnetic production in the surface waters of boreal lakes of different sizes. Limnol. Oceanogr. **46**: 1054–1064. doi:10.4319/lo.2001.46.5.1054

Kirk, J. T. O. 1994. Light and photosynthesis in aquatic ecosystems, Cambridge Univ. Press. doi: 10.1017/CBO9780511623370

Labasque, T., C. Chaumery, A. Aminot, and G. Kergoat. 2004. Spectrophotometric Winkler determination of dissolved oxygen: re-examination of critical factors and reliability. **88**: 53–60. doi: 10.1016/j.marchem.2004.03.004

Latasa, M.,A.M. Cabello, X.A.G. Morán, R. Massana, and R. Scharek. 2017. Distribution of phytoplankton groups within the deep chlorophyll maximum. Limnol. Oceanogr. **62**: 665–685. doi:10.1002/lno.10452

Leach, T. H., B. E. Beisner, C. C. Carey, and others. 2018. Patterns and drivers of deep chlorophyll maxima structure in 100 lakes: The relative importance of light and thermal stratification. Limnol. Oceanogr. **63**: 628–646. doi:10.1002/lno.10656

Martin, J., J. É. Tremblay, J. Gagnon, and others. 2010. Prevalence, structure and properties of subsurface chlorophyll maxima in Canadian Arctic waters. Mar. Ecol. Prog. Ser. **412**: 69–84. doi:10.3354/meps08666

Matthews, R., and E. Deluna. 2008. Metalimnetic Oxygen and Ammonium Maxima in Lake Whatcom, Washington (USA). Matthews DeLuna Northwest Sci. **82**: 18–29. doi:10.3955/0029-344X-82.1.18

Monorey, J. . 2001. Carbon concentrating mechanisms in aquatic photosynthetic organisms: a report on CCM 2001. J. Phycol. **37**: 926–928. doi:10.1046/j.1529-8817.2001.37601.x

Morales-Pineda, M., B. Úbeda, A. Cózar, and B. Obrador. 2016. Organic carbon sedimentation dominates over CO 2 emission in two net heterotrophic Mediterranean reservoirs during stratification. Aquat. Sci. **78**: 279–290. doi:10.1007/s00027-015-0423-6

Nixdorf, B., A. Fyson, and H. Krumbeck. 2001. Review: Plant life in extremely acidic waters. Environ. Exp. Bot. **46**: 203–211. doi:10.1016/S0098-8472(01)00104-6

Nixdorf, B., H. Krumbeck, J. Jander, and C. Beulker. 2003. Comparison of bacterial and phytoplankton productivity in extremely acidic mining lakes and eutrophic hard water lakes. **24**.

Nixdorf, B., K. Wollmann, and R. Deneke. 1998. Ecological potentials for planktonic development and food web interactions in extremely acidic mining lakes in Lusatia (Eastern Germany). In W. Geller, H. Klapper and W. Salomons (eds), Acidic mining lakes. Springer Verlag: 147–168. doi: 10.1007/978-3-642-71954-7_8

Okubo, A., and S. Levin. 2001. Diffusion and Ecological Problems: Modern Perspectives. Springer-Verlag, New York. doi: 10.1007/978-1-4757-4978-6

Osborn, T. R. 1980. Estimates of the Local Rate of Vertical Diffusion from Dissipation Measurements. J. Phys. Oceanogr. **10**: 83–89. doi:10.1175/1520-0485(1980)010<0083:EOTLRO>2.0.CO;2

Pace, M. L., and Y. T. Prairie. 2005. Respiration in Lakes. In: del Giorgio, P.A. and Williams, P.J.B., Eds., Respiration in Aquatic Ecosystems, Oxford University Press, New York, 103-121. doi: 10.1093/acprof:oso/9780198527084.003.0007

Revsbech, N. P., B. Thamdrup, T. Dalsgaard, and D. E. Canfield. 2011. Construction of STOX oxygen sensors and their application for determination of O2 concentrations in oxygen minimum zones, p. 325–341. *In* Methods in enzymology. Elsevier.

Reynolds, C. S., and A. E. Irish. 1997. Modelling phytoplankton dynamics in lakes and reservoirs : the problem of in-situ growth rates. 349: 5–17. doi: 10.1023/A:1003020823129

Ritchie, R. J. 2008. Universal chlorophyll equations for estimating chlorophylls. **46**: 115–126. doi: 10.1007/s11099-008-0019-7

Sadro, S., J. M. Melack, and S. MacIntyre. 2011. Depth-integrated estimates of ecosystem metabolism in a high-elevation lake (Emerald Lake, Sierra Nevada, California). Limnol. Oceanogr. **56**: 1764–1780. doi:10.4319/lo.2011.56.5.1764

Sánchez España J., M. Diez, and E. Santofimia. 2012. Mine pit lakes of the Iberian Pyrite Belt: Some basic limnological, hydrogeochemical, and microbiological considerations. Acidic Pit Lakes: The Legacy of Coal and Metal Surface Mines (W Geller, M Schultze, B Kleinmann & C Wolkersdorfer, eds), pp. 315– 342. Springer-Verlag, Berlin, Germany.

Santofimia, E., E. González-Toril, E. López-Pamo, M. Gomariz, R. Amils, and Á. Aguilera. 2013. Microbial Diversity and Its Relationship to Physicochemical Characteristics of the Water in Two Extreme Acidic Pit Lakes from the Iberian Pyrite Belt (SW Spain). PLoS One **8**. doi:10.1371/journal.pone.0066746

Satake, K., and Y. Saijo. 1974. Carbon dioxide content and metabolic activity of microorganisms in some acid lakes in Japan. Limnol. Oceanogr. **19**: 331–338. doi:10.4319/lo.1974.19.2.0331

Schindler, D.W. 1975. Factors affecting gas exchange in natural waters. Limnol. Oceanogr. 20, 1053-105. doi: 10.4319/lo.1975.20.6.1053a

Smith, E. M., and Y. T. Prairie. 2004. Bacterial metabolism and growth efficiency in lakes: The importance of phosphorus availability. Limnol. Oceanogr. **49**: 137–147. doi:10.4319/lo.2004.49.1.0137

Soetaert, K., and P. M. Herman. 2009. ecolMod:" A practical guide to ecological modelling-using R as a simulation platform". R Packag. version **1**.

Soetaert, K., and F. Meysman. 2012. R-package ReacTran: Reactive Transport Modelling in R. Environ. Model. Softw. **32**: 49–60. doi: 10.1016/j.envsoft.2011.08.011

Soetaert, K., P. M. J. Herman, J. J. Middelburg, C. Heip, C. L. Smith, P. Tett, and K. Wild-allen. 2001. Numerical modelling of the shelf break ecosystem : reproducing benthic and pelagic measurements. Deep. Res. Part I Oceanogr. Res. Pap. **48**: 3141–3177. doi:10.1016/S0967-0645(01)00035-2

Soetaert, K., T. Petzoldt, and F. J. R. Meysman. 2010. MARELAC: tools for aquatic science. R Packag. version 2.1.2 Software.

Staehr, P. A., J. P. A. Christensen, R. D. Batt, and J. S. Read. 2012. Ecosystem metabolism in a stratified lake. Limnol. Oceanogr. **57**: 1317–1330. doi:10.4319/lo.2012.57.5.1317

Sterner, R. W. 2010. In situ-measured primary production in Lake Superior. J. Great Lakes Res. **36**: 139–149. doi:10.1016/j.jglr.2009.12.007

Tiano, L., E. Garcia-Robledo, and N. P. Revsbech. 2014. A new highly sensitive method to assess respiration rates and kinetics of natural planktonic communities by use of the switchable trace oxygen sensor and reduced oxygen concentrations. PLoS One **9**. doi:10.1371/journal.pone.0105399

Tiedje, J. M. 1988. Ecology of denitrification and dissimilatory nitrate reduction to ammonium. p. 179-244. In A.J.B. Zehnder (ed), Environmental Microbiology of Anaerobes. John Wiley and Sons, New York.

Tittel, J., V. Bissinger, U. Gaedke, and N. Kamjunke. 2005. Inorganic carbon limitation and mixotrophic growth in Chlamydomonas from an acidic mining lake. Protist **156**: 63–75. doi:10.1016/j.protis.2004.09.001

Tittel, J., V. Bissinger, B. Zippel, U. Gaedke, E. Bell, A. Lorke, and N. Kamjunke. 2003. Mixotrophs combine resource use to outcompete specialists: Implications for aquatic food webs. Proc. Natl. Acad. Sci. **100**: 12776–12781. doi:10.1073/pnas.2130696100

Torres, E., C. Ayora, C. R. Canovas, E. García-Robledo, L. Galván, and A. M. Sarmiento. 2013. Metal cycling during sediment early diagenesis in a water reservoir affected by acid mine drainage. Sci. Total Environ. **461**–**462**: 416–429. doi:10.1016/j.scitotenv.2013.05.014

Torres, E., C. Ayora, J. L. Jiménez-Arias, E. García-Robledo, S. Papaspyrou, and A. Corzo. 2014. Benthic metal fluxes and sediment diagenesis in a water reservoir affected by acid mine drainage: A laboratory experiment and reactive transport modeling. Geochim. Cosmochim. Acta **139**: 344–361. doi:10.1016/j.gca.2014.04.013

Torres, E.,R. M. Couture, B. Shafei, A. Nardi, C. Ayora, and P. Van Cappellen. 2015. Reactive transport modeling of early diagenesis in a reservoir lake affected by acid mine drainage : Trace metals , lake overturn , benthic fl uxes and remediation. Chem. Geol. **419**: 75–91. doi:10.1016/j.chemgeo.2015.10.023

Torres, E., L. Galván, C. R. Cánovas, S. Soria-Píriz, M. Arbat-Bofill, A. Nardi, S. Papaspyrou, and C. Ayora. 2016. Oxycline formation induced by Fe(II) oxidation in a water reservoir affected by acid mine drainage modeled using a 2D hydrodynamic and water quality model - CE-QUAL-W2. Sci. Total Environ. **562**: 1–12. doi:10.1016/j.scitotenv.2016.03.209

Van den Meersche, K., J. J. Middelburg, K. Soetaert, P. Van Rijswijk, H. T. S. Boschker, and C. H. R. Heip. 2004. Carbon-nitrogen coupling and algal-bacterial interactions during an experimental bloom : Modeling a 13 C tracer experiment. Limnol. Oceanogr. **49**: 862–878. doi:10.4319/lo.2004.49.3.0862

Wang, X. J., M. Behrenfeld, R. Le Borgne, R. Murtugudde, and E. Boss. 2009. Regulation of phytoplankton carbon to chlorophyll ratio by light, nutrients and temperature in the equatorial pacific ocean: A basin-scale model. Biogeosciences **6**: 391–404. doi:10.5194/bg-6-391-2009

Wilkinson, G. M., J. J. Cole, M. L. Pace, R. A. Johnson, and M. J. Kleinhans. 2015. Physical and biological contributions to metalimnetic oxygen maxima in lakes. Limnol. Oceanogr. **60**: 242–251. doi:10.1002/lno.10022

Wuest, A., G. Piepke, and D. C. Van Senden. 2000. Turbulent kinetic energy balance as a tool for estimating vertical diffusivity in wind-forced stratified waters. Limnol. Oceanogr. **45**: 1388–1400. doi:10.4319/lo.2000.45.6.1388

Yacobi, Y. Z., and T. Zohary. 2010. Carbon:Chlorophyll a ratio, assimilation numbers and turnover times of Lake Kinneret phytoplankton. Hydrobiologia **639**: 185–196. doi:10.1007/s10750-009-0023-3

7. Supplementary Material

7.1 Material and methods

7.1.1 Microbial community cell biovolume, carbon and biomass estimates

Cell biovolume (BV) was calculated from cell diameter assuming a spherical form and cell diameter was estimated from the side scatter signal (Echevarria et al. 2009), calibrated with reference beads (0.49, 1.1, 4.2 and 9.9 µm, FluoSpheres® Molecular Probes Inc.™). Cell carbon of photosynthetic prokaryotes was calculated from the BV, using a conversion factor of 235 fg C μm^{-3} (Shalapyonok et al. 2001; Worden et al. 2004), while cell carbon of photosynthetic eukaryotes were calculated with the equation (Eppley et al. 1970):

$$\text{Log C} = 0.94\text{Log BV} - 0.6 \qquad (1)$$

Cell carbon of heterotrophic prokaryotes was calculated from (Posch et al. 2001):

$$\text{C} = 218\ \text{BV}^{0.86} \qquad (2)$$

Biomass of each group (in µg C L^{-1}) was estimated from the cell carbon (µg C $cell^{-1}$) and abundance (cell L^{-1}).

7.1.2 Primary production estimations and photosynthesis-Irradiance curves

Net primary production (*Pn*) and respiration in darkness (*Rd*) rates were calculated as the slope of O_2 concentration versus time. *Rd* rates at the *in situ* T of every depth were estimated using a $Q_{10} = 2$ (Walsby 2001). Gross primary production (*Pg*) data were fitted to a photosynthesis-irradiance (*P-E*) curve model (Jassby and Platt 1976) according to equation 3:

$$Pg = Pn + Rd = Pg^{\max} \cdot tanh\left(\alpha \cdot \frac{E}{Pg^{\max}}\right) \qquad (3)$$

where *Pn* is the net primary production, *Rd* is the respiration rate in the dark, Pg^{max} is the maximum gross primary production, α is the photosynthetic efficiency and *E* is the irradiance. The compensation irradiance (E_c) was determined as the quotient between *Rd* and α, and the light-saturation of photosynthesis (E_k) as the quotient between Pg^{max} and α.

7.1.3 Code description (R script) for the DCM - CO_2 model

This section describes the R code used to find a numerical solution to the model proposed for DCM development. Note that this program has been designed for a particular aim and applied to a specific data structure. Caution should be taken when it is run for a different purpose, in which case slight modifications should be considered.

Two main steps were carried out by two independent scripts, i.e. a calibration of parameters and a steady-state solution for chlorophyll a (Chl *a*) and carbon dioxide (CO_2) profiles, named as "DIC" in the script. Given that the code is quite similar in both cases i.e. calibration script and solution script, only the steady-state solution is detailed line by line, whereas the calibration method is briefly outlined.

Once a set of parameters have been estimated by inverse modelling, the steady-state script begins with an input of their values, as well as a specification of numerical strategy (i.e. from purely backward=1 to purely forward=0), grid resolution (dz) and maximum depth. The ReacTran R package (Soetaert and Meysman 2012) should be firstly invoked.

```
##########################Install package#####################################

install.packages("Reactran")
library(ReacTran)
##############################################################################

omega<-1    #0-1, weight of backward values in numerical simulation

########################Parameters and constrains#############################

dz<- ##m, spatial grid resolution

depth_max<-##m, maximum depth

depth<-seq (0,depth_max,by=dz)

N<-length(depth)

grid <- setup.grid.1D(x.up=0,L=depth_max,N=N)

mumax <- ##day-1, Maximum reproductive rate

DIC_Half <- ##mmol m-3, Half-saturation coefficient for DIC uptake

l<- ##day-1, mortality rate

vz<- ##m day-1, sedimentation rate

ki<-##mmol m-3, Half-saturation constant for oxygen inhibition

ks<-##mmol m-3, Half-saturation constant for oxygen uptake

R_a<-##mmol C cell-1 day-1, Value for specific bacterial respiration

C_Chla_Epi<- ##mg C mg Chla-1, Value of the ratio for phytoplankton in the epilimnion

C_Chla_Meta<- ##mg C mg Chla-1, Value of the ratio for phytoplankton in the
metalimnion

Rmin <- ##d-1, minimum respiration rate (independent of gross production).

Gresp <- ##fraction of respiration associated to gross production

Q10<- ##Enhancement factor of respiration due to temperature increase

R_an_R_a<- ##Ratio of maximum specific respirations

kpiston<- ##m day-1, piston velocity for CO2

C_eq<- ##mmol m-3, CO2 equilibrium concentration with atmosphere

To<- ##ºC, maximum surface temperature

bo<- ##mg Chla m-3, biomass at the surface boundary (depth=0)

bf<- ##mg Chla m-3, biomass at the bottom boundary

Flux_down<- ##mmol m-2 day-1, flux of CO2 from the sediment-water interface
##(negative: from the sediment to the water column)

##############################################################################
```

Coefficients of turbulent diffusion are defined for epilimnion, metalimnion and hypolimnion at defined intervals of depth.

```
###Coefficients of turbulent diffusion
D_Epi<- ##m2 day-1, turbulent diffusion coefficient for epilimnion
depth_Epi_Meta<- ##m, depth limit of epilimnion
D_Meta<- ##m2 day-1, turbulent diffusion coefficient for metalimnion
depth_Meta_Hypo<- ##m, depth limit of metalimnion
D_Hypo<- ##m2 day-1, turbulent diffusion for hypolimnion
#############################################################################
```

Given that the spatial resolution needed for numerical calculus is higher than the sampling resolution, environmental variables (irradiance, temperature and oxygen concentrations) and state variables of the community (light saturation point and bacterial abundances) are linearly interpolated or splined. The resulting values are attached to the grid of depth.

```
###Splining and interpolating data in agreement with grid resolution
Irradiance<-read.table("[Name of file data].csv",sep = ",",header = T)
z_Irradiance<-Irradiance[,1]
raw_I<-Irradiance[,2]
Spline_Iz <- smooth.spline(z_Irradiance,raw_I)
Prediction_Iz<- function(x) {predict(Spline_Iz,x)$y}
Iz<-Prediction_Iz(depth)
###Ik is linearly interpolated (instead of splined)
Ik<-read.table("[Name of file data].csv",sep = ",",header = T)
z_Ik<-Ik[,1]
raw_Ik<-Ik[,2]
Ikzmatrix<-matrix(c(z_Ik,raw_Ik),nrow=length(raw_Ik),ncol=2)
###Bacterial abundance
Abundance_Bact<-read.table ("[Name of file data].csv",sep = ",",header = T)
 z_Bact<-Abundance_Bact [,1]
raw_Bact<-Abundance_Bact [,2]
Bactzmatrix<-matrix(c(z_Bact,raw_Bact),nrow=length(raw_Bact),ncol=2)
###Oxygen
O2<-read.table("[Name of file data].csv",sep = ",",header = T)
z_O2<-O2[,1]
O2_raw<-O2[,2]
O2zmatrix<-matrix(c(z_O2,O2_raw),nrow=length(O2_raw),ncol=2)
```

```
###Temperature

Temp<-read.table("[Name of file data].csv",sep = ",",header = T)

z_Temp<-Temp[,1]

Temp_raw<-Temp[,2]

Tempzmatrix<-matrix(c(z_Temp,Temp_raw),nrow=length(Temp_raw),ncol=2)

#############################################################################

###Defining a profile of turbulent diffusivity (Dz)

Dz<-c(rep(D_Epi,each=(depth_Epi_Meta/dz)),rep(D_Meta,each=((depth_Meta_Hypo-
depth_Epi_Meta)/dz)),rep(D_Hypo,each=(((depth_max-depth_Meta_Hypo)/dz)+1)))

#############################################################################
```

Given that different ratios of particulate organic carbon-to-chlorophyll *a* (C: Chl *a*) were assumed for epilimnion and metalimnion, a binary matrix (0,1) allows to assign the proper value within each layer.

```
###Defining a profile of binary-matrix (0,1) for the calibration of C_Chla

epsilon_Epi<-c(rep(1,each=(depth_Epi_Meta/dz)),rep(0,each=(((depth_max-
depth_Epi_Meta)/dz)+1)))

epsilon_Meta<-c(rep(0,each=(depth_Epi_Meta/dz)),rep(1,each=(((depth_max-
depth_Epi_Meta)/dz)+1)))

###Defining the grid of variables and parameters

Iz.grid <- setup.prop.1D(func=Prediction_Iz,grid=grid)

Ikz.grid<-setup.prop.1D(xy=Ikzmatrix,interpolate="linear",grid=grid)

Bactz.grid<-setup.prop.1D(xy=Bactzmatrix,interpolate="linear",grid=grid)

O2z.grid<-setup.prop.1D(xy=O2zmatrix,interpolate="linear",grid=grid)

Tempz.grid<-setup.prop.1D(xy=Tempzmatrix,interpolate="linear",grid=grid)

#########################################################################

###Diffusion matrix

Dz_matrix<-t(rbind(depth,Dz))

Dz.grid<-setup.prop.1D(xy=Dz_matrix,interpolate="linear",grid=grid)

###Epsilon matrix for epilimnion and metalimnion#################

epsilon_Epi_matrix<-t(rbind(depth,epsilon_Epi))

epsilon_Epi.grid<-
setup.prop.1D(xy=epsilon_Epi_matrix,interpolate="linear",grid=grid)

epsilon_Meta_matrix<-t(rbind(depth,epsilon_Meta))

epsilon_Meta.grid<-
setup.prop.1D(xy=epsilon_Meta_matrix,interpolate="linear",grid=grid)

#########################################################################
```

Next lines allow to visualize the data input and check for accuracy.

```
####Plots
plot(z_Irradiance,raw_I)
lines(depth,Iz)
x11()
plot(z_Ik,raw_Ik)
lines(Ikzmatrix[,1],Ikzmatrix[,2])
x11()
plot(z_Bact, raw_Bact)
lines(Bactzmatrix[,1],Bactzmatrix[,2])
x11()
plot(z_O2, O2_raw)
lines(O2zmatrix[,1],O2zmatrix[,2])
x11()
plot(z_Temp, Temp_raw)
lines(Tempzmatrix[,1],Tempzmatrix[,2])
x11()
plot(Dz_matrix[,1],Dz_matrix[,2])
x11()
plot(epsilon_Epi_matrix[,1],epsilon_Epi_matrix[,2])
x11()
plot(epsilon_Meta_matrix[,1],epsilon_Meta_matrix[,2])
##############################################################################################
```

On the other hand, both Chl *a* and CO_2 profiles, as well as values of gross production have to be turned into the workspace in order to compare with model predictions.

```
#######Raw Phyto and DIC data (to obtain sampled depths and calculate costs)
Abundance_Phyto<-read.table("[Name of file data].csv",sep = ",",header = T)
z_Phyto<-Abundance_Phyto[,1]
raw_Phyto<-Abundance_Phyto[,2]
positions1<-which(depth %in% z_Phyto )
DICdata<-read.table("[Name of file data].csv",sep = ",",header = T)
z_DIC<-DICdata[,1]
raw_DIC<-DICdata[,2]
positions_DIC<-which(depth %in% z_DIC)
max_positions<-max(positions1)
positions2<-max_positions+positions_DIC
```

```
Grossprod_data<-read.table("[Name of file data].csv", sep = ",",header = T)

z_gross_prod2<-Grossprod_data[,1]

raw_gross_prod2<-Grossprod_data[,2]

positions3<-which(depth %in% z_gross_prod2)

print(positions3)
```

The last lines properly assign indexes to the Chl *a* and CO_2 outputs, in order to compare with positions of available measurements. Furthermore, they help to identify values of gross production within the grid. The R code is structured to input parameters as a combined argument. Therefore, transport and production terms are formulated within the same function.

```
#########################################################################

###########Defining the model to solve steady state#####################

parameters<-
c(mumax=mumax,DIC_Half=DIC_Half,l=l,vz=vz,ki=ki,ks=ks,R_a=R_a,C_Chla_Epi=C_Chla_Epi
,C_Chla_Meta=C_Chla_Meta,Q10=Q10,Flux_down=Flux_down,Rmin=Rmin,Gresp=Gresp)

model<-function(time, state, parameters){

with(as.list(c(parameters)),{

############Initialisation of state variables#######

b<-state[1:N]

DIC <- state[(N+1):(2*N)]

######Transport and production terms for Chlorophyll a#####

####For Chl a, Flux=0 at the surface#####################

########Chl a is a known value at the bottom###############

tran1<-tran.1D(C=b,C.down=bf,flux.up=0,D=Dz.grid,v=vz,AFDW=omega,VF=1,dx=grid)$dC

prod1<-((mumax*pmin(tanh(Iz.grid$mid/Ikz.grid$mid),(DIC/(DIC+DIC_Half))))-l)*b

#########Transport and production terms for CO2############################

#########For CO2, Piston flux at the water-atmosphere interface###############

#########Flux from sediment is a known value at the bottom###################

tran2<-tran.1D(C=DIC,flux.down=Flux_down,C.up=C_eq,a.bl.up=kpiston,
D=Dz.grid,v=0,AFDW=omega,VF=1,dx=grid)$dC

 prod2<-
((mumax*pmin(tanh(Iz.grid$mid/Ikz.grid$mid),(DIC/(DIC+DIC_Half)))))*b*(C_Chla_Epi*e
psilon_Epi.grid$mid+C_Chla_Meta*epsilon_Meta.grid$mid)*(1/12)

resp2<-

(Bactz.grid$mid*(Q10^((Tempz.grid$mid-
To)/10))*(R_a*(O2z.grid$mid/(O2z.grid$mid+ks))+

R_an_R_a*R_a*(1-O2z.grid$mid/(O2z.grid$mid+ki))))

#################Estimating gross production rates################

gross_prod2<<-
```

```
(1/(1-
Gresp))*((mumax*pmin(tanh(Iz.grid$mid/Ikz.grid$mid),(DIC/(DIC+DIC_Half))))+Rmin)*b*

(C_Chla_Epi*epsilon_Epi.grid$mid+C_Chla_Meta*epsilon_Meta.grid$mid)*(1/12)
```

These lines require further clarification. In both Chl *a* (the state variable '*b*') and CO_2 profiles, boundary conditions are specified within the function '*tran.1d*'. The upper boundary condition for CO_2 is delimited by the equilibrium concentration with atmosphere ('C_eq') and the mass transfer coefficient ('kpiston'). The argument '*VF*' equals 1 because water column is 100% fluid. The factor 1/12 simply converts mg C to mmol C. Gross production is calculated from biomass growth and respiration parameters; the operator '<<-' extracts spatial grid to the workspace. Recall that each command should be typed in one single line, as part of the function '*model*'. The code lines described below yield rates of change to find a zero-solution from an initial guess of the modelled variables.

```
################################################################################

################ Assemble the total rate of change#########################

db<-tran1+prod1

dDIC<-tran2-prod2+resp2

return(list(c(db=db,dDIC=dDIC)))

  })}

################### State variables and initial conditions########

b_in<-rep(bo,length.out=N)

DIC_in <- rep(C_eq,length.out=N)

state <- c(b_in,DIC_in)

################################################################################
```

Finally, the steady state is estimated by indicating a standard method, the number of modelled variables ('*nspec*=2') and the restriction to only positive outcomes ('*pos=TRUE*'). The output is double checked, i.e. (1) by corroborating that deviations are under an acceptable threshold for the stationary condition ('*attributes*') and (2) by plotting results ('Output') against real data.

```
################## Steady state calculation ################################

Output <- steady.1D(y=state, func=model, parms=parameters, method="stode",nspec=2,
pos=TRUE)

 steady.state.reached <- attributes(Output)$steady

if (steady.state.reached) {b<-Output$y[1:N];DIC <- Output$y[(N+1):(2*N)]} else
{stop}

print                                                    (sum(((Output$y[positions1]-
raw_Phyto)/(max(raw_Phyto)))^2)+sum(((Output$y[positions2]-
raw_DIC)/(max(raw_DIC)))^2)+sum(((gross_prod2[positions3]-
raw_gross_prod2)/(max(raw_gross_prod2)))^2))

print(attributes(Output)$steady)

print(attributes(Output)$prec)

################################################################################
```

```
#################Plotting the results#########################################
x11()
plot(z_Phyto,raw_Phyto)
lines(depth,Output$y[1:N])
x11()
plot(z_DIC,raw_DIC)
lines(depth,Output$y[(N+1):(2*N)])
alldata_gross_prod<-data.frame(raw_gross_prod2,gross_prod2[positions3])
x11()
barplot(t(as.matrix(alldata_gross_prod)),names.arg=z_gross_prod2,beside=TRUE,horiz=
TRUE,ylab="Depth(m)",xlab="Gross production rates mmol m-3 d-1", col=c("white",
"grey"),xlim=c(0,2.5))
 legend("right",legend=c("Observed","Predicted"),fill=c("white", "grey"))
#############################################################################
```

Goodness of fit is estimated with the observations versus predictions line. Both intercept and determination coefficient (R^2) are tested for significance. The slope is statistically compared with a 1:1 line by means of a t-test.

```
#################Plotting the predictions-observations line##################
Expected1<-Output$y[positions1]
x11()
plot(Expected1,raw_Phyto)
lines(c(min(raw_Phyto),max(raw_Phyto)),c(min(raw_Phyto),max(raw_Phyto)))
Data_Phyto<-data.frame(Expected1,raw_Phyto)
Reg1<-lm(raw_Phyto~Expected1,data=Data_Phyto)
summary(Reg1)
############Testing slope is not significantly different than 1################
print(coef(summary(Reg1))[2,1])
print(coef(summary(Reg1))[2,2])
t_value1<- (coef(summary(Reg1))[2,1]-1)/(coef(summary(Reg1))[2,2])
p_value1<- 2*pt(-abs(t_value1),df=length(raw_Phyto)-2)
print(t_value1)
print(p_value1)
#############################################################################
```

Similar code lines should be applied for CO_2 profiles, in order to obtain an indicator of the quality of fit. The R script is ended with a data save instruction and the detachment of external R packages.

```
write.csv(b,file='[Name of file data].csv')

write.csv(DIC,file='[Name of file data].csv')

detach(package:ReacTran)

##############################################################################
```

The code for parameters calibration mostly includes all of the steps above described. Instead of specific values, minimum and maximum limits are indicated for each parameter. The function '*model*' does not yield the expected profiles of Chl *a* and CO_2, but a combination of costs of fitting, according to:

```
Negative<-which(Output$y<0)

final_costs<-ifelse(length(Negative)>0,Inf,sum(((Output$y[positions1]-
raw_Phyto)/(max(raw_Phyto)))^2)+sum(((Output$y[positions2]-
raw_DIC)/(max(raw_DIC)))^2)+sum(((gross_prod2[positions3]-
raw_gross_prod2)/(max(raw_gross_prod2)))^2))
```

where the target minimum squares are normalized by the respective maximum values of Chl *a*, CO_2, and gross production. Note that this code line should be joined with a specification that exclude any negative prediction, e.g. by making the associated costs infinite. Value of costs are then used by the function '*pricefit*' to iteratively select the set of parameters that minimizes deviations. Depending on the number of iterations chosen, the computer performance and the code structure, a solution with the best 50 set of parameters is reached in few minutes to several hours. In our case, number of iterations were around 25000.

```
#########################Install package#####################################

install.packages("ecolMod")
library(ecolMod)
##############################################################################

inverse_modelling<-pricefit(par=c(mumax=mumax_ini,DIC_Half=DIC_Half_ini,
[…]),minpar=c(mumax=mumax_min,DIC_Half=DIC_Half_min,[…]),maxpar=c(mumax=mumax_max,D
IC_Half=DIC_Half_max, […]),func=cost,numiter=25000)

print(inverse_modelling)

detach(package:ecolMod)
```

where […] are the rest of parameters, the subscript '*_min*' indicates the lowest limit and the subscript '*_max*' indicates the highest limit. More information about inverse modelling procedures can be found in Soetaert and Herman (2009).

7.1.4 References

Echevarria, F., L. Zabala, A. Corzo, G. Navarro, L. Prieto, and D. Macías. 2009. Spatial distribution of autotrophic picoplankton in relation to physical ´ diz , Strait of forcings : the Gulf of Ca ´ n Sea case study Gibraltar and Albora. J. Plankton Res. **31**. doi:10.1093/plankt/fbp070

Eppley, R. W., F. M. H. Reid, and J. D. H. Strickland. 1970. Estimates of Phytoplankton Crop Size, Growth Rate, and Primary Production, *In* The Ecology of the Plankton Off La Jolla, California, in the Period April Through September, 1967.

Jassby, A. D., and T. Platt. 1976. Mathematical formulation of the relationship between photosynthesis and light

for phytoplankton. Limnol. Oceanogr. **21**: 540–547.

Posch, T., M. Loferer-Krößbacher, G. Gao, A. Alfreider, J. Pernthaler, and R. Psenner. 2001. Precision of bacterioplankton biomass determination: A comparison of two fluorescent dyes, and of allometric and linear volume-to-carbon conversion factors. Aquat. Microb. Ecol. **25**: 55–63. doi:10.3354/ame025055

Shalapyonok, A., R. J. Olson, and L. S. Shalapyonok. 2001. Arabian Sea phytoplankton during Southwest and Northeast Monsoons 1995: composition, size structure and biomass from individualcellpropertiesmeasuredby#owcytometry. Deep. Res. Part II Top. Stud. Oceanogr. **48**: 1–31. doi:10.1016/S0967-0645(00)00137-5

Smith, E. M., and Y. T. Prairie. 2004. Bacterial metabolism and growth efficiency in lakes: The importance of phosphorus availability. Limnol. Oceanogr. **49**: 137–147. doi:10.4319/lo.2004.49.1.0137

Soetaert, K., and P. M. Herman. 2009. ecolMod:" A practical guide to ecological modelling-using R as a simulation platform". R Packag. version **1**.

Soetaert, K., and F. Meysman. 2012. R-package ReacTran: Reactive Transport Modelling in R. Environ. Model. Softw. **32**: 49–60.

Walsby, A. E. 2001. Erratum: Determining the photosynthetic productivity of a stratified phytoplankton population (Aquatic Sciences (2001) 63 (18-43)). Aquat. Sci. **63**: 502. doi:10.1007/s00027-001-8048-3

Worden, A. Z., G. Drive, L. Jolla, and J. K. Nolan. 2004. Assessing the dynamics and ecology of marine picophytoplankton : The importance of the eukaryotic component. **49**: 168–179.

7.2 Figures

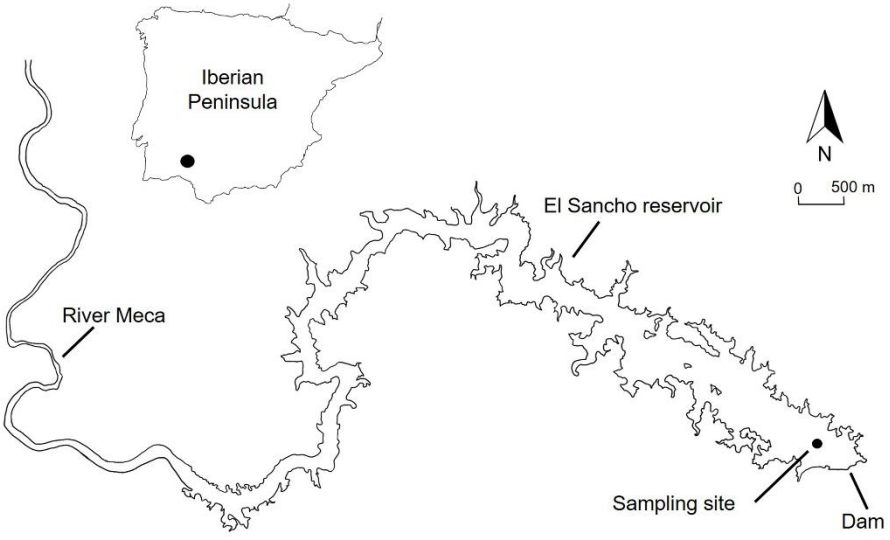

Fig.S1. *Map* of El Sancho reservoir showing the sampling site during the stratification period in 2013.

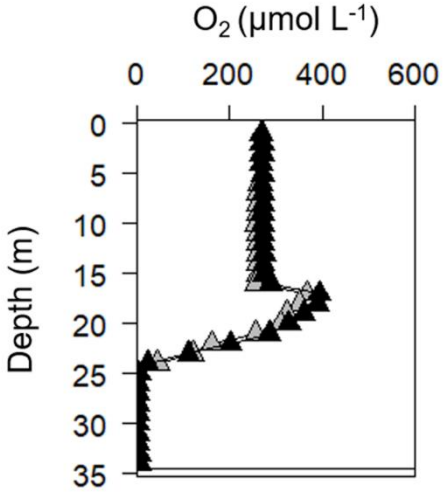

Fig.S2. *Water column* depth profiles of high resolution oxygen on 2th (△) and 8th (▲) October 2013 in El Sancho reservoir. The bottom of reservoir is shown with a horizontal black line

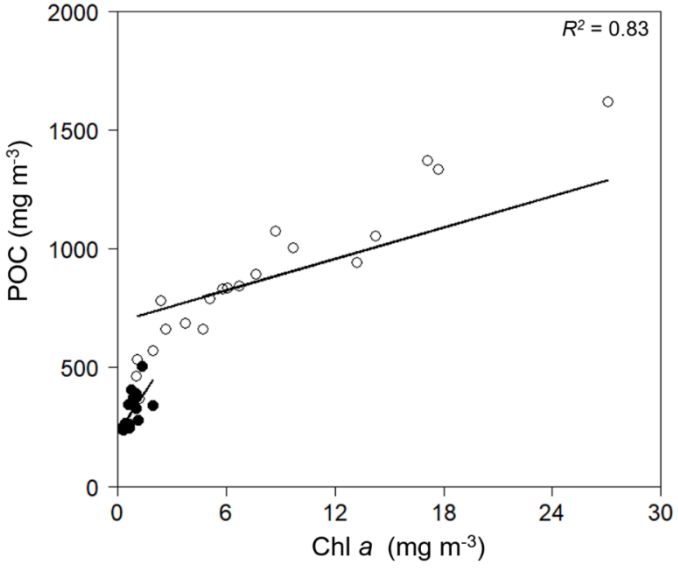

Fig.S3. *Relationship* between particulate organic carbon (POC) and chlorophyll *a* (Chl *a*) experimental data in the epilimnion (●) and metalimnion (○). Data fit significantly to the corresponding POC:Chl *a* ratio (slope of lines) obtained from the model in both lake compartments on 25th September.

CHAPTER V

Changes in phylogenetic composition and single-cell traits of bacterioplankton community between stratification and mixing in an acidic reservoir

Changes in phylogenetic composition and single-cell traits of bacterioplankton community between stratification and mixing in an acidic reservoir

Sara Soria-Píriz [1*], Alfonso Corzo[1], Juan Luís Jiménez-Arias[1], Juan M. González [2], Sokratis Papaspyrou[1].

[1]Department of Biology, Faculty of Marine and Environmental Sciences, University of Cádiz, Campus of International Excellence (CEIMAR), Polígono Rio San Pedro s/n 11510 Puerto Real, (Cádiz) Spain.
[2] Institute of Natural Resources and Agrobiology Spanish National Research Council. Avda. Reina Mercedes 10, 41012-Sevilla, Spain
* corresponding author: Department of Biology, Faculty of Marine and Environmental Sciences, University of Cádiz, Polígono Río San Pedro s/n 11510 Puerto Real (Cádiz), Spain Tel. 34-956-016774. E-mail:

ABSTRACT: Spatio-temporal changes on phylogenetic composition and single-cell traits of bacterioplankton are poorly known in acid lakes. El Sancho reservoir (Iberian Pyritic belt, Huelva, SW Spain) is an acid mine drainage impacted holomictic water body (pH < 4). We examined the variation of the bacterioplankton community in terms of phylogenetic composition, abundance and single-cell traits of the high nucleic acid (HNA) and low nucleic acid (LNA) assemblages in response to shifts in environmental conditions in space and time. Canonical correspondence analysis indicated that phylogenetic bacterial composition was mainly regulated by oxygen, chlorophyll a, temperature, pH and DOC and bacterial cell-traits by temperature, pH and ammonium. Procrustes analysis showed that both canonical correspondence analyses were highly correlated (r = 0.42, p = 0.02) but they seem to be explained by different environmental drivers. This covariation at multiple community structural levels and the differences in the drivers involved suggests that bacterial community dynamics are complex even in this relatively simple system. Our results point out to a strong role of environmental selection in the occupation of the different microbial niches since microbial dispersion was no or little limited.

KEYWORDS: bacterial community structure, drivers, flow cytometry, composition, acid lake, gradients

1. Introduction

Bacterioplankton plays a crucial role in pelagic systems, being involved in all key biogeochemical processes and channelling matter and energy to higher trophic levels through the microbial loop (Azam 1998, Cotner and Biddanda 2002, Mühlenbruch et al 2018). A major challenge for microbial ecology is to link bacterial physiology, abundance and diversity to ecological functioning in order to understand seasonal and long term biogeochemical changes in aquatic systems and eventually be able to predict them under the present scenario of increasing anthropogenic pressures (Comte and del Giorgio 2009, 2010, Wallenstein and Hall 2012, Krause et al 2014, Glassman et al 2018). This aim requires the application of complementary approaches, i.e. molecular techniques, flow cytometry (FCM), determination of metabolic and growth rates, and suitable statistical tools to integrate the multidimensional information obtained (Comte and del Giorgio 2009, Krause et al 2014, Read et al 2015, Crognale et al 2017).

Bacterioplankton communities can exhibit spatial variability at scales ranging from millimetres to thousands of kilometres (Martiny et al. 2006). In the last decades, relationships among different structural levels of bacterial community (single-cell traits, physiology, metabolism and taxonomy) in response to environmental conditions have been explored at large spatial scales across interconnected systems at basin scale (Comte and del Giorgio 2009, 2010, Niño-García et al 2016a,b), long downstream systems (del Giorgio and Bouvier 2002, Fortunato et al 2012, Read et al. 2015, Zhang et al 2019), latitudinal gradients or geographic distance (Lindström 2006, Schiaffino et al 2013, Liu et al 2015) including the factor time (Shade et al 2008, Nelson et al 2009, Comte and del Giorgio 2009, 2010, Liu et al 2013). Studies have reached different conclusions on the importance of environmental factors in shaping structural aspects of microbial communities, likely because the microbial dispersal factor influences the spatial patterns of the microbial community composition (Reche et al 2005, Crump et al 2007, Findlay et al 2010). However, less information exists on the potential changes in the structure of microbial community at different levels along environmental gradients at smaller spatiotemporal scales (Kent et al 2007, Shade et al 2008, Nelson et al 2009) where differences between sites are not limited by dispersion and environmental selection is probably more important in shaping the microbial community.

Freshwater lakes and reservoirs are ideal systems to examine the community dynamics of bacterioplankton in response to changes in environmental drivers and the resulting habitat heterogeneity both in space and time within the same water body. In many freshwater systems, environmental conditions change dramatically during the annual thermal cycle, leading to a combination of sharp biogeochemical vertical gradients during stratification across thermal layers (Selig et al., 2004; Tammert et al., 2005; Tonno et al., 2005; Boucher et al., 2006). In contrast, during the colder months the water column turns over disrupting the bacterial niches created by thermal stratification and mixing vertically biogeochemical elements and communities alike, resetting the system (Fenchel and Finlay 2008, Shade et al. 2008, 2012, Morrison et al 2017).

Acid mine drainage (AMD) impacted systems are considered extreme environment due to the low pH and high concentration of toxic heavy metals, which affect the abundance and diversity of microbial communities (Nixdorf et al. 1998, Williamson et al 2008, Zhang et al 2019). However, AMD systems have been long recognized as model systems for the quantitative analysis of microbial ecology and community function due to their relative biological simplicity (Baker and Banfield 2003; Huang, Kuang and Shu 2016). El Sancho Reservoir (SW Spain) is one such acidified environment due to

chronic pollution by AMD. Previous studies in El Sancho have demonstrated the existence of different ecological niches in the strongly stratified water column in summer, a close coupling between bacterial abundance and CO_2 production in the hypolimnion and the existence of a deep chlorophyll maximum (DCM) located in the metalimnion (Soria-Píriz et al. 2019). However, no information exists on the bacterial community structure in this reservoir. In addition, little information exists on the single-cell traits dynamics of bacterial communities in this and other acidic lakes and reservoirs, let alone on whether possible single cell traits shifts are synchronous to changes in the phylogenetic composition and what factors are responsible.

In the present study we aimed to assess to what degree the bacterial composition - determined by molecular DNA-based techniques- and bacterial abundance and single-cell traits - determined by flow cytometry (FCM) - are linked across different microbial niches defined by spatiotemporal changes of environmental properties. For this purpose, we sampled during the thermal stratification and mixing periods at different depths in the El Sancho Reservoir. Our study shows that analysis of both phylogenetic composition and single-cell characteristics of bacterioplankton are able to discriminate the communities in different niches of the stratification and mixed periods in this reservoir. In addition, the changes observed at the two community structural levels between different niches are synchronous, i.e. changes in cells traits occur in parallel with changes in phylogenetic composition; however, they seem to be explained by different environmental drivers. This double shift at multiple community structural levels and the differences in the drivers involved suggests that bacterial community dynamics are complex even in this relatively simple system, affecting most likely the flows of matter and energy, and, ultimately, ecosystem-scale functioning.

2. Materials and Methods

2.1. Study site and sampling

El Sancho reservoir is located within the Iberian Pyrite Belt (SW Spain), one of the world's largest accumulations of AMD polluted environments (Sanchez-España et al. 2005). El Sancho is a holomictic water body heavily polluted by AMD, with a pH ranging from 3.5 to 4.5 depending on season (Torres et al., 2013). During stratification the hypolimnion becomes hypoxic and a deep chlorophyll maximum develops in the metalimnion (Torres et al. 2016, Soria-Píriz et al. 2019).

Field measurements and water samplings were carried out at a single site (37°27'49''N, 6°59'3''W), located at the deepest part of the reservoir (~ 35 m depth), during the stratification (12th September, 18th September, 25th September and 8th October, 2013) and the mixing periods (8th January, 25th January and 4th February, 2014).

2.2. Environmental variables

Vertical profiles of temperature (T, ºC), pH, and fluorescence (relative units, r.u.) were obtained using a multiparameter probe (Hydrolab MS5). Water samples were collected using a 10 L Van Dorn bottle from similar depths during both seasons (0, 5, 10, 15-16, 20, 22/26, 32/33 m depth).

High-resolution O_2 profiles in the water column were determined during the stratification (2th and 8th October) and during the mixing periods (8th January, 25th January and 4th February, 2014) with a modified MP4 Miniprofiler (UNISENSE). TCO_2 samples (n = 1 per depth) were collected in 5 mL

Exetainer tubes, fixed with 100 µL saturated $HgCl_2$ and stored in darkness at 4 °C until analysis on an InfraRed Gas Analyzer (Qubit systems, S151 CO_2 analyzer) (Limit of detection, LOD: 6.8 µmol L^{-1}), following Hall and Aller (1992).

Inorganic nutrients samples were filtered in situ (MF 300, 0.7 µm, 47 mm, Fisherbrand™), stored on ice and frozen at -20 ºC once in the laboratory. Nutrients were analysed using standard protocols (ammonium: Bower and Holm-Hansen 1980; nitrate and nitrite: García-Robledo et al. 2014) with a limit of detection between 0.1 and 0.5 µmol L^{-1}.

For the determination of chlorophyll *a* (Chl *a*), water samples (0.5 - 1 L) were filtered *in situ* through pre-combusted filters (GF/F glass fiber filters, 0.7 µm, 47 mm, Whatman®). Filters were stored on ice in darkness and frozen at -20 °C upon return to the laboratory. Chlorophyll *a* was extracted at 4 °C for 12 hours with 4 mL of acetone 90%, tubes centrifuged (2200 x g, 5 min) and the absorbance of the extracts measured on a UV 1700 Pharmaspec Shimadzu spectrophotometer. Chlorophyll *a* concentrations were calculated according to Ritchie (2008).

Dissolved organic carbon (DOC) samples (approximately 20 mL) were filtered through nylon filters (Nylon Syringe filters,0.2 µm, 30 mm, Thermo Scientific™) in acid washed glass vials (n = 1) and stored at 4ºC. DOC concentration was determined on a Shimadzu TOC-5050 analyzer after sample acidification (1 mL of phosphoric acid 1:3) (ICMAN-CSIC external services).

2.3. DNA sequences

To examine the composition of bacterial community, water from each depth was filtered through a Sterivex filter (0.22 µm, Millipore®) until saturating the filter and fixed with RNALater® according to the manufacturer's instructions. DNA extractions were performed with the PowerWater Sterivex DNA Isolation kit (MoBio Laboratories, Inc., Carlsbag, CA) with an additional initial wash in an acidic buffer (pH 1.8; 0.1 M KCl, 0.04 M HCl) followed by neutralization in TE buffer (10 mM Tris-HCl, 1 mM EDTA, pH 8.0). Amplicon based libraries for the 16S rRNA gene were pyrosequenced on a FLX Titanium Genome Sequencer (Roche Applied Sciences, 454 Life Sciences, Branford, CT, USA) following Bowers et al. (2009). DNA sequences were analysed with the QIIME software (Caporoso et al., 2010). Operational phylogenetic units (OTUs) were determined based at the 97% sequence similarity using the molecular web GREENGENES database (DeSantis et al., 2006).
In this study, the phylas > 0.1% of their mean relative abundance across all samples were defined as abundant, while phyla with relative abundance < 0.1% were pooled in the "Others" category.

2.4. Flow cytometry

Water samples were fixed in cryotubes (4.5 mL) using glutaraldehyde (1% final concentration) (Vaulot et al. 1989) and frozen at –80 ºC until analysis. Samples were left to thaw at room temperature, 1 mL aliquots were immediately stained with 10 µL of SYBR® Green-I nucleic acid gel stain (Molecular Probes #S7563) (2.5 µM final concentration) and incubated for 10 min at room temperature in darkness before analysis (Lebaron et al. 2001; Corzo et al. 2005). A known amount of autofluorescent beads (1.1 µm diameter, Ex/Em: 430/465 nm, FluoSpheres® Molecular Probes Inc.™) were added to each sample as an internal standard. Reference beads and stained bacterial cells were excited at 488 nm and detected according to their 90° light scatter (SSC) and green fluorescence (FL). Samples from stratification and mixing were analyzed on a Dako CyAnTM ADP (Beckman Coulter™)

and on a CytoFLEX (Beckman Coulter™) flow cytometers respectively. All samples were analyzed by the same researcher at medium flow rate, and were run until at least 30000 counts were recorded.

Two heterotrophic bacterial populations were discriminated based on their signature in the FL vs SSC cytogram: HNA (high nucleic acid content) and LNA (low nucleic acid contents) (Fig. S1) (Lebaron et al. 1998, Gasol and del Giorgio 2000, Corzo et al 2005).

The values of cell traits, FL, and SSC for the HNA and LNA subpopulation were calculated as the average channel number for each trait and each subpopulation divided by the average channel number of FL and SSC of the reference beads added to the sample.

2.5. Statistical analysis

Total bacterial abundance, FL, SSC and FL/SSC of both HNA and LNA cells and environmental variables (i.e. T, O_2, pH, CO_2, NH_4^+, NO_x, Chl *a* and DOC) were scaled (0 to 1) to remove differences in scales prior to multivariate statistical analyses. To assess the significant variability of the total bacterial abundance and the %, FL and SSC of HNA and LNA cells through the water column and between seasons, we used two-way ANOVA and Tukey-Kramer means post-hoc comparison tests ($\alpha = 0.05$).

Variation in phylogenetic composition and single-cell traits through the water column and between seasons was related to the environmental variables using two different canonical correspondence analysis (CCA) (R package Vegan version 2.5-4) (Oksanen et al. 2010). In the first CCA, phyla were used as "species", while in the second one, the "species" were the total bacterial abundance, % LNA and the single-cell traits (i.e. FL, SSC) of both LNA and HNA cells. Environmental variables were used as constraining variables. Before the CCA analysis, environmental variables with high correlation (> 0.8) were eliminated to avoid collinearity using the ggpairs() function (R package GGally: Extension to 'ggplot2' version 1.4.0) (Schloerke et al 2018). Collinearity between temperature and NO_3^- and between NH_4^+ and CO_2 were found. Only temperature and NH_4^+ were included in the analysis. A forward-selection procedure using the AIC criterion with 9999 permutations was used to choose the environmental variables best explaining the variations in each CCAs ($p < 0.05$) (R package vegan version 2.5-4) (Oksanen et al. 2010, Borcard et al 2011). The congruence between both CCAs was tested using the procrustes() function (R package vegan version 2.5-4) (Oksanen et al. 2010). This method determines the best superimposition that maximizes the fit through scales and rotations processes by matching corresponding points (depths in this study) from both multivariate data sets. The significance of the procrustes statistics was evaluated using the protest() function with 999 permutations (R package vegan version 2.5-4) (Jackson 1995, Oksanen et al. 2010).

To assess possible seasonal patterns between the most abundant bacterial classes, bacterial abundance and the single-cell traits of HNA and LNA fractions data were pooled (without distinguishing potential microbial niches) and tested by Spearman correlations using the rcorr() function (R package Hmisc version 4.2-0) (Harrel et al. 2016) and the corrplot() function for visualization (R package corrplot version 0.84) (Wei and Simko 2016).

3. Results

3.1. Biogeochemical structure of the water column

The differences in the thermal structure of the water column determined large changes in biogeochemical characteristics between stratification and mixing, including the presence of a deep chlorophyll maximum (DCM) (Fig. 1, Table S1). To investigate the relationship between the environmental variability and bacterial cellular traits, abundance and community taxonomic composition, we distinguished six microbial niches with different environmental conditions, which include spatial and temporal segregation (Table S1). During summer, the epilimnion, metalimnion and hypolimnion differed clearly in a number of biogeochemical properties (Table S1). Furthermore, within the metalimnion three niches were defined (Fig. 1), which are likely to harbour different bacterial communities and cellular traits: the O_2 peak, the upper layer of the DCM (above DCM), associated to the net production maximum (Soria-Píriz et al. 2019), and the DCM peak, where the maxima of fluorescence, Chl *a* and POC occur (Table S1, Soria-Píriz et al. 2019). In contrast, during the mixing period, the water column was assumed to represent one potential microbial niche since changes in the biogeochemical variables were little.

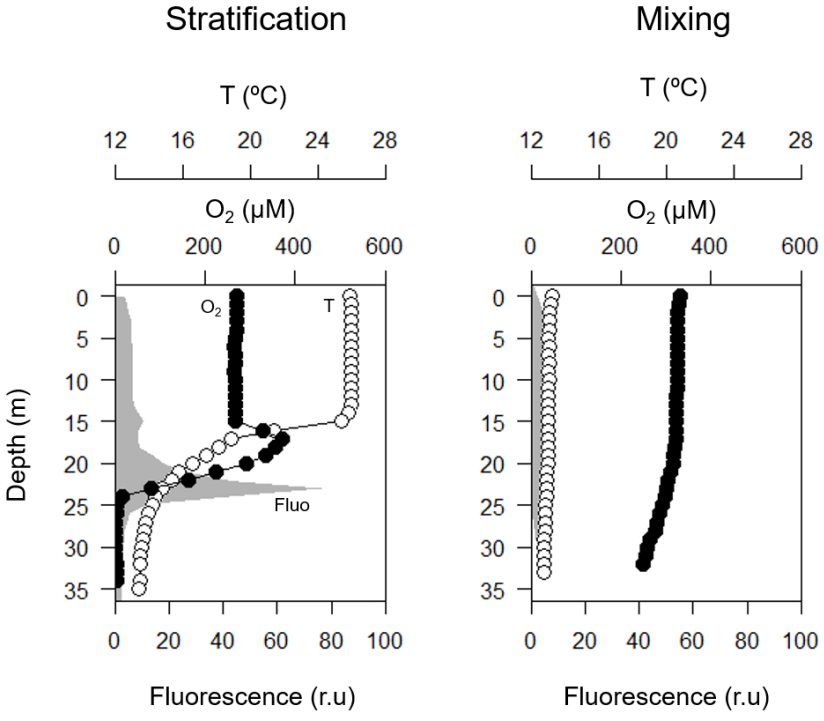

Fig.1: Depth profiles showing the vertical distribution of temperature (T), dissolved oxygen (O_2), and fluorescence (Fluo, shaded curve) in El Sancho reservoir during stratification (summer) and mixing (winter).

3.2. Phylogenetic composition of bacterioplankton community

A total of 1,922,474 sequences were generated, averaging 13000 sequences per depth, comprising a total of 20186 operational phylogenetic units (OTUs). Diversity indices (Shannon,

Simpson, Chao1) based on OTUs relative abundance increased from the epilimnion to the hypolimnion during stratification whereas in mixing were more homogeneous along the water column (Fig. S2).

Ordination analysis of the most abundant bacterial phyla revealed clear separation between the different niches (Fig. 2a), being explained significantly by axes CCA1 (42.2 %, $F_{1,\ 21}$ = 55.73, p =0.001), CCA2 (23.9%, $F_{1,\ 21}$ = 31.58, p = 0.001) and CCA3 (9.7 %, $F_{1,\ 21}$ = 17.64, p = 0.001) (Fig. 2a). O_2, Chl *a*, temperature, pH, and DOC (variables selected by Forward-selection procedure) explained together 83.32% of the variation in the bacterial phylogenetic composition-based ordination at the phylum level.

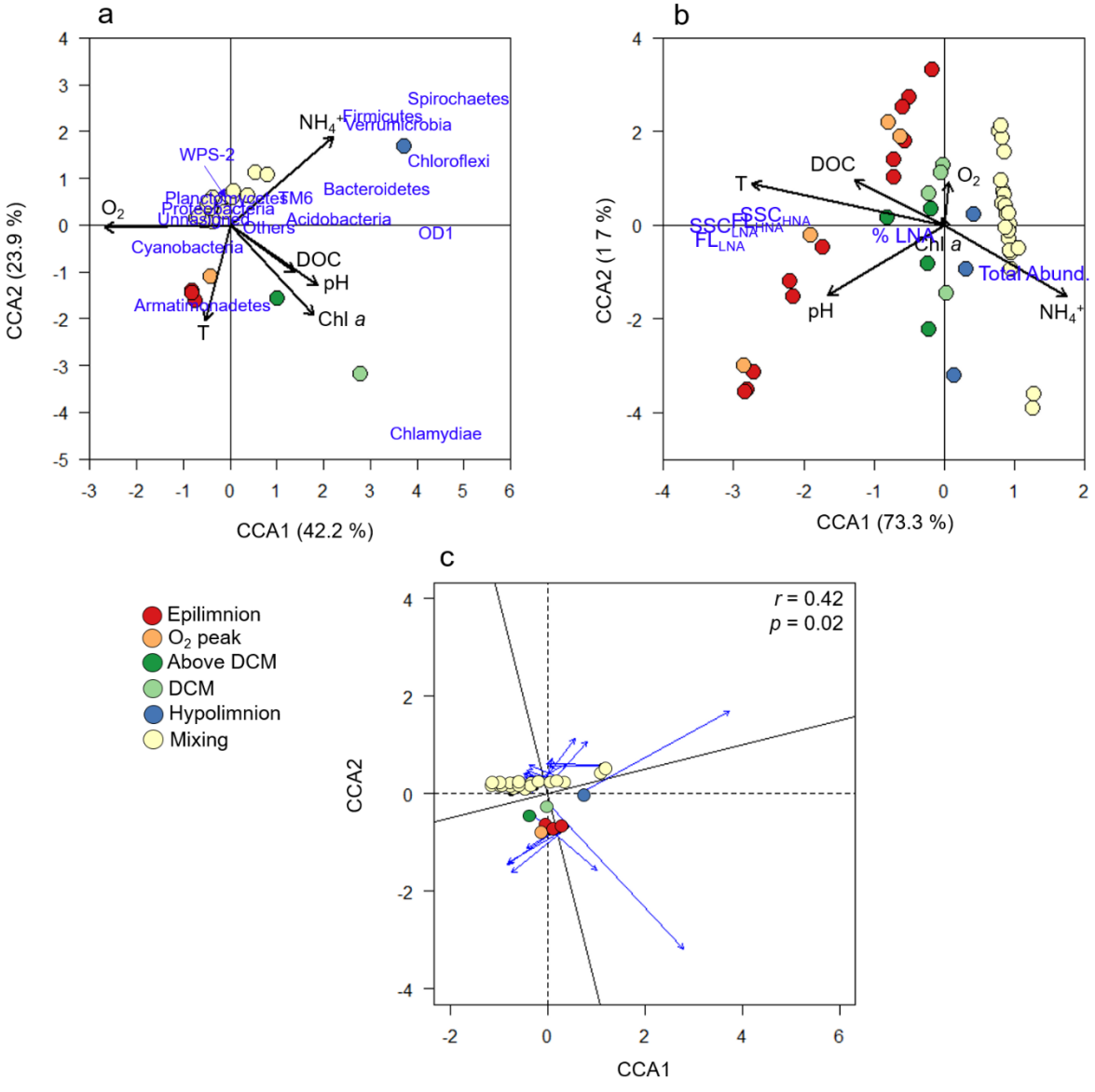

Fig.2: (a) Canonical correspondence analysis (CCA) ordination of microbial niches distinguished in El Sancho (Table 1) based in the relative abundance (%) of the most abundant bacterial phyla i.e. Acidobacteria,

Armatimonadetes, Bacteroidetes, Chamydiae, Chloroflexi, Cyanobacteria, Firmicutes, OD1, Planctomycetes, Proteobacteria, Spirochaetes, TM6, Verrucomicrobia, WPS-2 and Unassigned while "Others" includes all phyla with relative abundance < 0.1%. (blue letters). Circles in color represent sampling points. Correlations between environmental variables and the microbial niches ordination are represented by the black arrows. One sampling during stratification (summer) (n = 7) and three samplings during mixing (winter) (n = 21). (b) CCA ordination of the microbial niches based on the total abundance (Total abund.), % of LNA and cytometric characteristics (FL and SSC) of HNA and LNA subpopulations (blue letters) and circles in color represent sampling points. Correlations between environmental variables and the microbial niches ordination are represented by the black arrows. The data used comprised four sampling during stratification (n = 28) and three samplings during mixing (n = 21). Total abundance, the single cell cytometric characteristics (FL and SSC) and environmental data were scaled (0 to 1). (c) Procrustes superimposition plot comparing the most abundant classes and the single-cell traits structures of bacterial community. Blue line represents the Procrustes residual from both canonical correspondence analysis ordinations in each microbial niche. Correlation (*r*) and significance values (*p*) were calculated using the protest function (Vegan R package).

Proteobacteria was the most abundant phylum across all niches representing between 33.5 and 48.1 % of the total community during stratification and up to 60% during mixing. Cyanobacteria contributed about 30% of the total community in the epilimnion decreasing downwards. Armatimonadetes represented ~ 16 % of total community from the surface down to the DCM, but was little abundant in the hypolimnion and in mixing. The number of phyla increased clearly from the epilimnion downwards to the hypolimnion as did diversity. Bacteroidetes, Acidobacteria, Chlamydiae, Chloroflexi, Firmicutes, Planctomycetes, Spirochaetes, Verrucomicrobia, candidates division to OD1, TM6, WPS-2 and "Others" were more abundant in the DCM and the hypolimnion.

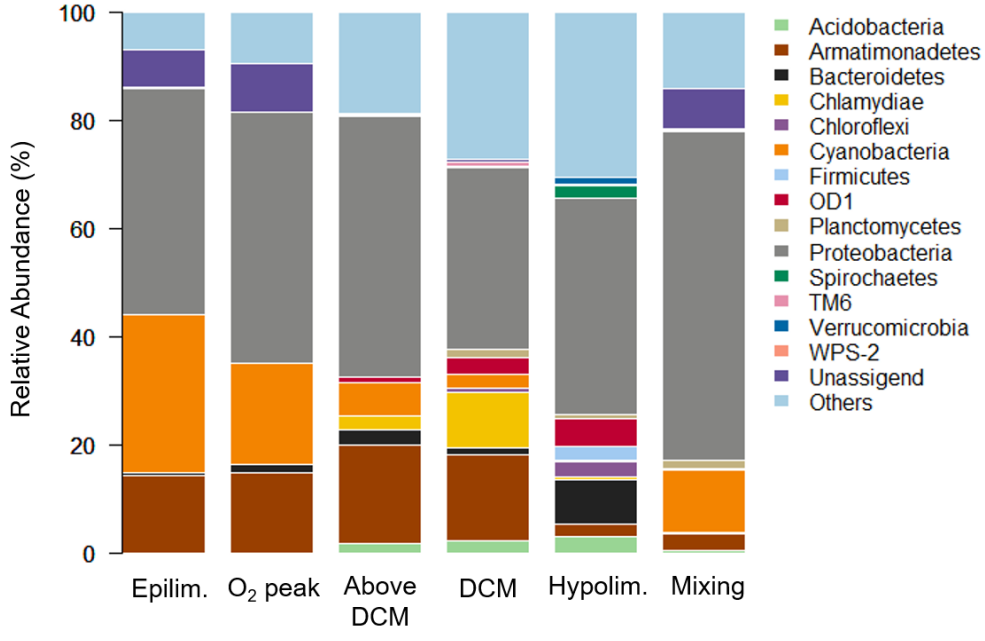

Fig.3. Relative abundance of the most abundant bacterial phyla in the microbial niches in El Sancho reservoir during stratification and mixing. The data used comprised one sampling during stratification (summer) (n = 7) and three samplings during mixing (winter) (n = 21). Bacterial phyla with an average relative abundance > 0.1% are shown, while "Others" includes all phyla with relative abundance < 0.1%. "Unassigned" included the unclassified bacterial phyla.

The most abundant bacterial classes were *α-proteobacteria*, around 40% of total community in the epilimnion during stratification and mixing, and *Fimbriimonadia* (~12% during stratification) (Fig. 4). Seasonally, the vertical distribution of the different bacterial classes was largely variable during stratification and even in mixing for some classes (Fig. S3). The class *α-proteobacteria* decreased through the water column in summer and winter while *β- and γ-*p*roteobacteria* increased. The highest richness at the class level occurred in hypolimnion as well, where about 50% of the classes showed their maxima relative abundance. Some classes were mainly associated with the DCM (*Acidobacteriia*, *Chlamydiia* and *SJA-4)* and the O_2 peak (*Flavobacteriia*) (Fig. 4, Fig. S3).

3.3. Abundance and cellular traits of bacterioplankton community

Microbial niches were also clearly separated in the ordination analysis based on the abundance and single-cell traits along CCA1 (73.3 %, $F_{1,\ 43} = 131.8$, $p = 0.001$) but not along CCA2 (1.7 %, $F_{1,\ 43} = 3.1$, $p = 0.56$) or any other axes (Fig.2). Forward selection identified temperature, pH and NH_4^+ as the main environmental variables in the bacterial abundance and single-cell traits -based ordination, and explained together 74.11% of the variation.

HNA and LNA bacterial cells were identified in all samples although their appearance on cytograms was highly variable between samples (Fig. S1). Total bacterial abundance (HNA + LNA) increased with depth during summer while it did not show a clear pattern in winter (Fig. 5a, b). Two-way ANOVA followed by post-hoc comparison of total bacterial abundance showed a marked difference between the Epilimnion and "O_2 peak" and the other niches (Fig. 5c). LNA bacteria were on average more abundant than HNA in all microbial niches (Fig. 6a). The percentage of LNA vs HNA cells changed little between niches, about 70 and 30 %, respectively, being the differences statistically no significant. Differences between niches were more evident in cellular traits, i.e.: FL (Fig. 6b) and SSC (Fig. 6c) of both HNA and LNA fractions. Among the cellular traits, FL_{HNA} showed the highest variability between niches (ANOVA, $F_{5,\ 43} = 133.3$, $p < 10^{-5}$) followed by SSC_{HNA} (ANOVA, $F_{5,\ 43} = 65.17$, $p < 10^{-5}$), SSC_{LNA} (ANOVA, $F_{5,\ 43} = 47.48$, $p < 10^{-5}$) and FL_{LNA} (ANOVA, $F_{5,\ 43} = 28$, $p < 10^{-5}$) (Fig. 6b-c). FL of both HNA and LNA fractions were significantly smaller during mixing than the other niches (Two-way ANOVA, post-hoc comparison, $p < 0.05$) (Fig. 6b). Similar patterns of variability were observed in SSC HNA and SSC LNA. Epilimnion and O_2 peak were significantly different from the other niches and mixing showed the smallest values (Two-way ANOVA, post-hoc comparison, $p < 0.05$) (Fig. 6c). The content of nucleic acid normalized by cell size (FL/SSC) of both HNA and LNA fractions showed a peak in the Above DCM layer (Fig. S4). However, only FL/SSC_{LNA} differed greatly in this niche from the rest (Two-way ANOVA, post-hoc comparison, $p < 0.05$) (Fig. 6d).

Seasonally (polling all the stratification samples), abundance and cellular traits (i.e.: FL and SSC) of HNA and LNA fractions covaried more during stratification than in mixing (Table S2). Abundance of HNA and LNA fractions showed negative correlations with FL and SSC (Table S2) during stratification. Cells traits did not show any significant correlation with %HNA or %LNA during stratification. FL of HNA and LNA showed significant positive correlation with SSC of both bacterial fractions during stratification but not in mixing. SSC of both subpopulations was negatively correlated with abundance and % of HNA and positively with % LNA in mixing.

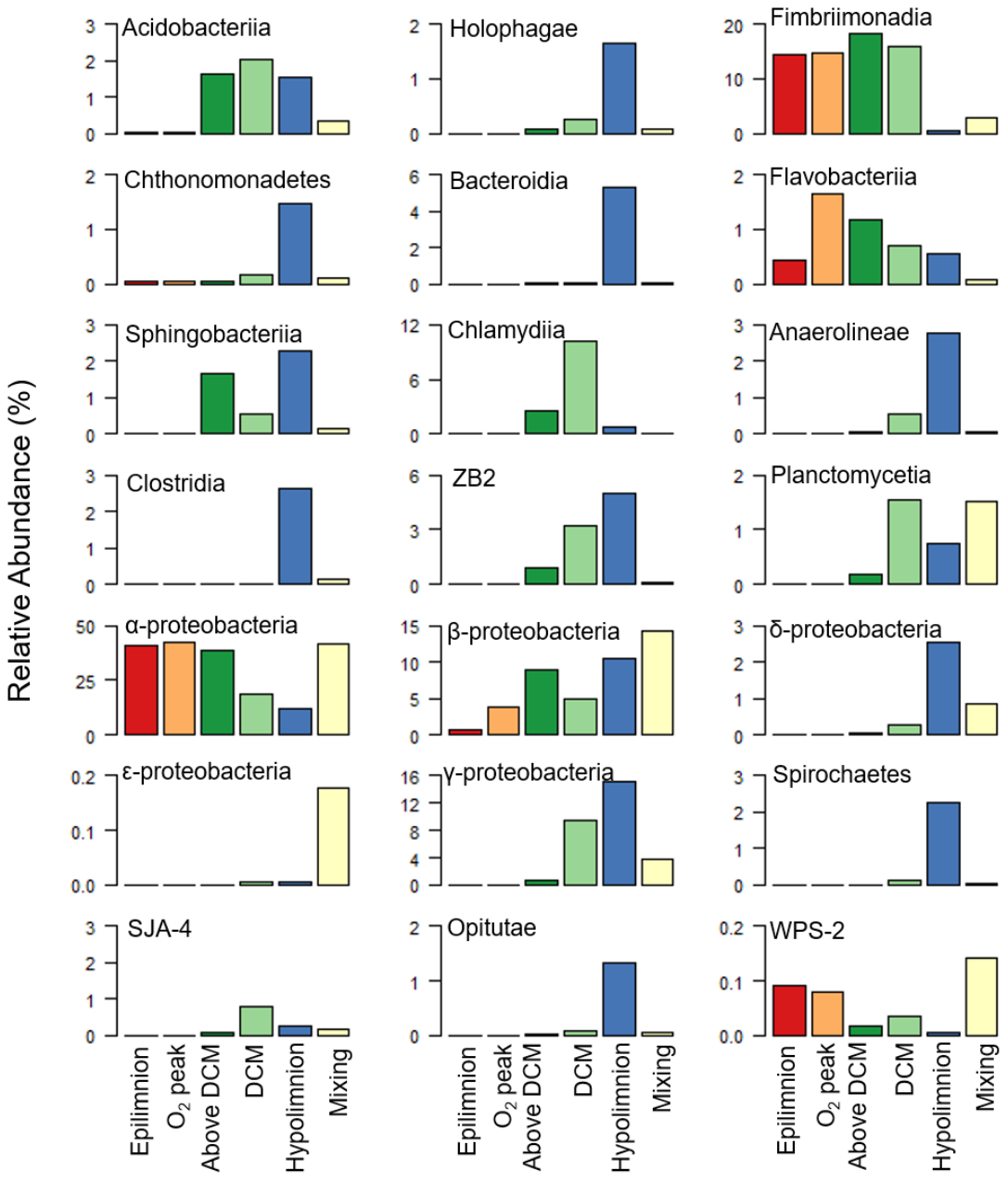

Fig 4: Relative abundance (%) of most abundant bacterial classes in the microbial niches distinguished in El Sancho in stratification (one sampling, n=7) and in mixing (three samplings, n = 21).

3.4. Relationship between phylogenetic composition, abundance and single-cell traits of the bacterioplankton community

The correspondence between the ordinations of the most abundant bacterial classes and single-cell traits structures of bacterial community was good, with a high correlation (Protest, $r = 0.42$, $p = 0.02$) (Fig. 2c). Microbial environments displayed short distances (small Procrustes residual), except for the DCM and the hypolimnion (largest Procrustes residual) (Fig. 2c).

Seasonally (with all microbial niches were pooled), the correlation analysis between the most abundant classes and the cellular traits structure revealed several significant correlations in both seasons (Fig. 7). Five classes, *Holophagae, Planctomycetia, Spirochaetes, SJA-4 and Opitutae* were positively correlated to both HNA and LNA bacterial abundances during summer and Clostridia, ε- and *γ-Proteobacteria* only to LNA bacterial abundances (Fig. 7). Most of the classes showed negative correlations with SSC of both HNA and LNA subgroups, except Cyanobacteria which showed positive correlation with FL of HNA and SSC of both HNA and LNA or no correlation i.e. *Fimbriimonadia*, *Flavobacteria*, *Clostridia*, *α-Proteobacteria* and *WPS-2*. In particular, *Acidobacteriia*, *Bacteroidia*, *Chlamydiia*, *Anaerolineae*, *ZB2*, *β-*, *δ-* and *γ-Proteobacteria*, *Spirochaetes* and *Opitutae* showed negative correlations with FL and SSC of both HNA and LNA fractions (Fig. 7). During mixing, *Acidobacteria*, *Sphingobacteriia*, *Chlamydiia*, *β-Proteobacteria*, *Spirochaetes* and *Opitutae* showed positive correlation with HNA abundance. *α-Proteobacteria* were positively correlated to FL of LNA and to SSC of LNA whereas that of *Bacteroidia* and *Anaerolineae* classes showed negative correlations with FL of both HNA and LNA fractions. *Holophagae*, ZB2 and *SJA-4* with FL and SSC of LNA (Fig. 7).

4. Discussion

4.1 Diversity of microbial niches in the water column in space and time

The microbial niches discriminated here include a wide amplitude of environmental conditions from the highly illuminated, warm and oxic epilimnion to the dim light conditions prevailing above the DCM, and the dark, cold and hypoxic conditions prevailing at the hypolimnion and different degrees of water column mixing (Fig. 1, Table S1). The niche separation was also reflected in the CCA analysis of the phylogenetic composition of the bacterial community and the abundance and single-cell traits of HNA and LNA subpopulations (Fig. 6a, b) in El Sancho. A previous study has shown that the environmental differences represent a segregation of niches for phytoplankton as well (Soria-Píriz et al 2019). PicoEukaryotes were the main primary producers in the epilimnion while a *Synechococcus*-like population was abundant at the DCM, although the chlorophyte *Carteria* sp. largely dominated photoautotrophic biomass this niche (Soria-Píriz et al 2019). The quantity and quality of dissolved organic compounds released by primary producers were likely very different due to changes in the phytoplankton community structure and in the environmental conditions along the water column (Fogg 1983, Baines and Pace 1991, Corzo et al. 2000, Thornton 2014). Thus, a more refractory DOC is probably present in the epilimnion, which can be significantly affected by photooxidation due to high irradiance at this latitude (Salonen and Vähätalo 1994, Miller and Moran 1997). In contrast, in the hypolimnion, the dominant source of organic substrates are decomposing phytoplanktonic cells settling from the photic layer, which provide a higher diversity of organic substrates, of both intra and

extracellular origin, favoring microbial diversity (Salcher et al 2013, Yang et al 2015, Sperling et al 2017).

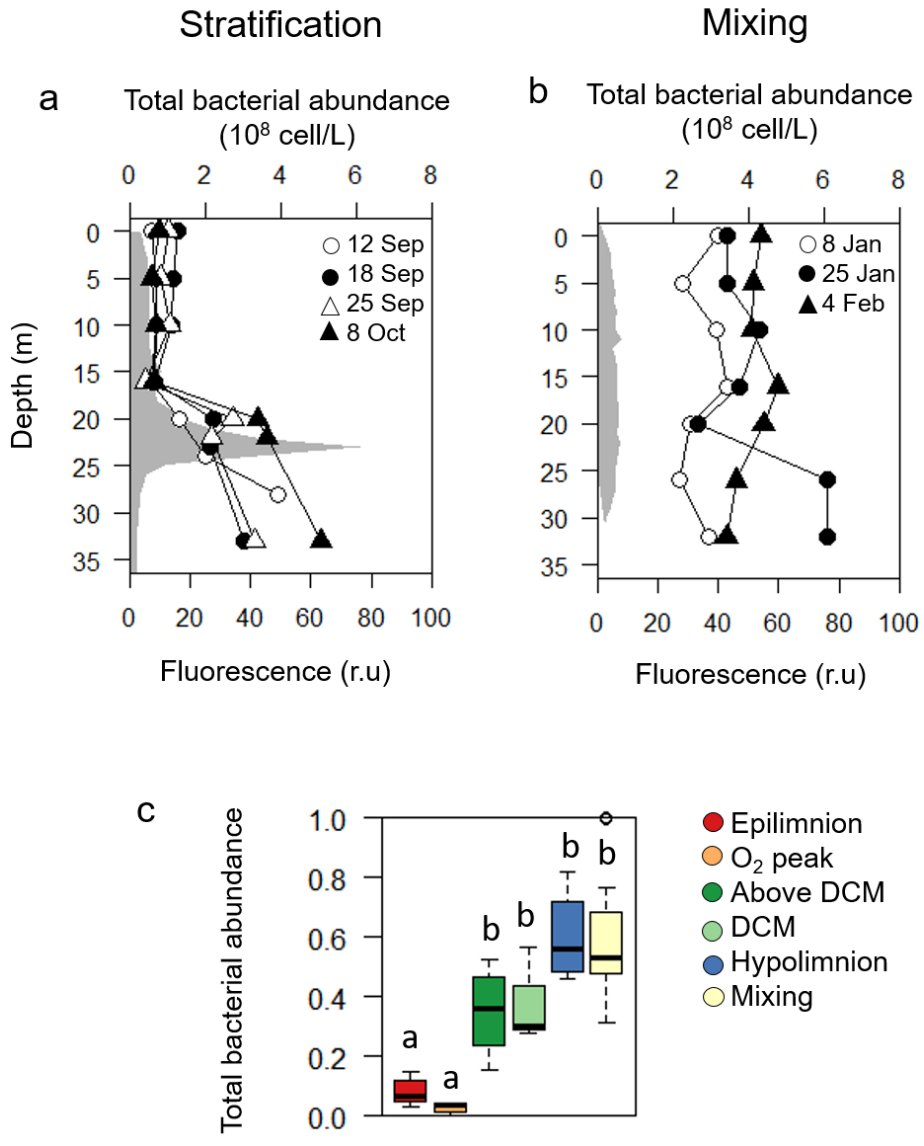

Fig. 5: Depth profiles showing the vertical distribution of total bacteria abundance (cell/L) in El Sancho reservoir during (a) stratification and (b) mixing. Fluorescence ( ) profiles are also shown for spatial reference. (c) Box plots showing the normalized total bacterial abundance (0 to 1) in the microbial niches discriminated during stratification and mixing. Lower to upper values are indicated, respectively, 10%, 25%, 50% (median), 75% and 90% percentiles. Bacterial niches connected by the same letter are not significantly different ($p > 0.05$).

4.2. Environmental drivers of the bacterioplankton community composition

The most striking features of the changes in the phylogenetic structure of the bacterial community from El Sancho was the increase in phylum and class richness with depth during the stratification period (Fig. 3, 4). Bacterial community abundance and diversity can be affected by

bottom-up drivers like temperature, UV radiation inhibiting of bacterial growth and inorganic and organic substrates limiting growth (Lindell and Ending 1996, Van Wambeke et al 2009, Berdjeb et al 2011, Ávila et al 2017) and top-down mechanisms, like grazing and viral lysis (Epstein and Shiaris 1992, Weinbauer and Höfle 1998, Tammert et al. 2005). The increase of bacterial abundance and diversity with depth and in particular in the hypolimnion covaried with the availability of potential substrates (DOC and particulate organic carbon and total nitrogen) (Soria-Piriz et al. 2019) originating from the dead phytoplankton being remineralised. This was also reflected in the increase of NH_4^+ and CO_2 and DOC with depth (Table 1). In fact, DOC explained up to 16.7% of the variations in the phylogenetic community composition between niches alone (Fig. 6a). Another important factor related to niche determination is oxygen availability. Higher bacterial diversity has been observed in stratified waters in the transition zones between oxic and anoxic conditions, and in environments with low oxygen concentration, likely due to a higher diversity of inorganic and organic substrates and potential electron acceptors which favour higher metabolic diversity as well (Crump et al 2007, Stevens and Ulloa 2008, Zaikova et al., 2010, Barberán and Casamayor 2011, Ávila et al 2017). In fact, in El Sancho, O_2 contributed largely (42.1%) to explain the niches separation at the phylum level, confirming the above.

Proteobacteria dominated all microbial niches (Fig. 3), being likely very important in shaping the functional response of the bacterial community to the physicochemical changes with depth and between seasons in El Sancho. The classes within Proteobacteria differed clearly in their niche occupation. *α-Proteobacteria* dominated the upper layers and decreased with depth in both seasons (Fig. 3, Fig. S2). *α-Proteobacteria* are common in a wide range of freshwater ecosystems including acid pit lakes (Percent et al 2008, Santofimia et al 2013, Yu et al 2014, Ávila et al 2017), likely due to their versatility regarding substrate demands, grazing resistance and growth conditions (Pinhassi and Berman 2003, Newton et al 2011 and references therein). Interestingly, *Cyanobacteria* were found abundant in upper waters layers by molecular techniques but we did not Synechococcus by FCM in the epilimnion (Soria-Píriz et al 2019). Contrary to *α-Proteobacteria*, the relative abundance of *β-, δ-* and *γ-Proteobacteria* increased with depth in stratification and even in mixing, despite the homogeneity of environmental factors and the high turbulent diffusion coefficients during the latter (Fig. 4, Fig. S2, Table S1). *Acidobacteriia, Chlamydiia, Planctomycetia* and *SJA-4* classes increased around the DCM (Fig 3, Fig. S2). All members of *Acidobacteriia* class are heterotrophic and most of them show aerobic metabolism (Kielak et al. 2016). Some members of Planctomycetes are associated with the occurrence of algal blooms (Pizzetti et al 2011) and also have been reported in acidic environments (Santofimia et al 2013). The hypolimnetic microbial community was clearly different from that of upper layers, being dominated by *Holophagae*, *Clostridia*, *Planctomycetia*, *ε-* and *γ-Proteobacteria, Spirochaetes, SJA-4* and *Opitutae* (Fig. 4). These classes have been found in different environments expressing a wide range of metabolisms relevant to the conditions of the El Sancho hypolimnion: strictly anaerobic (e.g. *Clostridia*), both aerobic and anaerobic metabolisms, or associated with DCMs or algae (e.g. *γ-proteobacteria, Planctomycetia, Opitutae*) (Crump et al 2007, Lage and Bondoso 2014, Cabello-Yeves 2017, Andrei et al. 2019). During mixing, most bacterial classes reduced their relative abundance or almost disappeared, but other increased their relative importance (*β-Proteobacteria*, *ε-Proteobacteria*, WPS-2) (Fig. 4, Fig. S2), confirming that there are direct linkages between changes in biogeochemical conditions due to hydrodynamic forcing and the phylogenetic composition of the bacterial community within the same water body (Shade et al 2012, Avila et al 2017).

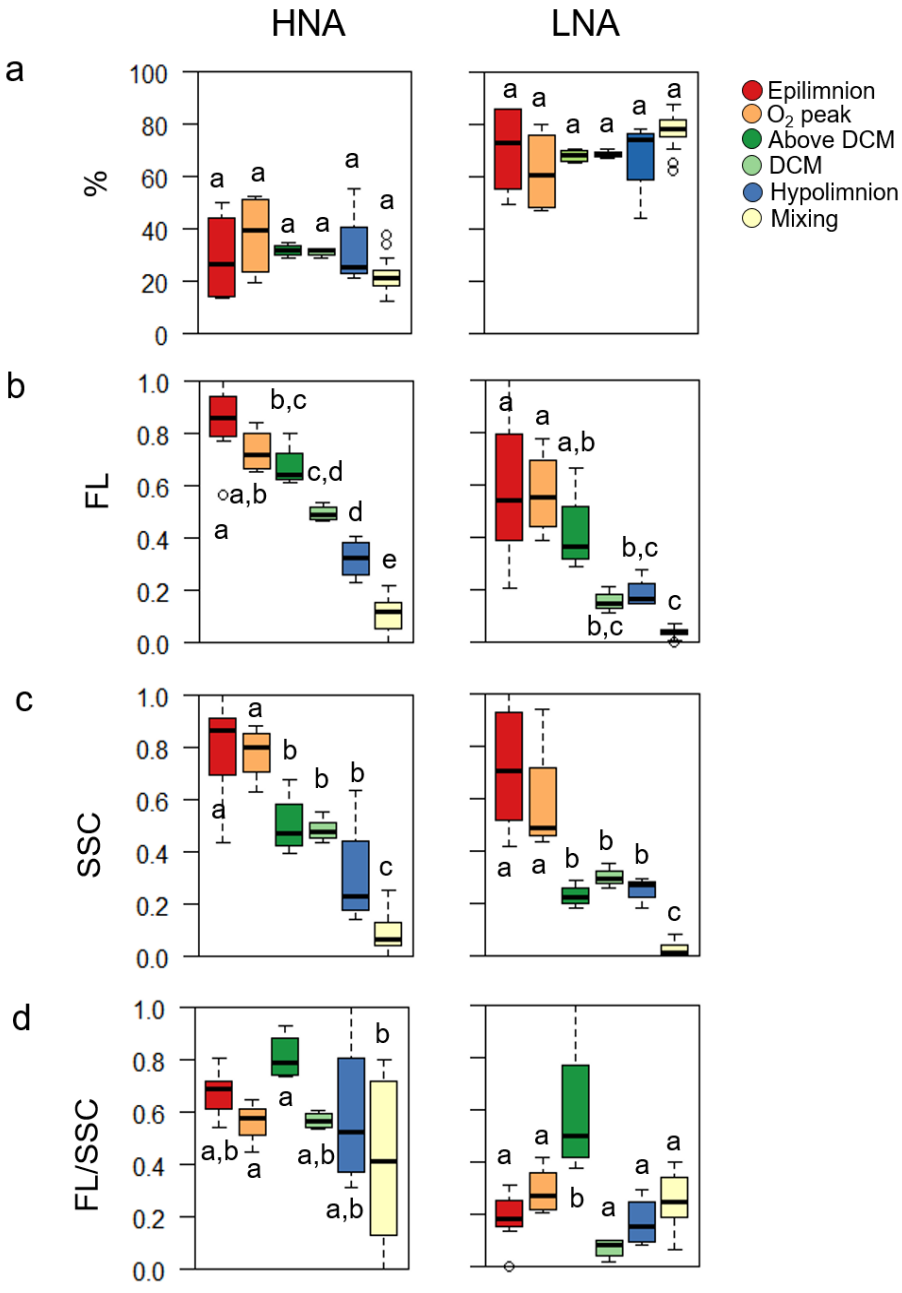

Fig. 6: Box plots showing (a) the percent respect total bacteria (%), (b) cell content of nucleic acid (FL), (c) cell side scatter (SSC) and (d) FL normalized by cell size (FL/SSC) of HNA and LNA cells both for the microbial niches during stratification (one sampling, n=7) and during mixing (three samplings, n = 21) in El Sancho reservoir. All variables were normalized (0 to 1) except % of LNA and HNA. Lower to upper values are indicated, respectively, 10%, 25%, 50% (median), 75% and 90% percentiles. Bacterial niches connected by the same letter are not significantly different ($p > 0.05$).

4.3. Environmental drivers of bacterioplankton community abundances and single cell traits

Bacterial abundance in El Sancho was in the range reported in other AMD impacted systems (Nixdorf et al. 1998, Kamjunke et al. 2004, Wendt-Potthoff et al 2011), which are typically one or two orders of magnitude lower than those reported in neutral lakes (Cole et al. 1993, Nishimura et al. 2005, Tammert et al 2005, Dorigo et al 2006). The % HNA in El Sancho (around 30%) was rather constant, slightly lower than the mean value found in lakes (~ 42%) and close to the ocean average (~ 35%) (Bouvier et al 2007), confirming the oligotrophic conditions of this acidic lake.

The constancy in % HNA and % LNA with depth and season in El Sancho, in contrast to the clear changes in other cellular traits, suggests that the ratio HNA:LNA might not be always a reliable estimator of bacterial growth rate and metabolic activity (Jellet et al. 1996, Gasol et al 1999, Corzo et al. 2005, Bouvier et al. 2007, Schiaffino et al. 2013). The highest values of SSC and FL for HNA and LNA in the epilimnion (Fig. 5b,c), however, do suggest a higher overall growth rate in this microbial niche, decreasing toward the hypolimnion and during mixing (Gasol et al. 1995, 1999, Bouvier et al 2007, Vadia et al 2017). Yet, when the content of nucleic acid was normalized by cell size (FL/SSC), the differences between the bacterial niches for both HNA and LNA subpopulations in space and seasonally were small (Fig. 5d), except above the DCM niche. There a peak in FL/SSC of LNA coincided with the maximum autotrophic growth rate (Soria-Píriz et al 2019), suggesting an increase in bacterial activity associated to the vicinity of DCMs (Talarmin et al 2011, Van Wambeke et al. 2011).

The decrease of bacterial growth rate and activity with depth, as suggested by the FL and SSC vertical patterns during stratification (Fig. S4), contradicts both the vertical distribution of potential organic substrates and of the bacterioplankton abundance and phylogenetic diversity. At present, it is unclear what ecological drivers, bottom-up or top-down, are responsible for these opposite patterns (abundance vs fluorescence and size) during stratification. The lower bacterial abundance in the epilimnion compared to bottom layers could be due to a top-down mechanism like grazing or viral lysis as reported in other neutral and acid lakes (Kamjunke et al. 2004, Tammert et al 2005). Photosynthetic picoeukaryotes dominate the epilimnion of El Sancho (Soria-Píriz et al 2017) and might include mixotrophs able to graze upon the bacterial community (Massana 2011, McKie-Krisberg and Sanders 2014, Mitra et al. 2014) given the CO_2 limitation (Sara-Píriz et al 2019). In addition, a possible limitation with phosphate of bacterial growth might exist since PO_4^{3-} was below detection limit (Soria-Píriz et al. 2019).

During mixing bacterial growth rates were lower than during stratification, as confirmed by the smaller cells (Fig. 5c) and as expected from the lower temperature and substrate availability (Table S1). During this period, interestingly, the widely accepted interpretation of the HNA fraction representing the most active cells, and the LNA fraction the inactive and dormant cells with low levels of activity (Li et al 1995, Gasol et al 1999, Lebaron et al 2002) seems to hold well since the relative abundance of the LNA fraction increased during this season in comparison to stratification (Fig. S3a) and the FL/SSC of HNA decreased (Fig. S3c), indicating a possible lower activity in HNA fractions with lower DOC availability during mixing (Table S1) (Cuevas et al 2011).

4.4. Links between cellular traits, abundance and composition of bacterioplankton community

The correspondence between the ordinations of the most abundant bacterial classes and single-cell traits structures of bacterial community in El Sancho was high (Fig. 6c). Both sets of response variables seemed to be able to discriminate the different niches communities, despite the a priori lower expected discriminatory capacity (less variables included) of the cell trait vs phylogenetic groups analysis. The synchrony between spatiotemporal changes of community composition at the class and the single-cell traits and abundance levels, indicate that in this acidic reservoir the community responds simultaneously in multiple ways, in order to adapt to the changing environment. Bottom-up processes are known to impact multiple aspects of bacterial communities, such as physiological structure, composition and metabolism (Nishimura et al 2005, Crump et al 2007, Comte and del Giorgio 2009). However, the factors that best explained these changes in El Sancho depended on the aspect of the community studied, except for T and pH which contributed to both. Changes in the bacterial phylogenetic composition were better explained by the availability of O_2 and Chl *a* (phytoplankton biomass), and DOC, determining the transitions between an aerobic, hypoxic and anaerobic communities and communities with different capacities to metabolise the organic material available (phytoplankton exudates, dead cells etc). In contrast, the "physiological" cell traits state of the bacterial community was best explained by temperature. Changes in nutrients (NH_4^+) and temperature are considered the main factors determining bacterial metabolism and growth rates in temperate lakes (Vrede 2005), which in turn produce changes in the size of cells (del Giorgio and Gasol 2008).

No universal relationships were observed between the abundance and single-cell traits of HNA and LNA fractions and the different bacterial classes during stratification and mixing, with the few significant correlations observed within each phase being classes specific (Fig. 7). Some studies have concluded that there are no phylogenetic differences between HNA and LNA fractions (Servais et al 2003, Longnecker et al 2005), while others have found specific groups associated with one of the two fractions (i.e. SAR11 clade belonging to *α-Proteobacteria* with the LNA fraction) (Mary et al 2006). Here, the increase of HNA and LNA abundances downward during stratification highly correlated with several bacterial classes (i.e. *Holophagae, Planctomycetia, Spirochaetes, SJA-4 and Opitutae)* suggesting an increase in the relative abundance of these classes in both HNA and LNA fractions. As mentioned previously, these classes are known to be active in niches such those found with depth in El Sancho, justifying their increase with depth in both cell fractions. Clostridia, ε- and *γ-Proteobacteria* were positively correlated to LNA abundances as well, suggesting that LNA fractions could be more diverse than HNA fraction towards the bottom. *Acidobacteria*, *Sphingobacteriia, Chlamydiia, β-Proteobacteria, Spirochaetes* and *Opitutae* only showed positive correlation with HNA abundance during mixing while no correlations were found with LNA abundances. This could be interpreted as the existence of intrinsic differences in the composition between HNA and LNA cells in this season, where each fraction presents its own phylogenetic composition. Finally, in terms of cell size, the inverse relationship of the cellular size of both HNA and LNA with the relative abundance of *Acidobacteriia*, *Bacteroidia, Sphingobacteriia, Chlamydiia*, *Anaerolineae*, *ZB2*, *β-*, *δ-* and *γ-Proteobacteria*, *Spirochaetes* and *Opitutae* during stratification could indicate a change in cell growth and, thus, changes in bacterial metabolism downwards (del Giorgio and Gasol 2008). This pattern was also observed in terms of fluorescence, suggesting a link between the content in acid nucleic and the cellular size in both HNA and LNA fractions. Therefore, the phylogenetic identity of HNA and LNA bacteria changes between systems and ecological conditions as do the relative importance of

"physiological/ecological" mechanisms (growth rate, cell cycle phase, damaged and death cells, etc.), involved in the exchange of cells between both fractions.

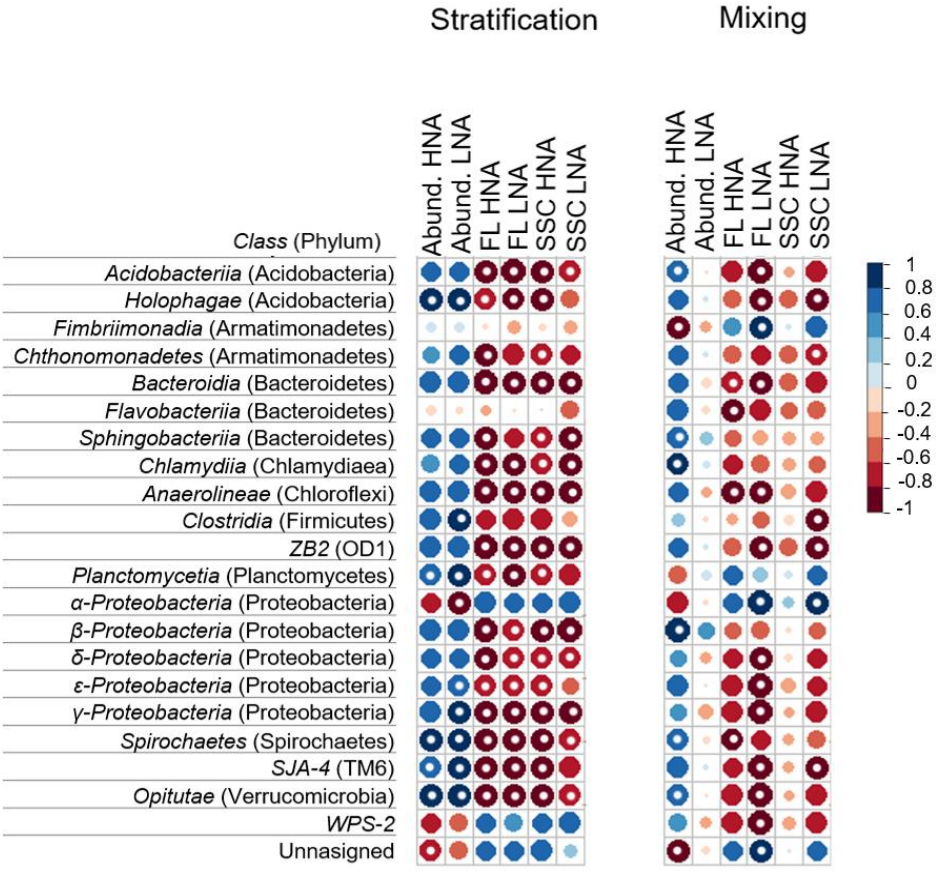

Fig. 7: Correlation matrix between the abundance, cell content of nucleic acid (FL) and the cell side scatter (SSC) of HNA and LNA subpopulations and the relative abundance contribution at the class level of bacterioplankton. The data used for correlations were the mean dataset of the four samplings during stratification (summer) (n = 28) and the mean dataset of the three samplings during mixing (winter) (n = 21), except for the relative contribution at the class level during the stratification (n = 7). The colour bar represents the Spearman correlation coefficient with blue data for positive and red for negative relationship. The size and tone of the dots is directly related to the magnitude of the correlation. Significant correlations are labelled with a white dot ($p < 0.05$).

In conclusion, our results show that multiple aspects of the bacterial community are strongly influenced by spatiotemporal changes in the environmental variables (NH_4^+, CO_2, O_2, Chl *a*, DOC, T and pH). In addition, the simultaneous analyses of the shifts in cellular traits and phylogenetic composition of the community opens new perspectives and questions in the ecological interpretation of the distribution of bacterial abundance and composition, and their relationships with the environmental conditions. Exploring the links between these community structure levels and how these change between different niches and across ecosystems will allow us to fill important gaps in understanding how seasonal and long term biogeochemical changes in aquatic systems affect the transfer or energy and matter and the ecosystem function overall.

5. Acknowledgement

The research was funded by projects P11-RNM-7199 from the Junta de Andalucía, CTM2017-82274-R from the Spanish I+D+I Program and 20.DG.UE.II.05 from University of Cadiz.

6. References

Andrei, A.-Ş., M. M. Salcher, M. Mehrshad, P. Rychtecký, P. Znachor, and R. Ghai. 2019. Niche-directed evolution modulates genome architecture in freshwater Planctomycetes. ISME J. **13**: 1056–1071. doi:10.1038/s41396-018-0332-5

Ávila, M. P., P. A. Staehr, F. A. R. Barbosa, E. Chartone-Souza, and A. M. A. Nascimento. 2017. Seasonality of freshwater bacterioplankton diversity in two tropical shallow lakes from the Brazilian Atlantic Forest. FEMS Microbiol. Ecol. **93**: 1–11. doi:10.1093/femsec/fiw218

Azam, F. 1998. Microbial Control of Oceanic Carbon Flux: The Plot Thickens. Science (80-.). **280**: 694 LP-696. doi:10.1126/science.280.5364.694

Baines, S. B., and M. L. Pace. 1991. The production of dissolved organic matter by phytoplankton and its importance to bacteria: Patterns across marine and freshwater systems. Limnol. Oceanogr. **36**: 1078–1090. doi:10.4319/lo.1991.36.6.1078

Baker, B. J., and J. F. Banfield. 2003. Microbial communities in acid mine drainage. FEMS Microbiol. Ecol. **44**: 139–152. doi:10.1016/S0168-6496(03)00028-X

Barberán, A., and E. O. Casamayor. 2011. Euxinic Freshwater Hypolimnia Promote Bacterial Endemicity in Continental Areas. Microb. Ecol. **61**: 465–472. doi:10.1007/s00248-010-9775-6

Berdjeb, L., J. F. Ghiglione, and S. Jacquet. 2011. Bottom-up versus top-down control of hypo-and epilimnion free-living bacterial community structures in two neighboring freshwater lakes. Appl. Environ. Microbiol. **77**: 3591–3599. doi:10.1128/AEM.02739-10

Borcard D, F. Gillet, P. Legendre. 2011. Numerical Ecology with R. New York, Dordrecht London Heidelberg

Boucher, D., L. Jardillier, D. Debroas, and B. Pascal. 2005. Succession of bacterial community composition over two consecutive years in two aquatic systems : a natural lake and a lake-reservoir.doi:10.1111/j.1574.6941.2005.00011.x

Bouvier, T., P. A. del Giorgio, and J. M. Gasol. 2007. A comparative study of the cytometric characteristics of High and Low nucleic-acid bacterioplankton cells from different aquatic ecosystems. Environ. Microbiol. **9**: 2050–2066. doi:10.1111/j.1462-2920.2007.01321.x

Bower and Holm-Hansen. 1980. A salicylate-Hypochlorite method for determining amonia in seawater. Can. J. Fish. Aquat. Sci. **37**: 794–798. doi:10.1139/f80-106

Bowers, R. M., C. L. Lauber, C. Wiedinmyer, M. Hamady, A. G. Hallar, R. Fall, R. Knight, and N. Fierer. 2009. Characterization of Airborne Microbial Communities at a High-Elevation Site and Their Potential To Act as Atmospheric Ice Nuclei □. Appl. Environ. Microbiol. **75**: 5121–5130. doi:10.1128/AEM.00447-09

Cabello-Yeves, P. J., R. Ghai, M. Mehrshad, A. Picazo, A. Camacho, and F. Rodriguez-Valera. 2017. Reconstruction of diverse verrucomicrobial genomes from metagenome datasets of freshwater reservoirs. Front. Microbiol. **8**. doi:10.3389/fmicb.2017.02131

Caporaso, J. G., J. Kuczynski, J. Stombaugh, and others. 2010. correspondEnce QIIME allows analysis of high-throughput community sequencing data Intensity normalization improves color calling in SOLiD sequencing. Nat. Methods **7**: 335–336. doi:10.1038/nmeth0510-335

Cole, J. J., M. L. Pace, N. F. Caraco, and G. S. Steinhart. 1993. Bacterial biomass and cell size distributions in lakes: More and larger cells in anoxic waters. Limnol. Oceanogr. **38**: 1627–1632. doi:10.4319/lo.1993.38.8.1627

Comte, J., and P. A. del Giorgio. 2009. Links between resources, C metabolism and the major components of bacterioplankton community structure across a range of freshwater ecosystems. Environ. Microbiol. **11**: 1704–1716. doi:10.1111/j.1462-2920.2009.01897.x

Comte, J., and P. A. del Giorgio. 2010. Linking the patterns of change in composition and function in bacterioplankton successions along environmental gradients. Ecology **91**: 1466–1476. doi:10.1890/09-0848.1

Corzo, A., J. L. Jiménez-Arias, E. Torres, E. García-Robledo, M. Lara, and S. Papaspyrou. 2018. Biogeochemical changes at the sediment–water interface during redox transitions in an acidic reservoir: exchange of protons, acidity and electron donors and acceptors. Biogeochemistry **139**: 241–260. doi:10.1007/s10533-

018-0465-7
Corzo, A., J. A. Morillo, and S. Rodríguez. 2000. Production of transparent exopolymer particles (TEP) in cultures of Chaetoceros calcitrans under nitrogen limitation. Aquat. Microb. Ecol. **23**: 63–72. doi:10.3354/ame023063
Corzo, A., S. Rodríguez-Gálvez, L. Lubian, C. Sobrino, P. Sangrá, and A. Martínez. 2005. Antarctic marine bacterioplankton subpopulations discriminated by their apparent content of nucleic acids differ in their response to ecological factors. Polar Biol. **29**: 27–39. doi:10.1007/s00300-005-0032-2
Cotner, J. B., and B. A. Biddanda. 2002. Small Players , Large Role : Microbial Influence on Biogeochemical Processes in Pelagic Aquatic Ecosystems. Ecosystems **5**: 105–121. doi:10.1007/s10021-001-0059-3
Crognale, S., S. Zecchin, S. Amalfitano, S. Fazi, B. Casentini, A. Corsini, L. Cavalca, and S. Rossetti. 2017. Phylogenetic structure and metabolic properties of microbial communities in Arsenic-rich waters of geothermal origin. Front. Microbiol. **8**. doi:10.3389/fmicb.2017.02468
Crump, B. C., C. Peranteau, B. Beckingham, and J. C. Cornwell. 2007. Respiratory succession and community succession of bacterioplankton in seasonally anoxic estuarine waters. Appl. Environ. Microbiol. **73**: 6802–6810. doi:10.1128/AEM.00648-07
Desantis, T. Z., P. Hugenholtz, N. Larsen, and others. 2006. Greengenes , a Chimera-Checked 16S rRNA Gene Database and Workbench Compatible with ARB. Appl. Environ. Microbiol. **72**: 5069–5072. doi:10.1128/AEM.03006-05
Dorigo, U., D. Fontvieille, and J. F. Humbert. 2006. Spatial variability in the abundance and composition of the free-living bacterioplankton community in the pelagic zone of Lake Bourget (France). FEMS Microbiol. Ecol. **58**: 109–119. doi:10.1111/j.1574-6941.2006.00139.x
Epstein, S. S., and M. P. Shiaris. 1992. Size-selective grazing of coastal bacterioplankton by natural assemblages of pigmented flagellates, colorless flagellates, and ciliates. Microb. Ecol. **23**: 211–225. doi:10.1007/BF00164097
Fenchel, T., and B. Finlay. 2008. Oxygen and the spatial structure of microbial communities. Biol. Rev. **83**: 553–569. doi:10.1111/j.1469-185X.2008.00054.x
Findlay, S. 2010. Stream microbial ecology. J. North Am. Benthol. Soc. **29**: 170–181. doi:10.1899/09-023.1
Fogg, G. E. 1983. The Ecological significane of extracellular products of phytoplankton. Bot. Mar. **26**: 3–14. doi:10.1515/botm.1983.26.1.3
Fortunato, C. S., L. Herfort, P. Zuber, A. M. Baptista, and B. C. Crump. 2012. Spatial variability overwhelms seasonal patterns in bacterioplankton communities across a river to ocean gradient. ISME J. **6**: 554–563. doi:10.1038/ismej.2011.135
García-Robledo, E., A. Corzo, and S. Papaspyrou. 2014. A fast and direct spectrophotometric method for the sequential determination of nitrate and nitrite at low concentrations in small volumes. Mar. Chem. **162**: 30–36. doi:10.1016/j.marchem.2014.03.002
Gasol, J. M., and P. A. del Giorgio. 2000. Using flow cytometry for counting natural planktonic bacteria and understanding the structure of planktonic bacterial communities. Sci. Mar. **64**: 197–224. doi:10.3989/scimar.2000.64n2197
Gasol, J. M., P. A. Del Giorgio, R. Massana, and C. M. Duarte. 1995. Active versus inactive bacteria: size-dependence in a coastal marine plankton community. Mar. Ecol. Prog. Ser. **128**: 91–97. doi:10.3354/meps128091
Gasol, J. M., U. Li Zweifel, F. Peters, J. A. Fuhrman, and Å. Hagström. 1999. Significance of size and nucleic acid content heterogeneity as measured by flow cytometry in natural planktonic bacteria. Appl. Environ. Microbiol. **65**: 4475–4483. doi:10.13039/501100000780
del Giorgio, P. A., and T. C. Bouvier. 2002. Linking the physiologic and phylogenetic successions in free-living bacterial communities along an estuarine salinity gradient. Limnol. Oceanogr. **47**: 471–486. doi:10.4319/lo.2002.47.2.0471
del Giorgio, P. A., and J. M. Gasol. 2008. Physiological Structure and Single-Cell Activity in Marine Bacterioplankton. Microb. Ecol. Ocean. Second Ed. 243–298. doi:10.1002/9780470281840.ch8
Glassman, S. I., C. Weihe, J. Li, and others. 2018. Decomposition responses to climate depend on microbial community composition. Proc. Natl. Acad. Sci. U. S. A. **115**: 11994–11999. doi:10.1073/pnas.1811269115
Hall, P. O. J., and R. C. Aller. 1992. Rapid, small volume, flow injection analysis for CO2 and NH4+ in marine and freshwaters. Limnol. Ocean. **37**: 1113–1119. doi:http://www.jstor.org/stable/2837857
Harrell, F. E. Jr., with contributions from Charles Dupont and many others. 2019. Hmisc: Harrell Miscellaneo. R package version 4.3-0.

Huang, L. N., J. L. Kuang, and W. S. Shu. 2016. Microbial Ecology and Evolution in the Acid Mine Drainage Model System. Trends Microbiol. **24**: 581–593. doi:10.1016/j.tim.2016.03.004

Jellett, J. F., W. K. W. Li, P. M. Dickie, A. Boraie, and P. E. Kepkay. 1996. Metabolic activity of bacterioplankton communities assessed by flow cytometry and single carbon substrate utilization. Mar. Ecol. Prog. Ser. **136**: 213–225. doi:10.3354/meps136213

Kamjunke, N., U. Gaedke, J. Tittel, G. Weithoff, and E. M. Bell. 2004. Strong vertical differences in the plankton composition of an extremely acidic lake. Arch. fur Hydrobiol. **161**: 289–306. doi:10.1127/0003-9136/2004/0161-0289

Kent, A. D., A. C. Yannarell, J. A. Rusak, E. W. Triplett, and K. D. Mcmahon. 2007. Synchrony in aquatic microbial community dynamics. 38–47. doi:10.1038/ismej.2007.6

Kielak, A. M., C. C. Barreto, G. A. Kowalchuk, J. A. van Veen, and E. E. Kuramae. 2016. The ecology of Acidobacteria: Moving beyond genes and genomes. Front. Microbiol. **7**: 1–16. doi:10.3389/fmicb.2016.00744

Krause, S., X. Le Roux, P. A. Niklaus, and others. 2014. Trait-based approaches for understanding microbial biodiversity and ecosystem functioning. Front. Microbiol. **5**: 1–10. doi:10.3389/fmicb.2014.00251

Lage, O. M., and J. Bondoso. 2014. Planctomycetes and macroalgae, a striking association . Front. Microbiol. **5**: 267.

Lebaron, P., N. Parthuisot, P. Catala, and O. Oce. 1998. Comparison of Blue Nucleic Acid Dyes for Flow Cytometric Enumeration of Bacteria in Aquatic Systems Comparison of Blue Nucleic Acid Dyes for Flow Cytometric Enumeration of Bacteria in Aquatic Systems. Appl. Environ. Microbiol. **64**: 1725.

Lebaron, P., P. Servais, H. Agogué, C. Courties, and F. Joux. 2001. Does the High Nucleic Acid Content of Individual Bacterial Cells Allow Us to Discriminate between Active Cells and Inactive Cells in Aquatic Systems? Appl. Environ. Microbiol. **67**: 1775–1782. doi:10.1128/AEM.67.4.1775-1782.2001

Lebaron, P., P. Servais, A. Baudoux, M. Bourrain, C. Courties, and N. Parthuisot. 2002. Variations of bacterial-specific activity with cell size and nucleic acid content assessed by flow cytometry.doi:10.3354/ame028131

Li, W. K. W., J. Jellett, and P. A. I. Dickie. 1995. DNA distribut : ions in planktonic bacteria stained with TOT0 or TO-PRO POT01 & D. Enzyme **40**: 1485–1495.

Lindell, M., and H. Edling. 1996. Influence of light on bacterioplankton in a tropical lake. Hydrobiologia **323**: 67–73. doi:10.1007/BF00020548

Liu, L., J. Yang, X. Yu, G. Chen, and Z. Yu. 2013. Patterns in the Composition of Microbial Communities from a Subtropical River : Effects of Environmental , Spatial and Temporal Factors. **8**: 1–10. doi:10.1371/journal.pone.0081232

Liu, L., J. Yang, Z. Yu, and D. M. Wilkinson. 2015. The biogeography of abundant and rare bacterioplankton in the lakes and reservoirs of China. ISME J. **9**: 2068–2077. doi:10.1038/ismej.2015.29

Longnecker, K., B. F. Sherr, and E. B. Sherr. 2005. Activity and phylogenetic diversity of bacterial cells with high and low nucleic acid content and electron transport system activity in an upwelling ecosystem. Appl. Environ. Microbiol. **71**: 7737–7749. doi:10.1128/AEM.71.12.7737-7749.2005

Martiny, J. B. H., B. J. M. Bohannan, J. H. Brown, and others. 2006. Microbial biogeography: Putting microorganisms on the map. Nat. Rev. Microbiol. **4**: 102–112. doi:10.1038/nrmicro1341

Mary, I., J. L. Heywood, B. M. Fuchs, R. Amann, G. A. Tarran, P. H. Burkill, and M. V Zubkov. 2006. SAR11 dominance among metabolically active low nucleic acid bacterioplankton in surface waters along an Atlantic meridional transect. **45**: 107–113.

Massana, R. 2011. Eukaryotic Picoplankton in Surface Oceans. Annu. Rev. Microbiol. **65**: 91–110. doi:10.1146/annurev-micro-090110-102903

McKie-Krisberg, Z. M., and R. W. Sanders. 2014. Phagotrophy by the picoeukaryotic green alga Micromonas: Implications for Arctic Oceans. ISME J. **8**: 1953–1961. doi:10.1038/ismej.2014.16

Miller, W. L., and M. A. Moran. 1997. Interaction of photochemical and microbial processes in the degradation of refractory dissolved organic matter from a coastal marine environment. Limnol. Oceanogr. **42**: 1317–1324. doi:10.4319/lo.1997.42.6.1317

Mitra, A., K. J. Flynn, J. M. Burkholder, and others. 2014. The role of mixotrophic protists in the biological carbon pump. Biogeosciences **11**: 995–1005. doi:10.5194/bg-11-995-2014

Morrison, J. M., K. D. Baker, R. M. Zamor, S. Nikolai, M. S. Elshahed, and N. H. Youssef. 2017. Spatiotemporal analysis of microbial community dynamics during seasonal stratification events in a freshwater lake (Grand Lake, OK, USA). PLoS One **12**. doi:10.1371/journal.pone.0177488

Mühlenbruch, M., H. P. Grossart, F. Eigemann, and M. Voss. 2018. Mini-review: Phytoplankton-derived

polysaccharides in the marine environment and their interactions with heterotrophic bacteria. Environ. Microbiol. **20**: 2671–2685. doi:10.1111/1462-2920.14302

Nelson, C. E. 2009. Phenology of high-elevation pelagic bacteria: The roles of meteorologic variability, catchment inputs and thermal stratification in structuring communities. ISME J. **3**: 13–30. doi:10.1038/ismej.2008.81

Newton, R. J., S. E. Jones, A. Eiler, K. D. McMahon, and S. Bertilsson. 2011. A Guide to the Natural History of Freshwater Lake Bacteria,.

Niño-García, J. P., C. Ruiz-González, and P. A. del Giorgio. 2016a. Landscape-scale spatial abundance distributions discriminate core from random components of boreal lake bacterioplankton. Ecol. Lett. **19**: 1506–1515. doi:10.1111/ele.12704

Niño-García, J. P., C. Ruiz-González, and P. A. Del Giorgio. 2016b. Interactions between hydrology and water chemistry shape bacterioplankton biogeography across boreal freshwater networks. ISME J. **10**: 1755–1766. doi:10.1038/ismej.2015.226

Nishimura, Y., C. Kim, and T. Nagata. 2005. Vertical and seasonal variations of bacterioplankton subgroups with different nucleic acid contents: Possible regulation by phosphorus. Appl. Environ. Microbiol. **71**: 5828–5836. doi:10.1128/AEM.71.10.5828-5836.2005

Nixdorf, B., and J. Jander. 2003. Bacterial activities in shallow lakes – a comparison between extremely acidic and alkaline eutrophic hard water lakes. 697–705.

Nixdorf, B., K. Wollmann, and R. Deneke. 1998. Ecological potentials for planktonic development and food web interactions in extremely acidic mining lakes in Lusatia, p. 147–167. *In* Acidic mining lakes. Springer.

Oksanen, J. , F. Guillaume Blanchet, Michael Friendly, Roeland Kindt, Pierre Legendre, Dan McGlinn, Peter R. Minchin, R. B. O'Hara, Gavin L. Simpson, Peter Solymos, M. Henry H. Stevens, Eduard Szoecs and Hele ne Wagner 2019. vegan: Community Ecology Package. R package version 2.5-6.

Percent, S. F., M. E. Frischer, P. A. Vescio, and others. 2008. Bacterial community structure of acid-impacted lakes: What controls diversity? Appl. Environ. Microbiol. **74**: 1856–1868. doi:10.1128/AEM.01719-07

Pinhassi, J., and T. Berman. 2003. Differential growth response of colony-forming α- and γ-proteobacteria in dilution culture and nutrient addition experiments from Lake Kinneret (Israel), the Eastern Mediterranean Sea, and the Gulf of Eilat. Appl. Environ. Microbiol. **69**: 199–211. doi:10.1128/AEM.69.1.199-211.2003

Pizzetti, I., B. M. Fuchs, G. Gerdts, A. Wichels, K. H. Wiltshire, and R. Amann. 2011. Temporal variability of coastal Planctomycetes clades at Kabeltonne station, North Sea. Appl. Environ. Microbiol. **77**: 5009–5017. doi:10.1128/AEM.02931-10

Read, D. S., H. S. Gweon, M. J. Bowes, L. K. Newbold, D. Field, M. J. Bailey, and R. I. Griffiths. 2015. Catchment-scale biogeography of riverine bacterioplankton. ISME J. **9**: 516–526. doi:10.1038/ismej.2014.166

Reche, I., E. Pulido-Villena, R. Morales-Baquero, and E. O. Casamayor. 2005. Does Ecosystem Size Determine Aquatic Bacterial Richness? Ecology **86**: 1715–1722.

Ritchie, R. J. 2008. Universal chlorophyll equations for estimating chlorophylls. **46**: 115–126.

Salcher, M. M., T. Posch, and J. Pernthaler. 2013. In situ substrate preferences of abundant bacterioplankton populations in a prealpine freshwater lake. ISME J. **7**: 896–907. doi:10.1038/ismej.2012.162

Sánchez-España, J., E. López Pamo, E. Santofimia, O. Aduvire, J. Reyes, and D. Barettino. 2005. Acid mine drainage in the Iberian Pyrite Belt (Odiel river watershed, Huelva, SW Spain): Geochemistry, mineralogy and environmental implications. Appl. Geochemistry **20**: 1320–1356. doi:10.1016/j.apgeochem.2005.01.011

Santofimia, E., E. González-Toril, E. López-Pamo, M. Gomariz, R. Amils, and Á. Aguilera. 2013. Microbial Diversity and Its Relationship to Physicochemical Characteristics of the Water in Two Extreme Acidic Pit Lakes from the Iberian Pyrite Belt (SW Spain). PLoS One **8**. doi:10.1371/journal.pone.0066746

Schiaffino, M. R., J. M. Gasol, I. Izaguirre, and F. Unrein. 2013. Picoplankton abundance and cytometric group diversity along a trophic and latitudinal lake gradient. Aquat. Microb. Ecol. **68**: 231–250. doi:10.3354/ame01612

Schloerke, B., J. Crowley, D. Cook, F. Briatte, M. Marbach, E. Thoen, A. Elberg and J. Larmarange 2018. GGa lly: Extension to 'ggplot2'. R package version 1.4.0.

Selig, U., T. Hübener, R. Heerkloss, and H. Schubert. 2004. Vertical gradient of nutrients in two dimictic lakes – influence of phototrophic sulfur bacteria on nutrient balance. Aquat. Sci. **66**: 247–256. doi:10.1007/s00027-004-0684-y

Servais, P., E. O. Casamayor, C. Courties, P. Catala, N. Parthuisot, and P. Lebaron. 2003. Activity and diversity

of bacterial cells with high and low nucleic acid content. Aquat. Microb. Ecol. **33**: 41–51.

Shade, A., S. E. Jones, and K. D. McMahon. 2008. The influence of habitat heterogeneity on freshwater bacterial community composition and dynamics. Environ. Microbiol. **10**: 1057–1067. doi:10.1111/j.1462-2920.2007.01527.x

Shade, A., J. S. Read, N. D. Youngblut, and others. 2012. Lake microbial communities are resilient after a whole-ecosystem disturbance. ISME J. **6**: 2153–2167. doi:10.1038/ismej.2012.56

Soria-Píriz, S., M. Lara, J. L. Jiménez-Arias, and others. 2019. What supports the deep chlorophyll maximum in acidic lakes? The role of the bacterial CO2 production in the hypolimnion. Limnol. Oceanogr. 1–18. doi:10.1002/lno.11391

Sperling, M., J. Piontek, A. Engel, K. H. Wiltshire, J. Niggemann, G. Gerdts, and A. Wichels. 2017. Combined carbohydrates support rich communities of particle-associated marine bacterioplankton. Front. Microbiol. **8**: 1–14. doi:10.3389/fmicb.2017.00065

Stevens, H., and O. Ulloa. 2008. Bacterial diversity in the oxygen minimum zone of the eastern tropical South Pacific. Environ. Microbiol. **10**: 1244–1259. doi:10.1111/j.1462-2920.2007.01539.x

Talarmin, A., F. Van Wambeke, P. Catala, C. Courties, and P. Lebaron. 2011. Flow cytometric assessment of specific leucine incorporation in the open Mediterranean. Biogeosciences **8**: 253–265. doi:10.5194/bg-8-253-2011

Tammert, H., V. Kisand, and T. No. 2005. Lake Verevi, Estonia — A Highly Stratified Hypertrophic Lake. Lake Verevi, Est. — A Highly Stratif. Hypertrophic Lake. doi:10.1007/1-4020-4363-5

Thornton, D. C. O. 2014. Dissolved organic matter (DOM) release by phytoplankton in the contemporary and future ocean. Eur. J. Phycol. **49**: 20–46. doi:10.1080/09670262.2013.875596

Tõnno, I., K. Ott, and T. Nõges. 2005. Nitrogen dynamics in the steeply stratified, temperate Lake Verevi, Estonia, p. 63–71. *In* I. Ott and T. Kõiv [eds.], Lake Verevi, Estonia --- A Highly Stratified Hypertrophic Lake. Springer Netherlands.

Torres, E., C. Ayora, C. R. Canovas, E. García-Robledo, L. Galván, and A. M. Sarmiento. 2013. Metal cycling during sediment early diagenesis in a water reservoir affected by acid mine drainage. Sci. Total Environ. **461**–**462**: 416–429. doi:10.1016/j.scitotenv.2013.05.014

Torres, E., L. Galván, C. R. Cánovas, S. Soria-Píriz, M. Arbat-Bofill, A. Nardi, S. Papaspyrou, and C. Ayora. 2016. Oxycline formation induced by Fe(II) oxidation in a water reservoir affected by acid mine drainage modeled using a 2D hydrodynamic and water quality model - CE-QUAL-W2. Sci. Total Environ. **562**: 1–12. doi:10.1016/j.scitotenv.2016.03.209

Vadia, S., J. L. Tse, R. Lucena, Z. Yang, D. R. Kellogg, J. D. Wang, and P. A. Levin. 2017. Fatty Acid Availability Sets Cell Envelope Capacity and Dictates Microbial Cell Size. Curr. Biol. **27**: 1757–1767.e5. doi:10.1016/j.cub.2017.05.076

Vaulot, D., C. Courties, and F. Partensky. 1989. A simple method to preserve oceanic phytoplankton for flow cytometric analyses. Cytom. Part A **10**: 629–635.

Vrede, K. 2005. Nutrient and temperature limitation of bacterioplankton growth in temperate lakes. Microb. Ecol. **49**: 245–256. doi:10.1007/s00248-004-0259-4

Wallenstein, M. D., and E. K. Hall. 2012. A trait-based framework for predicting when and where microbial adaptation to climate change will affect ecosystem functioning. Biogeochemistry **109**: 35–47. doi:10.1007/s10533-011-9641-8

Van Wambeke, F., P. Catala, M. Pujo-Pay, and P. Lebaron. 2011. Vertical and longitudinal gradients in HNA-LNA cell abundances and cytometric characteristics in the Mediterranean Sea. Biogeosciences **8**: 1853–1863. doi:10.5194/bg-8-1853-2011

Van Wambeke, F., J.-F. Ghiglione, J. Nedoma, G. Mével, and P. Raimbault. 2009. Bottom up effects on bacterioplankton growth and composition during summer-autumn transition in the open NW Mediterranean Sea. Biogeosciences **6**: 705–720. doi:10.5194/bg-6-705-2009

Wei T. and V. Simko. 2017. R package "corrplot": Visualization of a Correlation Matrix (Version 0.84).

Weinbauer, M. G., and M. G. Höfle. 1998. Distribution and life strategies of two bacterial populations in a eutrophic lake. Appl. Environ. Microbiol. **64**: 3776–3783.

Wendt-Potthoff, K., M. Koschorreck, M. Diez Ercilla, and J. Sánchez España. 2012. Microbial activity and biogeochemical cycling in a nutrient-rich meromictic acid pit lake. Limnologica **42**: 175–188. doi:10.1016/j.limno.2011.10.004

Williamson, C. E., W. Dodds, T. K. Kratz, and M. P. Palmer. 2008. Lakes and streams as sentinels of environmental change in terrestrial and atmospheric processes. Connect. Connect. Connect. **6**: 247–254.

doi:10.1890/070140
Yang, X., T. Huang, and H. Zhang. 2015. Effects of seasonal thermal stratification on the functional diversity and composition of the microbial community in a drinking water reservoir. Water (Switzerland) **7**: 5525–5546. doi:10.3390/w7105525
Yu, Z., J. Yang, S. Amalfitano, X. Yu, and L. Liu. 2014. Effects of water stratification and mixing on microbial community structure in a subtropical deep reservoir. Sci. Rep. **4**: 1–7. doi:10.1038/srep05821
Zaikova, E., D. A. Walsh, C. P. Stilwell, W. W. Mohn, P. D. Tortell, and S. J. Hallam. 2010. Microbial community dynamics in a seasonally anoxic fjord: Saanich Inlet, British Columbia. Environ. Microbiol. **12**: 172–191. doi:10.1111/j.1462-2920.2009.02058.x
Zhang, X., S. Tang, M. Wang, and others. 2019. Acid mine drainage affects the diversity and metal resistance gene profile of sediment bacterial community along a river. Chemosphere **217**: 790–799. doi:10.1016/j.chemosphere.2018.10.210

7. Supplementary Material

7.1 Tables

Table S1: Mean ± standard error of temperature (T), dissolved oxygen (O_2), pH, carbon dioxide (CO_2), ammonium (NH_4^+), Nitrate + Nitrite (NO_x), chlorophyll a (Chl *a*), dissolved organic carbon (DOC) and turbulent diffusion coefficient (K_d) for six different microbial niches in El Sancho reservoir water column. Five of them are spatially separated along the water column during stratification (summer): epilimnion (0 - 10 m depth), O_2 peak (16 m depth), above DCM (20 m depth), DCM (22 - 24 m depth) and hypolimnion (28 - 33 m depth). The sixth one includes the whole water column during mixing (winter), representing a temporally separate environment from the rest. < LOD: below limit of detection.

	Stratification					Mixing
	Epilimnion (n =12)	O_2 peak (n = 4)	Above DCM (n = 4)	DCM (n = 4)	Hypolimnion (n = 4)	(n = 21)
T (ºC)	25.6 ± 0.2	22.1 ± 0.8	16.4 ± 0.1	15 ± 0.2	13.7 ± 0.2	12.7 ± 0.1
O_2 (µM)	267 ± 0.9	327.3 ± 15.8	291.7 ± 14.9	57.8 ± 21.9	2.7 ± 0.6	306.8 ± 7.1
pH	3.5 ± 0.03	3.6 ± 0.04	3.6 ± 0.04	3.6 ± 0.04	4.1 ± 0.04	3.1 ± 0.01
CO_2 (µM)	< LOD	< LOD	11 ± 1	140 ± 35	574 ± 69	25 ± 3
NH_4^+ (µM)	16 ± 0.5	27 ± 3	38 ± 1	49 ± 3	97 ± 8	45 ± 1
NO_x (µM)	3 ± 0.04	2 ± 0.3	2 ± 0.1	1 ± 0.03	< d. l	1 ± 0.05
Chl a (µg/L)	1 ± 0.1	1 ± 0.2	4 ± 1	19 ± 3	2 ± 1	1 ± 0.1
DOC (µM)	151 ± 11.5	188 ± 10	175 ± 9	202 ± 16	207 ± 15	83 ± 15
K_d (m^2/s)	$7.3 \times 10^{-5} \pm 4 \times 10^{-5}$	$5.2 \times 10^{-7} \pm 1.4 \times 10^{-8}$	$5.2 \times 10^{-7} \pm 1.4 \times 10^{-8}$	$5.2 \times 10^{-7} \pm 1.4 \times 10^{-8}$	$8.6 \times 10^{-6} \pm 5.4 \times 10^{-7}$	$1.9 \times 10^{-4} \pm 6.7 \times 10^{-5}$

Table S2: Seasonal relationships between the abundance (Abund.), the relative contribution (%), the cell content of nucleic acid (FL) and the cell side scatter (SSC) of HNA and LNA cells. The data for correlations comprised four sampling during stratification (n = 28) and three samplings during mixing (n = 21). Statistically significant Spearman correlations coefficients ($p < 0.05$) are marked in bold

		Abund. HNA.	Abund. LNA	% HNA	% LNA	FL_{HNA}	FL_{LNA}	SSC_{HNA}	SSC_{LNA}
Stratification (n = 28)	Abund. HNA	1							
	Abund. LNA	**0.73**	1						
	% HNA	**0.41**	-0.3	1					
	% LNA	**-0.41**	0.3	-1	1				
	FL_{HNA}	**-0.52**	**-0.71**	0.22	-0.22	1			
	FL_{LNA}	**-0.43**	**-0.76**	0.35	-0.35	**0.88**	1		
	SSC_{HNA}	**-0.47**	**-0.74**	0.30	-0.30	**0.89**	**0.81**	1	
	SSC_{LNA}	**-0.58**	**-0.75**	0.21	-0.21	**0.80**	**0.76**	**0.80**	1
Mixing (n =21)	Abund. HNA	1							
	Abund. LNA	0.33	1						
	% HNA	**0.47**	**-0.48**	1					
	% LNA	**-0.47**	**0.48**	-1	1				
	FL_{HNA}	-0.39	-0.43	-0.22	0.22	1			
	FL_{LNA}	**-0.48**	**-0.51**	-0.14	0.14	**0.86**	1		
	SSC_{HNA}	**-0.47**	0.04	**-0.54**	**0.54**	-0.13	0.13	1	
	SSC_{LNA}	-0.26	0.36	**-0.68**	**0.68**	-0.20	0.20	**0.55**	1

7.2. Figures

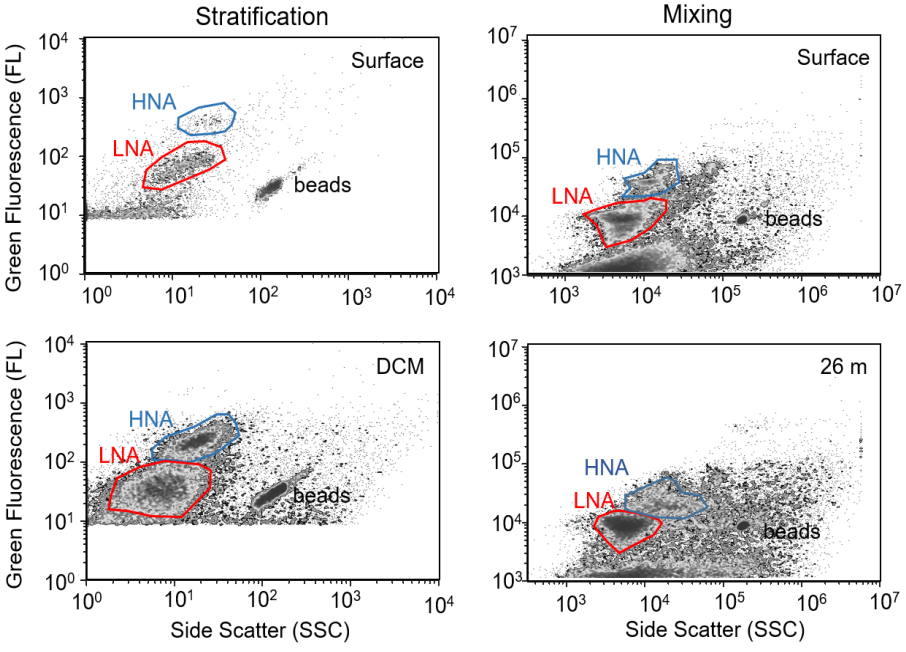

Fig. S1: Examples of four cytograms obtained after SyBR green I staining of surface (0 m depth) and DCM samples (22 m) during stratification (summer) and surface and 26 m depth during mixing (winter). The regions for high nucleic acid (HNA) cells (blue) and low nucleic acid (LNA) cells (red) were slightly adjusted when needed for every sample. Beads (1.1 µm) were added to every sample as internal standard.

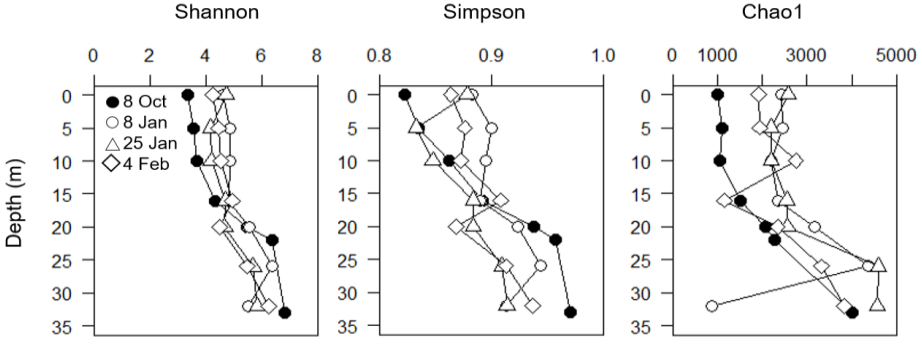

Fig. S2: Depth profiles showing the vertical distribution of the Diversity indices (Shannon, Simpson, Chao1) in El Sancho reservoir in one sampling during stratification (summer) and in three samplings during mixing (winte

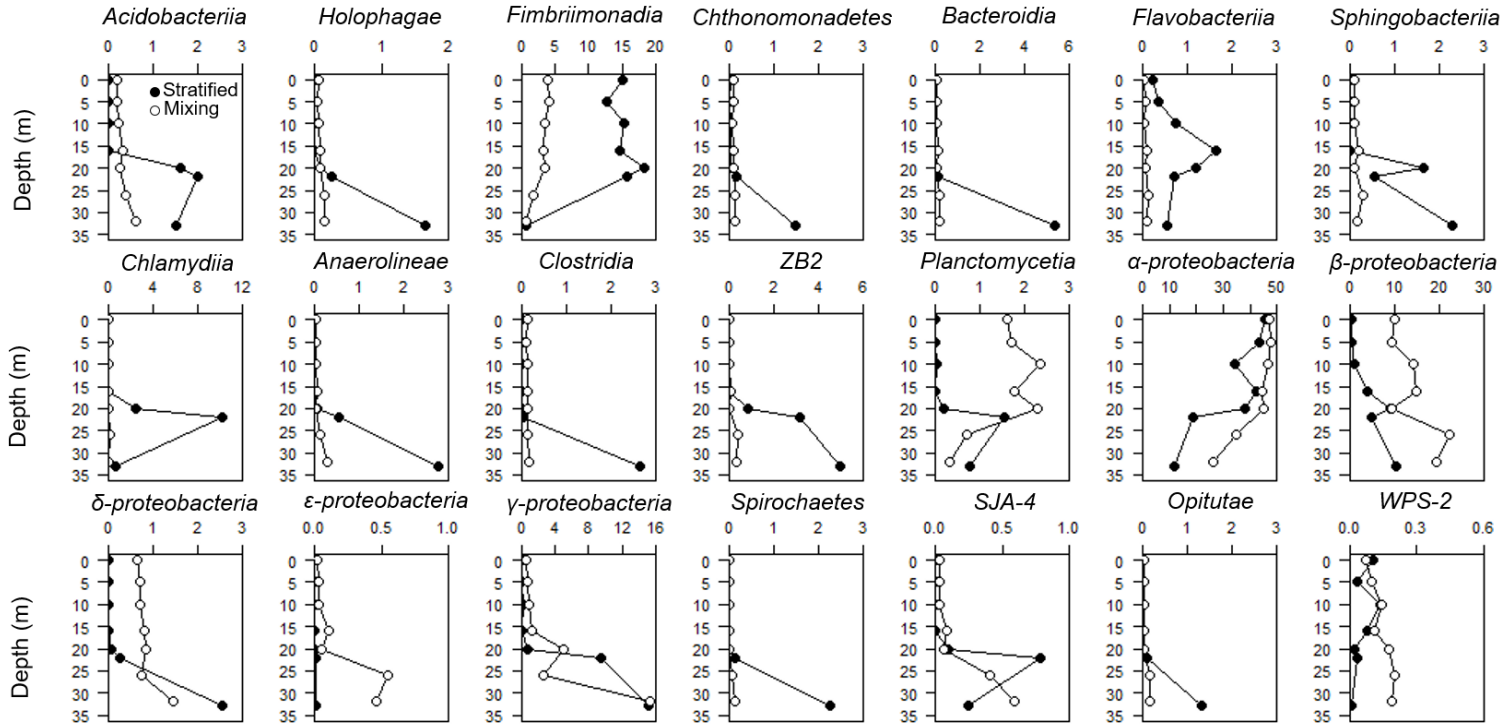

Fig. S3: Depth profiles showing the vertical distribution of the relative abundance (%) of the most abundant bacterial classes in El Sancho reservoir during stratification (summer) and mixing (winter).

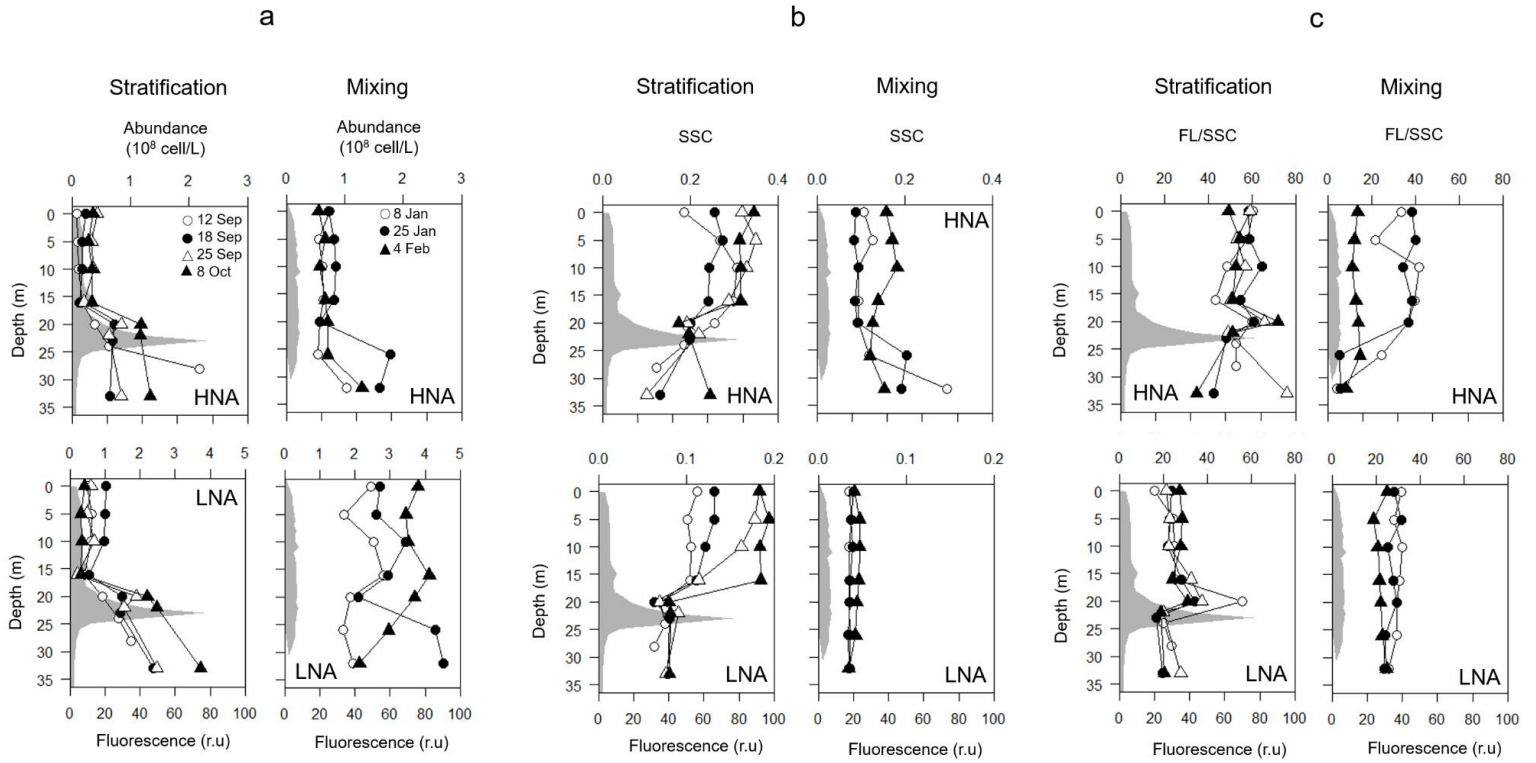

Fig. S4: Depth profiles showing the vertical distribution of the (a) abundance, (b) SSC and (c) FL/SSC of both HNA and LNA fractions in El Sancho reservoir during stratification (summer) and mixing (winter). Fluorescence ( ) profiles are also shown for spatial reference

CHAPTER VI

General Discussion and Conclusions

1. GENERAL DISCUSSION

1.1. Interactions of microbial communities along environmental gradients

The studies presented here as separate chapters (Chapters II - V) were designed to test specific hypothesis on the interactions of microbial communities along environmental gradients which were addressed by *in situ* and laboratory measurements, field observations and modelling approaches. The study of planktonic microbial communities and biogeochemical variables along environmental gradients allowed to identify and define ecological niches and specific microbial interactions depending on the spatial and temporal scales of each gradient which largely affect ecosystemic functions. In this chapter, I will summarize the main results from each individual study in order to offer an overall view of the biogeochemistry and microbial interactions along the two environmental gradients selected. Hopefully, these findings can be used in the future as guide points for other studies on similar ecological gradients in different environments. Therefore, this chapter is divided into four sections: (1) the biogeochemistry in aquatic ecosystems dominated by gradients; (2) primary production, limiting resources and net metabolism zonation along ecological gradients; (3) zonation of microbial community structure based on size fractionated net metabolism, cell traits and phylogenetic composition along environmental gradients; and (4) microbial community ordination in space and time and interactions along ecological gradients

1.2. The biogeochemistry in aquatic ecosystems dominated by gradients

The two ecosystems selected in this PhD thesis provide new insights on the environmental gradient concept in aquatic ecosystems based on an integrated approach including biogeochemistry and microbial community aspects, which had been poorly studied to date in both types of ecosystems. As expected in a gradient environment, a wide amplitude of environmental conditions both in space and in time could be observed in both ecosystems.

In the inner part of the Gulf of Nicoya, the spatial gradient defined by salinity was the main feature along the longitudinal transect. This salinity gradient varied seasonally affecting the hydrological circulation, water column stability and residence time, as a consequence of the variability of the freshwater discharges from the Tempisque River, which represents the main supply of inorganic nutrients, and dissolved and particulate matter in the inner part of the Gulf of Nicoya (Gocke et al. 2001; Kress et al. 2002; Palter et al. 2007; Seguro et al. 2015). In addition, since salinity is considered a conservative property and the key driving force that defines estuaries as unique aquatic environments (Boyle et al. 1974; Fisher et al. 1988; Geyer 2010; Telesh and Khlebovich 2010; Cloern et al. 2017) it allowed to identify the dilution process by mixing with seawater as the main process responsible for the decrease of inorganic nutrients along the estuary (Chapter II). Nonetheless, the high NO_3^-, NO_2^- and PO_4^{3-} concentrations observed close to the sediment at Sta. 1 and Sta. 2 were related to intense remineralization processes in this part of the estuary, rather than the river discharge. In addition, flocculation occurred at Sta. 2 as a consequence of the high suspended solid concentrations, favored by the mixing between freshwater and marine water detected in this zone (Gómez-ramírez et al. 2019). The high increase of CDOM during the rainy season was related to a higher contribution of refractory organic compounds, characteristic of terrestrial soils (Bianchi et al. 1997; Abril et al. 2002). This was supported by the increase of the slope of the CDOM spectra along the estuary (Chapter III).

In El Sancho reservoir, the spatial gradient was determined by the temperature (T), resulting in the vertical stratification of the water column in different layers. The intensity of the thermal stratification defined the intense compartmentalization of the pelagic environment from the highly illuminated, warm and oxic epilimnion to the dim light conditions prevailing above the DCM, and the dark, cold and hypoxic conditions prevailing at the hypolimnion (Chapter IV and V). The thermal gradient allowed us to determine the vertical turbulent diffusion coefficient (K_d) and the net rates of O_2, CO_2, NH_4^+ and NO_3^- within every layer of the water column. The lowest K_d was found in the metalimnion indicating that this layer shows the strongest stability, limiting turbulent diffusion not only of solutes but also of the plankton community (Eberly 1964; Martin et al. 2010). In fact, this high stability (low turbulent diffusivity) led to a metalimnetic O_2 maximum in the upper part of this layer (Chapter IV), as seen in other lakes (Matthews and Deluna 2008; Wilkinson et al. 2015; Latasa et al. 2017). The formation and persistence of this O_2 maximum was related to the highly positive net photosynthetic O_2 production due to a higher light availability at that depth (Chapter IV) (Clegg et al. 2012; Latasa et al. 2017). The quick O_2 decrease with depth was associated to its consumption in the aerobic oxidation of organic matter (OM) and the oxidation of reduced inorganic compounds formed during the anaerobic mineralization of OM by heterotrophic bacteria. In addition, the strong positive correlations of CO_2 and NH_4^+ with the bacterial abundance support the role of microbial degradation as the main source of CO_2 in the hypolimnion (Chapter IV). During mixing, the sharp nutrients and oxygen gradients disappeared when the entire water column was homogeneous as a consequence of the decrease in temperature in winter (Chapter V). The very high values for the turbulent diffusion coefficient led to the whole water column being well mixed, and thus it was considered the same bacterial environment. Moreover, the dissolved organic substrates from autochthonous sources (phytoplankton) decreased as well, which were key drivers for supporting the bacterial communities (Chapter IV and V).

1.3. Primary production, limiting resources and net metabolism zonation along ecological gradients

The measurements of primary production and net metabolism, along the inner part of the Gulf of Nicoya, allowed us to increase the scarce information available on phytoplanktonic primary production of estuarine-coastal tropical ecosystems (Cloern et al. 2014). The higher phytoplankton production measured in the Gulf of Nicoya (Chapter II), compared to other tropical systems (Lewis 1974; Hernández J. and Gocke 1990; Burford et al. 2008) confirmed that the current estimates might substantially underestimate the contribution of primary production from this type of ecosystems at a global scale, as a consequence of the lower number of studies in tropical zones (Cloern et al. 2014). Therefore, measurements of phytoplankton primary production in these sites will be of special relevance for a better appraisal of the contribution of tropical estuaries to the current global estimates, largely biased by the higher number of temperate estuaries in global databases so far. The information obtained from El Sancho reservoir is also highly relevant. The measurements of primary production and net metabolism in this system during stratification (Chapter IV), contributed to enlarge the scarce available information about primary production and metabolism in acidic lakes or reservoir, particularly in the Iberian Pyritic Belt (IPB). Despite the harsh conditions of low pH and high metals concentration, the phytoplankton community was metabolically active even at the DCM, under limiting light conditions. Thus, El Sancho could be a reference for primary production and metabolism for acidic holomictic water bodies affected by acid mine drainage in the IPB.

Limiting factors for primary producers varied depending on ecosystems. Light availability was identified as the main limiting factor for the net primary production (Pn) in the inner part of the Gulf of Nicoya by the relation between Pn, the incident irradiance (I_o) and the extinction coefficient of light (k) in Chapter II (Cole and Cloern 1984, 1987), also observed in other estuarine systems (Cloern 1987; Burford and Rothlisberg 1999; Cloern et al. 2017). The attenuation of light was very pronounced along the estuarine gradient independently on seasons. The highest light attenuation coefficient was found in the estuarine head stations, and was associated to the river-transported sediments (Chapter II, III). This factor is important for photosynthesis levels in the estuary since it defines the photic depth (Cloern 1987). In contrast, El Sancho reservoir was characterized by clear waters where photic layer reached up to middle of the metalimnion (~ 20 m) (Chapter IV). In acidic systems, the chemistry of the water is considered as the main factor determining the survival and growth of the organisms (Nixdorf et al. 1998, 2001). Thus, in El Sancho reservoir, dissolved inorganic carbon was below our analytical detection limit in the epilimnion, identifying it as one of the principal nutrients limiting phytoplankton primary production. Moreover, a strong coupling between bacterial CO_2 production in the hypolimnion and phytoplankton CO_2 assimilation within the DCM structure located in the lower part of the metalimnion was demonstrated through the 1-D reactive transport model in Chapter IV.

Despite that the main limiting factors of primary producers were different depending on the ecosystem, equivalent zonations in terms of primary production and net metabolism could be considered in both ecosystems, as a consequence of the compromise between the distribution main driving factors for the phytoplankton growth, i.e. nutrients and light availability, and the stability of the water column. Firstly, the maximum values of Pn, chlorophyll a (Chl *a*) and particulate organic carbon (POC) were registered in the middle of the estuary which corresponded to the end of the maximum salinity gradient (Fig. 1) (Cloern 1987; Humborg et al. 1997). In this area, the ideal conditions for phytoplankton growth occurred. The photic layer was deeper than the mixing layer due to a decrease in turbidity (Seguro et al. 2015) and an increase in thermohaline stratification. This resulted in higher residence time for phytoplankton in the photic layer under high nutrient conditions (Cole and Cloern 1984; Cloern 1987; Lancelot and Muylaert 2011). Similarly, in the case of El Sancho reservoir, the peak of net primary production was located in the upper part of the metalimnion, where *in situ* irradiance conditions were above the compensation irradiance, and the CO_2 was above the limiting conditions for phytoplankton growth (Fig. 2). In this case, the primary production peak occurred 3 - 4 m above the maximum of biomass (DCM), being this difference dependent on the sinking rate of the phytoplankton and the turbulent diffusivity coefficient (Gong et al. 2015). Nonetheless, the physical and biogeochemical properties that define the metalimnion allowed the development of the maxima of both growth and biomass of the phytoplankton since this layer showed the highest stability, and the resource gradients of light and nutrients interacted in the right proportion (Eberly 1964, Abbott et al. 1984; Camacho 2006; Martin et al. 2010; Durham and Stocker 2012). The second similar metabolic zone between both ecosystems may be characterized by low primary production rates, intense planktonic microbial respiration and mixing depth exceeding the euphotic depth. The riverine stations of the inner part of the Gulf of Nicoya showed these features (Fig. 1). This zone is associated to both the mixing depth exceeded the euphotic depth (Grobbelaar 1985; Domingues et al. 2011) and the intense planktonic microbial respiration due to the input of allochthonous organic matter (Chapter II). The similar zone in El Sancho could is the hypolimnion. This layer was located below the photic layer and the concentrations of CO_2, ammonium (NH_4^+) and bacterioplankton were much higher than that in the epi- and metalimnion, suggesting a strong microbial degradation process leading to hypoxic conditions (Fig. 2) (Chapter IV).

Finally, the third equivalent metabolic zone between both gradients were formed by the more marine stations in the estuary and the epilimnion layer in the reservoir. Both zones were characterized by high light availabilty conditions but lower primary production, possibly as a consequence of lower inorganic nutrients concentrations and suspended material (Chapter II and IV).

1.4. Zonation of microbial community structure based on size fractionated net metabolism, cell traits and phylogenetic composition along environmental gradients

The characterization of the pelagic microbial community in the inner part of the Gulf of Nicoya allowed us to increase the scarce information available on tropical and subtropical aquatic ecosystems in compared to temperate ones (Xia et al. 2017). We investigated the spatiotemporal distributions of four photoautotrophic assemblages and two heterotrophic assemblages in terms of abundance, fluorescence (FL, related to pigment content or nucleic acid) and side scatter (SSC, relate to size and granularity). The photoautotrophic assemblage was form by two *Synechococcus* (Syn) populations: one phycocyanin (PC)-rich cells and another phycoerythrin (PE)-rich cells, PicoEukaryotes (PEuk) and NanoEukaryotes (NEuk). In the bacterioplankton assemblage we distinguished high nucleic acid content (HNA) and low nucleic acid contents (LNA) bacteria. Their spatiotemporal dynamics suggested that phyto- and bacterioplankton subgroups occupy different ecological niches along the inner part of the Gulf of Nicoya.

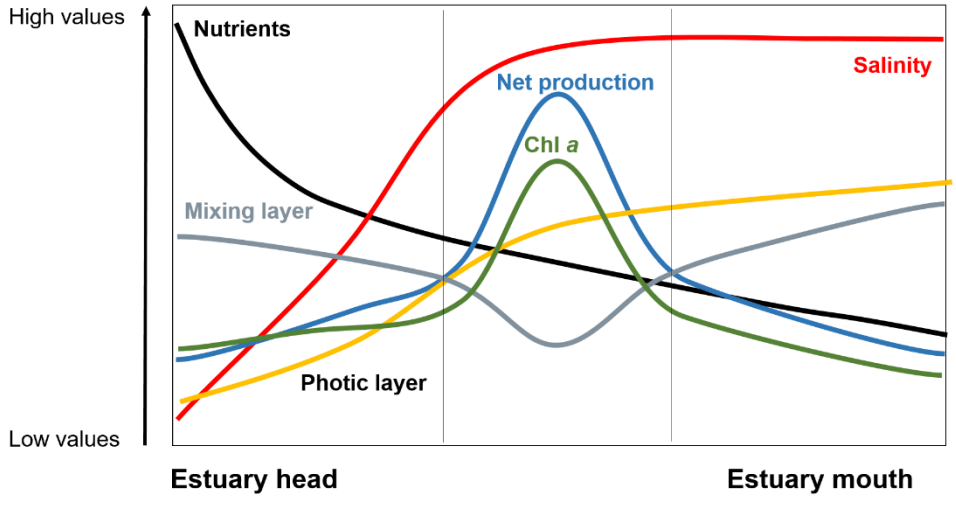

Fig. 1: A schematic diagram showing the *longitudinal cross section* of the main environmental gradients studied in this PhD along the inner part of the Gulf of Nicoya.

The uncoupling between the relative contribution of different size classes to total phytoplankton biomass and net primary production (Pn) observed in the inner part of the Gulf of Nicoya (Chapter II) has been typically explained either as a consequence of a top-down control of the phytoplankton

community by grazers (Banse 1995) or by physiological changes that affect the photosynthetic efficiency of phytoplankton (Chisholm 1992; Geider et al. 1997; Cermeno et al. 2006).

Nanoplanktonic fraction dominated in the inner part of the Gulf of Nicoya as in other estuaries (Iriarte and Purdie 1994; Sin et al. 2000), although its contribution to the phytoplankton abundance and biomass decreased along the estuarine gradient and the contribution of microplankton tended to increase seawards (Chapter II, III). The coincidence of higher abundances of PicoEukaryotes (PEuk) with a positive depth-integrated plankton community production (NCP) is consistent with the increase of relative importance of PEuk with an increase of Chl *a* in nutrient-rich ecosystems due to their higher growth rates than picocyanobacteria (Raven 1986, Weisse 1993, Bec et al 2005).

The inverse spatial segregation between Syn-PC, more abundant in the riverine stations, and Syn-PE, more abundant in the seawater stations, are coincident with other studies where the abundance and diversity of the Synechococcus assemblage has been shown to be affected by nutrient availability (nitrate and phosphate) and salinity as main factors (Rajaneesh and Mitbavkar 2013; Xia et al. 2015, 2017; Sohm et al. 2016). The dominance of Syn-PC in rich-nutrients and high turbid waters and Syn-PE in oligotrophic and transparent waters observed in other aquatic ecosystems (Pick 1991; Vörös et al. 1998; Camacho et al. 2003; Stomp et al. 2007) might explain the inverse spatial pattern of Synechococcus assemblages observed in the Gulf of Nicoya (Chapter III).

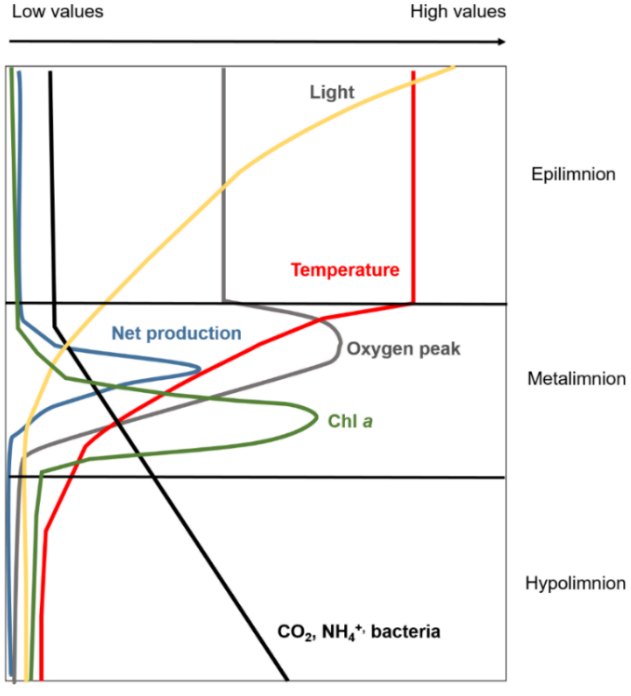

Fig. 2: A schematic diagram showing the *cross-section* of the biochemical structure, net production and microbial distributions studied in this PhD in El Sancho reservoir during stratification.

The increase of abundance of high nucleic acid content (HNA) bacterial and of low nucleic acid contents (LNA) bacterial assemblages seaward has been observed in some temperate estuaries in the transition zone where fresh and marine water mix (del Giorgio and Bouvier 2002; Cottrell and David

2003) but not in others (Urakawa et al. 2013; Li et al. 2017). The variability in bacterial abundance and structure along the estuary has been suggested to be affected by differences in water residence time (Crump et al. 2004). Moreover, higher turbidity, POC and total respiration rate measured at Sta. 1 in the Gulf of Nicoya suggest a higher importance of the attached bacterial community in the estuary head particularly that has not been studied so far (Seguro et al 2015, Soria-Píriz et al 2017).

In terms of SSC, whereas SSC of Syn-PC and Syn-PE decreased seaward, SSC of PEuk and NEuk tended to increase along the estuarine gradient. They could be associated to changes in metabolism and growth in response to the nutrient and light availability along the estuarine gradient (DeLong et al. 2010; Marañón 2015). The variability of SSC between HNA and LNA along the estuarine gradient suggest that HNA and LNA fractions comprise of different compositions and/or the cells size of both LNA and HNA fractions could differed in their response to increasing levels of nutrients and Chl *a* (Corzo et al. 2005, Liu et al 2017).

The considerable seasonal change of FL/SSC observed in PicoEukaryotes (PEuk) and NanoEukaryotes (NEuk) in the surface water layer during the rainy season respect to the dry season might be related to both changes in the phylogenetic composition and to physiological changes to increase fitness to changing condition along the estuarine gradient (Demers et al. 1989; Olson et al. 1990). The increase of FL/SSC of both HNA and LNA fractions seaward coincided with the increase in the slopes of the CDOM spectra along the estuary in both seasons (Chapter III), indicating a relative increase of more labile DOM, likely from autochthonous phytoplankton origin, stimulating production and growth of the bacterial community (Bertilsson and Tranvik 1998; Stedmon and Markager 2003; Bertilsson et al. 2005; Galgani et al. 2011).

In El Sancho reservoir, a clear microbial zonation was observed during stratification. Picoeukaryotes (PEuk) were the only type of primary producer found in the epilimnion in El Sancho reservoir (Chapter IV). This layer seems to be a harsh environment for bacterioplankton since the low phylogenetic diversity was coincident with a low bacterial abundance as well (Chapter V). Bottom-up drivers like UV inhibition of bacterial growth and limitation by inorganic nutrients and organic substrates have been suggested in several aquatic systems (Lindell and Edling 1996; Van Wambeke et al. 2009; Berdjeb et al. 2011; Ávila et al. 2017), whereas top-down mechanisms, like grazing by picoeukaryotes and nanoflagellates or viral lysis have been proposed in others (Epstein and Shiaris 1992; Weinbauer and Höfle 1998; Tammert et al. 2005). An increase in bacterial diversity and biomass occurred downwards (Chapter V). Interestingly, a FL/SSC peak in both HNA and LNA fractions was evident at the Above DCM niche, where the maximum in net primary production occurred (Chapter IV). Most likely in this layer, more DOC was released from phytoplankton cells supporting high rates of bacterial production (Nagata 2000). In both this and the DCM layer, Synechococcus was the most abundant group, although the chlorophyte *Carteria* sp. largely dominated photoautotrophic biomass (Chapter IV). In this remarkable ecological niche (DCM), as in other stratified waters (Cullen 2015; Leach et al. 2018; Reintjes et al. 2019), the low light compensation point (*Ec*) and the particulate organic carbon to chlorophyll *a* ratio (POC: Chl *a*) suggested that phytoplankton community could present photoacclimation mechanisms to survive under low light conditions (Fennel and Boss 2003; Clegg et al. 2012). In the hypolimnion, changes in bacterial abundance and phylogenetic composition were likely driven by a high supply of labile DOC produced by phytoplankton exudation and decomposing phytoplankton cells settling from the photic layer (Chapter IV) (Van Hannen et al. 1999; Auer and Powell 2004; Pinhassi et al. 2004; Teeling et al. 2012) which likely include a higher diversity of organic substrates and contributed to favor microbial diversity as well. In fact, the higher phylogenetic bacterial

diversity observed in the hypoxic hypolimnion of El Sancho acidic reservoir is consistent with trends observed in neutral systems as well (Chapter V). The intense microbial degradation of this detritus is reflected in the increase of NH_4^+ and CO_2 in the hypolimnion and the correlation of these variables with phylogenetic differences and bacterial biomass in the niche ordination (Chapter V). In addition, higher bacterial diversity has been observed in stratified waters, in the transition zones between oxic and anoxic conditions, and in environments with low oxygen concentration, likely due to a higher diversity of inorganic and organic substrates and potential electron acceptors which ultimately lead to higher metabolic diversity (Crump et al. 2007; Stevens and Ulloa 2008; Zaikova et al. 2010; Barberán and Casamayor 2011).

1.5. Microbial community ordination in space and time and interactions along ecological gradients

Multivariate ordinations based on the different microbial assemblages allowed us to conclude that the component of the pelagic trophic web were more linked during the dry season along the estuarine gradient of the Gulf of Nicoya (Chapter III). By contrast, the weak similarities in the ordination patterns within the phyto- and bacterioplankton assemblages during the rainy season, suggests that their dynamics are more uncoupled and they could be under different abiotic and/or biotic drivers during this period of the year (Huete-Stauffer and Morán 2012; Liu et al. 2016). The uncoupling between bacterial assemblages from phytoplankton during the rainy season have been attributed to the higher allochthonous organic carbon discharges from the Tempisque River and the lower autochthonous NCP as in other estuaries (Barrera-Alba et al. 2008; Figueroa et al. 2016; Andersson et al. 2018). Under non-limiting DOC conditions, bacterioplankton out-competes phytoplankton for N and P taking advantages of their low surface/volume ratio (Le et al. 1994; Findlay 2003; Hitchcock and Mitrovic 2010). Therefore, during the rainy season, the strong DOC inflows to the Gulf of Nicoya could potentially change the system to an allochthonous C dominated system, with enhanced importance of bacterioplankton in the transfer of carbon to higher trophic levels, via the detrital food chain (Fig. 3a) (Jassby et al. 1993; Sherr and Sherr 2000; Barrera-Alba et al. 2009). The greater coincidences in the spatial ordinations based on phyto- and bacterial assemblages during the dry season was likely the consequence of a higher coupling between these two functional components of the pelagic trophic web due to a higher autochthonous primary production and the lower DOC inflows from the river discharges, increasing the dependence of bacterial production from local primary production (Fig. 3b).

There are many studies on DCM dynamics, both descriptive and theoretical including modelling, in both lakes and oceans (Cullen 1982; Abbott et al. 1984; Barbiero and Tuchman 2004; Huisman et al. 2006; Clegg et al. 2012; Latasa et al. 2017). Our results (Chapter IV) confirm prior studies in several aspects, but here we show that CO_2, can be as an important limiting nutrient for phytoplankton growth in acidic conditions, as N or P in neutral systems. In addition, most of this CO_2 maintaining the DCM comes from bacterial community respiration in the underlying water and sediments. These microbial interactions were unravelled through the 1-D reactive transport model in which the vertical distribution of Chl *a* was modelled as a function of phytoplankton net growth - dependent on the opposite vertical gradients of CO_2 and light-, turbulent mixing processes and sedimentation (Huisman and Sommeijer 2002; Fennel and Boss 2003; Gong et al. 2015). The CO_2 distribution through the water column was explained basically by the bacterial respiration in the water column despite the fact that the model took into account three CO_2 inputs to the water column i.e. from

the atmosphere (upper boundary flux), from bacterial respiration in the water column and from the sediment (lower boundary flux). Moreover, the modelled CO_2 distribution improved by including a term of anaerobic respiration. This confirmed that the magnitude and vertical position of the DCM in El Sancho reservoir depends on both the light penetration depth and the supply of CO_2 by the hypolimnetic heterotrophic bacteria respiration (aerobic and anaerobic) (Fig. 4).

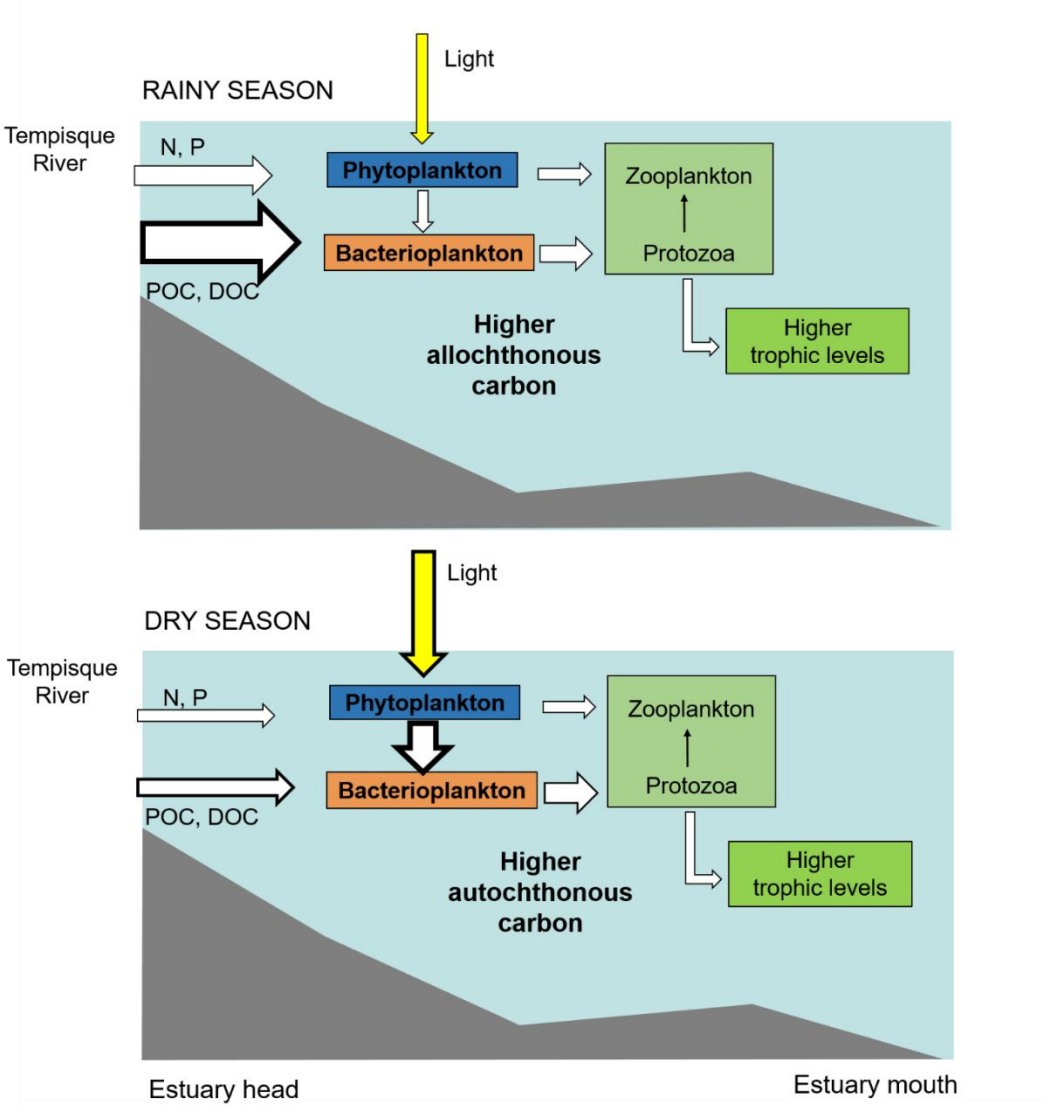

Fig. 3: A schematic diagram of the seasonal differences between phyto- and bacterioplankton assemblages in the inner part of the Gulf of Nicoya. (a) During the rainy season the strong DOC inflows from the Tempisque River could potentially change the system to an allochthonous carbon dominated system, with enhanced importance of bacterioplankton in the transfer of carbon to higher trophic levels. (b) During the dry season a higher autochthonous primary production and the lower DOC inflows from the Tempisque River could increase the dependence of bacterioplankton production from local phytoplankton primary production.

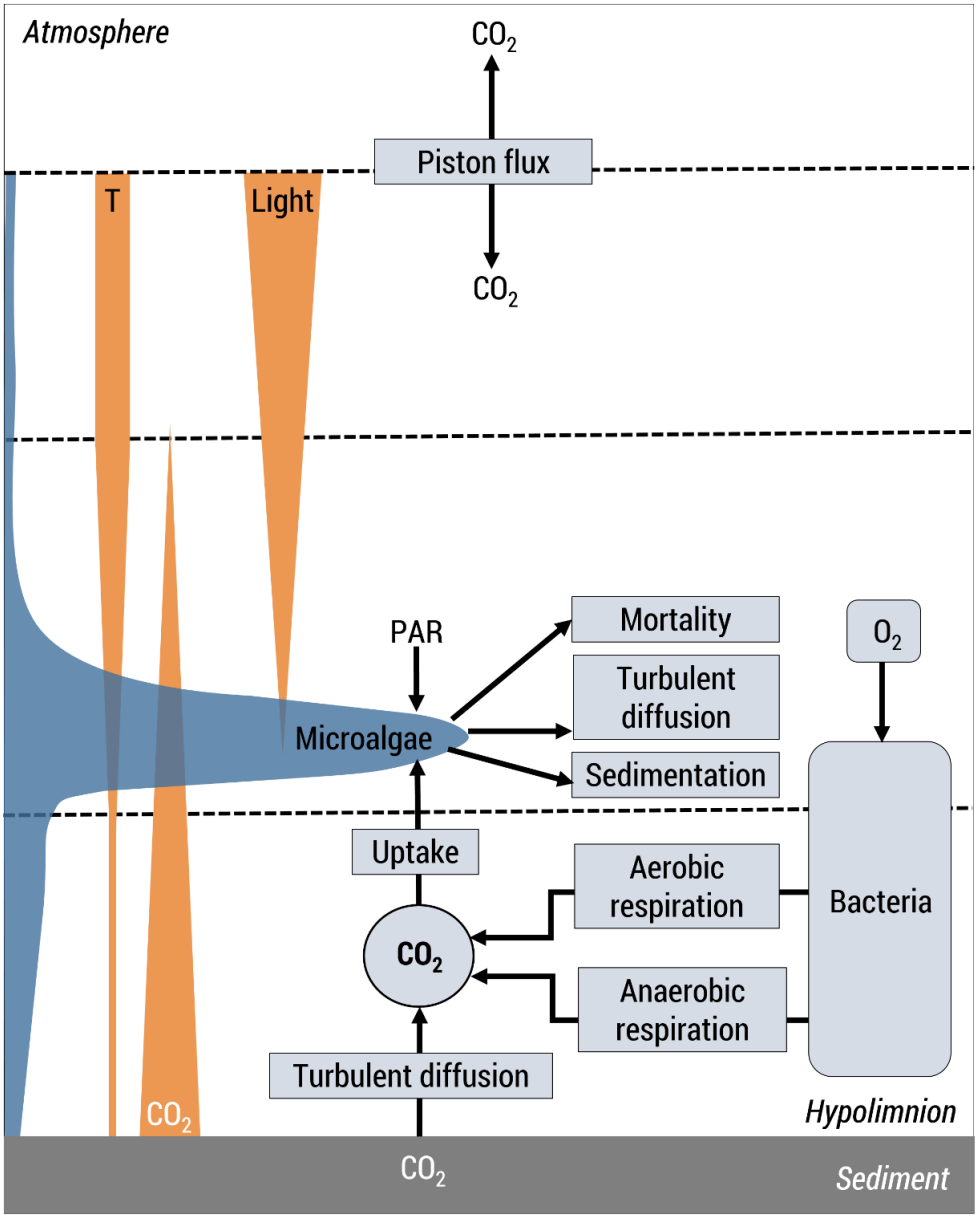

Fig. 4: A schematic diagram of the 1D reactive transport model developed throughout the different layers of the water column and sediment in El Sancho reservoir showing the coupling between phytoplankton and bacterioplankton. The orange triangles are the major variables considered responsible for the formation and positioning of the DCM. Chl *a* (microalgae) and CO_2 are state variables, main processes considered by rectangles and fluxes by black arrows. Non-modelled input data are indicated by a rectangle with smoothed angles.

The strong coupling between changes at the level of phylogenetic composition and abundance and cell traits of the bacterioplankton community over space and time suggests that bacterial community is affected by environmental changes at different structural levels, from physiological to phylogenetic, having implications in the flows of matter and energy, and ultimately, ecosystem-scale dynamic (Chapter V). Thus, these aspects of bacterial community could act as an environmental indicator (Paerl

et al. 2010). Both spatial and temporal variation of microbial assemblages should be considered when assessing the impact of environmental factors on microbial community. Therefore, exploring the links between different community structure levels and how they change among different niches and ecosystems will allow us to understand how seasonal and long term biogeochemical changes in aquatic systems affect the transfer of energy, matter and the ecosystem function overall.

2. References

Abbott, M. R., K. L. Denman, T. M. Powell, P. J. Richerson, R. C. Richards, and C. R. Goldman. 1984. Mixing and the dynamics of the deep chlorophyll maximum in Lake Tahoe. Limnol. Oceanogr. **29**: 862–878. doi:10.4319/lo.1984.29.4.0862

Abril, G., M. Nogueira, H. Etcheber, G. Cabec, and E. Lemaire. 2002. Behaviour of Organic Carbon in Nine Contrasting European Estuaries. 241–262. doi:10.1006/ecss.2001.0844

Andersson, A., S. Brugel, J. Paczkowska, O. F. Rowe, and D. Figueroa. 2018. Estuarine , Coastal and Shelf Science In fl uence of allochthonous dissolved organic matter on pelagic basal production in a northerly estuary. **204**: 225–235. doi:10.1016/j.ecss.2018.02.032

Auer, M. T., and K. D. Powell. 2004. Heterotrophic bacterioplankton dynamics at a site off the southern shore of Lake Superior. J. Great Lakes Res. **30**: 214–229. doi:10.1016/S0380-1330(04)70387-1

Ávila, M. P., P. A. Staehr, F. A. R. Barbosa, E. Chartone-Souza, and A. M. A. Nascimento. 2017. Seasonality of freshwater bacterioplankton diversity in two tropical shallow lakes from the Brazilian Atlantic Forest. FEMS Microbiol. Ecol. **93**: 1–11. doi:10.1093/femsec/fiw218

Banse, K. 1995. Community response to IRONEX. Nature **375**: 112.

Barberán, A., and E. O. Casamayor. 2011. Euxinic Freshwater Hypolimnia Promote Bacterial Endemicity in Continental Areas. Microb. Ecol. **61**: 465–472. doi:10.1007/s00248-010-9775-6

Barbiero, R. P., and M. L. Tuchman. 2004. The Deep Chlorophyll Maximum in Lake Superior. **30**: 256–268.

Barrera-Alba, J., M. Flores, G. Aparecida, O. Moser, and M. P. Saldanha-corre. 2009. Estuarine , Coastal and Shelf Science Influence of allochthonous organic matter on bacterioplankton biomass and activity in a eutrophic , sub-tropical estuary. **82**: 84–94. doi:10.1016/j.ecss.2008.12.020

Barrera-Alba, J. J., S. M. Gianesella, G. A. Oliveira Moser, and F. M. Prado Saldanha-COrrea. 2008. Bacterial and phytoplankton dynamics in a sub-tropical estuary. Hydrobiologia 229–246. doi:10.1007/s10750-007-9156-4

Berdjeb, L., J. F. Ghiglione, and S. Jacquet. 2011. Bottom-up versus top-down control of hypo-and epilimnion free-living bacterial community structures in two neighboring freshwater lakes. Appl. Environ. Microbiol. **77**: 3591–3599. doi:10.1128/AEM.02739-10

Bertilsson, S., O. Berglund, M. J. Pullin, and S. W. Chisholm. 2005. Release of dissolved organic matter by Prochlorococcus. Vie Milieu **55**: 225–231.

Bertilsson, S., and L. J. Tranvik. 1998. Photochemically produced carboxylic acids as substrates for freshwater bacterioplankton. **43**: 885–895.

Bianchi, T. S., M. Baskaran, J. Delord, and M. Ravichandran. 1997. Carbon cycling in a shallow turbid estuary of Southeast Texas: The use of plant pigment biomarkers and water quality parameters. Estuaries **20**: 404–415. doi:10.2307/1352353

Boyle, E., R. Collier, A. T. Dengler, J. M. Edmond, A. C. Ng, and R. F. Stallard. 1974. On the chemical mass-balance in estuaries. Geochimica **38**: 1719–1728.

Burford, M. A., D. M. Alongi, A. D. McKinnon, and L. A. Trott. 2008. Primary production and nutrients in a tropical macrotidal estuary, Darwin Harbour, Australia. Estuar. Coast. Shelf Sci. **79**: 440–448. doi:10.1016/j.ecss.2008.04.018

Burford, M. A., and P. C. Rothlisberg. 1999. Factors limiting phytoplankton production in a tropical continental shelf ecosystem. Estuar. Coast. Shelf Sci. **48**: 541–549. doi:10.1006/ecss.1999.0471

Camacho, A. 2006. On the occurrence and ecological features of deep chlorophyll maxima (DCM) in Spanish stratified lakes. Limnetica **25**: 453–478.

Camacho, A., M. R. Miracle, and E. Vicente. 2003. Which factors determine the abundance and distribution of picocyanobacteria in inland waters? A comparison among different types of lakes and ponds. Arch. für Hydrobiol. **157**: 321–338. doi:10.1127/0003-9136/2003/0157-0321

Cermeno, P., E. Maranón, V. Pérez, P. Serret, E. Fernández, and C. G. Castro. 2006. Phytoplankton size structure

and primary production in a highly dynamic coastal ecosystem (Ría de Vigo, NW-Spain): Seasonal and short-time scale variability. Estuar. Coast. Shelf Sci. **67**: 251–266.

Chisholm, S. W. 1992. Phytoplankton size, p. 26. *In* P.G. Falkowski and A.D. Woodhead [eds.], Primary productivity and Biogeochemical Cycles in the Sea. Plenum Press, New York.

Clegg, M. R., U. Gaedke, B. Boehrer, and E. Spijkerman. 2012. Complementary ecophysiological strategies combine to facilitate survival in the hostile conditions of a deep chlorophyll maximum. 609–622. doi:10.1007/s00442-011-2225-4

Cloern, J. E. 1987. Turbidity as a control on phytoplankton biomass and productivity in estuaries. Cont. Shelf Res. **3**: 1367–1381.

Cloern, J. E., S. Q. Foster, and A. E. Kleckner. 2014. Phytoplankton primary production in the world ' s estuarine-coastal ecosystems. 2477–2501. doi:10.5194/bg-11-2477-2014

Cloern, J. E., A. D. Jassby, T. S. Schraga, E. Nejad, and C. Martin. 2017. Ecosystem variability along the estuarine salinity gradient: Examples from long-term study of San Francisco Bay. Limnol. Oceanogr. **62**: S272–S291. doi:10.1002/lno.10537

Cole, B. E., and J. E. Cloern. 1984. Significance of biomass and light availability to phytoplankton productivity in San Francisco Bay. **17**: 15–24.

Cole, B. E., and J. E. Cloern. 1987. An empirical model for estimating phytoplankton productivity in estuaries. Mar. Ecol. Prog. Ser. **36**.

Cottrell, M. T., and K. L. David. 2003. Contribution of major bacterial groups to bacterial biomass production (thymidine and leucine incorporation) in the Delaware estuary. Limnol. Oceanogr. **48**: 168–178.

Crump, B. C., C. S. Hopkinson, M. L. Sogin, and J. E. Hobbie. 2004. Microbial Biogeography along an Estuarine Salinity Gradient : Combined Influences of Bacterial Growth and Residence Time. **70**: 1494–1505. doi:10.1128/AEM.70.3.1494

Crump, B. C., C. Peranteau, B. Beckingham, and J. C. Cornwell. 2007. Respiratory succession and community succession of bacterioplankton in seasonally anoxic estuarine waters. Appl. Environ. Microbiol. **73**: 6802–6810. doi:10.1128/AEM.00648-07

Cullen, J. J. 1982. The deep chlorophyll maximum: comparing vertical profiles of chlorophyll a. Can. J. Fish. Aquat. Sci. **39**: 791–803.

Cullen, J. J. 2015. Subsurface Chlorophyll Maximum Layers: Enduring Enigma or Mystery Solved? Ann. Rev. Mar. Sci. **7**: 207–239. doi:10.1146/annurev-marine-010213-135111

DeLong, J. P., J. G. Okie, M. E. Moses, R. M. Sibly, and J. H. Brown. 2010. Shifts in metabolic scaling, production, and efficiency across major evolutionary transitions of life. Proc. Natl. Acad. Sci. **107**: 12941 LP-12945. doi:10.1073/pnas.1007783107

Demers, S., K. Davis, and T. L. Cucci. 1989. A flow cytometric approach to assessing the environmental and physiological status of phytoplankton. Cytometry **10**: 644–652. doi:10.1002/cyto.990100521

Domingues, R. B., T. P. Anselmo, A. B. Barbosa, U. Sommer, and H. M. Galvão. 2011. Estuarine , Coastal and Shelf Science Light as a driver of phytoplankton growth and production in the freshwater tidal zone of a turbid estuary. Estuar. Coast. Shelf Sci. **91**: 526–535. doi:10.1016/j.ecss.2010.12.008

Durham, W. M., and R. Stocker. 2012. Thin Phytoplankton Layers: Characteristics, Mechanisms, and Consequences. Ann. Rev. Mar. Sci. **4**: 177–207. doi:10.1146/annurev-marine-120710-100957

Eberly, W. R. 1964. Further Studies on the Metalimnetic Oxygen Maximum , with Special Reference to Its Occurrence Throughout the World The presence of excessively large amounts of dissolved oxygen in the metalimnion of lakes has been noted many times . Probably the earliest . **VI**: 103–139.

Epstein, S. S., and M. P. Shiaris. 1992. Size-selective grazing of coastal bacterioplankton by natural assemblages of pigmented flagellates, colorless flagellates, and ciliates. Microb. Ecol. **23**: 211–225. doi:10.1007/BF00164097

Fennel, K., and E. Boss. 2003. Surface maxima of phytoplankton and chlorophyll: Stady-state solutions from a simple model. Limnol. Ocean. **48**: 1521–1534.

Figueroa, D., O. F. Rowe, J. Paczkowska, C. Legrand, and A. Andersson. 2016. Allochthonous Carbon — a Major Driver of Bacterioplankton Production in the Subarctic Northern Baltic Sea. 789–801. doi:10.1007/s00248-015-0714-4

Findlay, S. 2003. 15 - Bacterial Response to Variation in Dissolved Organic Matter, p. 363–379. *In* S.E.G. Findlay and R.L.B.T.-A.E. Sinsabaugh [eds.], Aquatic Ecology. Academic Press.

Fisher, T. R., L. W. Harding Jr., D. W. Stanley, and L. G. Ward. 1988. Phytoplankton, Nutrients, and Turbidity in the CHesapeake, Delaware, and Hudson Estuaries. Estuarine **27**: 61–93.

Galgani, L., A. Tognazzi, C. Rossi, and others. 2011. Journal of Photochemistry and Photobiology B : Biology Assessing the optical changes in dissolved organic matter in humic lakes by spectral slope distributions. J. Photochem. Photobiol. B Biol. **102**: 132–139. doi:10.1016/j.jphotobiol.2010.10.001

Geider, R. J., H. L. MacIntyre, and T. M. Kana. 1997. Dynamic model of phytoplankton growth and acclimation: Responses of the balanced growth rate and the chlorophyll a:carbon ratio to light, nutrient-limitation and temperature. Mar. Ecol. Prog. Ser. **148**: 187–200. doi:10.3354/meps148187

Geyer, W. R. 2010. Estuarine salinity structure and circulation. Contemp. Issues Estuar. Phys. 12–26. doi:10.1017/CBO9780511676567.003

del Giorgio, P. A., and T. C. Bouvier. 2002. Linking the physiologic and phylogenetic successions in free-living bacterial communities along an estuarine salinity gradient. Limnol. Oceanogr. **47**: 471–486. doi:10.4319/lo.2002.47.2.0471

Gocke, K., J. Cortés, M. M. Murillo, and others. 2001. The annual cycle of primary productivity in a tropical estuary : The inner regions of the Golfo de Nicoya , Costa Rica Study area : The Golfo de Nicoya is a tropical estuary situated on the Pacific coast of Costa. 289–306.

Gómez-ramírez, E. H., A. Corzo, E. Garcia-robledo, J. Bohórquez, A. Agüera-jaquemet, F. Bibbó-sánchez, S. Soria-píriz, and J. L. Jiménez-arias. 2019. Estuarine , Coastal and Shelf Science Benthic-pelagic coupling of carbon and nitrogen along a tropical estuarine gradient (Gulf of Nicoya , Costa Rica). Estuar. Coast. Shelf Sci. **228**: 106362. doi:10.1016/j.ecss.2019.106362

Gong, X., J. Shi, H. W. Gao, and X. H. Yao. 2015. Steady-state solutions for subsurface chlorophyll maximum in stratified water columns with a bell-shaped vertical profile of chlorophyll. Biogeosciences **12**: 905–919. doi:10.5194/bg-12-905-2015

Grobbelaar, J. U. 1985. Phytoplankton productivity in turbid waters*. J. Plankton Res. **7**: 653–663. doi:10.1093/plankt/7.5.653

Van Hannen, E. J., W. Mooij, M. P. Van Agterveld, H. J. Gons, and H. J. Laanbroek. 1999. Detritus-dependent development of the microbial community in an experimental system: Qualitative analysis by denaturing gradient gel electrophoresis. Appl. Environ. Microbiol. **65**: 2478–2484.

Hernández J., C. A., and K. Gocke. 1990. Productividad Primaria En La Cienaga Grande De Santa Marta, Colombia. An. Inst. Invest. Mar. Punta Merín. doi:10.25268/bimc.invemar.1990.19.0.430

Hitchcock, J. N., and S. M. Mitrovic. 2010. Responses of Estuarine Bacterioplankton , Phytoplankton and Zooplankton to Responses of Estuarine Bacterioplankton , Phytoplankton and Zooplankton to Dissolved Organic Carbon (DOC) and Inorganic Nutrient Additions.doi:10.1007/s12237-009-9229-x

Huete-Stauffer, T. M., and X. A. G. Morán. 2012. Dynamics of heterotrophic bacteria in temperate coastal waters: Similar net growth but different controls in low and high nucleic acid cells. Aquat. Microb. Ecol. **67**: 211–223. doi:10.3354/ame01590

Huisman, J., N. N. Pham Thi, D. M. Karl, and B. Sommeijer. 2006. Reduced mixing generates oscillations and chaos in the oceanic deep chlorophyll maximum. Nature **439**: 322–325. doi:10.1038/nature04245

Huisman, J., and B. Sommeijer. 2002. Population dynamics of sinking phytoplakton in light-limited environments: simulation techniques and critical parameters. J. Sea Res. **48**: 83–96.

Humborg, C., V. Ittekkot, A. Cociasu, and B. V. Bodungen. 1997. Effect of Danube River dam on Black Sea biogeochemistry and ecosystem structure. Nature **386**: 385–388. doi:10.1038/386385a0

Iriarte, A., and D. A. Purdie. 1994. Size distribution of chlorophyll a biomass and primary production in a temperate estuary (Southampton Water): the contribution of photosynthetic picoplankton.

Jassby, A. D., J. E. Cloern, and T. M. Powell. 1993. Organic carbon sources and sinks in San Francisco Bay: variability induced by river flow. Mar. Ecol. Prog. Ser. **95**: 39–54.

Kress, N., S. Leon, C. L. Brenes, and S. Brenner. 2002. Horizontal transport and seasonal distribution of nutrients , dissolved oxygen and chlorophyll -a in the Gulf of Nicoya , Costa Rica : a tropical estuary. **22**: 51–66.

Lancelot, C., and K. Muylaert. 2011. Trends in Estuarine Phytoplankton Ecology, Elsevier Inc.

Latasa, M., A. M. Cabello, X. A. G. Morán, R. Massana, and R. Scharek. 2017. Distribution of phytoplankton groups within the deep chlorophyll maximum. Limnol. Oceanogr. **62**: 665–685. doi:10.1002/lno.10452

Le, J., J. D. Wehr, and L. Campbell. 1994. Uncoupling of bacterioplankton and phytoplankton production in fresh waters is affected by inorganic nutrient limitation. Appl. Environ. Microbiol. **60**: 2086–2093.

Leach, T. H., B. E. Beisner, C. C. Carey, and others. 2018. Patterns and drivers of deep chlorophyll maxima structure in 100 lakes: The relative importance of light and thermal stratification. Limnol. Oceanogr. **63**: 628–646. doi:10.1002/lno.10656

Lewis. 1974. Primary Production in the Plankton Community of a Tropical Lake. Ecol. Monogr. **44**.

Li, J., X. Jiang, Z. Jing, G. Li, Z. Chen, L. Zhou, and C. Zhao. 2017. Spatial and seasonal distributions of bacterioplankton in the Pearl River Estuary : The combined e ff ects of riverine inputs , temperature , and phytoplankton. **125**: 199–207. doi:10.1016/j.marpolbul.2017.08.026

Lindell, M., and H. Edling. 1996. Influence of light on bacterioplankton in a tropical lake. Hydrobiologia **323**: 67–73. doi:10.1007/BF00020548

Liu, J., Z. Hao, L. Ma, Y. Ji, M. Bartlam, and Y. Wang. 2016. Spatio-temporal variations of high and low nucleic acid content bacteria in an exorheic river. PLoS One **11**. doi:10.1371/journal.pone.0153678

Marañón, E. 2015. Cell Size as a Key Determinant of Phytoplankton Metabolism and Community Structure. Ann. Rev. Mar. Sci. **7**: 241–264. doi:10.1146/annurev-marine-010814-015955

Martin, J., J. É. Tremblay, J. Gagnon, and others. 2010. Prevalence, structure and properties of subsurface chlorophyll maxima in Canadian Arctic waters. Mar. Ecol. Prog. Ser. **412**: 69–84. doi:10.3354/meps08666

Matthews, R., and E. Deluna. 2008. Metalimnetic Oxygen and Ammonium Maxima in Lake Whatcom, Washington (USA). Matthews DeLuna Northwest Sci. **82**: 18–29. doi:10.3955/0029-344X-82.1.18

Nagata, T. 2000. Production mechanisms of dissolved organic matter. Microb. Ecol. Ocean.

Nixdorf, B., A. Fyson, and H. Krumbeck. 2001. Review: Plant life in extremely acidic waters. Environ. Exp. Bot. **46**: 203–211. doi:10.1016/S0098-8472(01)00104-6

Nixdorf, B., K. Wollmann, and R. Deneke. 1998. Ecological potentials for planktonic development and food web interactions in extremely acidic mining lakes in Lusatia, p. 147–167. *In* Acidic mining lakes. Springer.

Olson, R. J., S. W. Chisholm, E. R. Zettler, and E. V. Armbrust. 1990. Pigments, size, and distributions of Synechococcus in the North Atlantic and Pacific Oceans. Limnol. Oceanogr. **35**: 45–58. doi:10.4319/lo.1990.35.1.0045

Paerl, H. W., K. L. Rossignol, S. N. Hall, B. L. Peierls, and M. S. Wetz. 2010. Phytoplankton community indicators of short- and long-term ecological change in the anthropogenically and climatically impacted neuse river estuary, North Carolina, USA. Estuaries and Coasts **33**: 485–497. doi:10.1007/s12237-009-9137-0

Palter, J., S. L. Coto, and D. Ballestero. 2007. The distribution of nutrients , dissolved oxygen and chlorophyll a in the upper Gulf of Nicoya , Costa Rica , a tropical estuary. **55**: 427–436.

Pick, F. 1991. The abundance and composition of freshwater picocyanobacteria in relation to light penetration. Limnol. Oceanogr. **36**: 1457–1462. doi:10.4319/lo.1991.36.7.1457

Pinhassi, J., H. Havskum, F. Peters, and others. 2004. Changes in Bacterioplankton Composition under Different Phytoplankton Regimens Changes in Bacterioplankton Composition under Different Phytoplankton Regimens †. Appl. Environ. Microbiol. **70**: 6753–6766. doi:10.1128/AEM.70.11.6753

Rajaneesh, K. M., and S. Mitbavkar. 2013. Factors controlling the temporal and spatial variations in Synechococcus abundance in a monsoonal estuary. Mar. Environ. Res. **92**: 133–143. doi:https://doi.org/10.1016/j.marenvres.2013.09.010

Reintjes, G., H. E. Tegetmeyer, M. Bürgisser, and others. 2019. On-Site Analysis of Bacterial Communities of the Ultraoligotrophic South Pacific Gyre H. Nojiri [ed.]. Appl. Environ. Microbiol. **85**: e00184-19. doi:10.1128/AEM.00184-19

Seguro, I., C. M. García, S. Papaspyrou, J. A. Gálvez, and E. García-robledo. 2015. Seasonal changes of the microplankton community along a tropical estuary. Reg. Stud. Mar. Sci. **2**: 189–202. doi:10.1016/j.rsma.2015.10.006

Sherr, E. B., and B. F. Sherr. 2000. Microbial Ecology of the Oceans ed DL Kirchman.

Sin, Y., R. L. Wetzel, and I. C. Anderson. 2000. Seasonal variations of size-fractionated phytoplankton along the salinity gradient in the York River estuary , Virginia (USA). **22**: 1945–1960.

Sohm, J. A., N. A. Ahlgren, Z. J. Thomson, C. Williams, J. W. Moffett, M. A. Saito, E. A. Webb, and G. Rocap. 2016. Co-occurring Synechococcus ecotypes occupy four major oceanic regimes defined by temperature, macronutrients and iron. ISME J. **10**: 333–345. doi:10.1038/ismej.2015.115

Soria-Píriz, S., E. García-Robledo, S. Papaspyrou, V. Aguilar, I. Seguro, J. Acuña, A. Morales, and A. Corzo. 2017. Size fractionated phytoplankton biomass and net metabolism along a tropical estuarine gradient. Limnol. Oceanogr. doi:10.1002/lno.10562

Stedmon, C. A., and S. Markager. 2003. Behaviour of the optical properties of coloured dissolved organic matter under conservative mixing. **57**: 973–979. doi:10.1016/S0272-7714(03)00003-9

Stevens, H., and O. Ulloa. 2008. Bacterial diversity in the oxygen minimum zone of the eastern tropical South Pacific. Environ. Microbiol. **10**: 1244–1259. doi:10.1111/j.1462-2920.2007.01539.x

Stomp, M., J. Huisman, L. Vörös, F. R. Pick, M. Laamanen, T. Haverkamp, and L. J. Stal. 2007. Colourful

coexistence of red and green picocyanobacteria in lakes and seas. Ecol. Lett. **10**: 290–298. doi:10.1111/j.1461-0248.2007.01026.x

Tammert, H., V. Kisand, and T. No. 2005. Lake Verevi, Estonia — A Highly Stratified Hypertrophic Lake. Lake Verevi, Est. — A Highly Stratif. Hypertrophic Lake. doi:10.1007/1-4020-4363-5

Teeling, H., B. M. Fuchs, D. Becher, and others. 2012. Substrate-controlled succession of marine bacterioplankton populations induced by a phytoplankton bloom. Science (80-.). **336**: 608–611. doi:10.1126/science.1218344

Telesh, I. V., and V. V. Khlebovich. 2010. Principal processes within the estuarine salinity gradient: A review. Mar. Pollut. Bull. **61**: 149–155. doi:10.1016/j.marpolbul.2010.02.008

Urakawa, H., J. Ali, R. D. J. Ketover, S. D. Talmage, J. C. Garcia, I. S. Campbell, A. N. Loh, and M. L. Parsons. 2013. Shifts of Bacterioplankton Metabolic Profiles along the Salinity Gradient in a Subtropical Estuary L.B. Cahoon, J.L. Zhou, D. Alongi, M. Lipinski, and S. Ishman [eds.]. ISRN Oceanogr. **2013**: 410814. doi:10.5402/2013/410814

Van Wambeke, F., J.-F. Ghiglione, J. Nedoma, G. Mével, and P. Raimbault. 2009. Bottom up effects on bacterioplankton growth and composition during summer-autumn transition in the open NW Mediterranean Sea. Biogeosciences **6**: 705–720. doi:10.5194/bg-6-705-2009

Vörös, L., C. Callieri, K. V Balogh, and R. Bertoni. 1998. Freshwater picocyanobacteria along a trophic gradient and light quality range. Hydrobiologia **369**: 117–125. doi:10.1023/A:1017026700003

Weinbauer, M. G., and M. G. Höfle. 1998. Distribution and life strategies of two bacterial populations in a eutrophic lake. Appl. Environ. Microbiol. **64**: 3776–3783.

Wilkinson, G. M., J. J. Cole, M. L. Pace, R. A. Johnson, and M. J. Kleinhans. 2015. Physical and biological contributions to metalimnetic oxygen maxima in lakes. Limnol. Oceanogr. **60**: 242–251. doi:10.1002/lno.10022

Xia, X., W. Guo, S. Tan, and H. Liu. 2017. Synechococcus Assemblages across the Salinity Gradient in a Salt Wedge Estuary. **8**: 1–12. doi:10.3389/fmicb.2017.01254

Xia, X., N. K. Vidyarathna, B. Palenik, P. Lee, and H. Liu. 2015. Comparison of the seasonal variation of Synechococcus assemblage structure in estuarine waters and coastal waters of Hong Kong.doi:10.1128/AEM.01895-15

Zaikova, E., D. A. Walsh, C. P. Stilwell, W. W. Mohn, P. D. Tortell, and S. J. Hallam. 2010. Microbial community dynamics in a seasonally anoxic fjord: Saanich Inlet, British Columbia. Environ. Microbiol. **12**: 172–191. doi:10.1111/j.1462-2920.2009.02058.x

CONCLUSIONS

1. Different estuarine zones were clearly distinguished based on the strong physicochemical gradients in both seasons (rainy and dry) along the ecological gradients in the inner part of the Gulf of Nicoya. The opposing gradients of decreasing nutrients and CDOM and increasing salinity along the estuary and the clear difference in environmental conditions between Sta. 1 and the rest of the stations indicate that Tempisque River is the main contributor of allochthonous nutrients for the microbial community in the inner part of the Gulf of Nicoya in both seasons.

2. The size structure of the phytoplankton community changed considerably along the estuarine gradient in the Gulf of Nicoya, in terms of biomass, organic carbon and net metabolism (primary production and respiration). The uncoupling between the relative contribution of different size classes to total phytoplankton biomass and primary production suggested a possible top-down control of the phytoplankton community by grazers or physiological changes that affect the photosynthetic efficiency of phytoplankton.

3. A marked net metabolism zonation was observed based on daily integrated rates of organic carbon production and consumption. The middle of the estuary (Sta. 3) showed positive daily depth-integrated plankton community production indicating an autotrophic system which was favored by higher light conditions and residence time. Thus, light availability was identified as the main limiting factor for net primary production in the gulf of Nicoya.

4. Seasonal changes in terrestrial organic carbon inputs, inorganic nutrients, solar radiation and the amount of allochthonous DOC were the major driver of the coupling between the phyto- and bacterioplankton assemblages along the inner part of the Gulf of Nicoya. During the dry season, the spatial patterns of the microbial assemblages based on their cell traits were more similar than during the rainy season. This suggested a closer coupling between the bacterial assemblages and the production of DOC by phytoplankton.

5. In El Sancho reservoir, the differences in the thermal structure of the water column in stratification (summer period) and mixing periods (winter) led to large changes in its biogeochemical characteristics. This allowed to identify six sets of environmental conditions (or microbial niches) differentiated in space and time which sustained specific microbial communities. The synchrony between changes of the phylogenetic composition and the changes in cell traits of the bacterioplankton community as a response to the environmental gradients confirmed that there are direct linkages between changes in biogeochemical conditions due to hydrodynamic forcing and at different structural levels of the bacterial community within the same water body. This means that these parallel changes must affect profoundly the flows of matter and energy, and ultimately, ecosystem-scale dynamic.

6. A 1-D reactive transport model allowed to test the contribution of the bacterial community respiration in supporting the DCM (DCM-CO_2 coupled model) located in the bottom part of

the metalimnion during the stratification season in El Sancho reservoir. The vertical distribution of Chl *a* depended on phytoplankton net growth – being a function of the opposite vertical gradients of CO_2 and light-, turbulent mixing processes and sedimentation rates. In turn, the CO_2 distribution throughout the water column could be modelled by the bacterial respiration in the water column, even though three CO_2 inputs to the water column were considered i.e. from the atmosphere (upper boundary flux), from bacterial respiration in the water column and from the sediment (lower boundary flux). Moreover, the modelled CO_2 distribution improved by including a term of anaerobic respiration. This confirmed that the magnitude and vertical position of the DCM in El Sancho depends on both the light penetration depth and the supply of CO_2 by the hypolimnetic heterotrophic bacteria respiration (aerobic and anaerobic).